University of Windsor
Scholarship at UWindsor

Electronic Theses and Dissertations

1979

STATIC FIELD BREAKDOWN AND CORONA CHARACTERISTICS OF POSITIVE AND NEGATIVE ROD-PLANE GAPS FILLED WITH SULFUR-HEXAFLUORIDE - NITROGEN MIXTURES.

NAZAR HUSSAIN. MALIK
University of Windsor

Follow this and additional works at: http://scholar.uwindsor.ca/etd

Recommended Citation
MALIK, NAZAR HUSSAIN., "STATIC FIELD BREAKDOWN AND CORONA CHARACTERISTICS OF POSITIVE AND NEGATIVE ROD-PLANE GAPS FILLED WITH SULFUR-HEXAFLUORIDE - NITROGEN MIXTURES." (1979). *Electronic Theses and Dissertations.* Paper 3579.

This online database contains the full-text of PhD dissertations and Masters' theses of University of Windsor students from 1954 forward. These documents are made available for personal study and research purposes only, in accordance with the Canadian Copyright Act and the Creative Commons license—CC BY-NC-ND (Attribution, Non-Commercial, No Derivative Works). Under this license, works must always be attributed to the copyright holder (original author), cannot be used for any commercial purposes, and may not be altered. Any other use would require the permission of the copyright holder. Students may inquire about withdrawing their dissertation and/or thesis from this database. For additional inquiries, please contact the repository administrator via email (scholarship@uwindsor.ca) or by telephone at 519-253-3000ext. 3208.

National Library of Canada

Cataloguing Branch
Canadian Theses Division

Ottawa, Canada
K1A 0N4

NOTICE

The quality of this microfiche is heavily dependent upon the quality of the original thesis submitted for microfilming. Every effort has been made to ensure the highest quality of reproduction possible.

If pages are missing, contact the university which granted the degree.

Some pages may have indistinct print especially if the original pages were typed with a poor typewriter ribbon or if the university sent us a poor photocopy.

Previously copyrighted materials (journal articles, published tests, etc.) are not filmed.

Reproduction in full or in part of this film is governed by the Canadian Copyright Act, R.S.C. 1970, c. C-30. Please read the authorization forms which accompany this thesis.

THIS DISSERTATION
HAS BEEN MICROFILMED
EXACTLY AS RECEIVED

Bibliothèque nationale du Canada

Direction du catalogage
Division des thèses canadiennes

AVIS

La qualité de cette microfiche dépend grandement de la qualité de la thèse soumise au microfilmage. Nous avons tout fait pour assurer une qualité supérieure de reproduction.

S'il manque des pages, veuillez communiquer avec l'université qui a conféré le grade.

La qualité d'impression de certaines pages peut laisser à désirer, surtout si les pages originales ont été dactylographiées à l'aide d'un ruban usé ou si l'université nous a fait parvenir une photocopie de mauvaise qualité.

Les documents qui font déjà l'objet d'un droit d'auteur (articles de revue, examens publiés, etc.) ne sont pas microfilmés.

La reproduction, même partielle, de ce microfilm est soumise à la Loi canadienne sur le droit d'auteur, SRC 1970, c. C-30. Veuillez prendre connaissance des formules d'autorisation qui accompagnent cette thèse.

LA THÈSE A ÉTÉ
MICROFILMÉE TELLE QUE
NOUS L'AVONS REÇUE

NL-339 (3/77)

STATIC FIELD BREAKDOWN AND CORONA CHARACTERISTICS OF POSITIVE AND NEGATIVE ROD-PLANE GAPS FILLED WITH SF_6-N_2 MIXTURES

by

NAZAR HUSSAIN MALIK

A Dissertation

Submitted to the Faculty of Graduate Studies
through the Department of Electrical Engineering
in partial fulfillment of the requirements for
the Degree of Doctor of Philosophy at the
University of Windsor

Windsor, Ontario,
Canada

1979

© Nazar Hussain Malik - 1979

720785

I dedicate this work to my parents.

N.H. Malik

ABSTRACT

An experimental study of the static field breakdown and prebreakdown behavior of SF_6-N_2 mixtures in non-uniform field gaps for applied voltages of positive and negative polarities is described. Mixtures containing 0 to 100% SF_6 are investigated over a pressure range of 100 to 500 kPa using rod-plane gaps of various sizes and different degrees of field uniformity. An analysis of the prebreakdown currents, the photomultiplier outputs and the visual observations of the corona discharges indicate that static field anode and cathode corona discharges in SF_6 and SF_6-N_2 mixtures are considerably different from their counterparts in air. The results further show that for such gaps, the dielectric behavior of SF_6-N_2 mixtures is very similar to that of pure SF_6. A discontinuity is reported in the breakdown voltage-pressure characteristics of SF_6 and SF_6-N_2 mixtures when the rod electrode is positive. The pressure for which this discontinuity is observed is higher for the mixtures than for pure SF_6 and is affected by the mixture ratio. It is shown that for both positive and negative rod-plane gaps, breakdown can occur in the absence of any prebreakdown discharges above a critical pressure P_c. The value of this pressure is higher for the negative rod-plane gaps than for the positive ones and decreases with increasing SF_6 percentage in the mixtures. It is shown that depending on the experimental conditions, SF_6-N_2 mixtures can have a breakdown strength in some cases greater than that of pure SF_6, and in other cases lower than that of pure N_2. The experimental results are discussed in detail.

Based on the streamer criterion, a simple method is proposed to calculate the discharge inception voltages in SF_6-N_2 mixtures with SF_6 content between 1 and 100%. The calculated values are in good agreement with the experimental measurements for gaps having varying degrees of field non-uniformities. Using Pedersen's model, it is shown that SF_6-N_2 mixtures are less sensitive to the electrode surface imperfections than pure SF_6.

A semi-empirical criterion is proposed to estimate the minimum gas pressure at which corona free breakdown occurs in SF_6-N_2 mixtures. Based on this criterion, it is shown that the minimum pressure of corona free breakdown in SF_6-N_2 mixtures is a function of the radius of curvature of the anode and gas mixture ratio. These results are verified experimentally for hemispherically capped rod-plane gaps.

ACKNOWLEDGEMENTS

I would like to express my sincere thanks and appreciation to Prof. Dr. A.H. Qureshi for his encouragement, guidance and assistance throughout the progress of this thesis. I am also thankful to Dr. G.D. Theophilus and Dr. R. Hackam for their many valuable suggestions. Thanks are also due to Mrs. S. A. Ouellette for typing the dissertation and my wife for providing moral support during the course of this project.

I would like to thankfully acknowledge National Research Council of Canada, Ministry of Colleges and Universities of Province of Ontario and Government of Pakistan for providing the necessary funds for this project.

TABLE OF CONTENTS

Page

ABSTRACT i
ACKNOWLEDGEMENTS iii
TABLE OF CONTENTS. iv
LIST OF FIGURES. vi
LIST OF TABLES xiii
LIST OF SYMBOLS. xiv

I. INTRODUCTION. 1

1.1 Introduction.. 1
1.2 Nature of the Investigations.......................... 2

II. EXPERIMENTAL ARRANGEMENTS AND PROCEDURES 4

2.1 Pressure Vessel....................................... 4
2.2 Electrode Systems..................................... 4
2.3 Gas Mixing Procedure.................................. 6
2.4 High Voltage Supply and the Measurement Systems....... 8

III. PREBREAKDOWN STUDIES OF THE NEGATIVE ROD-PLANE GAPS 10

3.1 Introduction.. 10
3.2 The Cathode Corona in Nitrogen........................ 10
3.3 The Cathode Corona in SF_6.......................... 17
3.4 The Cathode Corona in SF_6-N_2 Mixtures........... 22
3.5 Corona Onset Levels in SF_6-N_2 Mixtures.......... 30
3.6 Prebreakdown Current Levels in SF_6-N_2 Mixtures.. 33

IV. BREAKDOWN STUDIES OF THE NEGATIVE ROD-PLANE GAPS 43

4.1 Breakdown Behavior of SF_6 and SF_6-N_2 Mixtures. 43
4.2 The Effect of Field Uniformity on the Breakdown Behavior of SF_6 48
4.3 The Effect of Field Configuration on the Breakdown Behavior of SF_6-N_2 Mixtures.................. 54

V. PREBREAKDOWN STUDIES OF THE POSITIVE ROD-PLANE GAPS 60

5.1 Introduction.. 60
5.2 The Anode Corona in Nitrogen.......................... 60
5.3 The Anode Corona in SF_6 and SF_6-N_2 Mixtures.. 66
5.4 The Corona Onset Voltage Levels....................... 77
5.5 The Prebreakdown Current Levels in SF_6-N_2 Mixtures.... 81

Page

VI. BREAKDOWN STUDIES OF THE POSITIVE ROD-PLANE GAPS. 87

6.1 Introduction.......... 87
6.2 The Breakdown Behavior of SF_6 87
6.3 The Breakdown Behavior of SF_6-N_2 Mixtures.......... 92
6.4 The Spark Trajectory Studies.......... 100
6.5 Discussion.......... 102

VII. THEORETICAL ANALYSIS OF THE DISCHARGE CHARACTERISTICS. . . 108

7.1 Breakdown Mechanisms in SF_6 108
7.2 Streamer Breakdown Criterion for SF_6 112
7.3 Streamer Breakdown Criterion for SF_6-N_2 Mixtures.......... 115
7.4 The Electrode Surface Roughness Effects in SF_6-N_2 Mixtures.......... 122
7.5 Comparison of Calculated and Measured Discharge Inception Voltages.......... 128

VIII. DISCUSSION OF THE EXPERIMENTAL RESULTS. 145

8.1 Introduction.......... 145
8.2 Prebreakdown Studies.......... 146
  8.2.1 Cathode corona in air.......... 147
  8.2.2 Cathode corona in SF_6 and SF_6-N_2 mixtures.......... 149
  8.2.3 Anode corona in air.......... 159
  8.2.4 Anode corona in SF_6 and SF_6-N_2 mixtures.......... 162
8.3 Breakdown Studies.......... 166
8.4 Corona Free Breakdown in SF_6 179
8.5 Corona Free Breakdown in SF_6-N_2 Mixtures.......... 182
8.6 Concluding Remarks.......... 184

REFERENCES. 190

VITA AUCTORIS 197

LIST OF FIGURES

Number	Page
2.1 Test chamber and electrode arrangement	5
2.2 Hard carbon steel needle electrode	7
3.1 Prebreakdown currents in a rod-plane gap using 1 mm diameter rod electrode and filled with N_2	11
3.2 Variations in the pulse repetition rate when applied voltage is changed	13
3.3 Relationship between the prebreakdown current and the photomultiplier output for glow corona in N_2	14
3.4 Variation in the prebreakdown current when applied voltage is changed	16
3.5 Prebreakdown current and photomultiplier output waveforms for rod-plane gaps filled with SF_6	18
3.6 Prebreakdown current and photomultiplier output waveforms for rod-plane gaps filled with SF_6-N_2 mixtures	23
3.7 Cathode coronas in rod-plane gaps filled with SF_6-N_2 mixtures	26
3.8 Cathode coronas in rod-plane gaps filled with SF_6-N_2 mixtures	28
3.9 Effect of pressure on cathode corona in a 40 mm gap filled with SF_6-N_2 mixtures	29
3.10 Cathode corona in nitrogen and an SF_6-N_2 mixture containing 0.05% SF_6	31
3.11 Effect of gas pressure and mixture ratio on the corona onset voltage of a 20 mm rod-plane gap using 1 mm diameter cathode	32

Number Page

3.12 Prebreakdown current in a 20 mm rod-plane gap as a function of the applied voltage and the mixture ratio 34

3.13 Prebreakdown current in a rod-plane gap as a function of the applied voltage and the gas pressure 35

3.14 Variations in the corona current prior to breakdown with gas mixture ratio 37

3.15 Variation of the prebreakdown current with the parameter $V[V - V_o]$ for a rod-plane gap filled with SF_6-N_2 mixtures 38

3.16 Variation of the constant C with gas mixture ratio 39

3.17 Variation of the constant C with total gas pressure 40

3.18 Effect of total gas pressure on the product PC for a 10% SF_6-N_2 mixtures 42

4.1 Breakdown voltage-pressure characteristics of SF_6, N_2 and 0.1% mixture for a 20 mm rod-plane gap using 1 mm diameter cathode 44

4.2 Breakdown voltage-mixture ratio characteristics of a 20 mm rod-plane gap for mixtures having low SF_6 content 46

4.3 Breakdown voltage-mixture ratio curve for a 20 mm negative rod-plane gap using 1 mm diameter rod electrode 47

4.4 Spark trajectories in a 20 mm negative rod-plane gap filled with SF_6 49

4.5 Influence of the rod diameter and gas pressure on the breakdown behavior of negative rod-plane gaps filled with SF_6 50

4.6 Influence of the gap length and the gas pressure on the breakdown behavior of negative rod-plane gaps filled with SF_6 53

Number		Page
4.7	Breakdown voltage-pressure characteristics of SF_6, N_2 and 10% SF_6-N_2 mixtures for a negative rod-plane gap	55
4.8	Influence of the mixture ratio on the critical pressure for negative rod-plane gaps	56
4.9	Breakdown voltage as a function of gas pressure and mixture ratio for a 20 mm negative rod-plane gap	57
5.1	Corona onset voltage levels for various corona modes in N_2	62
5.2	Prebreakdown current and photomultiplier output waveforms for various corona modes in N_2	63
5.3	Visual appearance of corona discharges in a 40 mm positive rod-plane gap filled with N_2	64
5.4	Prebreakdown current and photomultiplier output waveforms for rod-plane gaps filled with 1% SF_6-N_2 mixtures	67
5.5	Visual appearance of breakdown and prebreakdown streamers in a 20 mm rod-plane gap using 1 mm diameter rod anode	69
5.6	Prebreakdown current and light output oscillograms of corona discharges in rod-plane gaps filled with SF_6-N_2 mixtures	71
5.7	Visual appearance of corona discharges in a 40 mm rod-plane gap filled with SF_6-N_2 mixtures	76
5.8	Corona inception levels for a 40 mm rod-plane gap using 1 mm diameter rod electrode	78
5.9	Corona onset voltage-mixture ratio characteristics for a positive rod-plane gap	79

Number		Page
5.10	Corona onset voltage-mixture ratio characteristics for a positive rod-plane gap	80
5.11	Effect of applied voltage and gas mixture ratio on corona current in a positive rod-plane gap	82
5.12	Effect of gas pressure and mixture ratio on current prior to breakdown in SF_6-N_2 mixtures	83
5.13	Effect of gap length and gas pressure on the current prior to breakdown in SF_6-N_2 mixtures	84
5.14	Variation of the constant C with gas mixture ratio in a positive rod-plane gap	86
6.1	Breakdown voltage-pressure characteristics of SF_6 for a 20 mm positive rod-plane gap	88
6.2	Effect of the rod diameter on the breakdown voltage-pressure characteristics of SF_6 for a 20 mm positive rod-plane gap	90
6.3	Effect of the rod diameter on the breakdown voltage-pressure characteristics of SF_6 for a 40 mm positive rod-plane gap	91
6.4	Breakdown voltage-pressure characteristics of a 50% SF_6-N_2 mixture for a 20 mm rod-plane gap	93
6.5	Effect of gas pressure on breakdown and corona onset voltages of N_2 and 1.0% SF_6-N_2 mixture for a 45 mm rod-plane gap using 1 mm diameter rod anode	95
6.6	Variation of the discontinuity pressure P_d with gas mixture ratio	96

Number Page

6.7 Breakdown voltage-mixture ratio characteristics of a 20 mm rod-plane gap using 1 mm diameter rod anode 97

6.8 Breakdown voltage-mixture ratio characteristics for a 20 mm rod-plane gap using 1 mm diameter rod anode 99

6.9 Breakdown voltage-mixture ratio characteristics for a 40 mm rod-plane gap 101

6.10 Spark trajectories for a 20 mm positive rod-plane gap filled with a 50% SF_6-N_2 mixture 103

7.1 Effective ionization coefficients for SF_6-N_2 mixtures 118

7.2 Variation of $\left(\frac{E}{P}\right)^1_{lim}$ with gas mixture ratio 121

7.3 Relative limites for the onset of surface roughness effects in SF_6-N_2 mixtures 125

7.4 Effect of the variable RATIO on surface roughness factor ξ for SF_6 and SF_6-N_2 mixtures 126

7.5 Breakdown limitations in SF_6 and SF_6-N_2 mixtures from surface roughness 127

7.6 Measured and calculated values of uniform field breakdown voltages in SF_6-N_2 mixtures 129

7.7 Breakdown voltage as a function of gas mixture ratio and pressure for sphere-plane gaps filled with SF_6-N_2 mixtures 131

7.8 Measured and calculated values of breakdown voltages for sphere-sphere gaps filled with SF_6-N_2 mixtures 133

7.9 Measured and calculated values of static field breakdown voltages for SF_6-N_2 mixtures in coaxial electrode systems 134

Number Page

7.10 Dependence of the corona onset voltage on mixture ratio for SF_6-N_2 mixtures 136

7.11 Effect of pressure and mixture ratio on breakdown voltage of rod-plane gaps filled with SF_6-N_2 mixtures 137

7.12 Calculated and measured values of the minimum discharge voltage of SF_6 as a function of gas pressure and rod diameter 138

7.13 Calculated and measured values of the corona onset voltages of SF_6 for negative rod-plane gaps 139

7.14 Minimum discharge voltage as a function of gas pressure and rod diameter for a 50% mixture 140

7.15 Minimum discharge voltage as a function of gas pressure and rod diameter for a 50% mixture 141

7.16 Minimum discharge voltage as a function of gas pressure and rod diameter for a 10% mixture 142

7.17 Minimum discharge voltage as a funciton of gas pressure and rod diameter for a 10% mixture 143

8.1 Static field cathode corona in a 40 mm gap for 12.6 mm diameter rod electrode.

(a-e) = corona in N_2 containing less than 0.1% of air
(f) = corona in an SF_6-N_2 mixture containing 1.5% of SF_6 151

8.2 Effect of gas pressure on the breakdown voltage behavior of positive and negative rod-plane gap filled with SF_6 168

8.3 Effect of gas pressure on the breakdown voltage behavior of positive and negative rod-plane gap filled with SF_6 169

Name		Page
8.4	Breakdown voltage-pressure characteristics of SF_6 and 80% SF_6-He mixture for a 20 mm negative rod-plane gap using a 6.3 mm rod cathode	174
8.5	Breakdown voltage-pressure characteristics of SF_6 and SF_6-He mixtures for a 20 mm positive rod-plane gap using 1 mm diameter rod electrode	175
8.6	Effect of gas mixture ratio on the critical pressure of a 40 mm negative rod-plane gap using 6.3 mm diameter rod cathode and filled with SF_6-He mixtures	176
8.7	Effect of gas mixture ratio on the discontinuity pressure of 20 mm positive rod-plane gaps filled with SF_6-He mixtures	177
8.8	Effect of rod radius on the onset pressure for corona free breakdown in SF_6	183
8.9	Effect of gas mixture ratio on the critical pressure of a 20 mm positive rod-plane gap filled with SF_6-N_2 mixtures	185
8.10	Effect of rod radius on the onset pressure for corona free breakdown in SF_6 and SF_6-N_2 mixtures	186

LIST OF TABLES

Number Page

7.1 Variations of β_m, $\left(\frac{E}{p}\right)^{1}_{lim}$ and C_m with SF_6 content for SF_6-N_2 mixtures 119

7.2 Field utilization factors for sphere-plane and sphere-sphere gaps 130

8.1 Critical avalanche length X_c for SF_6-N_2 mixtures 157

LIST OF SYMBOLS

V – gap voltage

I – prebreakdown current

E – electric field intensity

P, p – gas pressure

d – gap length

U – field utilization factor

x_c – critical avalanche length

z – partial pressure ratio of SF_6

α – ionization coefficient

η – attachment coefficient

γ – second ionization coefficient

μ – photon absorption coefficient

ρ – gas density

ξ – roughness factor

CHAPTER I

INTRODUCTION

1.1. Introduction

Heavy gases belonging to the seventh group of the periodic table, e.g., fluorine, chlorine, etc., have a considerably higher dielectric strength compared to air under similar experimental conditions. The high breakdown strength depends mainly on their capability of taking up free electrons, thereby forming heavy negative ions. Gases having this property are called electronegative. Of the many available electronegative gases, sulphur-hexafluoride, SF_6, has especially gained in importance in recent years because of its chemical stability and good heat transfer properties in addition to its high dielectric strength. Therefore it is being used increasingly in high pressure, high voltage gas insulated systems capable of handling large amounts of energy.

Inspite of the excellent electrical properties, there are certain factors which adversely affect the choice of SF_6 in gas insulated systems. Besides being expensive, the dielectric strength of SF_6 is very sensitive to the presence of strong localized fields which are often encountered in gas insulated systems. These are due to electrode surface imperfections and the presence of contaminants, e.g., dirt and metallic particles, etc. Furthermore, SF_6 insulated systems utilizing gas pressures higher than about 600 kPa cannot be operated in colder climates because of the relatively high boiling temperature of the gas. Therefore, there is an increasing interest in the possible applications of mixtures of SF_6 with other common gases. The use of a mixture of SF_6 and a relatively inexpensive inert gas could eliminate some of the problems associated with pure SF_6 and also reduce the insulation cost.

A thorough study of the available literature on SF_6[1] and SF_6-gas mixtures [2] indicates that SF_6-N_2 mixtures are very promising for applications in high voltage gas insulated systems. Such mixtures are non-flammable, non-toxic and less expensive. Furthermore, such mixtures containing 50-60% of SF_6 by pressure have dielectric strength of upto 85-90% that of pure SF_6 [2]. They are also expected to be less sensitive to the presence of free conducting particles and electrode surface roughness and can be operated at pressures considerably higher than 600 kPa which is the upper limit for SF_6 insulated apparatus.

Inspite of the promise the mixtures show for applications as high voltage insulation, there is not enough information available about the electrical discharge characteristics of SF_6-N_2 mixtures especially in the non-uniform electric fields. An important aspect of the design of the high voltage gas insulated equipment is the prevention or minimization of corona discharge activity. Such activity results in an appreciable amount of power loss and causes deterioration of the insulation which can lead to the eventual breakdown of the device. Consequently, a thorough understanding of the corona related properties of SF_6 and its mixtures is required. Therefore it was decided to carry out a detailed investigation about the prebreakdown and breakdown behavior of SF_6, N_2 and SF_6-N_2 gas mixtures.

1.2. Nature of the Investigations

Experimental and theoretical investigations were carried out in order to obtain information which would contribute towards the understanding of the performance of SF_6 and its mixtures as a high voltage insulation. The following aspects of the mixtures were investigated:

1. Experimental study of the corona discharges from inception to the final breakdown of rod-plane gaps with hemispherically capped rods of various diameters and gap lengths insulated with SF_6, N_2 and SF_6-N_2 mixtures [3,4],

2. Experimental study of the breakdown behavior of rod-plane and sphere-plane gaps insulated with SF_6, N_2 and SF_6-N_2 mixtures [4,5],

3. A method based on streamer criterion was proposed to calculate the discharge inception levels in SF_6-N_2 mixtures with SF_6 content between 1 and 100% by pressure. The calculated numerical values of the discharge voltages in the mixtures were compared with our experimentally measured values as well as with those reported in the literature for electrode configurations producing varying degrees of field non-unifomities [6].

Throughout these investigations direct voltages were used with the highly stressed electrode acting both as anode and as cathode. Gas pressure ranged from a minimum of 100 kPa to a maximum of about 500 kPa. The SF_6 content of the mixtures varied between 0.05% and 100% by pressure. Hemispherically capped rod-plane electrode systems were used because they improve visual observation by localizing the ionization activity in the highly stressed region of the gap. Also since the plane electrodes exert negligible influence on the growth of ionization, such systems offer excellent conditions for the study of polarity effects in the breakdown and prebreakdown investigations of gaseous dielectrics.

CHAPTER II

EXPERIMENTAL ARRANGEMENTS AND PROCEDURES

2.1. Pressure Vessel

The investigations were carried out in a stainless steel pressure vessel 60 cm high and 36 cm in diameter fitted with a high voltage bushing and four viewing ports. The high voltage bushing is a General Electric 115 kV AC air blast breaker bushing which is filled with SF_6 at a pressure of 600 kPa. Three of the four viewing ports were utilized for the visual observation of the discharges in the test gap while the fourth served as a gas inlet port.

The high voltage electrode (rod/plane/sphere) was connected to the bushing through a 15 mm diameter rod. The low voltage electrode was connected to a bottom rod and was electrically isolated from the rest of the vessel which was permanently grounded. The bottom rod passed through the base plate and was connected to a vernier arrangement as shown in Figure 2.1. The low voltage electrode was electrically connected to a 50Ω coaxial cable.

The gap length was adjusted by first carefully lifting the bottom electrode until an ohmmeter indicated contact between the two electrodes. Proper gap length was then set by moving the low voltage electrode. Errors in the gap setting introduced by the tolerance limitations of thread and the backlash were insignificant. However, the elongation of the vessel walls resulting from pressurization introduced a small error which was corrected using the appropriate correction factors.

2.2. Electrode Systems

The plane electrode used throughout the investigation had a diameter of 130 mm and was machined from stainless steel to a 90° Rogowski

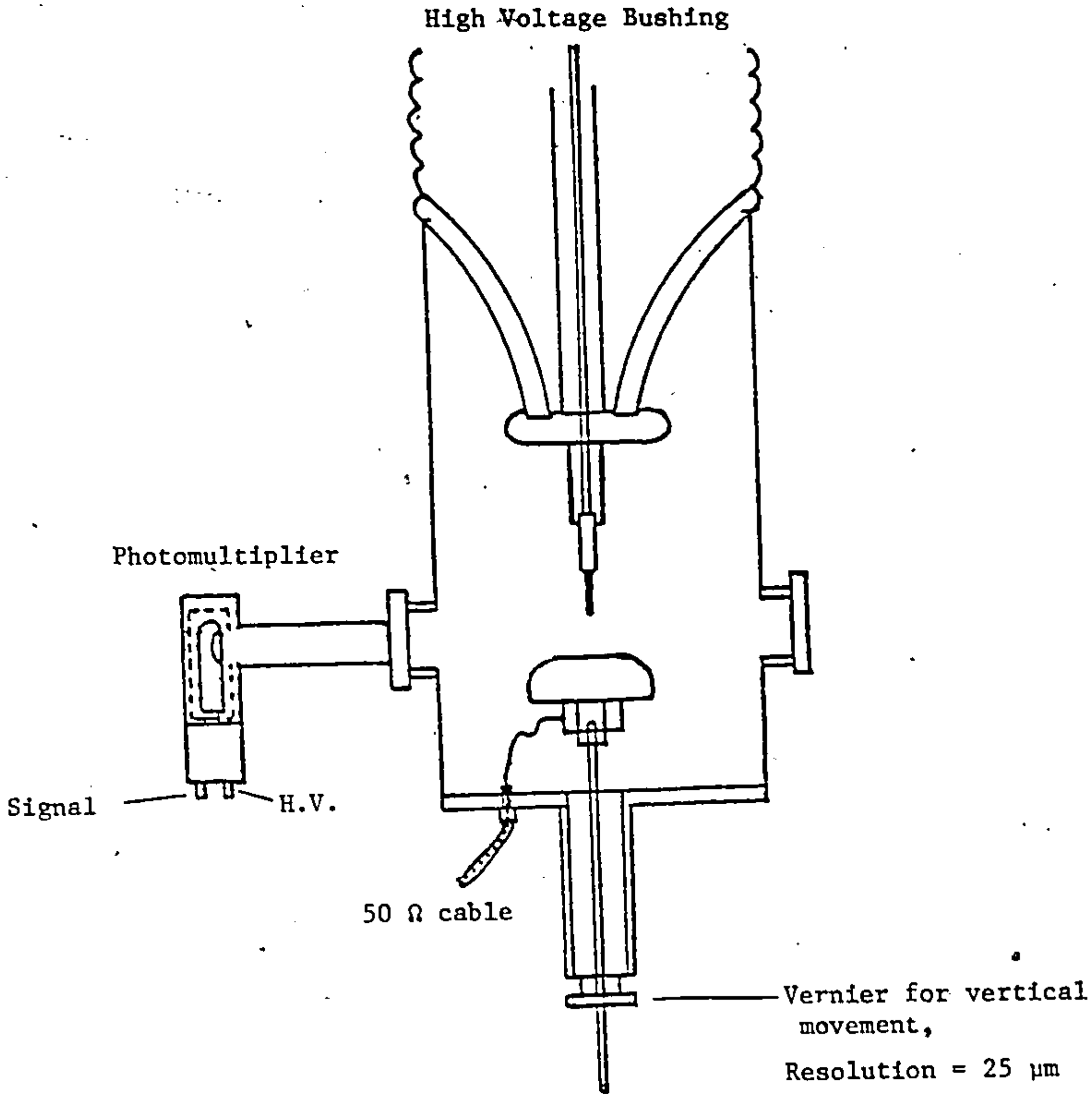
High Voltage Bushing
Photomultiplier
Signal
H.V.
50 Ω cable
Vernier for vertical movement,
Resolution = 25 μm

Figure 2.1 - Test chamber and electrode arrangement.

profile. Hemispherically capped rod electrodes of 1, 1.5, 2, 3.15, 6.25 and 12.6 mm diameter and 50 mm length were used for the study. Rod electrodes having a diameter of 1, 1.5 and 2 mm were made of stainless steel while the rest were made of brass. The ball point sewing machine needle used in some of the experiments was made of hard-carbon steel and had a profile as shown in Figure 2.2. The sphere electrode used was a 51 mm diameter brass sphere.

Before each series of tests, the electrodes were polished and cleaned thoroughly using the following procedure. The electrodes were first polished with a Brasso compound containing an abrasive chalk of maximum particle size of 20 µm. After cleaning with acetone, the electrodes were further polished using a red rouge lapping compound of 0.5 µm grain size. The electrode surfaces were then cleaned with acetone and freon solvents. Finally they were washed thoroughly with distilled water.

2.3. Gas Mixing Procedure

For measurements in SF_6 and N_2, the test chamber was first evacuated to a pressure of about 5 Pa and then flushed several times with the appropriate gas prior to pressurization. To study the discharge behavior of various mixtures, the gases were mixed by adjusting their partial pressure ratios. The chamber was first evacuated and the lower constituent was admitted to a partial pressure corresponding the desired mixture ratio. The second constituent was then added to a total pressure of about 500 kPa. To carry out measurements at lower pressures, the gas mixture was then leaked to the atmosphere to obtain the desired lower pressure. Unless otherwise mentioned, the percentage in the mixtures refer to the percentage of SF_6 by pressure.

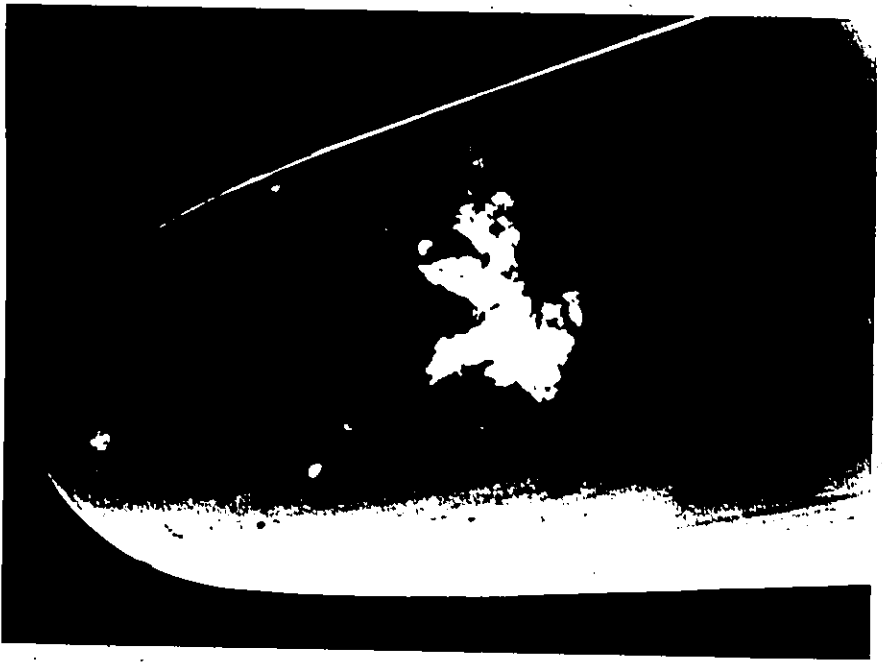

Figure 2.2 - Hard carbon steel needle electrode,magnification = 285 times.

The SF_6 used for these investigations was of commercial purity while the nitrogen and helium were of ultrapure grade. Before pressurizing the vessel, the gases were passed through a filter and a gas purifier containing a desiccant. A small quantity of silica gel and activated alumina was placed at the bottom of the pressure vessel. The silica gel served as a desiccant while the activated alumina was used to remove any chemically active compounds produced by the electrical discharges.

2.4. High Voltage Supply and the Measurement Systems

The power supply was a Deltaray high voltage D.C. generator capable of supplying upto 1 MV at 2 mA. The generator has a load regulation of 0.1% and peak to peak ripple of 0.1%. A 200 kΩ current limiting resistor was placed in series with the high voltage supply line. The output voltage of the generator was calibrated for applied voltages below 50 kV using an electrostatic voltmeter of ±0.5% accuracy. This calibration was extrapolated in the voltage range of 50 to 400 kV.

Prebreakdown current waveforms were observed on an oscilloscope connected through a 50Ω coaxial cable to the low voltage electrode. The cable was terminated in its characteristic impedance at the oscilloscope input. Average corona current levels were determined with the help of a D.C. microammeter connected in series with the test gap.

For optical measurements, a photomultiplier tube, EMI-9781 R was used. The photomultiplier was mounted on one of the chamber windows and was optically aligned to view the entire region of interest. The output signal from the photomultiplier tube was also measured with the oscilloscope using a 50Ω coaxial cable terminated in its characteristic impedance. Tektronix 549 storage oscilloscope with 1A1 or 1A7A plug-in unit was used for the oscillographic studies.

The 1A7A unit is a high gain, low noise amplifier with adjustable bandwidth and a maximum rise time of 350 nanoseconds. The use of this unit permits the measurement of currents as low as 2 x 10^{-10}A at a bandwidth of 10 Hz. The rise time of the 549 oscilloscope with the 1A1 plug-in unit is 13 nanoseconds.

CHAPTER III

PREBREAKDOWN STUDIES OF THE NEGATIVE ROD-PLANE GAPS

3.1. Introduction

Experimental investigations of the prebreakdown discharge behavior of hemispherically capped rod-plane gaps insulated with SF_6, N_2 and SF_6-N_2 mixtures were carried out. Most of these investigations were carried out using a 1 mm diameter rod electrode and a 20 mm long gap. However, measurements using other rod electrodes and gap separations were also carried out. Information about the prebreakdown current pulses and their dependence on the applied voltage, gas pressure, gas mixture ratio, gap length and the rod diameter was obtained. Furthermore, optical measurements using a photomultiplier tube were carried out in order to obtain a better understanding of the corona discharge behavior in the negative rod-plane gaps. The optical output of the corona discharges were photographed using a polaroid still camera and a 300 ASA black and white film. The experimental results of these studies are reported and discussed in the following sections.

3.2. The Cathode Corona in Nitrogen

In nitrogen, the prebreakdown current passed through four transitional stages before the final breakdown of the test gap occurred. As the applied voltage was gradually increased from zero, Trichel pulses appeared at the onset level which we denote as stage 1. These pulses were very regular in both their amplitude and frequency and are shown in figure 3.1(a). The frequency of these pulses increased with the applied voltage while their amplitude remained roughly the same. As the applied voltage was further increased, these pulses took the form

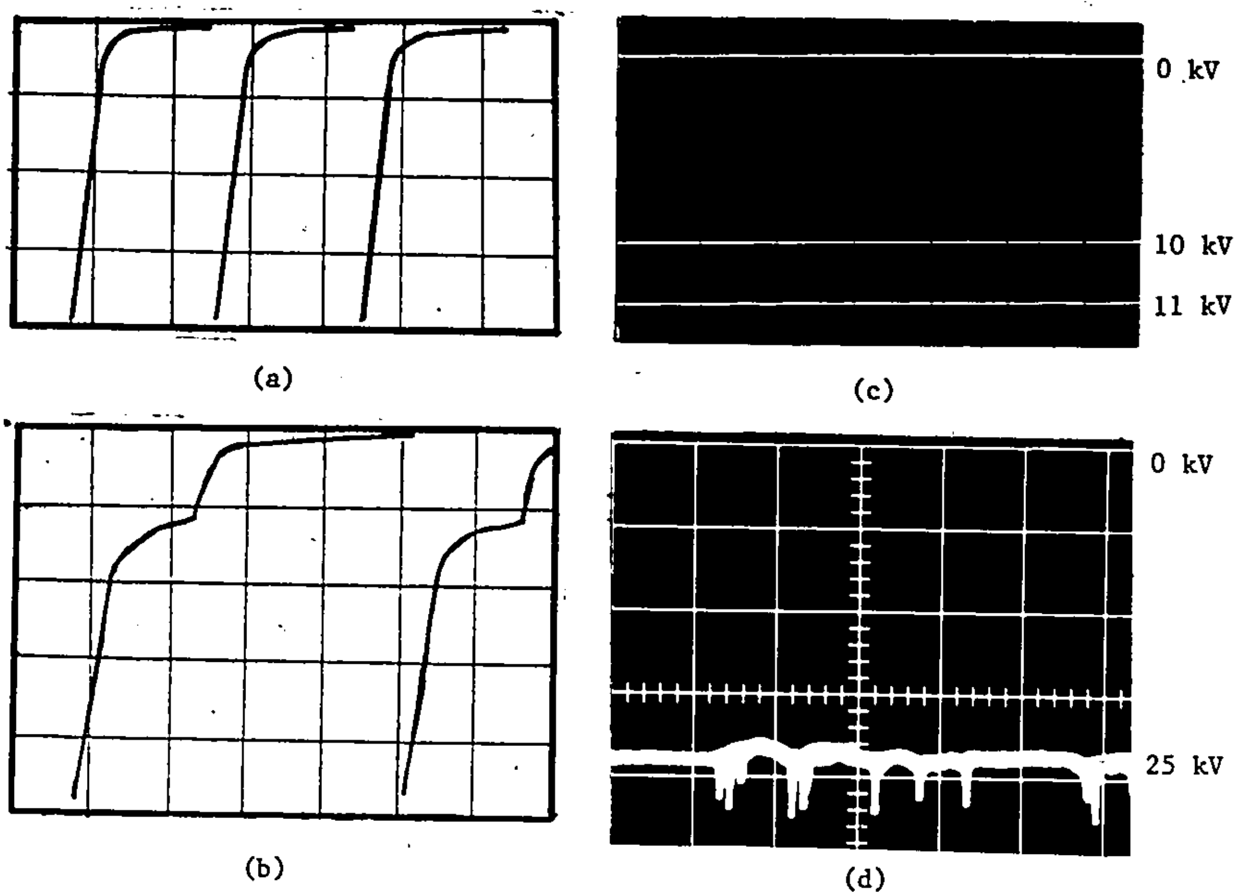

Figure 3.1 - Prebreakdown currents in a rod-plane gap using 1 mm diameter rod cathode and filled with N_2.

(a) Trichel pulse at 7 kV, horizontal scale = 50 μsec/div, vertical scale = 50 μA/div.

(b) Current pulse in stage 2 at 7.7 kV, horizontal scale = 20 μsec/div, vertical scale = 50 μA/div.

(c) Glow in stage 3, horizontal scale = 10 msec/div, vertical scale = 50 μA/div.

(d) Glow with pulses in stage 4, horizontal scale = 10 msec/div, vertical scale = 200 μA/div.

(a), (b) and (c) are for a 12 mm gap at a pressure of 100 kPa.
(d) is for a 20 mm gap at a pressure of 200 kPa.

of stage 2 as shown in figure 3.1(b). This is a transitional stage from the Trichel pulse corona to a glow corona. As in stage 1, the repetition rate of the pulses in stage 2 also increased with the applied voltage. Figure 3.2 shows the change in the repetition rate of the pulses in stage 1 and 2 with the applied voltage. With further increase in the applied voltage, the prebreakdown current became steady. The magnitude of this current increased with increasing applied voltage in stage 3 as shown in figure 3.1(c). As the applied voltage was further raised, irregular pulses appeared superimposed on the steady current leading to stage 4 as shown in figure 3.1(d). Visual observations during this stage of corona indicated the presence of a bright spot moving irregularly on the cathode tip. However, no discharge activity was detected on the cylindrical portion of the rod electrode. This behavior continued until the spark bridged the gap.

The photomultiplier output in stage 1 and 2 consisted of pulses similar to the current pulses discussed earlier. In stage 3 of the corona discharge, the photomultiplier output had a large steady component with a minute ripple. The signal from the photomultiplier output increased with the applied voltage. This output in stage 3 is plotted against the prebreakdown current in figure 3.3. Thus it appears that the light emitted in the glow stage of the corona discharge is almost proportional to the prebreakdown current. In the fourth stage, the photomultiplier output showed large variations with time.

When the applied voltage was gradually reduced, all the four stages occurred in the reverse order and their offset levels were somewhat lower than their onset levels. In general, the voltage ranges in which these four stages occur depend on the gas pressure. For instance, at low pressures such as 100 kPa, the first two stages might not be observed

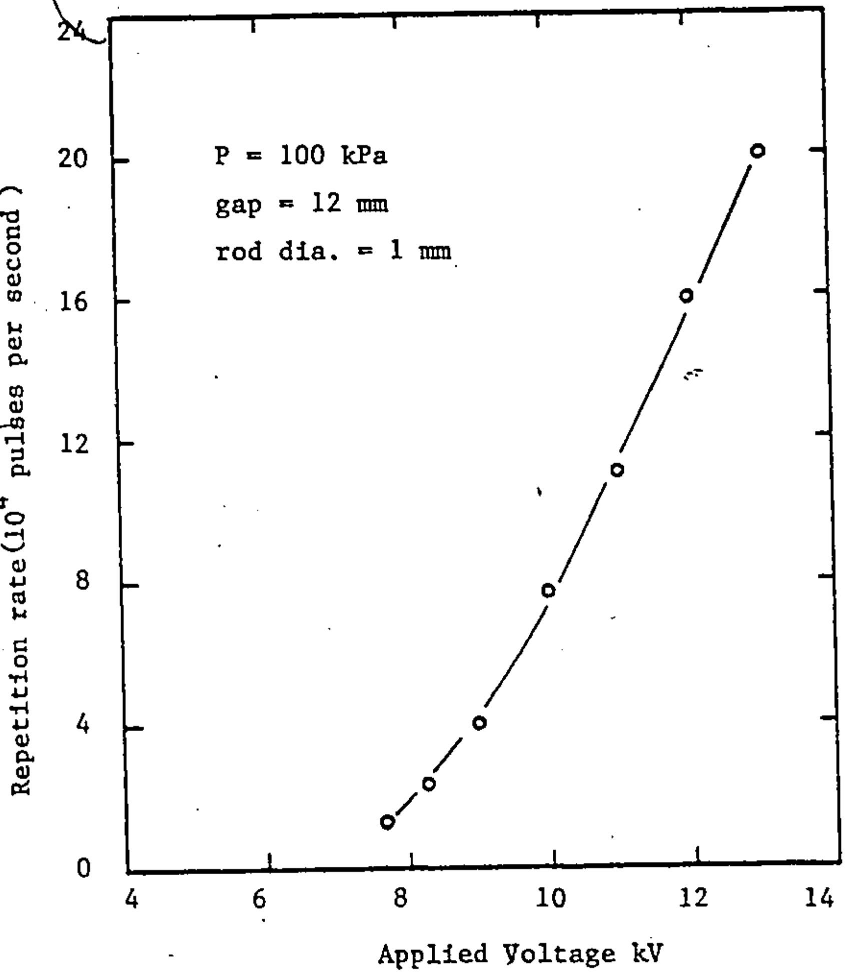

Figure 3.2 - Variations in the pulse repetition rate when applied voltage is changed.

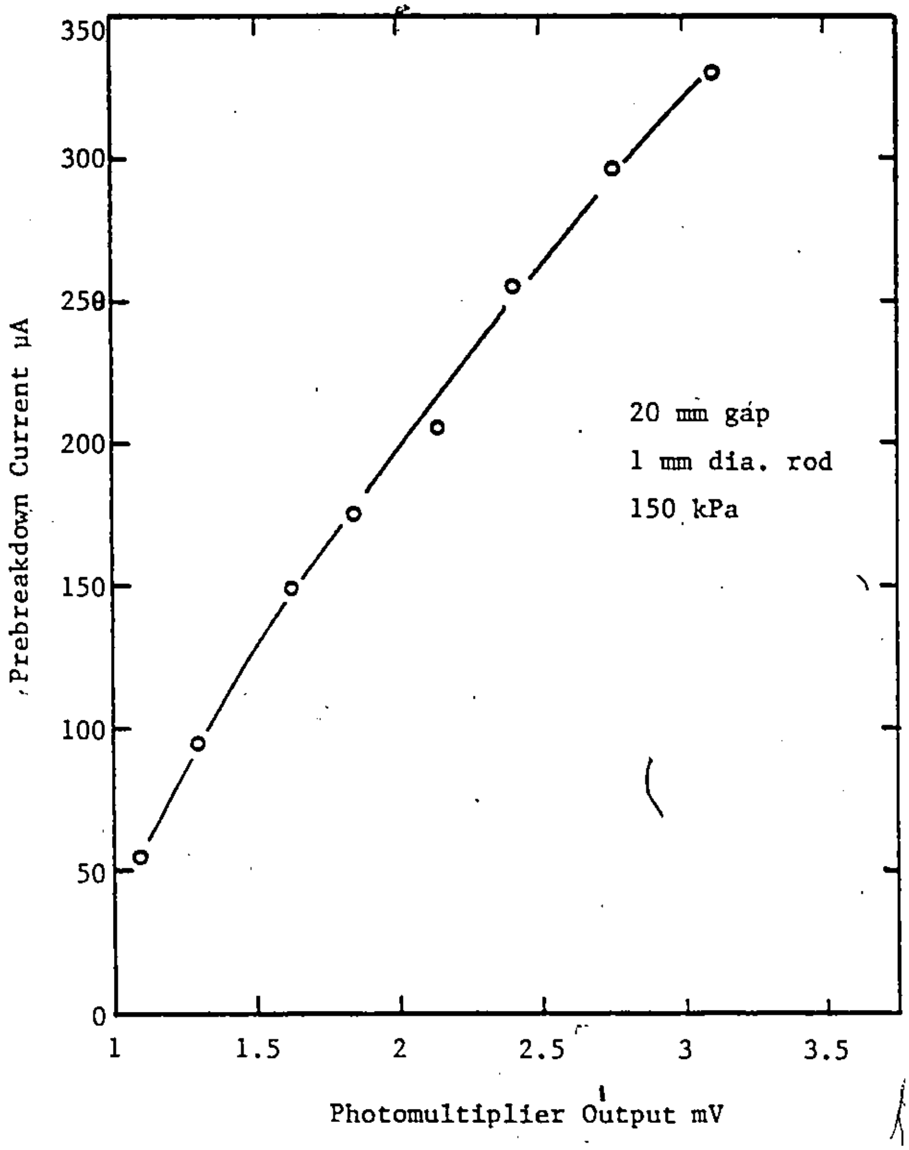

Figure 3.3 – Relationship between the prebreakdown current and the photomultiplier output for glow corona in N_2

when the applied voltage is raised from zero. In such cases, the onset current was of a glow nature. The magnitude of this current increased with the applied voltage as shown in figure 3.4. However, when the applied voltage was reduced gradually, the pulses of the second and the first stage appeared in sequence before the discharge extinction took place at a voltage level which was lower than the one where corona started (figure 3.4). It is interesting to note that the glow corona in stage 3 was observed at all the pressures investigated upto 500 kPa.

In pure non-attaching gases, the cathode corona is usually in the form of a glow discharge. Under such conditions, the positive ion cloud created by the corona discharges is at some distance from the cathode, thereby increasing the field between the cathode and this space charge. This increases the ionization in the vicinity of the cathode and thus produces a glow discharge. Any electronegative impurity prevents this discharge by building up a negative ion space charge and reducing the field near the cathode. The Trichel pulse corona observed in nitrogen indicates the presence of electronegative impurities such as H_2O or O_2 etc. Since these investigations were carried out using ultra pure nitrogen having electronegative impurities of less than ten parts per million and the test chamber was evacuated and flushed with N_2 several times prior to the measurements, the electronegative impurity in the final gas is expected to be less than $10^{-4}\%$. The Trichel pulse corona indicates that even such a small electronegative impurity is sufficient to build up a negative ion space charge cloud and interrupt the discharge especially near the threshold level. Earlier studies by Weissler [8] had indicated that Trichel pulse corona is observed in N_2 containing 0.1% O_2. The present results indicate that even the slightest electronegative impurity produces conditions favorable for Trichel pulse

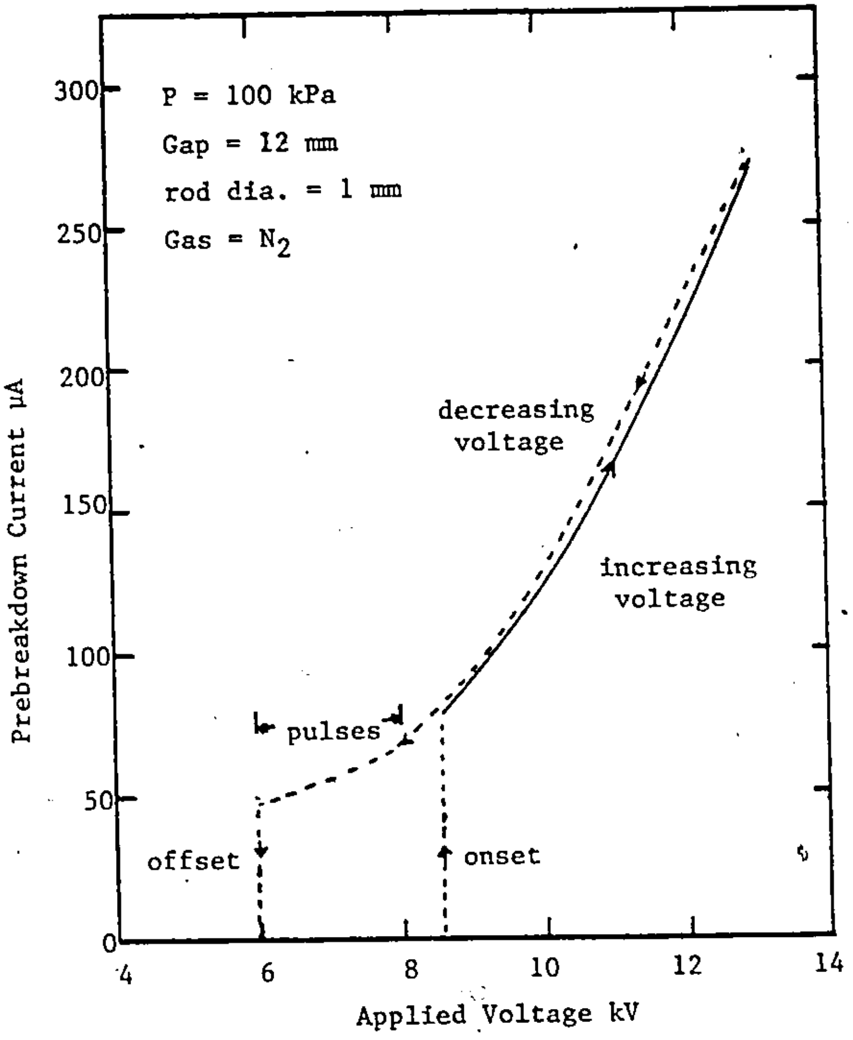

Figure 3.4 - Variation in the prebreakdown current when applied voltage is changed.

corona at the discharge onset level in non-attaching gas like N_2. However, when the applied voltage is increased, the negative ion space charge becomes less dominant and conditions for the establishment of a glow discharge prevail at higher voltage levels.

The presence of the irregular pulses in addition to the steady current in stage 4 is not surprising. The discharge in non-attaching gases is a cathode controlled phenomenon and is extremely sensitive to surface properties of the cathode material. Due to the continuous glow discharge, the positive ion bombardment sputters oxide films, gas films and the cathode material from the surface. Ambient gases reacting chemically or physically with the surface, as well as with ions driven into the surface due to their kinetic energy, will alter the surface properties in various and sometimes opposing fashions [9]. Thus depending on the current density and rate of gaseous diffusion, as well as on the kinetic energy of the ions, the surface conditions will change with time. This will force the discharge to wander over the surface and will also control the discharge magnitude thereby producing variations in the prebreakdown current magnitude.

3.3. The Cathode Corona in SF_6

With an increase in the applied voltage in SF_6, the first indication of the discharge activity was in the form of isolated current pulses as shown in figure 3.5(a). These pulses occurred at random with time intervals between two successive pulses varying between several milliseconds to a few minutes. The pulse amplitude also varied at random. The maximum amplitude of these pulses gradually increased with increasing applied voltages. In addition to single isolated pulses a series of pulses as shown in figure 3.5(b-e) were also observed near the onset level. These

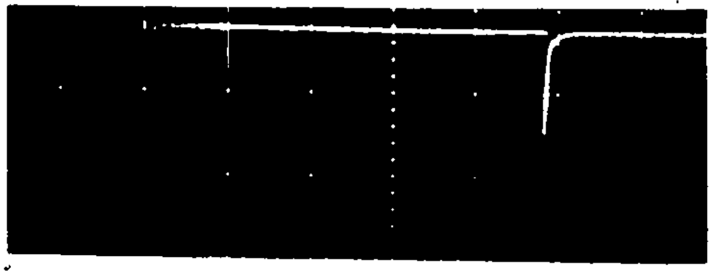

(a)

P = 100 kPa, V = 22 kV
5 msec/div, 20 μA/div.
Gap = 20 mm

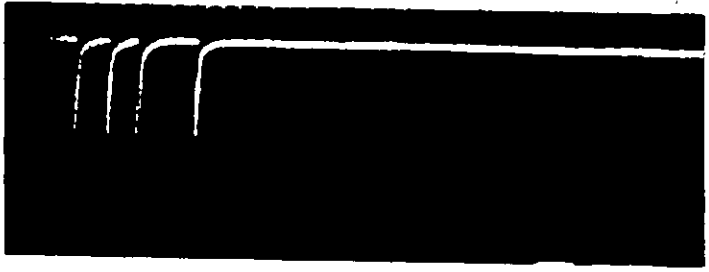

(b)

P = 100 kPa, V = 22 kV
5 msec/div, 20 μA/div.
Gap = 20 mm

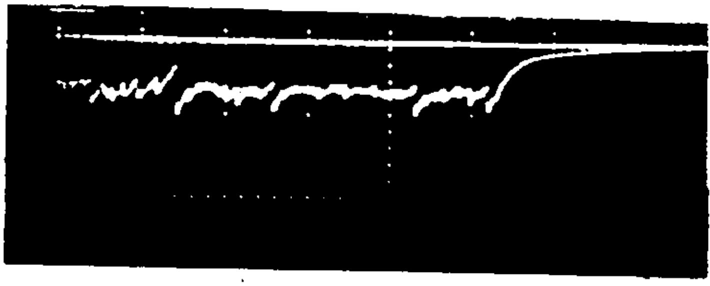

(c)

P = 100 kPa, V = 22.5 kV
50 μsec/div, 20 μA/div.
Gap = 20 mm

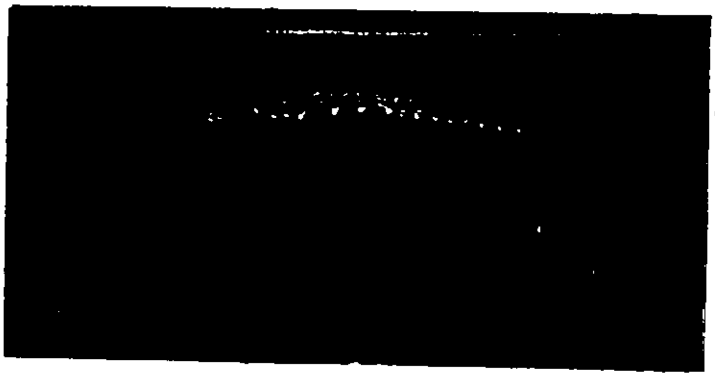

(d)

P = 450 kPa, V = 41 kV
2 μsec/div, 20 μA/div
Gap = 10 mm.

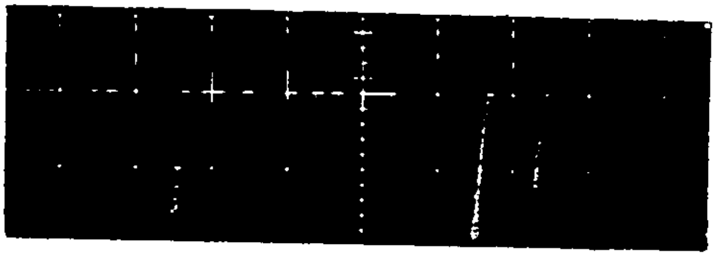

(e)

P = 100 kPa, V = 23 kV
50 μsec/div, 20 μA/div
Gap = 20 mm.

Figure 3.5 (cont'd)

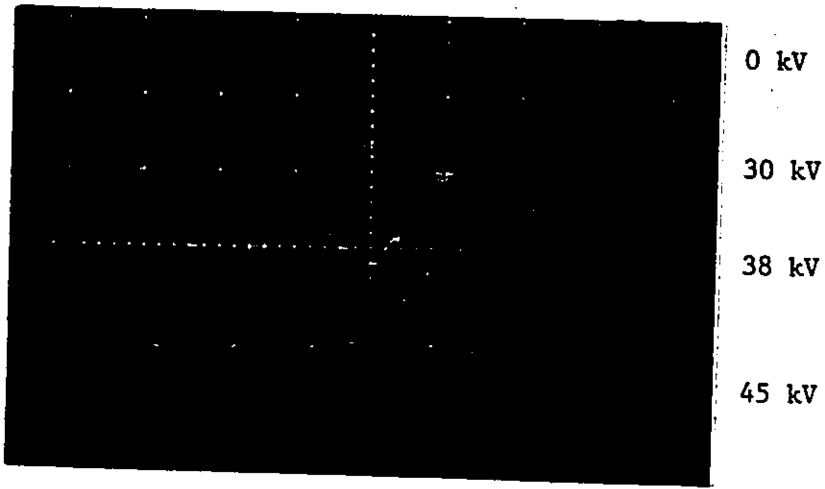

P = 100 kPa, Gap = 20mm
2 μsec/div, 10 μA/div.

(f)

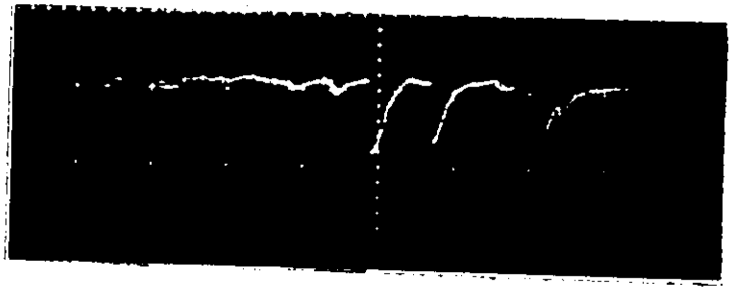

P = 100 kPa, V = 23 kV,
2 μsec/div, 0.1 mV/div.
Gap = 20 mm.

(g)

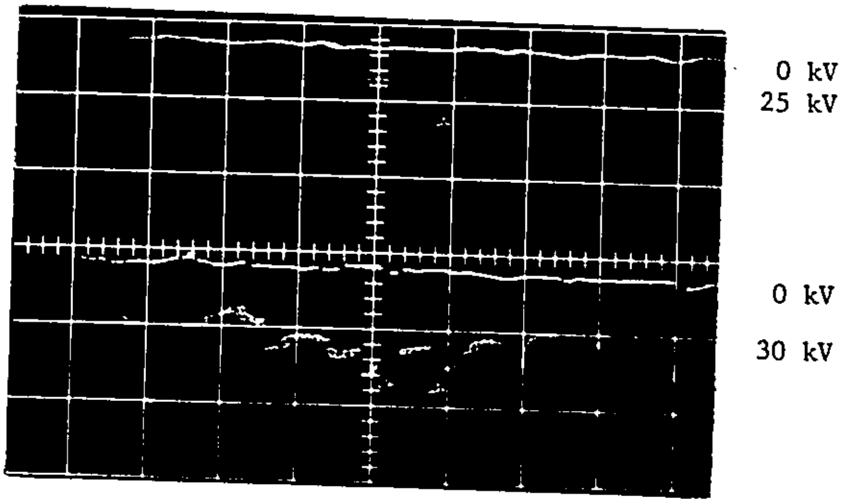

P = 100 kPa, Gap = 10 mm
1 μsec/div, 0.1 mV/div.

(h)

Figure 3.5 - Prebreakdown current and photomultiplier output waveforms for rod-plane gaps filled with SF_6. Diameter of the rod cathode is 1 mm.

(a) to (e) are the prebreakdown current waveform whereas (g) and (h) are the oscillograms of the photomultiplier output.

series of pulses or "momentary discharges" were more common at high pressures and discharge onset was usually in the form of pulses shown in figure 3.5(d). When the applied voltage was increased, the momentary discharges became more regular as shown in figure 3.5(e). This behavior continued until sustained corona occurred which was accompanied by a d.c. level of the prebreakdown current pulses. The average prebreakdown current as well as the repetition rate of the corona pulses increased with the applied voltage as shown in figure 3.5(f). This behavior of the prebreakdown current continued upto the breakdown voltage level.

The photomultiplier studies showed a good correlation between the prebreakdown current and the light emitted during the corona discharges. At the onset of a sustained discharge, the photomultiplier output was composed of small pulses irregularly spaced in time. These pulses had also different amplitude and had negligible d.c. level as shown in figure 3.5(g). An increase in the applied voltage resulted in an increase in the frequency and amplitude of these pulses. At higher voltage levels, the photomultiplier output contained a steady component in addition to the pulses as shown in figure 3.5(h). The steady component increased with the applied voltage. This behavior of the photomultiplier output continued upto the breakdown voltage level.

In SF_6, a steady glow corona was not observed in the range of pressures investigated. Though both the current and light output never reached zero values except near the discharge onset, the waveforms (e.g., figures 3.5(f) and 3.5(h)) appeared to indicate the presence of a series of pulses occurring in rapid succession, not necessarily from the same spot on the cathode. It was very difficult to resolve the nature of these pulses especially at higher voltage levels.

Visual observations of the test gap were also carried out. At the onset of steady corona discharge, faint bluish discharge filaments were seen at the tip of the rod electrode. These filaments were occurring at different points on the cathode. The length of these filaments and the cathode area covered by them increased with the applied voltage. At higher voltages, the discharge had a glow like spherical appearance at the tip of the cathode. The discharge activity spread to the cylindrical portion of the rod electrode as the applied voltage approached the breakdown level. Similar phenomenon could not be observed in the case of the pure nitrogen. The discharge in pure SF_6 was very faint at all the pressures and could not be photographed meaningfully.

When rod electrodes having diameters other than 1 mm were used, the discharge activity basically remained the same. Similarly a change in the gap length from 10 to 40 mm for rods having diameters of 1, 1.5, 2 and 3.15 mm did not produce any significant changes in the discharge behavior. An increase in the gas pressure introduced certain changes in the prebreakdown behavior of the test gaps. At higher pressures, the discharge seemed to spread laterally on the cathode surface rather than extending into the gap when the applied voltage approached the breakdown level. The gas pressure had a pronounced effect on the prebreakdown behavior when rod cathodes having diameters of 6.3 and 12.6 mm were used. At low pressures, the prebreakdown activity was similar to that observed for the 1 mm diameter cathode. As the pressure was increased, the discharge channels were shifted away from the spherical tip of the rod electrode. At still higher pressures, no prebreakdown activity of any kind was recorded prior to the breakdown of the gap. In such cases, the discharge onset directly resulted in the breakdown of the gap. The critical pressure, that is, the pressure above which no prebreakdown activity was observed, varied with diameter of the rod electrode.

3.4. The Cathode Corona in SF_6-N_2 Mixtures

Similar to the pure SF_6, the discharge onset in most of the SF_6-N_2 mixtures was in the form of isolated pulses which led to a sustained discharge when the applied voltage was increased. For mixtures having less than 10% of SF_6, the predominant type of prebreakdown current at the onset of the steady discharge was similar to the transitional pulses observed in the N_2 as shown in figure 3.6(a). Unlike pure SF_6 these pulses were quite regular in amplitude and in time separation. Their repetition rate increased with the applied voltage as shown in figure 3.6(a). With an increase in the SF_6 content of the mixture, more than one type of prebreakdown current pulses were recorded at the discharge onset. Figure 3.6(b) shows different forms of prebreakdown current pulses observed in a 20% SF_6-N_2 mixture. Although the separation between these pulses is not uniform, their amplitude is fairly regular. For mixtures having SF_6 content greater than 30%, the prebreakdown current pulses were generally similar to those observed in pure SF_6 as discussed in section 3.3. They were very irregular both in amplitude and time separation. At higher gas pressures, prebreakdown current pulses of the type shown in figure 4.6(c) and (d) were more common.

When the applied voltage was increased, the average corona current increased. Furthermore, in certain voltage ranges, steady currents like those in a glow corona could be observed for certain durations of time and were followed by pulses superimposed ~~on the~~ steady levels. This behavior was more common at low pressures such as 100 kPa and for mixtures having less than 20% SF_6. Figure 3.6(e) shows the prebreakdown current waveform for a mixture having 10% SF_6 at a total pressure of 100 kPa. Figure 3.6(f) shows the photomultiplier output under similar conditions.

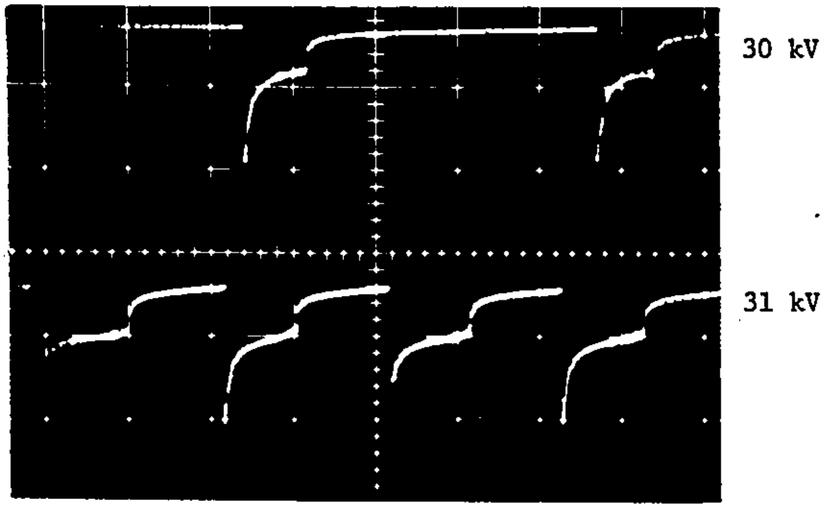

P = 300 kPa, 1.5% SF_6
20 μA/div, 0.2 msec/div.
20 mm gap, 1 mm dia.rod.

(a)

V = 23 kV, P = 200 kPa,
0.1 mA/div, 0.2 msec/div,
20% SF_6, 20 mm gap,
1 mm dia. rod.

(b)

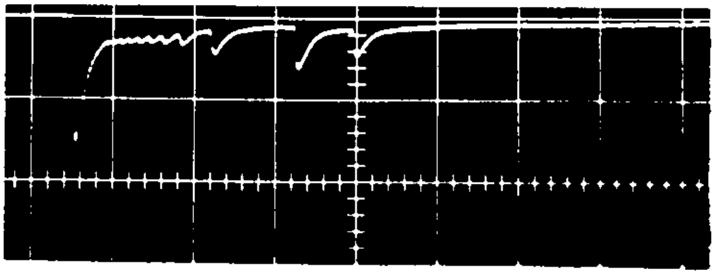

V = 30 kV, P = 400 kPa,
40 μA/div, 5 μsec/div,
0.1% SF_6, 20 mm gap,
1 mm dia. rod.

(c)

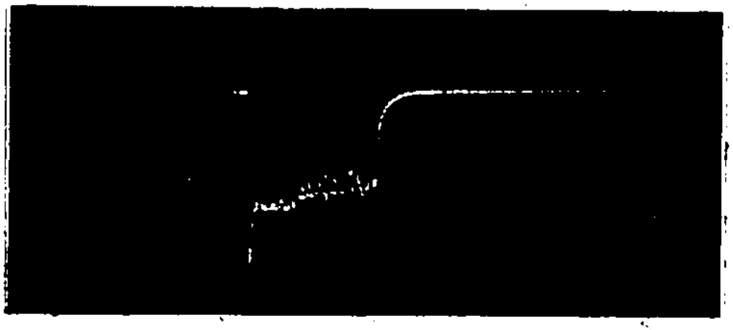

V = 52 kV, P = 500 kPa,
40 μA/div, 0.5 msec/div,
10% SF_6, 10 mm gap,
2 mm dia. rod.

(d)

Figure 3.6 (cont'd)

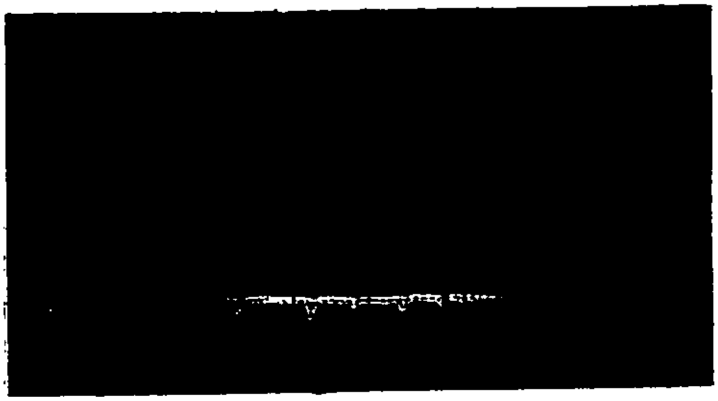

V = 76 kV, P = 100 kPa,
100 μA/div, 5 μsec/div,
10% SF_6, 40 mm gap,
1 mm dia. rod.

(e)

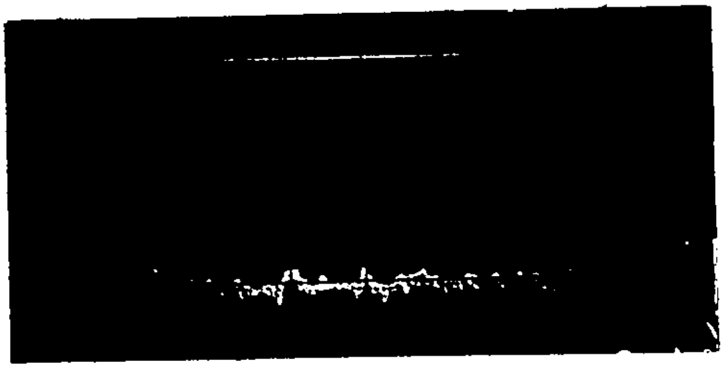

V = 76kV, P = 100 kPa,
10 mV/div, 5 μsec/div,
10% SF_6, 40 mm gap,
1 mm dia. rod. (PM output)

(f)

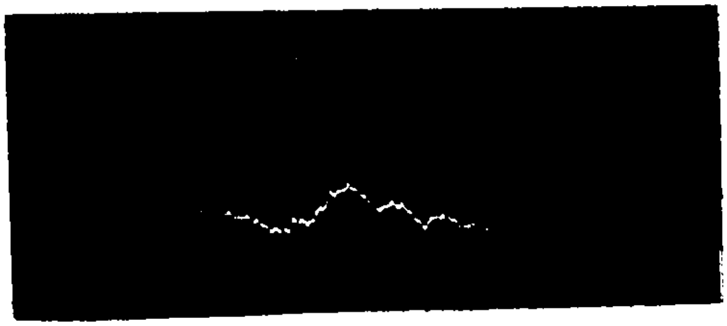

V = 155 kV, P = 300 kPa,
100 μA/div, 0.1 msec/div,
10% SF_6, 40 mm gap,
12.6 mm dia. rod.

(g)

Figure 3.6 – Prebreakdown current and photomultiplier output waveforms for negative rod-plane gaps filled with SF_6-N_2 mixtures.

(a) to (e) and (g) are the prebreakdown current waveforms whereas (f) is the oscillogram of the photomultiplier output.

In this case, both the current and photomultiplier outputs are fairly steady with relatively small pulses superimposed. For mixtures having either an SF_6 content of more than 20% or for gas pressures of ≥ 200 kPa. The prebreakdown current and the photomultiplier output appeared to be a collection of pulses in rapid succession. As the applied voltage approached the breakdown level, more and more pulses were observed superimposed on the d.c. component. These pulses were irregular in their amplitude and time separation for both the prebreakdown current and the photomultiplier outputs. This mode of corona discharge continued until a spark bridged the test gap.

There was a pressure above which no corona activity was observed prior to the breakdown in the case of 6.3 and 12.6 mm diameter rod cathrodes. This critical pressure was affected by the electrode gap configuration as well as the gas mixture ratio. These changes in the critical pressure will be discussed in detail in the next chapter.

Visual observations of the test gaps indicated that at the onset level a diffused channel appeared at the electrode tip as shown in figure 3.7(a). For mixtures having small SF_6 content, the discharge at the onset level was similar to that shown in figure 3.7(b). When the applied voltage was increased, the discharge spread on the cathode surface and extended into the gap. For 1 and 2 mm diameter rod cathodes, the discharge was very diffused and had a roughly spherical shape. The size of this glow like discharge increased with the applied voltage and ultimately the discharge spread towards the cylindrical part of the cathode. The size of the discharge was also affected by the total gas pressure and the mixture ratio as shown in figure 3.7(c) and (d). It is interesting to note that the prebreakdown current and photomultiplier output waveforms corresponding to the discharge shown in figure 3.7(c)

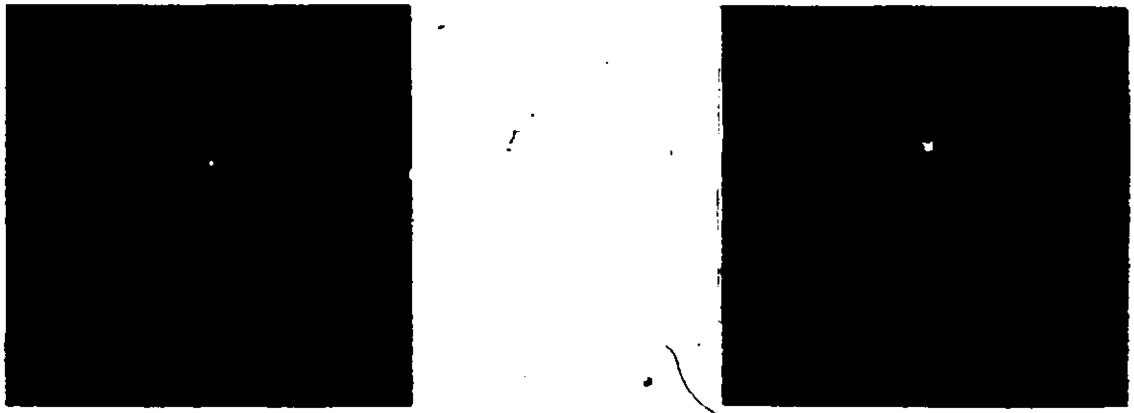

(a)

V = 50 kV, P = 100 kPa,
SF_6 = 50%, Gap = 40 mm
rod dia. = 3.16 mm
exposure time = 10 msec.

(b)

V = 16 kV, P = 100 kPa,
SF_6 = 1 %, Gap = 40 mm
rod dia. = 1 mm
exposure time = 10 msec.

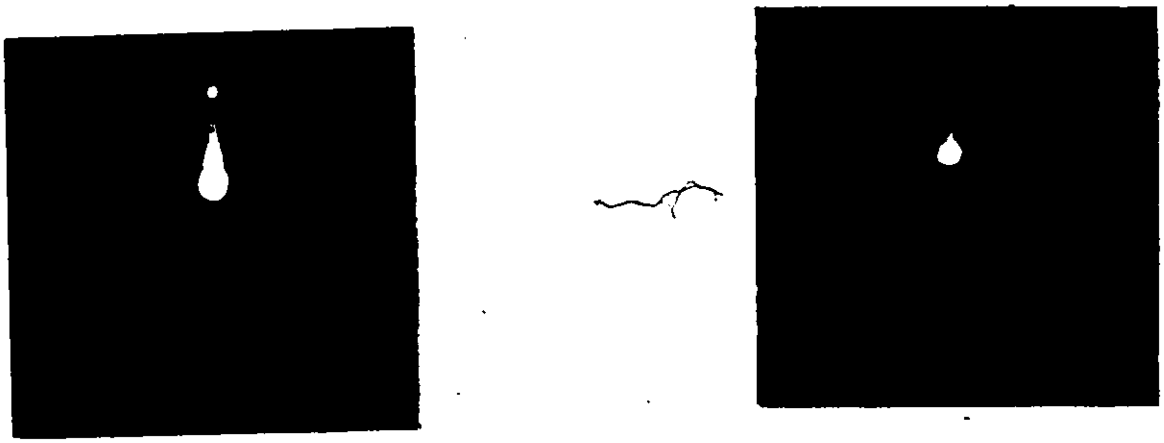

(c)

V = 76 kV, P = 100 kPa
SF_6 = 10%, Gap = 40 mm
rod dia = 1 mm
exposure time = 10 msec.

(d)

V = 90 kV, P = 100 kPa
SF_6 = 50%, Gap = 40 mm
rod dia = 1 mm
exposure time = 10 msec.

Figure 3.7 - Cathode coronas in rod-plane gaps filled with SF_6-N_2 mixtures.

contain a large steady component in addition to the pulses as shown in figure 3.6(e) and (f).

When cathodes of larger diameters were used, it was possible to observe the individual discharge filaments more clearly. Visual observations of a 12.6 mm diameter cathode indicated that the discharge was made of individual channels from the onset to the breakdown level. These channels were small in size and fewer in number at the onset level. They changed their position on the cathode surface in an irregular fashion. The number and size of these channels increased with the applied voltage as shown in figure 3.8(a) and (b) for a 30% SF_6-N_2 mixture. The number and size of these channels were also affected by the mixture ratio. Usually these were larger in size and possibly more numerous for lower SF_6 content. Figures 3.8(c) and (d) show this clearly for two different mixtures having otherwise identical conditions. The discharge appearance was also affected by the total gas pressure. It was observed that as the gas pressure increased, the surface area of the cathode covered by the discharge channels reduced gradually. At low pressures such as 100 kPa, the discharge fully covered the cathode tip and extended well into the gap. However, at higher pressures it tended to spread laterally to the cathode. At still higher pressures, the discharge materialized only on a small portion of the cathode. In such cases, the discharge channels were inclined to the axis of the rod electrode. Though the bundle of discharge channels changed its position on the cathode surface in a random fashion, their inclination to the rod axis at a particular pressure remained roughly the same. Figure 3.9(a) to (c) show the changes in discharge pattern when the total pressure of 1.5% SF_6-N_2 mixture is varied. Figure 3.9(d) to (f) show similar changes for a 10% mixture. The behavior was similar

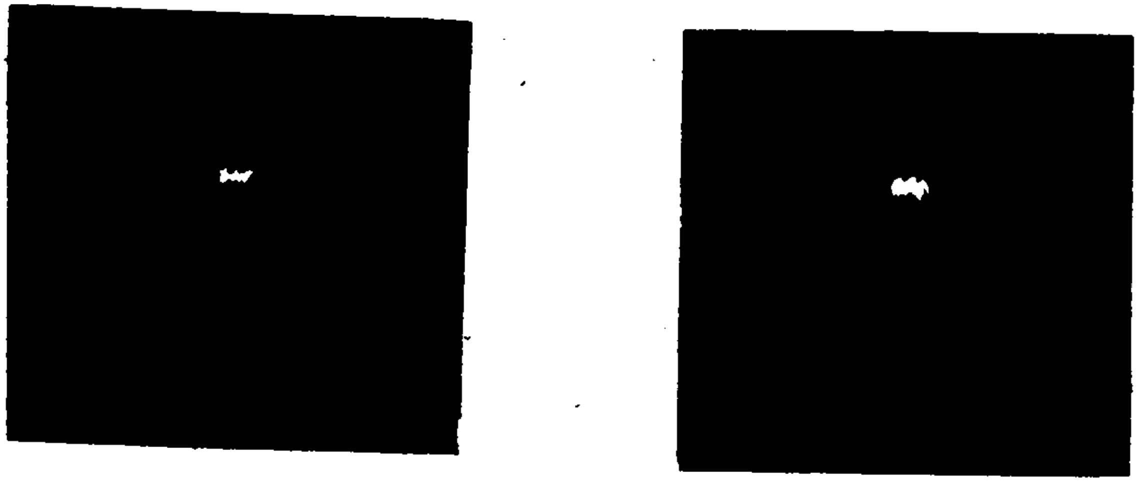

(a)

V = 90 kV, P = 100 kPa
SF_6 = 30%
gap = 40 mm
exposure time = 10 msec.

(b)

V = 100 kV, P = 100 kPa
SF_6 = 30%
gap = 40 mm
exposure time = 10 msec.

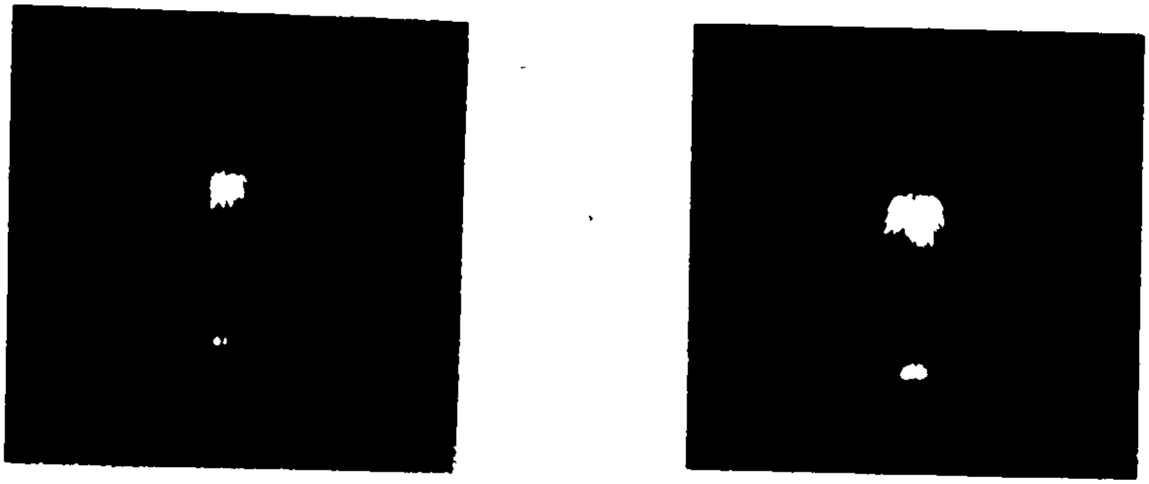

(c)

V = 86 kV, P = 100 kPa
SF_6 = 10%
gap = 40 mm
exposure time = 10 msec.

(d)

V = 86 kV, P = 100 kPa
SF_6 = 1.5%
gap = 40 mm
exposure time = 10 msec.

Figure 3.8 - Cathode coronas in rod-plane gaps filled with SF_6-N_2 mixtures. Rod dia. = 12.6 mm.

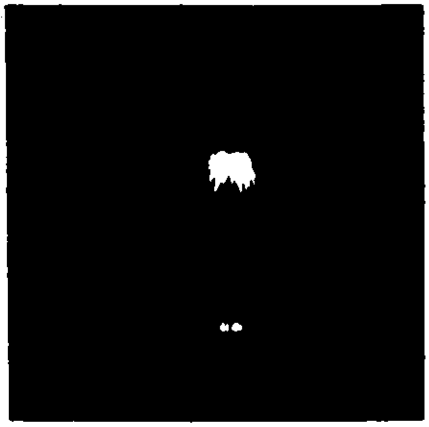

(a)

V = 82 kV, P = 100 kPa

(b)

V = 111 kV, P = 200 kPa

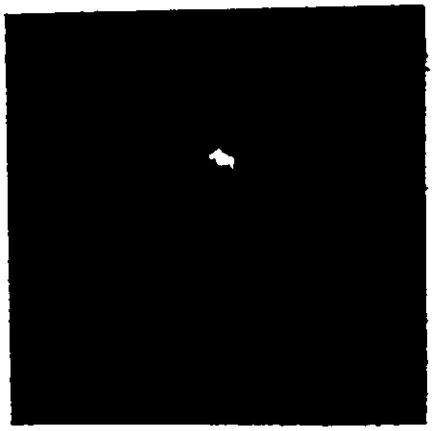

(c)

V = 141 kV, P = 335 kPa
(a-c) = 1.5% SF_6

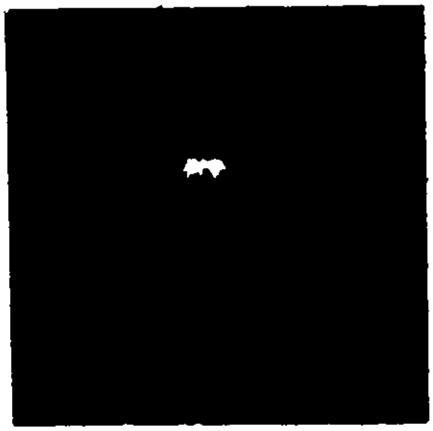

(d)

V = 46 kV, P = 60 kPa

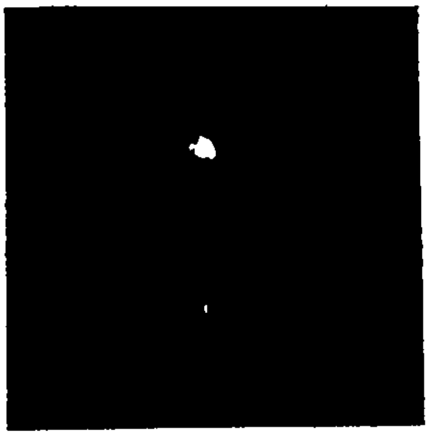

(e)

V = 128 kV, P = 200 kPa

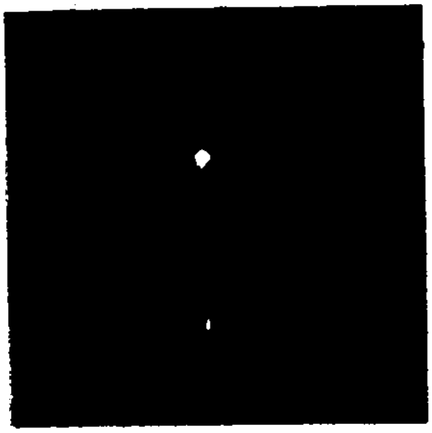

(f)

V = 155 kV, P = 300 kPa
(d-f) 10% SF_6

Figure 3.9 - Effect of pressure on cathode corona in a 40 mm gap filled with SF_6-N_2 mixtures. A 12.6 mm diameter rod cathode was used. Exposure time in all these cases is

in other mixtures as well as in pure SF_6. It is interesting to note the prebreakdown current waveform shown in figure 3.6(g) which does not contain pulses of any specific nature and appear to be due to some type of glow discharge. However, the visual appearance of discharge producing this current is made of individual filaments as shown in figure 3.9(f).

The brush-like discharges shown in figures 3.8 and 3.9 were observed in all the mixtures, even those containing 0.02% of SF_6. However, this type of discharge could not be observed in pure nitrogen. In nitrogen, the photons emitted at the cathode tip during corona discharge had enough intensity and meanfree paths that the plane anode as well as the chamber walls could be visually observed. Figure 3.10 shows the corona discharges in pure N_2 and in an SF_6-N_2 mixture having 0.05% SF_6. It is interesting to note that for the gap under discussion, the breakdown voltage of pure N_2 was practically the same as the corona onset voltage where as for 0.05% mixture, the breakdown voltage was more than double the corona inception voltage.

3.5. Corona Onset Levels in SF_6-N_2 Mixtures

As discussed in the previous section, the corona onset was in the form of isolated random pulses. When the applied voltage was increased, sustained discharge occurred. Usually the onset level for the single pulse corona activity was a few kV lower than the one at which the steady discharge appeared. The difference between the two levels increased with gas pressure, field uniformity and SF_6 content in the gas mixture. In this section the inception level for isolated pulse activity will be discussed. This is the minimum voltage at which discharge appears.

The corona onset voltage varied with the gas pressure, mixture ratio, gap length and the diameter of the rod electrode. Figure 3.11

(a)

V = 35 kV, P = 100 kPa
gas = nitrogen
exposure = 10 msec
gap = 40 mm
rod dia. = 12.6 mm

(b)

V = 80 kV, P = 100 kPa
SF_6 = 0.05%
exposure = 10 msec
gap = 40 mm
rod dia. = 12.6 mm

Figure 3.10 - Cathode corona in nitrogen and an SF_6-N_2 mixture containing 0.05% SF_6.

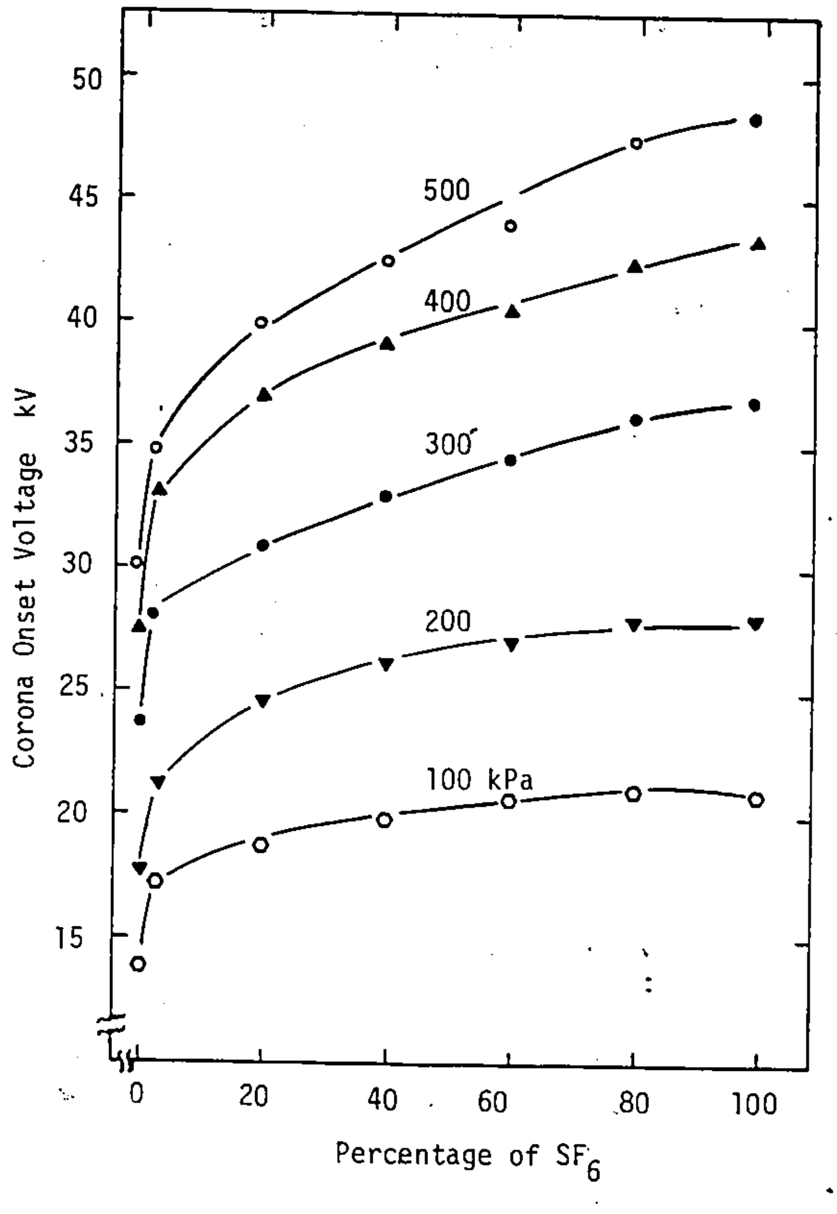

Figure 3.11 - Effect of gas pressure and mixture ratio on the corona onset voltage of a 20 mm rod-plane gap using 1 mm diameter cathode.

shows the variations in the onset voltage when the mixture ratio and gas pressure are changed using a 20 mm negative rod-plane gap and 1 mm diameter rod. Here it is seen that when the first few percents of SF_6 are added to N_2, the onset voltage increases significantly. However, a further increase of SF_6 content in the mixture does not result in a similar increase and the beneficial influence of SF_6 on the onset voltage of the SF_6-N_2 mixtures saturates at a fairly low SF_6 content. This behavior is very similar to the uniform field breakdown characteristics of SF_6-N_2 mixtures [10] which can be explained on the basis of the streamer breakdown criterion [6] and will be discussed in detail in chapter VII. The onset voltages for other gaps and rod cathodes having different diameters behaved similar to that of the 1 mm diameter rod. These levels increased with the field uniformity of the gap achieved by using larger diameters rod electrodes. The voltage levels at which the discharge extinction took place were always somewhat lower than the corresponding onset levels.

3.6. Prebreakdown Current Levels in SF_6-N_2 Mixtures

The prebreakdown currents showed variations with the applied voltage, gas pressure, mixture ratio, gap length and the diameter of the rod electrodes. Figure 3.12 shows the variations in the steady component of the prebreakdown current when the gap voltage and mixture ratio are changed. The measurements were carried out in a 20 mm rod-plane gap using a 1 mm diameter rod cathode at a total pressure of 300 kPa. Figure 3.13 shows the prebreakdown current as a function of the gas pressure and the applied voltage for a 10% SF_6-N_2 mixture.

When rods other than 1 mm in diameter and gap separations other than 20 mm were used, the variations in the prebreakdown current with gas

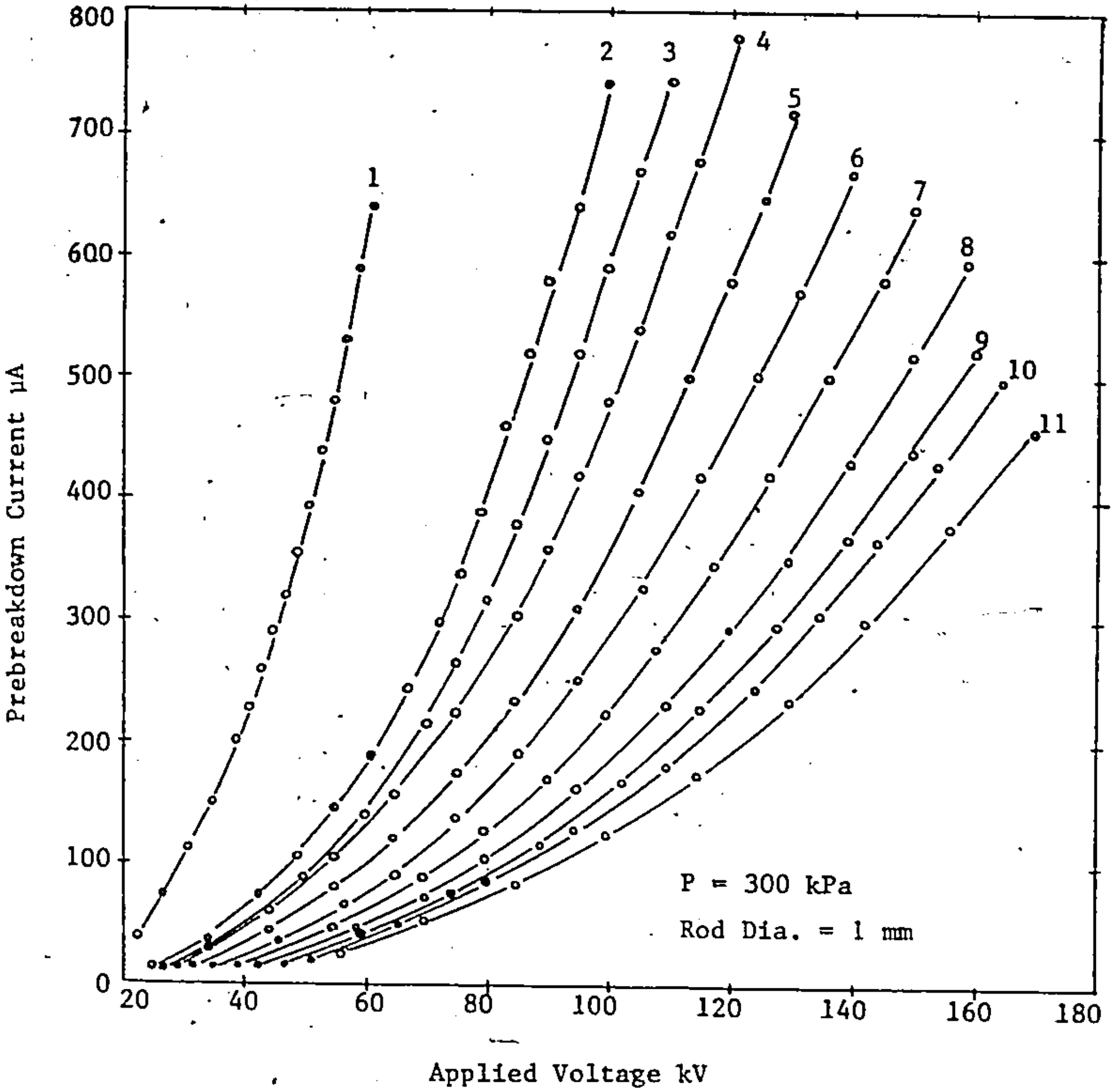

Figure 3.12 - Prebreakdown current in a 20 mm rod-plane gap as a function of the applied voltage and the mixture ratio. Ratios indicated on the diagram are (percentage of SF_6 in N_2).
(1) = 0%; (2) = 3.75%; (3) = 10%; (4) = 20%; (5) = 30%; (6) = 40%; (7) = 50 % ; (8) = 60%; (9) = 70%; (10) = 80%; (11) = 100%.

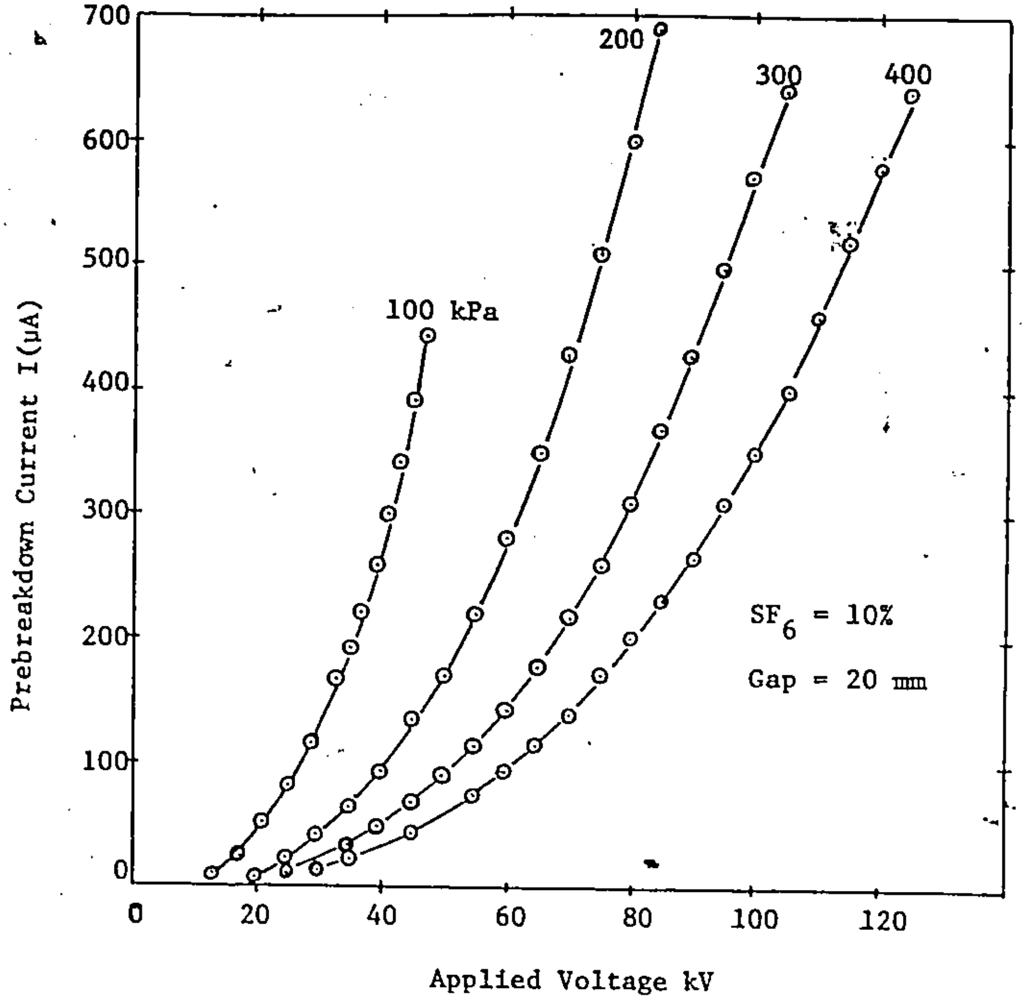

Figure 3.13 - Prebreakdown current in a rod-plane gap as a function of the applied voltage and the gas pressure.

pressure, mixture ratio and the applied voltage were similar to those shown in figures 3.12 and 3.13. Although the prebreakdown currents for a given electrode system and applied voltage were significantly different for different mixtures, the magnitude of the currents prior to breakdown did not change much with the mixture ratio. These currents exhibited a peak value for a certain mixture ratio as shown in figure 3.14. The gas mixture ratios for which maximum prebreakdown currents were observed were a function of the gas pressure.

The steady component of the prebreakdown current I is plotted as a function of the parameter $V[V-V_o]$ for SF_6 and several mixtures in figure 3.15. Here V is the applied voltage and V_o is the corona onset level. From the figure, one can express the voltage-current characteristics for SF_6 and SF_6-N_2 mixtures as

$$I = CV\,[V - V_o] \qquad (3.1)$$

where C is a constant which depends on the effective mobility of the charge carriers and is therefore affected by the gap length, rod diameter, gas pressure and the mixture ratio. This behavior of the prebreakdown current is typical for coronas in which field at the highly stressed electrode is limited by the space charge [9]. Values of the constant C were obtained for various mixtures at different pressures. Variations in the value of C with the mixture ratio are given in figure 3.16 for a 20 mm gap using 1 mm diameter rod cathode at a total gas pressure of 300 kPa. Figure 3.17 shows similar variations with the gas pressure for a mixture having 10% SF_6.

Since the constant C is a measure of the effective mobility of the charge carriers, the rapid decrease in the value of C with the addition of the first few parts percent of SF_6 indicates that most of the free

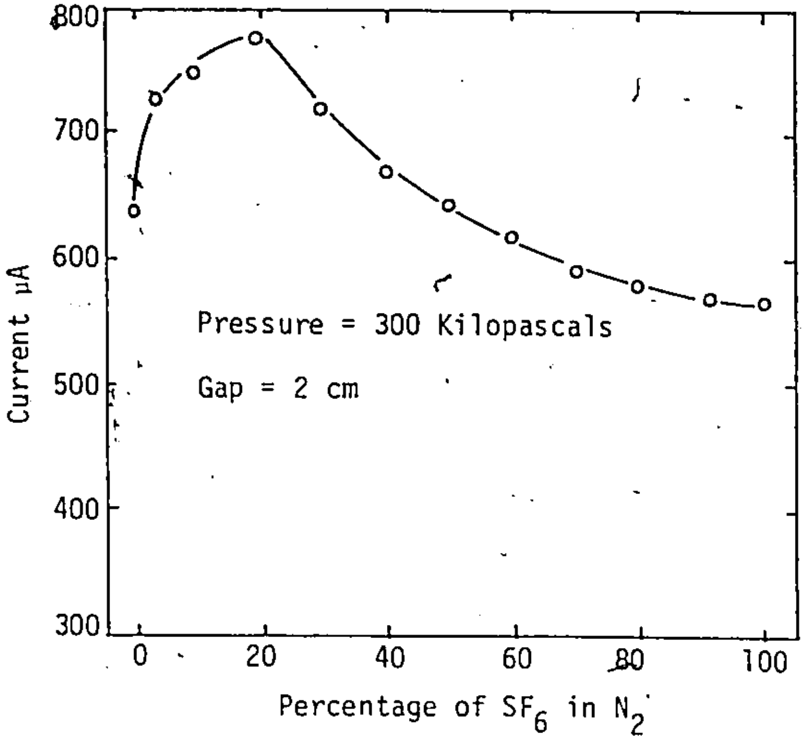

Figure 3.14 – Variations in the corona current prior to breakdown with gas mixture ratio.

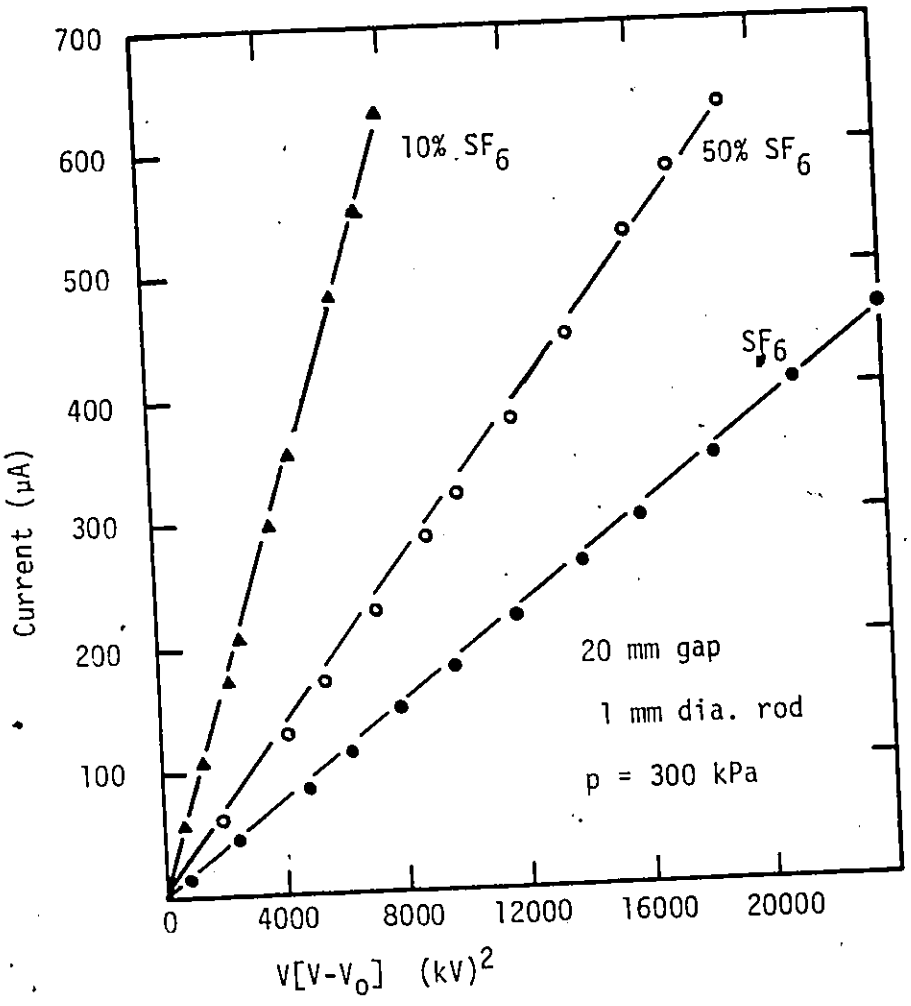

Figure 3.15 – Variation of the prebreakdown current with the parameter V[V-V$_o$] for a rod-plane gap filled with SF_6-N_2 mixtures.

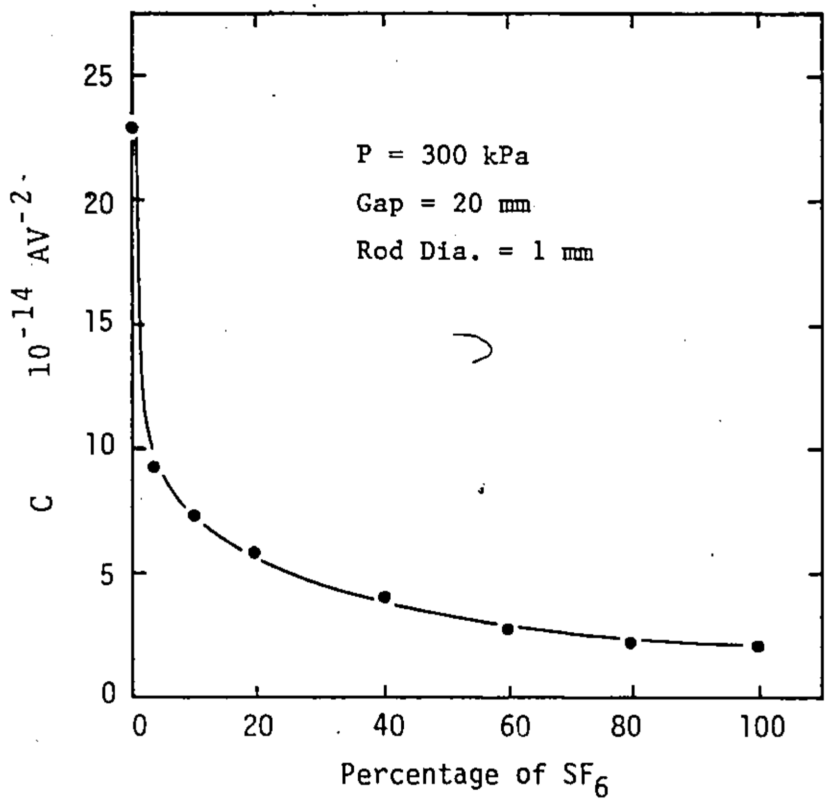

Figure 3.16 - Variation of the constant C with gas mixture ratio.

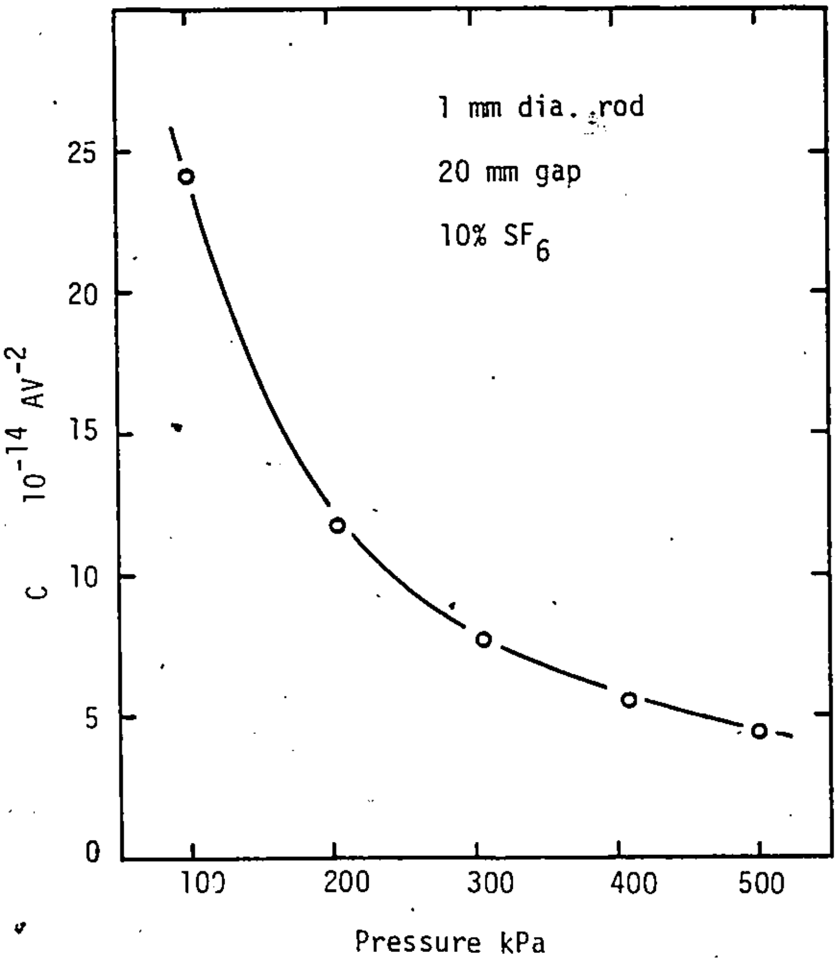

Figure 3.17 - Variation of the constant C with total gas pressure.

electrons are attached to the SF_6 gas molecules forming heavy negative ions with much reduced mobility. However, any further addition of SF_6 has a modest effect on the negative ion population and therefore the value of C does not change appreciably when SF_6 content is increased from about 10 to 100%. As mentioned earlier,since the constant C is a measure of the effective mobility, it should be inversely proportional to the gas pressure. In other words, the magnitude of the product of the gas pressure and the constant C should be independent of the gas pressure. From figure 3.18, it is clear that although, this product is slightly affected by the total gas pressure, it can be considered to be independent of the pressure.

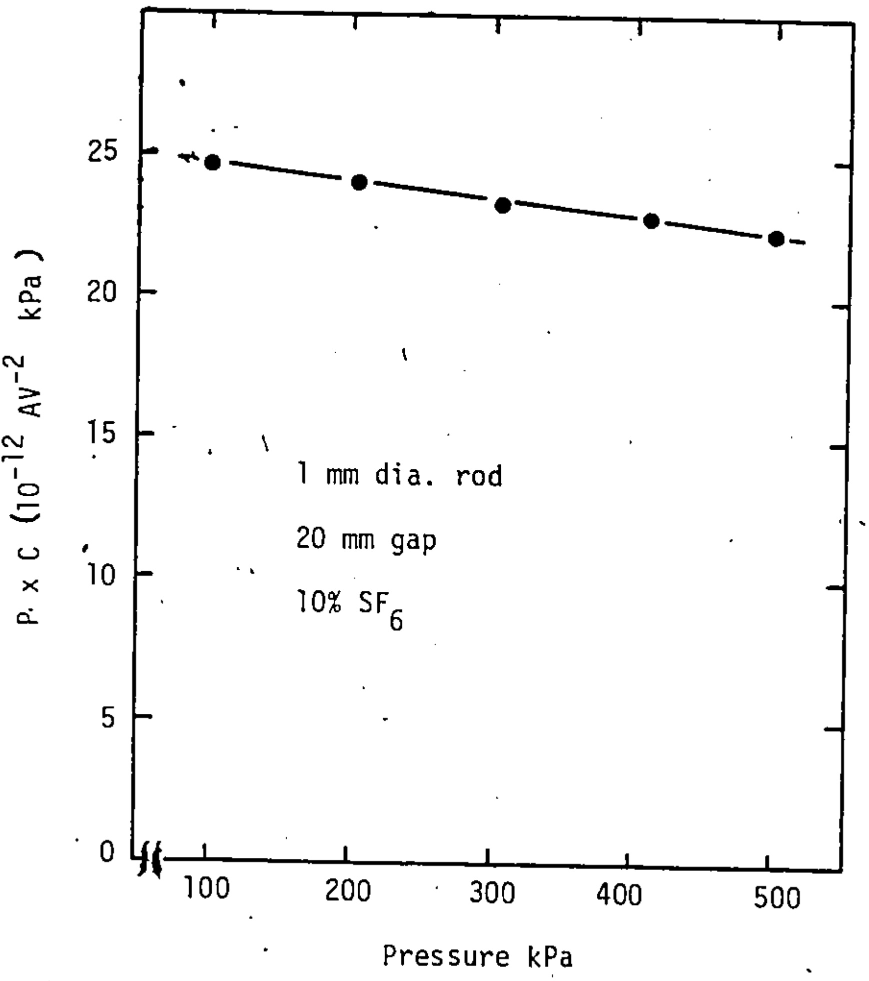

Figure 3.18 - Influence of total gas pressure on the product PC for a 10% SF_6-N_2 mixture

CHAPTER IV

BREAKDOWN STUDIES OF THE NEGATIVE ROD-PLANE GAPS

4.1. Breakdown Behavior of SF_6 and SF_6-N_2 Mixtures

Breakdown voltages for a 20 mm negative rod plane gap using 1 mm diameter rod electrode were measured for SF_6-N_2 mixtures in the pressure range of 100 to 500 kPa. Figure 4.1 shows the breakdown voltage as a function of gas pressure for SF_6, N_2 and 0.1% SF_6-N_2 mixture. For comparison the corona onset levels are also included in this figure. The breakdown voltage of SF_6 increases almost linearly with pressure in the range of 100 to 300 kPa. However the effect of gas pressure on the breakdown voltage is reduced as the gas pressure increases above 300 kPa. There is no peak in the breakdown voltage-pressure characteristics of SF_6, N_2 or 0.1% SF_6-N_2 mixture in the pressure range of 100 to 500 kPa. The difference between the onset and the breakdown voltages for a particular gas pressure is the highest for SF_6 and the lowest for N_2. Furthermore, the saturation of the breakdown voltage due to increasing pressure is less pronounced in N_2 and 0.1% mixture as compared to pure SF_6.

It is interesting to note that in figure 4.1, the breakdown voltage of N_2 is roughly 25% that of SF_6. However, an addition of 0.1% of SF_6 increases this level to about 50% that of pure SF_6. Besides the 0.1% mixture, other mixtures containing 0.05%, 0.18% and 1.5% of SF_6 were also investigated. The breakdown voltage-pressure characteristics of these and other mixtures studied were similar to that of pure SF_6. However, the breakdown levels of different mixtures were affected by the SF_6 content of the mixtures. The breakdown voltages of mixtures having low SF_6

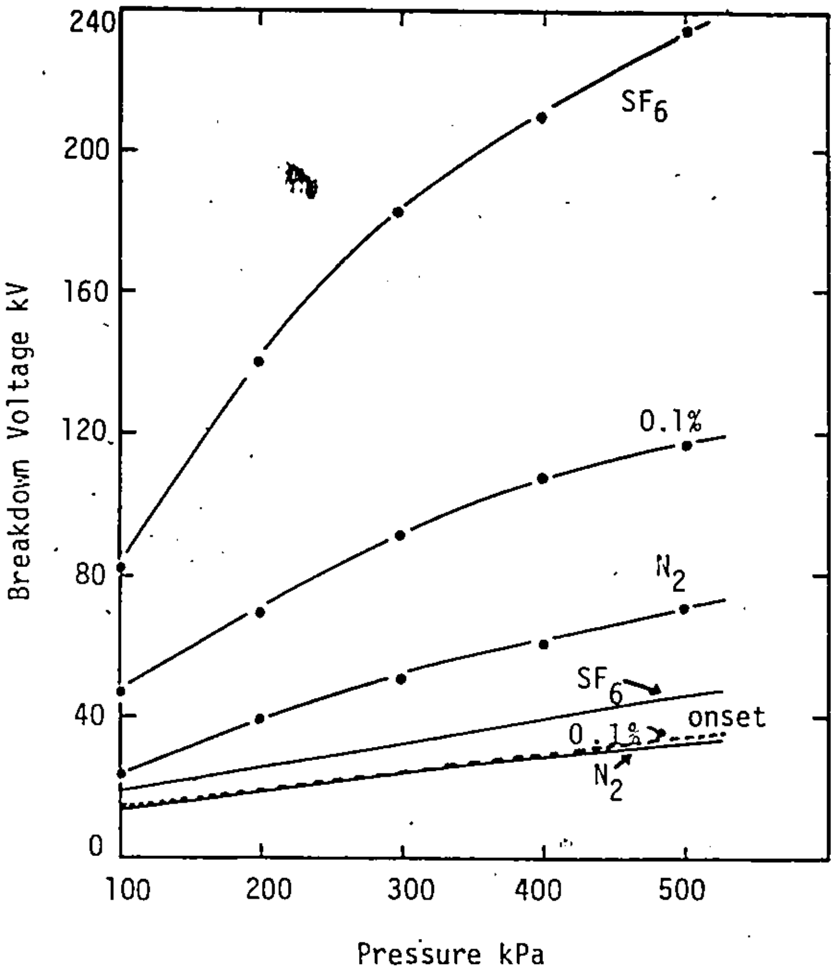

Figure 4.1 - Breakdown voltage-pressure characteristics of SF_6, N_2 and 0.1% mixture for a 20 mm rod-plane gap using 1 mm diameter cathode.

content are plotted in figure 4.2 as a function of the SF_6 content. The highest increase in the breakdown voltage is exhibited by mixtures with only minute traces of SF_6 and any further addition of SF_6 produces less dramatic effects. Figure 4.3 shows the breakdown voltages for mixtures having SF_6 content between 1.5 to 100%. A mixture containing about 5% SF_6 has a breakdown level which is about 65% that of pure SF_6. However, a further increase of the SF_6 component does not result in such a rapid increase in the breakdown strength and the breakdown voltage of a 50% mixtures is about 80% that of pure SF_6. Thus the beneficial influence of adding SF_6 on the breakdown properties of N_2 saturates at low SF_6 contents. Since SF_6 has a very high attachment cross-section at low energies of 0 to 0.4 eV, it appears that a modest amount of SF_6 added to N_2 could attach most of the low energy electrons resulting in an appreciable increase in the breakdown strength and any further addition of SF_6 has relatively little effect on the dielectric behavior of the mixture [10]. This is clearly evident in figures 3.11, 3.12, 3.16, 4.1, 4.2 and 4.3.

For 1 mm rod, in SF_6, N_2 and their mixtures, breakdown occurred in the presence of corona discharges. The difference between the corona onset and the breakdown levels was much higher in SF_6 and its mixtures than in pure N_2. For example, in figure 4.1, the corona onset level of the 0.1% mixture and N_2 are practically the same. However, the breakdown voltages of the 0.1% mixture are about 50% higher than those of pure N_2. The reason for this behavior is the fact that in mixtures containing SF_6, negative ions are formed readily. Despite the increase in the applied voltage, the electric field in most of the interelectrode gap region is stabilized by a negative ion space charge. This space charge is continuously generated as a result of corona discharges in the highest field

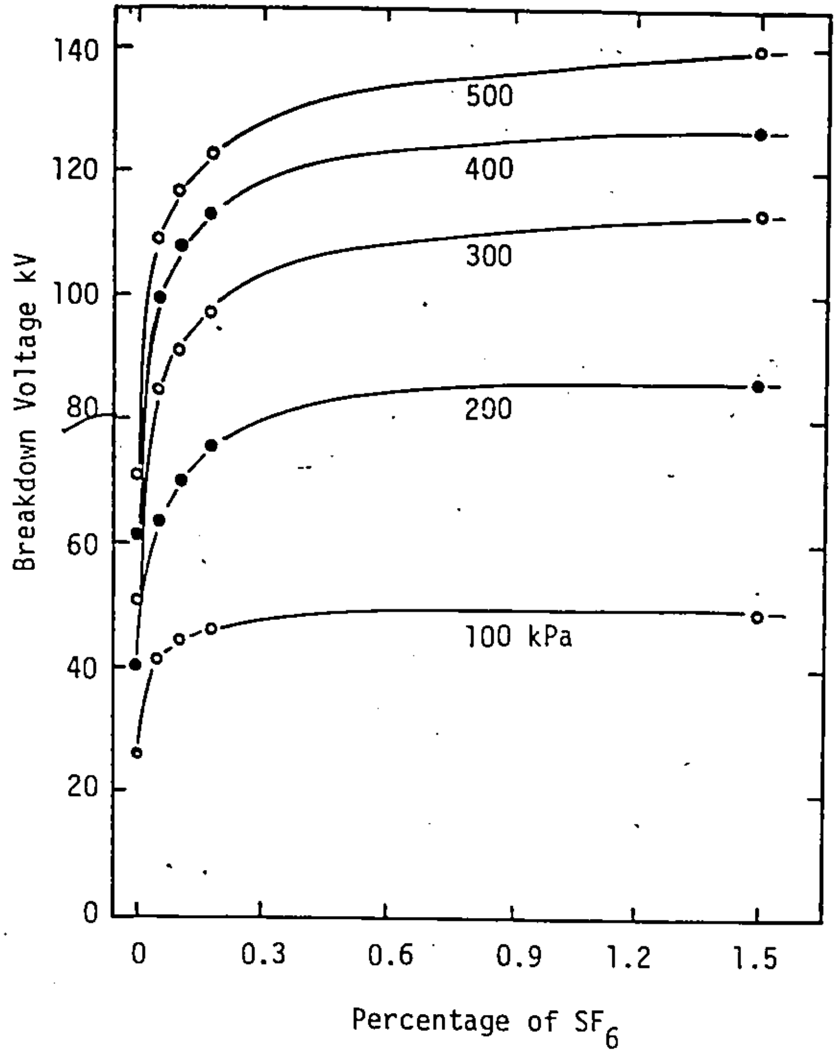

Figure 4.2 - Breakdown voltage-mixture ratio characteristics of a 20 mm rod-plane gap for mixtures having low SF_6 content. Diameter of the rod cathode is 1 mm.

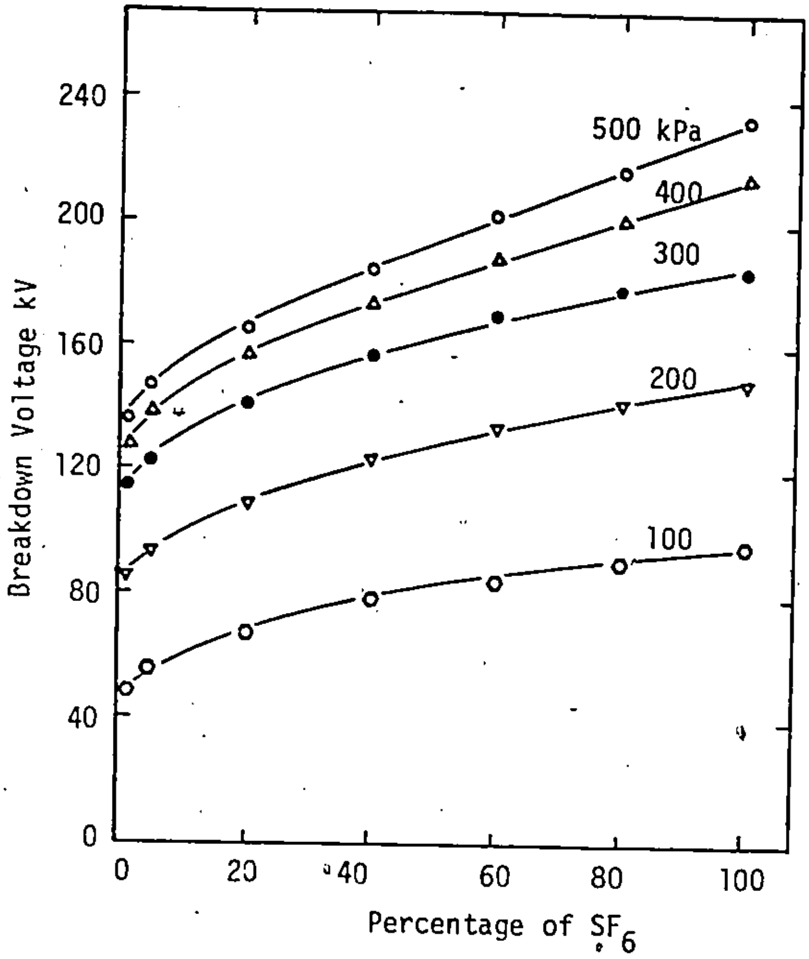

Figure 4.3 - Breakdown voltage-mixture ratio curve for a 20 mm negative rod-plane gap using 1 mm diameter rod electrode.

region. On the contrary, in pure N_2, negative ions are not formed and therefore the field increases as the applied voltage is increased. This results in increased ionization and therefore the breakdown streamers can propagate and bridge the gap at relatively lower applied voltages.

Spark channels were also monitored in this study. In the pressure range investigated the spark paths were almost straight in the case of pure N_2. However, in both SF_6 and its mixtures with N_2, the spark channels were affected by the total gas pressure. Figure 4.4 shows the general pattern of the spark trajectories in pure SF_6. The behavior in SF_6-N_2 mixtures was similar to that of pure SF_6. A look at figures 4.1 and 4.4 indicates that the spark paths are straight in the pressure region where the breakdown voltage increases linearly with the pressure. Above this pressure, however, the sparks do not follow the shortest interelectrode path available. It appears that the negative ion space charge in the interelectrode gap region inhibits the propagation of breakdown streamers along this path. This effect increases with pressure, most probably due to the increasing space charge density resulting from reduced diffusion at high pressures. Therefore, at high pressures, the breakdown streamers are more curved. Since in N_2, there is no negative ion space charge to inhibit the streamer growth, the discharge paths are straight.

4.2. The Effect of Field Uniformity on the Breakdown Behavior of SF_6.

Measurements of the breakdown and corona onset voltages were carried out in SF_6 insulated gaps using rod electrodes of various diameters. Fig.4.5 shows the breakdown voltage as a function of gas pressure for a 20 mm gap for different rod electrodes. Corona onset levels are shown using

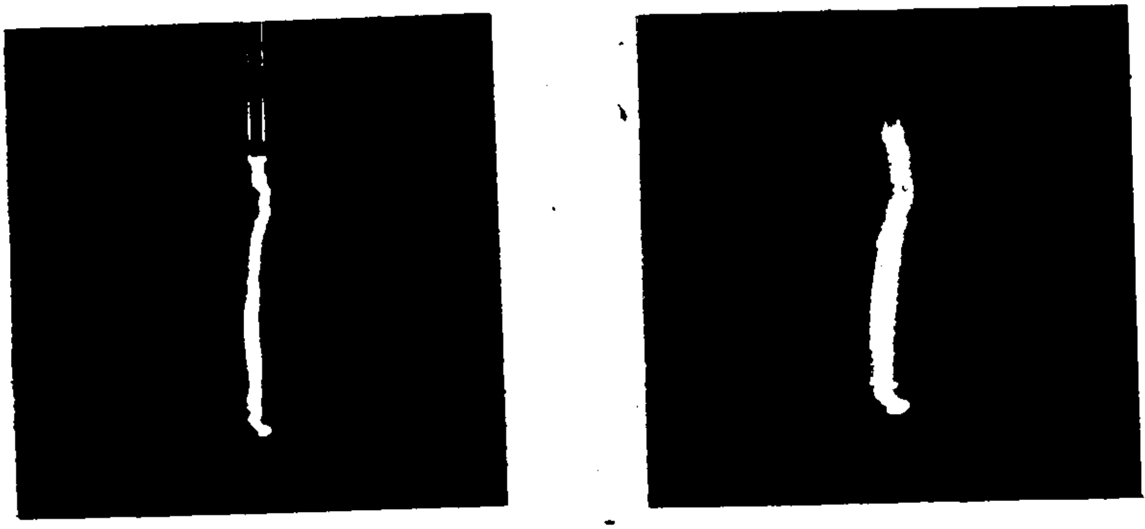

V = 81 kV, p = 100 kPa

V = 145 kV, P = 200 kPa

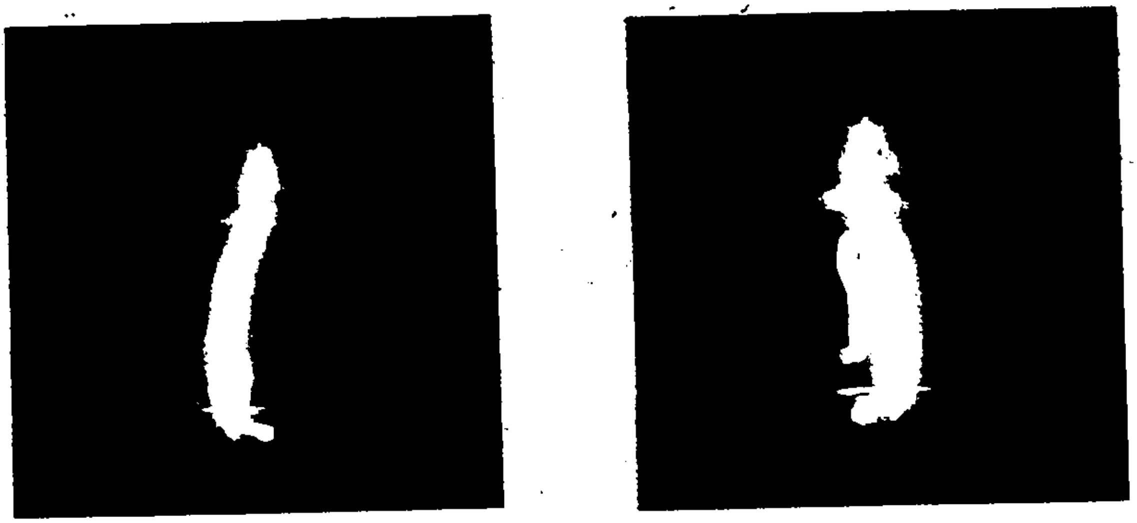

V = 181 kV, P = 300 kPa

V = 210 kV, P = 400 kPa

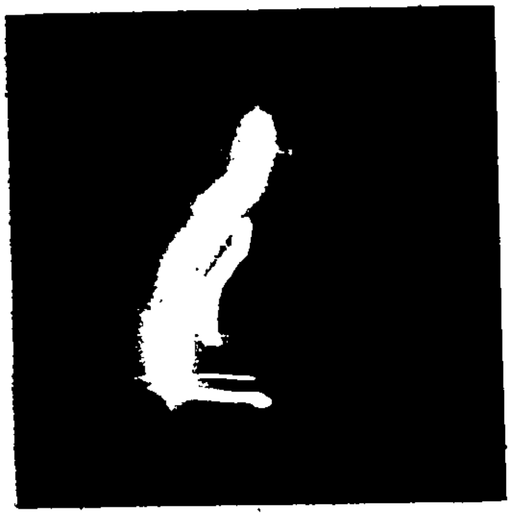

V = 236 kV, P = 500 kPa

Figure 4.4 - Spark trajectories in a 20 mm negative rod-plane gap filled with SF_6. Rod dia. = 1 mm.

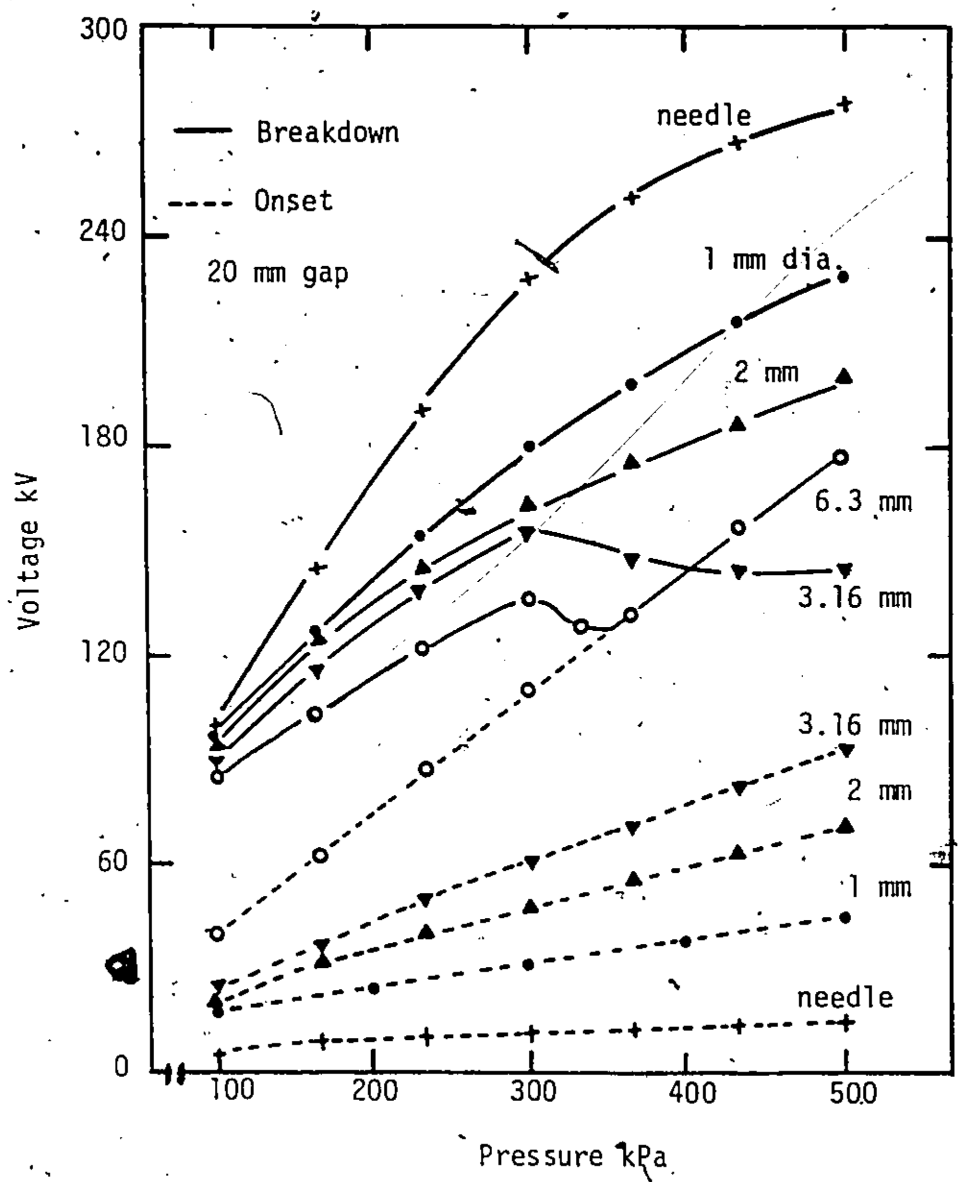

Figure 4.5 - Influence of the rod diameter and gas pressure on the breakdown behavior of negative rod-plane gaps filled with SF_6.

broken lines in the same figure. It is interesting to note that while corona onset voltages for different cathodes increase almost linearly with pressure, the same is not true for the breakdown voltages. Although these increase with gas pressure for the needle electrode (figure 2.2) and for 1 and 2 mm diameter electrodes, this is not the case for the 3.16 and the 6.3 mm diameter cathodes. For the 3.16 mm cathode, the breakdown voltage increases with pressure upto about 300 kPa. A further increase in the pressure results in an actual drop in the breakdown voltage. For the 6.3 mm cathode , the behavior is even more interesting. In this case, the breakdown voltage increases with pressure upto about 300 kPa. From 300 to 350 kPa, the breakdown voltage decreases. Above this pressure, it remains roughly constant over a small pressure region followed by an almost linear increase with pressure. The breakdown and corona onset levels coincide in this latter pressure range in which the discharge inception leads to the breakdown of the test gap. In general, the breakdown behavior of a 20 mm gap using 12.6 mm rod was similar to that of 6.3 mm rod electrode . Also the critical pressure P_c, the pressure above which the corona onset and breakdown levels are the same, was lower for the 12.6 mm diameter rod. Thus for rods having diameters of 6.3 mm and 12.6 mm, the breakdown is not always corona stabilized and there is a pressure above which the discharge directly leads to the breakdown. This critical pressure is affected by the diameter of the cathode and increases when diameter of the cathode is reduced. The peak in the breakdown voltage for the 3.16 mm rod in figure 4.5 suggests that the behavior of gaps using small diameter electrodes is similar to that observed using a 6.3 mm diameter rod electrode. However, the critical pressure for all these cases seems to be higher than 500 kPa which was beyond the experimental capabilities.

It is interesting to note that in figure 4.5, the breakdown voltage decreases with increasing rod diameters in the pressure regions where breakdown is corona stabilized. However, the behavior of corona onset voltages is exactly opposite and the higher breakdown levels of the gaps with smaller diameter cathodes are accompanied by the lower corona onset levels. Furthermore, in the highly non-uniform field gaps using smaller diameter rods, the prebreakdown current prior to the breakdown is extremely high. The magnitude of this current was so high in the case of the needle electrode that at pressures ≥ 300 kPa, the high voltage generator could not supply enough prebreakdown current. The low onset levels for extremely non-uniform field gaps are not surprising. However, the higher breakdown levels for such gaps need explanation. This will be discussed at a later stage (chapter VIII).

The discharge characteristics of SF_6 were also investigated using the same rod cathodes and varying gap lengths. Figure 4.6 shows the effect of gap length on the discharge characteristics using a 12.6 mm rod electrode. The breakdown voltage for the 40 mm gap is substantially higher than the onset level due to more effective corona stabilization in the more non-uniform field gaps. The increase in the onset voltage is greater when the gap is changed from 20 to 30 mm than when it is increased from 30 to 40 mm. This behavior of the corona onset voltage is very common in rod-plane gaps and can be explained on the basis of the streamer breakdown criterion [6]. It will be dealt with in more detail in chapter VII. It is also interesting to note that the critical pressure primarily depends on the radius of the cathode rather than the gap length for the non-uniform field gaps.

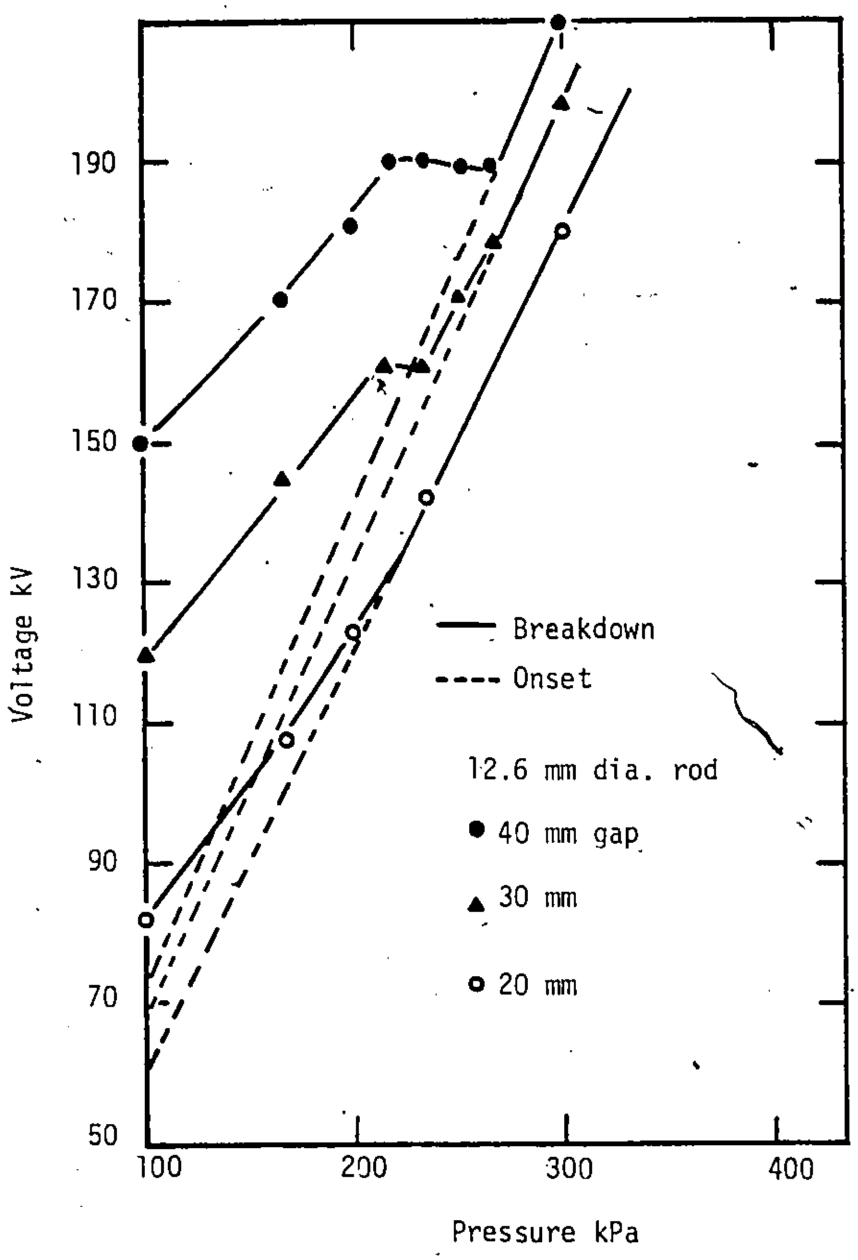

Figure 4.6 - Influence of the gap length and the gas pressure on the breakdown behavior of negative rod-plane gaps filled with SF_6.

4.3. The Effect of Field Configuration on the Breakdown Behavior of SF_6-N_2 Mixtures.

The behavior of the breakdown voltage as a function of the gas pressure and the mixture ratio for the needle electrode and the 2 mm rod electrode were similar to that of the 1 mm rod discussed in section 4.1. However, when electrodes of 6.3 and 12.6 mm diameter were used, the breakdown voltage-pressure characteristics of SF_6-N_2 mixtures showed a peak similar to that of pure SF_6. Also there was a pressure region in which breakdown occurred in the absence of any corona discharges.

Figure 4.7 shows the breakdown voltage-pressure characteristics for a 40 mm gap using 12.6 mm diameter rod and 10% SF_6-N_2 mixture. The breakdown behavior of the same gap when insulated with pure N_2 is also included in the figure. In nitrogen, the breakdown occurred in the absence of any significant corona discharges and the onset voltage was practically the same as the breakdown voltage. As seen in figure 4.7, the general breakdown behavior of the 10% SF_6-N_2 mixture is similar to that of pure SF_6. However, the critical pressure is different in the two cases. This pressure varied with the mixture ratio and the rod diameter. Figure 4.8 shows the variations in the critical pressure when the mixture composition is varied for the two gaps shown in the figure. In both cases, it is obvious that the critical pressure is practically constant for mixtures having SF_6 content $\geq$ 50%. However, for mixtures having SF_6 content below 50%, the critical pressure increases when the SF_6 component in the mixture is reduced.

Since the critical pressure of an SF_6-N_2 mixture depends on the percentage of SF_6, the breakdown voltage-mixture ratio characteristics are affected by the total gas pressure. Figure 4.9 shows the effect of gas

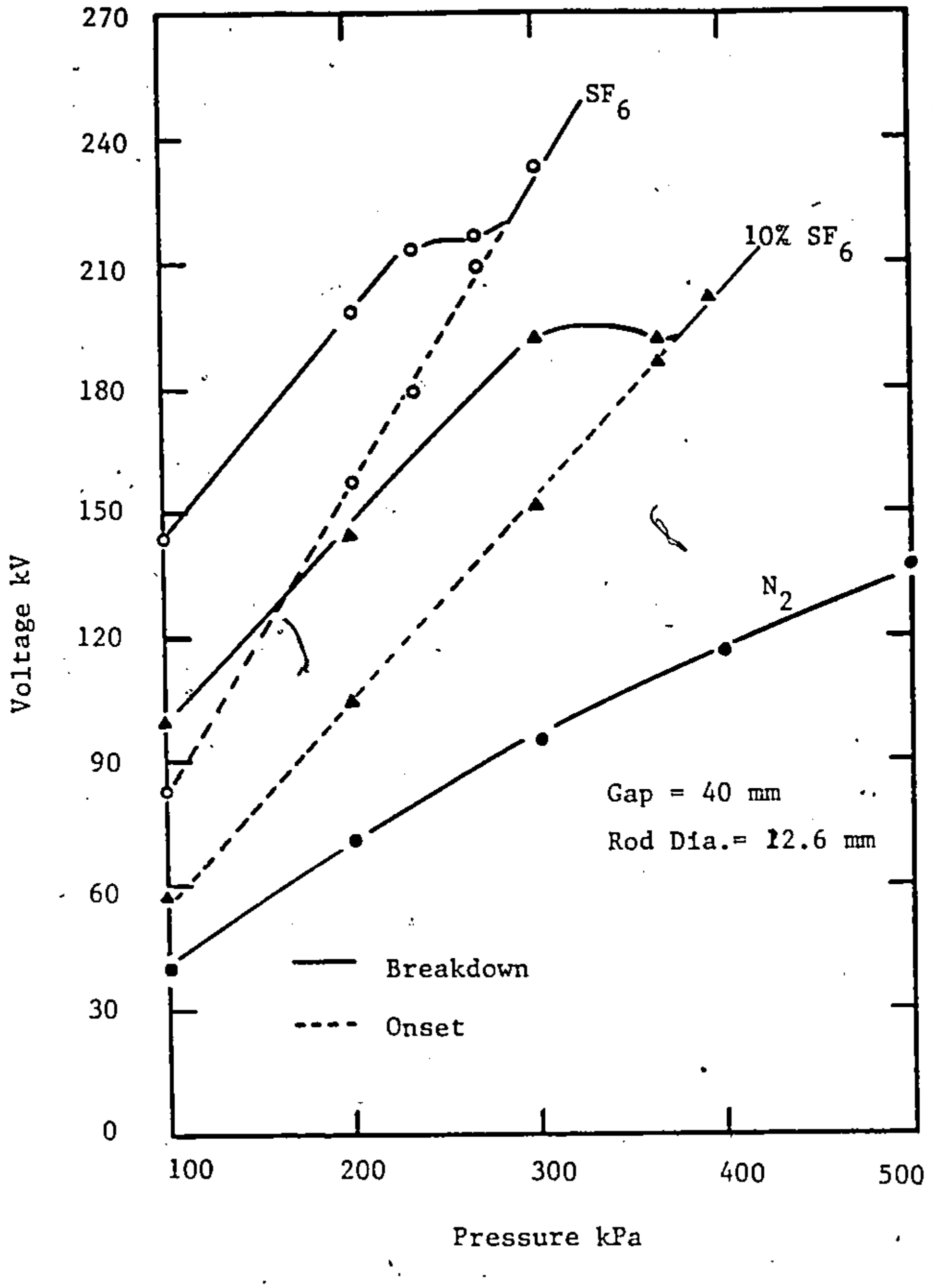

Figure 4.7 - Breakdown voltage-pressure characteristics of SF_6, N_2 and 10% SF_6-N_2 mixture for a negative rod-plane gap.

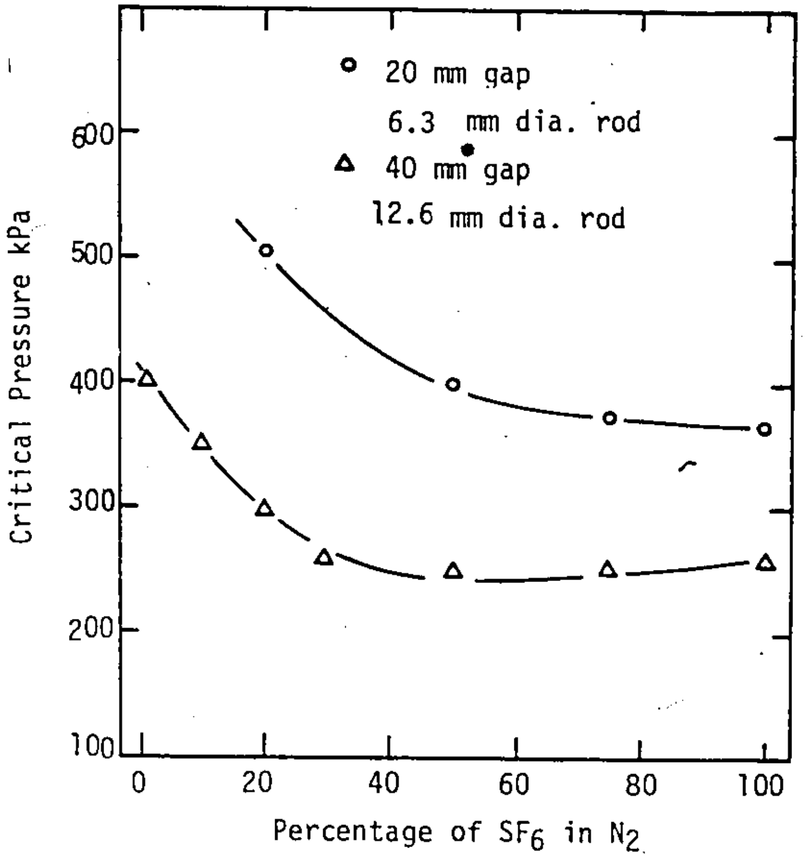

Figure 4.8 - Influence of the mixture ratio on the critical pressure for negative rod-plane gaps.

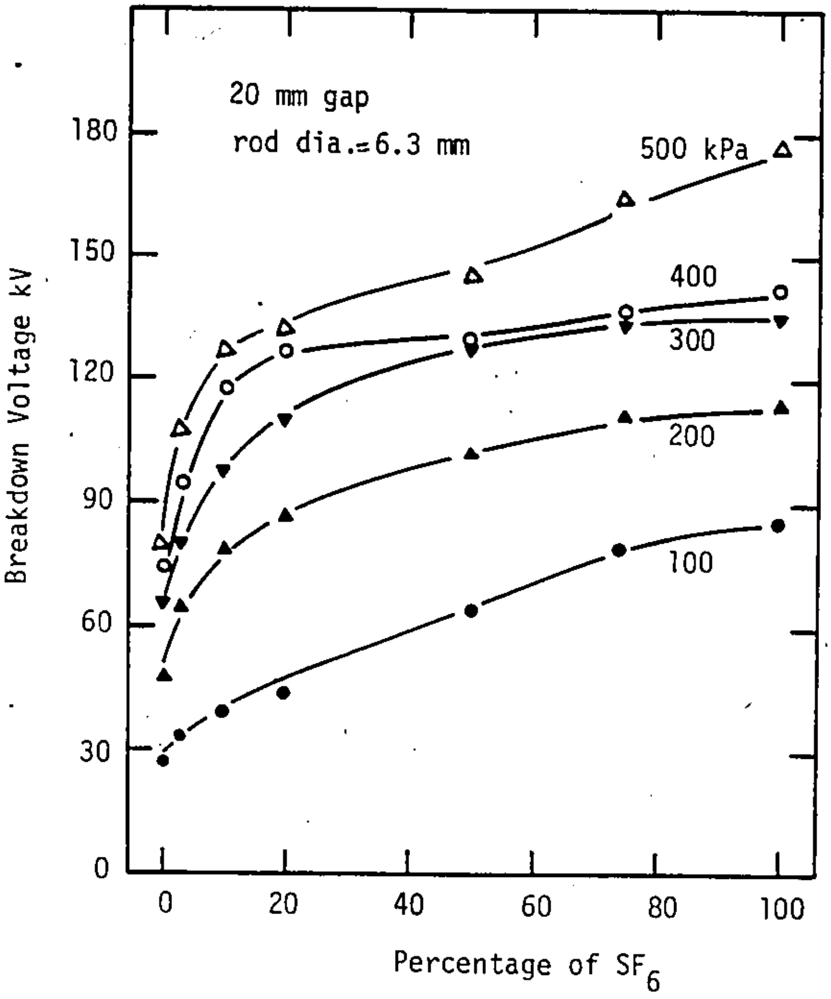

Figure 4.9 - Breakdown voltage as a function of gas pressure and mixture ratio for a 20 mm negative rod-plane gap.

pressure and mixture ratio on the breakdown voltage of a 20 mm gap using 6.3 mm cathode. Similar to figure 4.2, the breakdown voltage of nitrogen is very sensitive to the addition of the first few parts percent of SF_6. However, the extent of this effect is influenced by the total gas pressure as shown in Figure 4.9. For example at a total pressure of 400 kPa, the breakdown voltage of a 20% mixture is practically the same as that of the pure SF_6, whereas at a total pressure of 100 kPa, it is only about 55% that of pure SF_6. However, the onset voltage of 20% mixture is roughly 70% that of pure SF_6 at both these pressures. The difference in the breakdown voltage behavior is due to the fact that breakdown in SF_6 and SF_6-N_2 mixtures is corona stabilized in such non-uniform field gaps. The effectiveness of this corona stabilization depends on the partial pressure of SF_6 and the total pressure of the mixture. Therefore the breakdown voltage depends on the mixture ratio as well as the total gas pressure. Corona onset levels on the other hand depend primarily on the ionization and attachment properties of the gases. Therefore the ratio of the corona onset voltage of a particular mixture to that of pure SF_6 is not affected by the total gas pressure.

A study of the spark trajectories of these gases provided further information. Observations of the test gaps revealed that for SF_6 as well as SF_6-N_2 mixtures, the spark paths were relatively straight at lower pressures. This behavior continued in the pressure region in which the breakdown voltage increased linearly with the pressure. However, when the gas pressure further increased, the sparks exhibited a pronounced curvature to the axis of the rod electrode similar to figure 4.4. This curvature of the spark paths was quite appreciable in the pressure region where the breakdown voltage decreases with increasing pressure.

In this pressure region, even the corona discharges were inclined to the rod axis as shown in figure 3.9. However, when the gas pressure was further raised to levels where the breakdown occurred in the absence of any corona discharges, the spark channels were straight. This behavior is consistent with the arguments made in section 4.2 that the negative ion space charge inhibits the spark propagation and forces it around the space charge. Since at pressures above P_C, there are no corona discharges to introduce negative ion space charge in the interelectrode gap region, the spark channels are straight again.

CHAPTER V

PREBREAKDOWN STUDIES OF THE POSITIVE ROD-PLANE GAPS

5.1. Introduction

Investigations on the prebreakdown behavior of positive rod-plane gaps in SF_6, N_2 and SF_6-N_2 mixtures were carried out using various diameter rod anodes and gap lengths. Since the general behavior of the corona discharges varied little with the anode and gap size, only the results for 1 mm diameter anode will be discussed in this chapter. These investigations were carried out for rod-plane gaps of 10 to 50 mm length in the pressure range of 100 to 500 kPa.

5.2. The Anode Corona in Nitrogen

The prebreakdown behavior of rod-plane gaps insulated with pure N_2 was studied. At atmospheric pressure, no corona streamer were observed in the region of discharge threshold. Instead, the discharge was in the form of a succession of electron avalanches which formed in the relatively localized region of the highest field strength at the anode tip. The prebreakdown current waveform, though not absolutely steady, did not contain pulses of any specific character. The photomultiplier output, however, consisted of series of small pulses, with the separation between two consecutive pulses being of the order of 10 μsec. Visually corona appeared as a very faint discharge at the anode tip. As the applied voltage was increased, the magnitude and brightness of the discharge increased. This was accompanied by an increase in the average prebreakdown current and the repetition rate of the photomultiplier pulses. This behavior continued with increasing applied voltages until at a certain voltage level, weak prebreakdown streamers appeared. These streamers increased in number when the applied voltage was increased. Visual observations indicated that some of the streamers crossed the gap without causing a breakdown. With further increase in the applied voltage, a breakdown finally occurred.

With increasing pressure, the nature of the prebreakdown activity changed and prebreakdown current pulses were also recorded at the discharge onset. These pulses were quite regular in amplitude and time separation, their repetition rate being of the order of 10^3 pulses per second. However, an increase in the applied voltage established a pulseless current which had a general behavior as discussed earlier. Prior to the breakdown, the corona streamers appeared again in addition to the localized glow already present. The repetition rate of these pulses was of the order of 10^5 /sec. When the gas pressure was further increased, the region in which the pulseless current existed decreased gradually until at about 400 kPa, pulseless current was not recorded from the discharge onset to the ultimate breakdown of the test gap. The pulse repetition rate increased from about 10^3/sec at the discharge onset to about 10^5/sec near the breakdown level. The pulses prior to breakdown were an order of magnitude smaller in amplitude than those observed at the discharge onset level. However, both the photomultiplier as well as the current pulses near breakdown had a steady component in addition to the pulsating portion. It appears that this steady component was contributed by a localized glow discharge at the anode tip.

Figure 5.1 shows the voltage levels for different corona modes observed in nitrogen as pressure is varied. Figure 5.2 shows the prebreakdown current and light output waveforms for different types of the corona activity observed in nitrogen. Figure 5.3 shows the visual

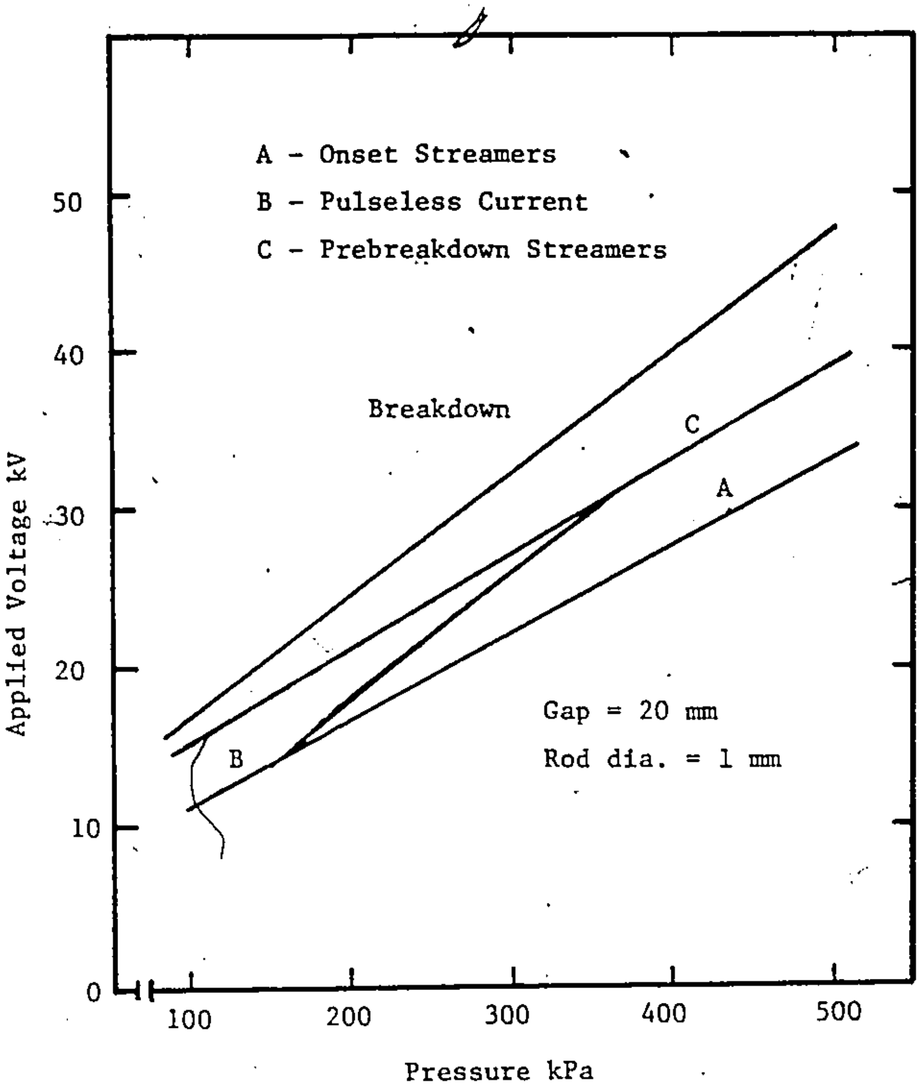

Figure 5.1 - Corona onset voltage levels for various corona modes in N_2.

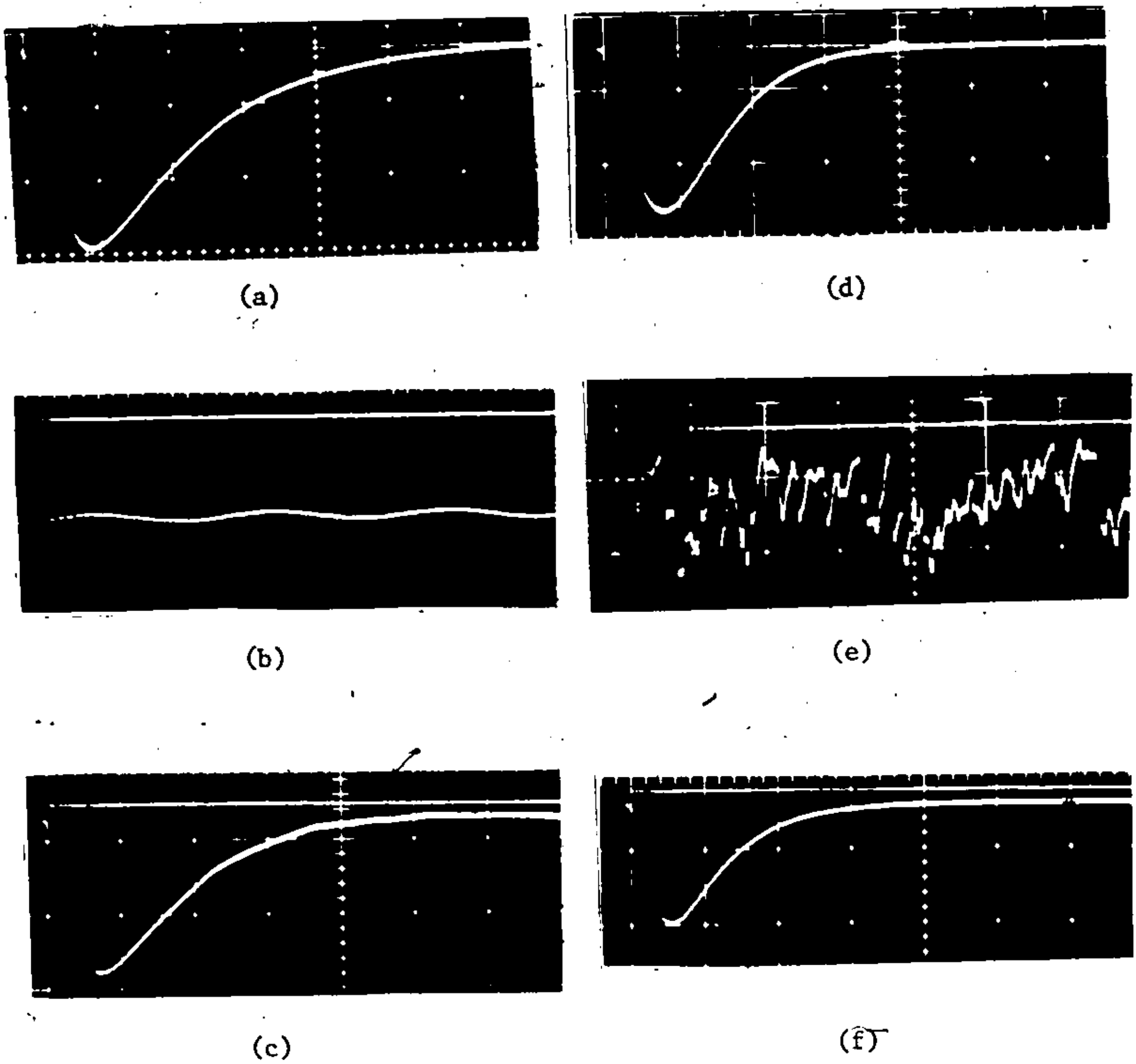

Figure 5.2.- Prebreakdown current and photomultiplier output waveforms for various corona modes in N_2. Gap = 20 mm. All the oscillograms shown are inverted.

(a) Current, region A, 500 kPa, 32 kV, 0.5 μsec/div, 20 mA/div.

(b) Current, region B, 300 kPa, 24 kV, 5 μsec/~~div~~ 20 μA/div.

(c) Current, region C, 500 kPa, 40 kV, 0.5 μsec/div, 4 mA/div.

(d) Light output, region A, 500 kPa, 32 kV, 0.5 μsec/div., 200 mV/div.

(e) Light output, region B, 300 kPa, 24 kV, 5 μsec/div., 1 mV/div.

(f) Light output, region C, 500 kPa, 40 kV, 0.5 μsec/div., 10 mV/div.

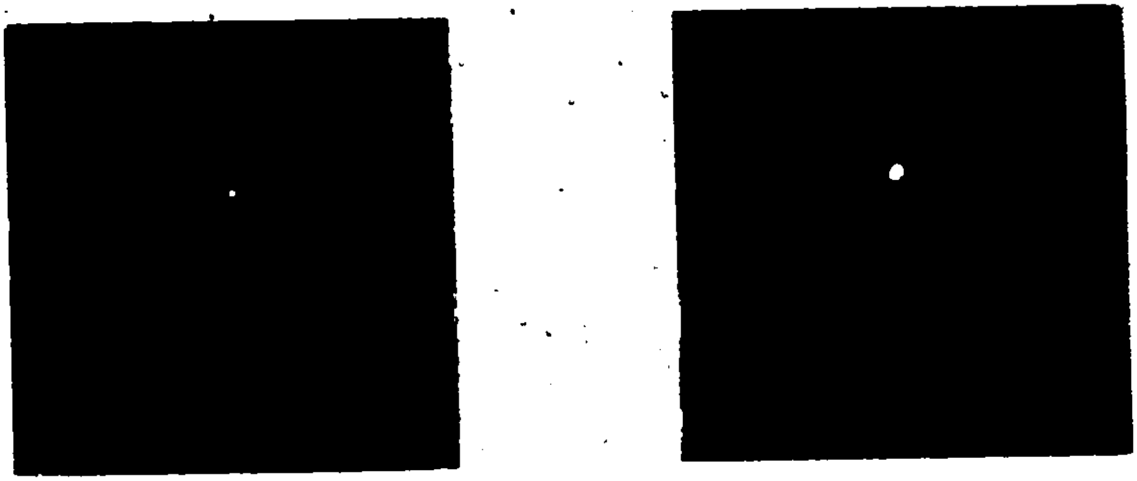

(a)

Pressure = 100 kPa
Voltage = 15 kV
Exposure = 10 msec

(b)

Pressure = 100 kPa
Voltage = 24.5 kV
Exposure = 10 msec

(c)

Pressure = 100 kPa
Voltage = 27 kV
Exposure = 10 msec

(d)

Pressure = 200 kPa
Voltage = 43 kV
Exposure = 10 msec

Figure 5.3 - Visual appearance of corona discharges in a 40 mm positive rod-plane gap filled with N_2. Diameter of the rod electrode is 1 mm. Figure (b), (c) and (d) show the pre-breakdown streamers while (a) shows a localized glow discharge.

appearance of the anode corona in stage B and C for a 40 mm gap and 1 mm diameter rod anode. It is interesting to note that some of the streamers in region C crossed the gap with out causing a breakdown. Also at higher pressures the discharge was concentrated in a narrow channel as compared to that at low pressures.

It is important to note that the magnitudes of both the prebreakdown current and light output in the glow corona in the case of a positive rod-plane gap were comparatively much lower than those for the negative rod-plane gaps. The reason for this behavior is that with a negative rod, the high field is concentrated about the cathode. Hence the necessary secondary processes such as photoionization in the gas, photoelectric effects at the cathode or the secondary electrons liberated by the positive ion bombardment take place in the high field region and therefore result in more effective ion multiplication. In the case of the positive rod-plane gaps, the main source of electrons available for maintaining a steady discharge is due to the photoelectric effect at the distant plate. The low fields at the plate electrode yield practically no electrons by positive ion bombardment. Furthermore, photoelectric emission from the plate is very weak. Hence, in this case the secondary ionization coefficient is small and therefore the prebreakdown currents are low. Also the photomultiplier output is so small that it is possible to differentiate between two successive avalanches. However, for the negative rod-plane gaps in nitrogen, the positive ions are accelerated in the high field region towards the rod electrode and hit the surface with energies 10 to 100 times higher than the energies associated with a positive rod-plane gap corona [9]. Therefore the secondary ionization coefficient takes on relatively large values, yielding high current and light outputs in the negative rod-plane gaps when compared to the positive rod-plane gaps under otherwise identical conditions.

5.3. The Anode Corona in SF_6 and SF_6-N_2 Mixtures

At low pressures such as 100 kPa and for SF_6-N_2 mixtures with SF_6 content below 1%, the discharge onset was usually in the form of pulseless currents. As the applied voltage was increased from zero, steady corona currents appeared at a certain threshold voltage level. Although there was some ripple in the prebreakdown current waveform, it did not contain pulses of any specific nature. However, with increase in the applied voltage, streamer pulses were always observed in addition to the pulseless currents. At higher gas pressures, streamer corona was more common. In such cases, the prebreakdown current usually had a large pulse followed by a series of small pulses as shown in figure 5.4(a). Whereas the large pulses had only one peak, the small pulses had one, two or even three peaks. In general the second peak was somewhat smaller than the first one, but in some cases pulses having second peaks larger than the first ones were also observed. The amplitude of the large pulse was substantially lower in mixtures than observed in pure nitrogen. When the applied voltage was increased, the large pulse disappeared and small pulses became more common. Usually these pulses were very regular in amplitude and time separation. Further increase in the applied voltage resulted in an increase in the average prebreakdown current and the frequency of these pulses. However,the current retained the same basic character as is evident from figure 5.4(b). The amplitude of the large pulse at the discharge onset was much higher than the average prebreakdown current recorded athigher voltage levels. Figure 5.4(c) shows the magnitude and waveshape of the large pulse observed at the discharge onset

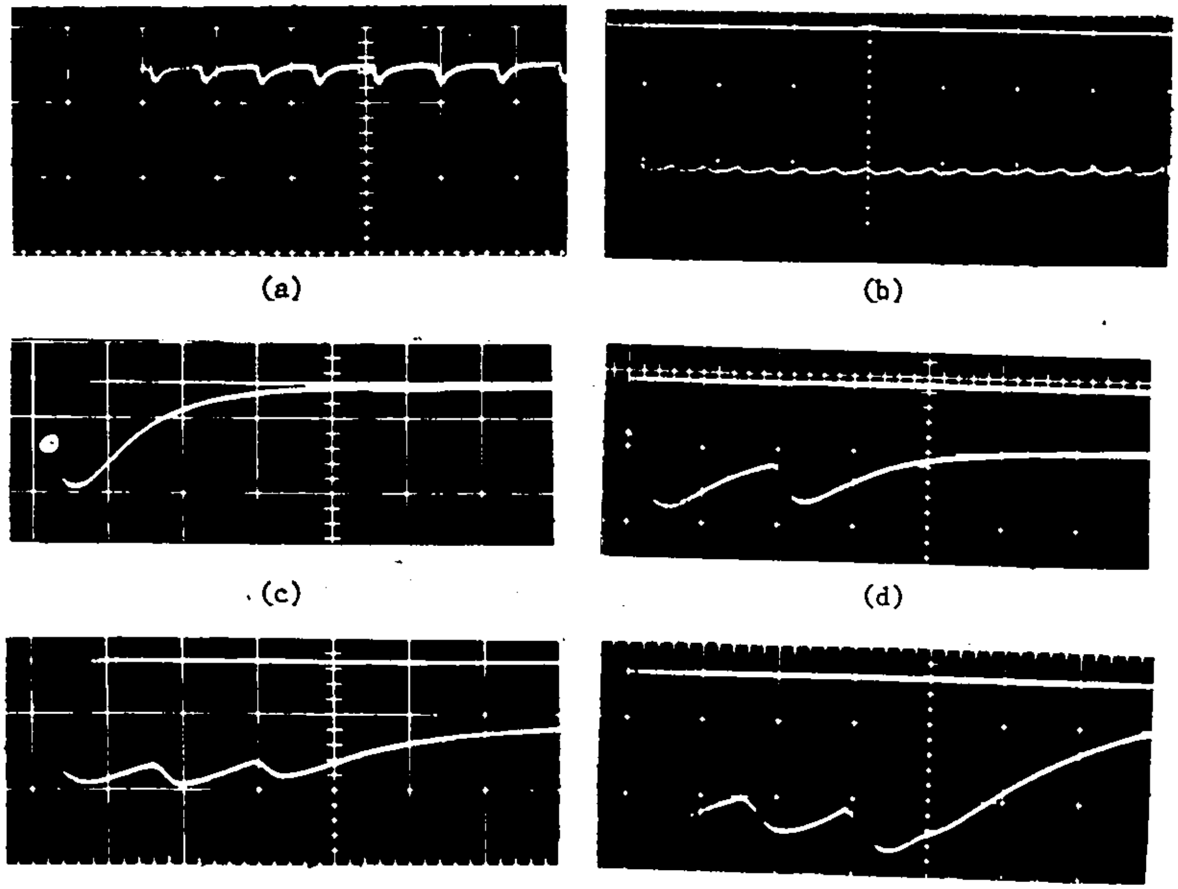

Figure 5.4 - Prebreakdown current and photomultiplier output waveforms for rod-plane gaps filled with 1% SF_6-N_2 mixture. Diameter of the rod anode is 1 mm. All the oscillograms shown are inverted.

(a) Current, 30 kV, 370 kPa, 20 mm gap, 0.4 mA/div, 20 μsec/div.

(b) Current, 45 kV, 370 kPa, 20 mm gap, 0.1 mA/div, 1 μsec/div.

(c) Current, 31 kV, 400 kPa, 20 mm gap, 0.4 mA/div, 0.5 μsec/div.

(d) Current, 41 kV, 400 kPa, 20 mm gap, 40 μA/div, 0.5 μsec/div.

(e) Current, 70 kV, 435 kPa, 45 mm gap, 40 μA/div, 0.5 μsec/div.

(f) Light output, 70 kV, 435 kPa, 45mm gap, 2 mV/div, 0.5 μsec/div.

whereas figure 5.4(d) shows the small pulses recorded at a higher voltage level. Both the prebreakdown current and photomultiplier output oscillograms had a steady component in addition to the pulses especially when the applied voltage approached the breakdown level. Figure 5.4(e) and (f) show a series of prebreakdown current and light output pulses at a voltage slightly below the breakdown level. The time period between two such successive series of pulses was of the order of 8 μsec.

When the prebreakdown current and the photomultiplier output contained pulses, the visual observations of the test gaps showed the existence of a bright channel as is shown in figure 5.5(a). This channel was very narrow and bright as compared to that observed in nitrogen and already shown in figure 5.3. This channel moved irregularly and in most cases was inclined to the axis of the rod electrode. The size and inclination of this channel were affected by the applied voltage, gas pressure and the mixture ratio. It was considerably extended into the gap for mixtures having SF_6 content less than 0.1% and at pressures below 150 kPa. In some cases two channels existed together simultaneously as shown in figure 5.5(b). Similar to the case of pure nitrogen, some of the streamers almost crossed the gap without causing a breakdown as shown in figure 5.5(a). This was more common at 100 kPa and for mixtures having SF_6 content less than 0.1%. Figures 5.5(c) and (d) show the corona and breakdown streamers for a 0.1% mixture. It is obvious that even at breakdown voltage levels, most of the corona streamers extend upto the middle of the test gap in contrast to N_2 and lower SF_6 content mixtures as shown in figures 5.3 and 5.5. When the SF_6 content was increased to about 1% the size and brightness of the streamer channels reduced considerably. In such cases, the discharge activity was usually confined to the vicinity

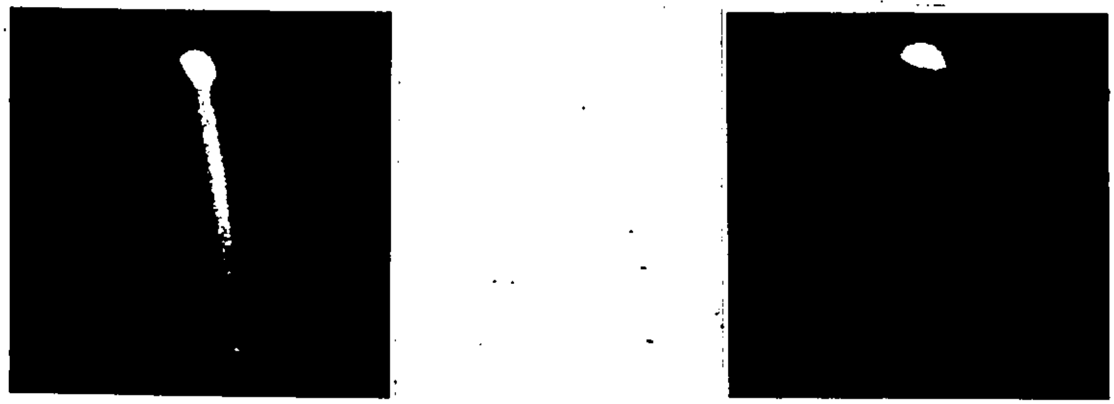

(a)

V = 23 kV

P = 100 kPa

SF_6 = 0.05%

Exposure = 10 msec.

(b)

V = 23 kV

P = 100 kPa

SF_6 = 0.05%

Exposure = 10 msec.

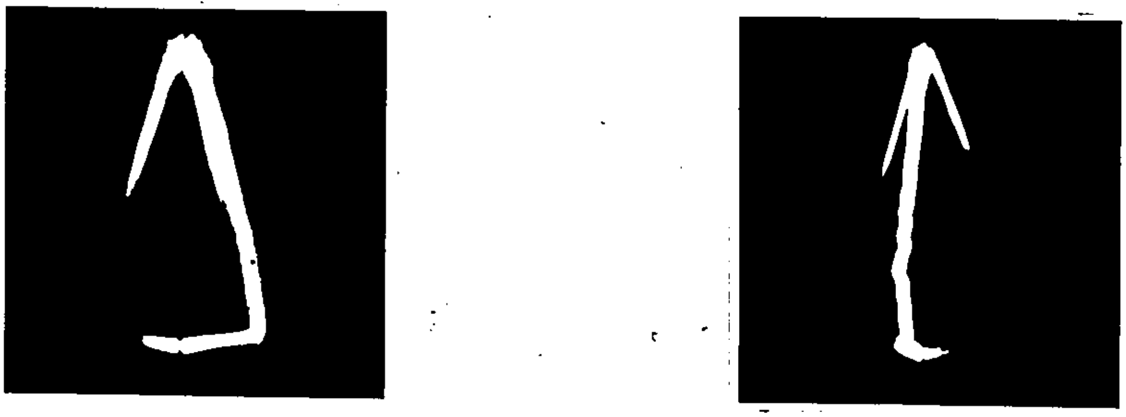

(c)

V = 25 kV

P = 100 kPa

SF_6 = 0.1%

Exposure = 10 msec.

(d)

V = 25 kV

P = 100 kPa

SF_6 = 0.1%

Exposure = 10 msec.

Figure 5.5 - Visual appearance of breakdown and prebreakdown streamers in a 20 mm rod-plane gap using 1 mm diameter rod anode.

of the anode. With the increase in the applied voltage, the discharge did not extend much into the gap even upto the breakdown voltage level.

For pure SF_6, and SF_6-N_2 mixtures with SF_6 content above 1%, pulseless currents could not be observed at any of the pressures investigated. The corona inception current in such cases was in the form of single isolated pulses as shown in figure 5.6(a). Such pulses occurred at random with intervals between successive pulses apparently independent of the voltage levels. These intervals were of the order of several seconds. The average time between such pulses increased with increasing gas pressure, SF_6 content and the field uniformity.

At voltages higher than the single pulse inception levels, similar to the negative rod-plane gaps, a discharge consisting of several pulses in rapid succession was occasionally observed. This type of discharge activity was earlier observed by Hazel [11] in pure SF_6 and was termed "momentary discharge". At the inception level of this type of discharge, the pulses appeared at random intervals, as in the case of the single pulse corona activity. The intervals between the momentary discharges ranged from milliseconds to seconds and decreased with increasing applied voltages. The momemtary discharges exhibited several types of waveforms depending on the gas pressure, mixture ratio, field configuration and the applied voltage. Figures 5.6(b-h) show some of the prebreakdown current waveforms observed. Photomultiplier output oscillograms were similar to those of the prebreakdown current.

The repetition rate of the momentary discharges generally increased with the applied voltage. A further increase in the gap voltage resulted in the establishment of a continuous discharge. Whereas the average corona current resulting from the momentary discharge activity was generally well below 1 μA throughout the voltage range of this activity,

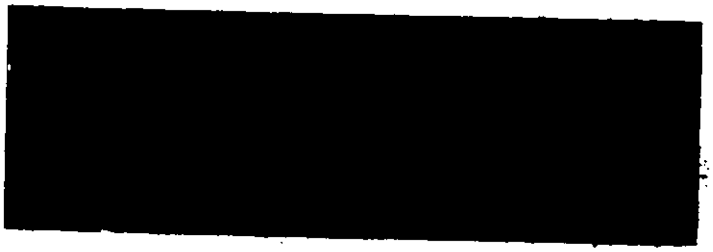

P = 400 kPa, V = 92 kV
SF$_6$ = 95%, Gap = 40 mm
20 μA/div, 10 μsec/div.

(a)

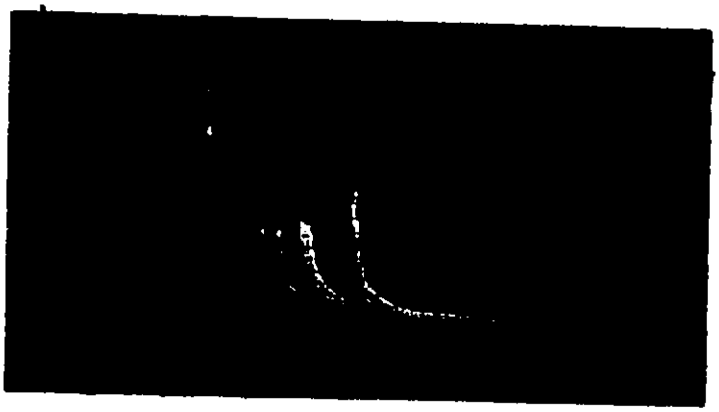

P = 235 kPa, V = 53 kV
SF$_6$ = 70%, Gap = 40 mm
20 μA/div, 5 μsec/div.

(b)

P = 360 kPa, V = 82 kV
SF$_6$ = 95%, Gap = 40 mm
20 μA/div, 10 μsec/div,

(c)

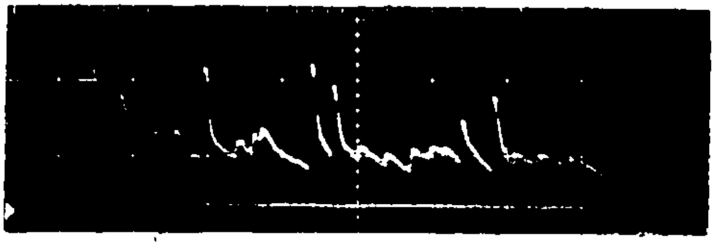

P = 375 kPa, V = 78 kV
SF$_6$ = 100%, Gap = 40 mm
20 μA/div, 5 μsec/div.

(d)

P = 400 kPa, V = 93 kV
SF$_6$ = 95%, Gap = 40 mm,
20 μA/div, 10 μsec/div

(e)

Figure 5.6 - continuted.

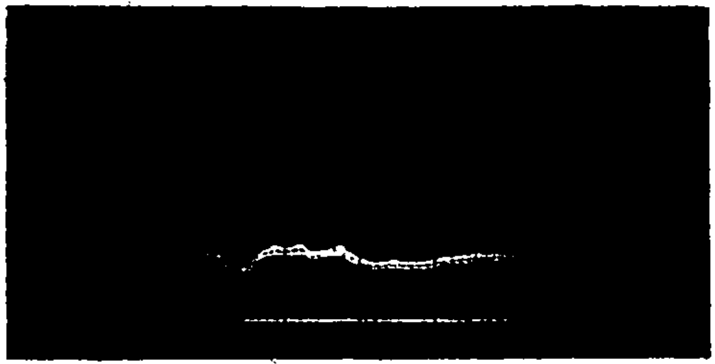

(f)

P = 440 kPa, V = 57.4 kV
SF_6 = 70%, Gap = 20 mm
20 μA/div, 5 μsec/div.

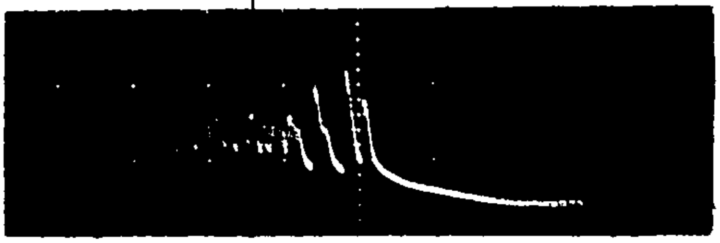

(g)

P = 340 kPa, V = 76.3 kV
SF_6 = 100%, Gap = 40 mm
20 μA/div, 5 μsec/div.

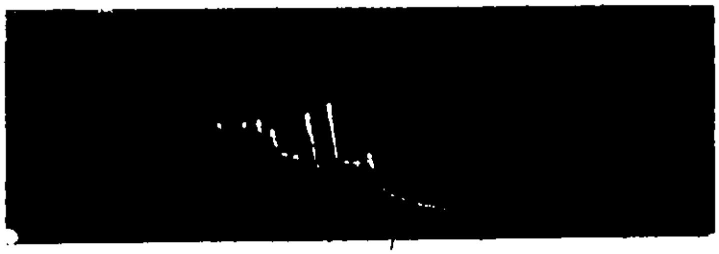

(h)

P = 340 kPa, V = 76.3 kV
SF_6= 100%, Gap = 40 mm
20 μA/div, 5 μsec/div.

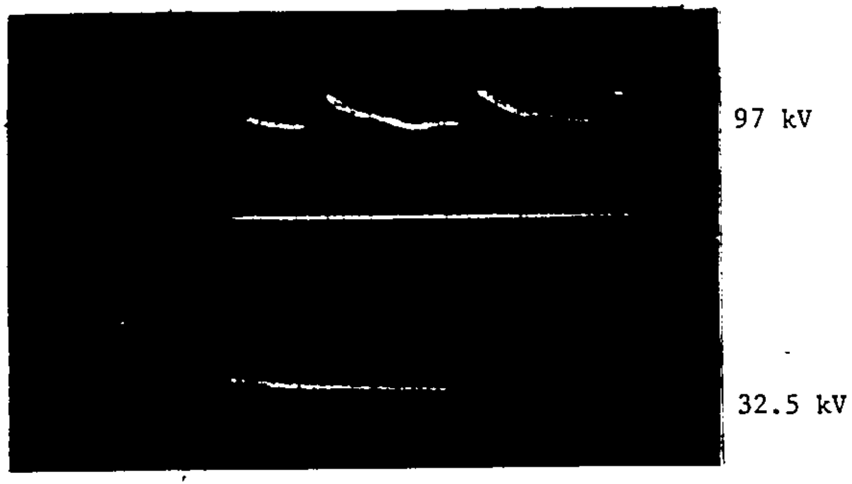

(i)

P = 200 kPa
SF_6 = 10%
Gap = 40 mm
100 μA/div
0.5 μsec/div.

Figure 5.6 - continued.

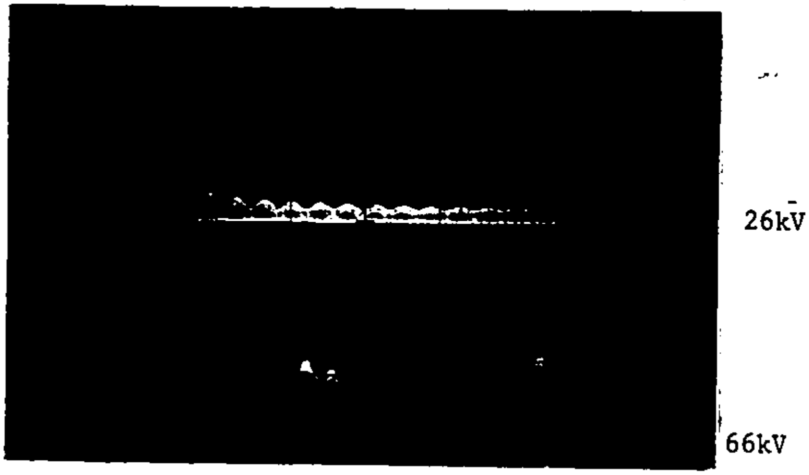

(j)

Light Output
$P = 100$ kPa
$SF_6 = 50\%$
Gap = 40 mm
20 mV/div
0.5 μsec/div

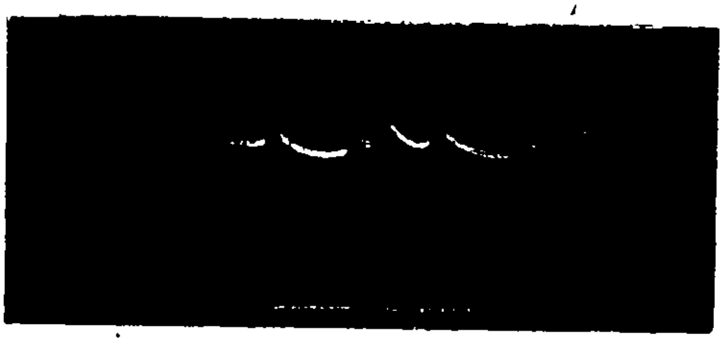

(k)

Current
$P = 200$ kPa, $V = 55$ kV
$SF_6 = 1\%$, Gap = 20 mm,
100 μA/div, 0.5 μsec/div.

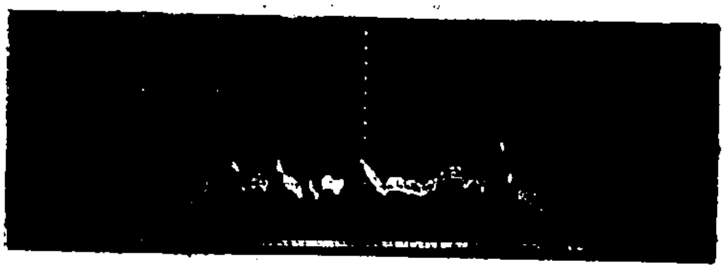

(ℓ)

Light Output
$P = 200$ kPa,
$V = 55$ kV,
$SF_6 = 1\%$,
Gap = 20 mm
50 mV/div, 0.5 μsec/div.

Figure 5.6 - Prebreakdown current and light output oscillograms of corona discharges in rod-plane gaps filled with SF_6-N_2 mixtures. Diameter of the rod anode is 1 mm.

the transition to a continuous discharge caused the microammeter to deflect suddenly and indicate a continuous current flow in the circuit. A transition from a continuous discharge to a momentary discharge occurred only when the applied voltage was reduced to a level somewhat lower than that at which the reverse transition occurred.

At the onset of a continuous discharge, both the prebreakdown current and the photomultiplier output were made up of pulses. These pulses were quite irregular in the amplitude and the time separation. When the applied voltage was increased, the frequency of current and light pulses as well as the d.c. level of the prebreakdown current increased. Figure 5.6(i) shows the prebreakdown current waveform at two different voltage levels whereas figure 5.6(j) shows the light output pulses at two values of the gap voltage. Prior to the breakdown of the test gap, both the prebreakdown current as well as the photomultiplier output had a steady component in addition to the pulses. Whereas the prebreakdown current had a large steady component for all the mixtures investigated, the same was not the case for the photomultiplier output. It had a large steady component only for the mixtures having low SF_6 content. Figures 5.6(k) and (ℓ) show the prebreakdown current and the light output oscillograms for a 1% SF_6-N_2 mixture at a voltage level close to breakdown.

For a particular mixture, the general discharge pattern remained the same with increasing gas pressure until a pressure was reached above which continuous discharge could not materialize and breakdown occurred. At and slightly above this pressure, only momentary discharges occurred prior to the breakdown. When the gas pressure was further increased, a critical pressure P_c was reached above which no discharge activity was observed prior to the breakdown. The critical pressure P_c and the pressure P_d above which no continuous discharges occurred were affected by the size of the anode and the gas mixture ratio and will be discussed in chapters VI and VIII.

Visual observations of the test gaps showed a bluish filament at the spherical tip of the anode at the onset of a continuous discharge. The root of the filament was brighter than the stem and the filament moved irregularly over the anode surface. As the applied voltage was increased, both the length of the filament and the rate of its motion on the anode surface increased. Further increase in the applied voltage resulted in multiple filaments which were more diffused in appearance than the single filament and moved more rapidly over the entire anode tip. The number of filaments, their length and their displacement from the rod tip increased with the increasing gap voltage. The discharge spread more on the anode surface than growing into the gap. At still higher voltage levels, the discharge filaments became so numerous and diffused that the discharge at the electrode surface appeared as a continuous glow. However, at the outer edge of the discharge, the individual filaments were still recognizable. The glow-like appearance was more common for anodes with smaller diameters at low pressures and in mixtures having low SF_6 content. With increasing applied voltage, the glow-like discharge extended into the gap as well as laterally on the anode. Depending on the gas pressure, mixture ratio, applied voltage and the rod diameter, the discharge activity could also be detected on the cylindrical portion of the rod anode. Figure 5.7 shows the photographs of these discharges is various mixtures for a 1 mm diameter anode.

At higher ~~gas~~ pressures, the discharge did not extend into the gap with the increasing gap voltage and spread laterally over the anode surface similar to the negative rod-plane gaps. Occasional long reddish discharge filaments were also observed, emanating primarily from the edge

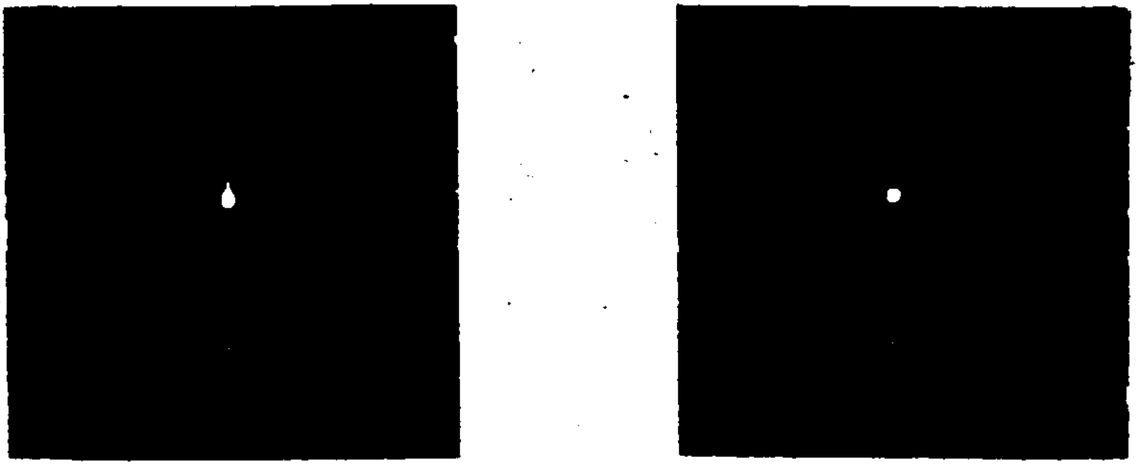

(a)

V = 108 kV
P = 100 kPa
SF_6 = 30%
Exposure = 10 msec.

(b)

V = 152 kV
P = 200 kPa
SF_6 = 30%
Exposure = 10 msec.

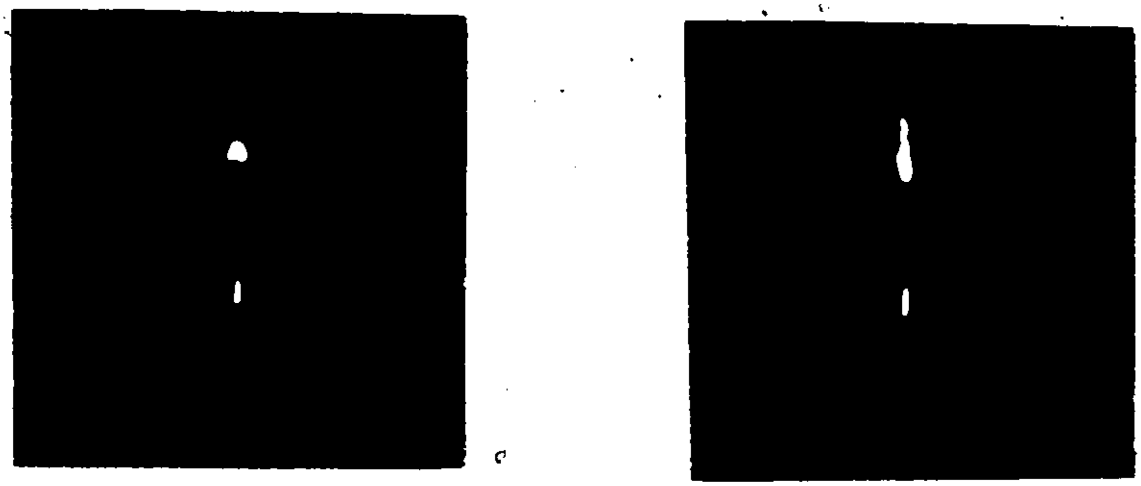

(c)

V = 80 kV
P = 100 kPa
SF_6 = 1%
Exposure = 10 msec.

(d)

V = 108 kV
P = 100 kPa
SF_6 = 10%
Exposure = 10 msec.

Figure 5.7 - Visual appearance of corona discharges in a 40 mm rod-plane gap filled with SF_6-N_2 mixtures. Diameter of the rod anode is 1 mm.

of the discharge region on the spherical tip of the anode. This behavior continued upto the breakdown voltage. In general, the discharge was brighter and extended more into the gap when the SF_6 content in the mixtures was low.

5.4. The Corona Onset Voltage Levels

As discussed in the previous section, the corona inception in SF_6-N_2 mixtures was in the form of random pulses which led to momentary and then continuous discharge when the applied voltage was raised. The onset levels for the single pulse corona were lower than those at which continuous discharges appeared. The difference between the two levels was affected by the gas pressure, mixture ratio and the field configuration. In general, the difference between the two inception levels increased with increasing gas pressure, gap length, rod diameter and the SF_6 content. Figure 5.8 shows the two inception levels at different pressures for 10 and 95% SF_6-N_2 mixtures. Since the single pulse inception levels are the lowest voltage levels at which any discharge is detected, only these are discussed in detail in this section.

The corona inception voltages varied with the gas pressure, mixture ratio, gap length and diameter of the rod electrode. These levels were 10-15% higher than those for the negative rod-plane gaps. Other than this difference in the absolute values of the corona onset voltages, other behavior of the onset voltages was similar to that of the negative rod-plane gaps. Figure 5.9 and 5.10 show the variation in the onset voltages with gas pressure and mixture ratio for 20 and 40 mm positive rod-plane gaps using 1 mm diameter anode. The behavior of corona onset voltages as a function of the mixture ratio shown in figures 5.9 and 5.10 is similar to that of the negative rod-plane gap and shown in figure 3.11. The behavior of the corona onset voltage as a function of the mixture ratio

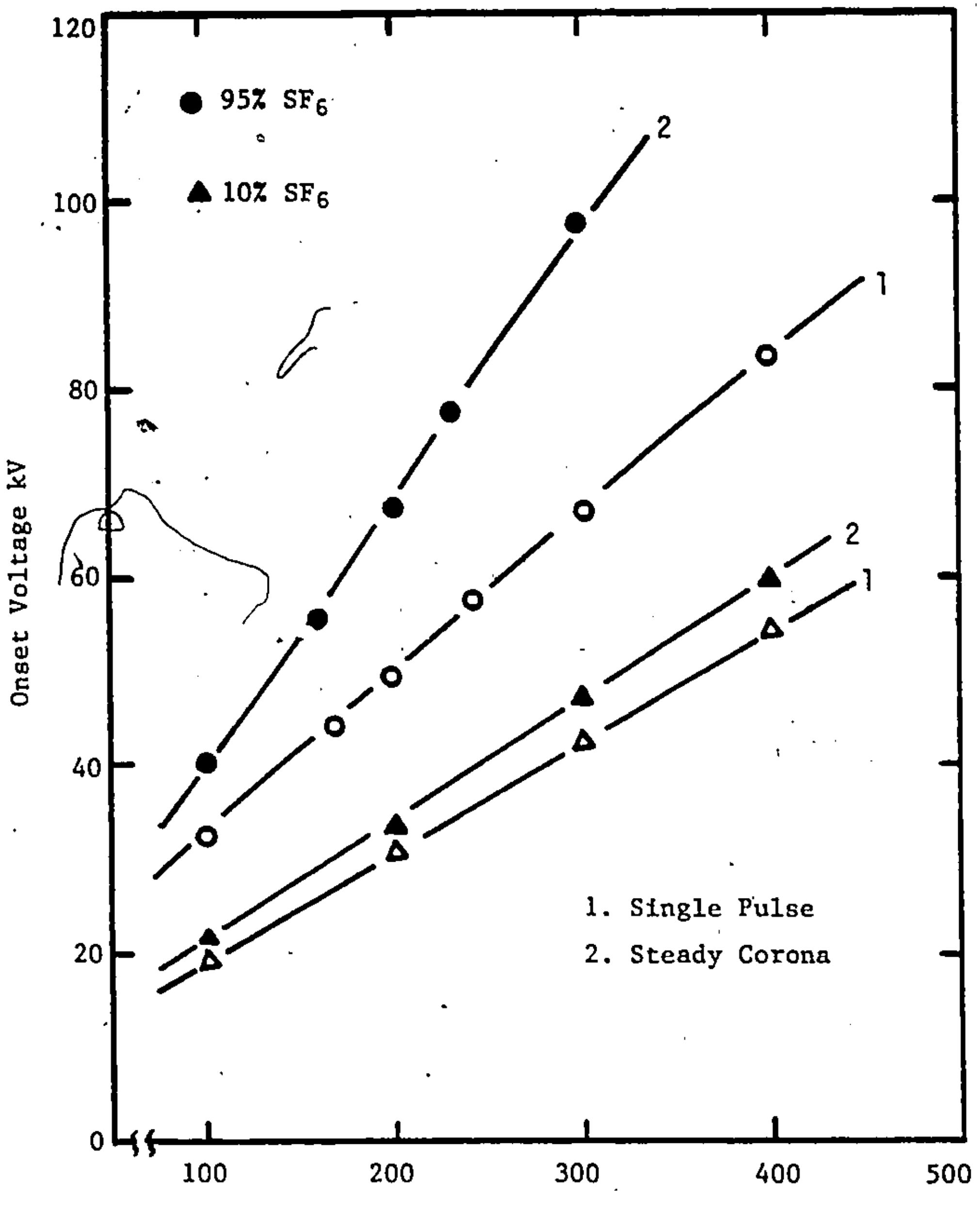

Figure 5.8 - Corona inception levels for a 40 mm rod-plane gap using 1 mm diameter rod electrode.

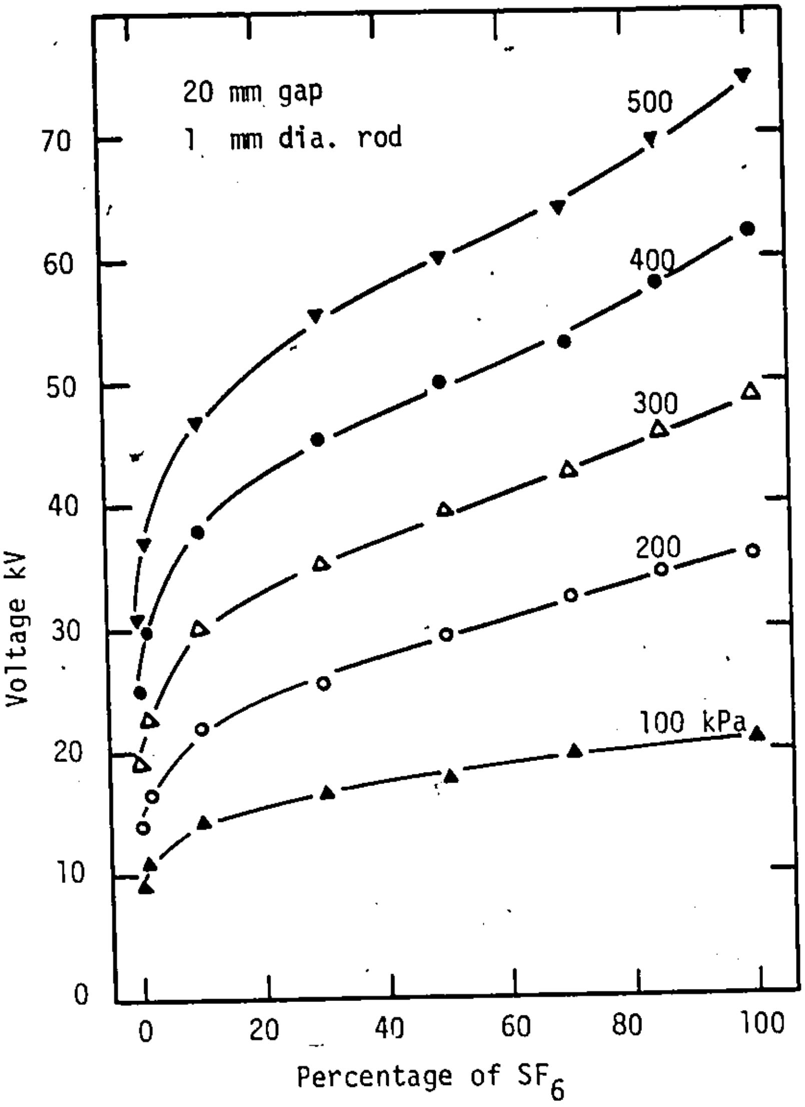

Figure 5.9 - Corona onset voltage-mixture ratio characteristics for a positive rod-plane gap.

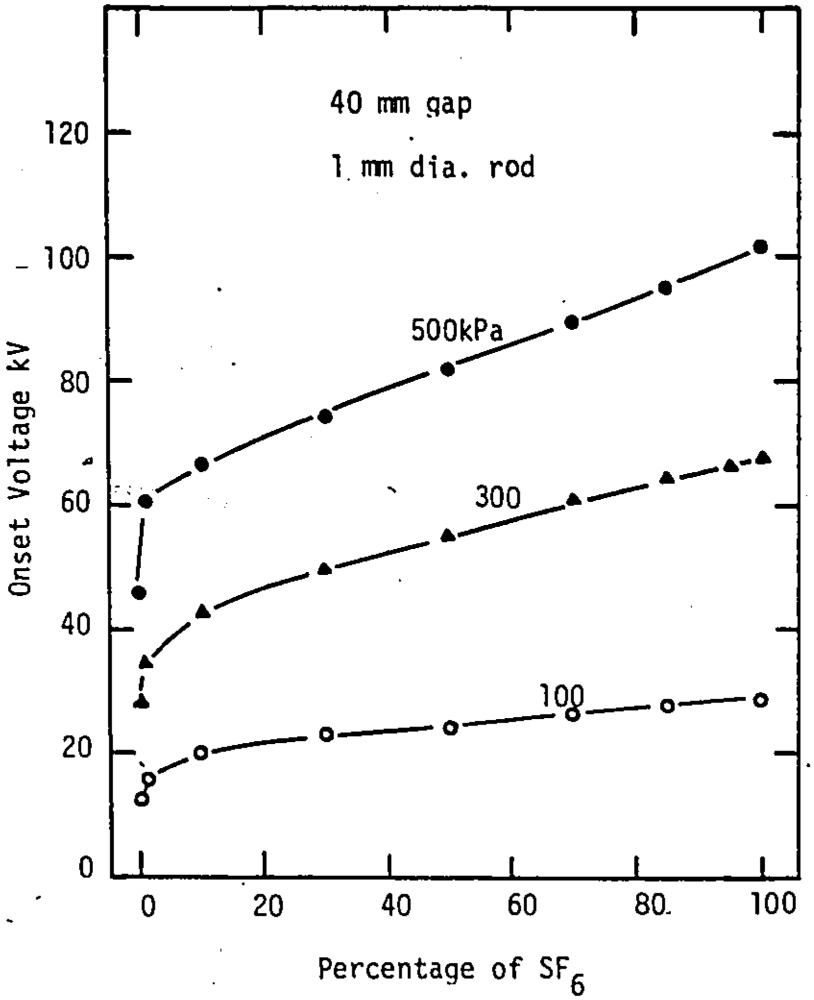

Figure 5.10- Corona onset voltage-mixture ratio characteristics for a positive rod-plane gap.

and the gas pressure for anodes having different diameters was similar to that of 1 mm diameter rod and therefore will not be discussed here.

5.5. The Prebreakdown Current Levels in SF_6-N_2 Mixtures

Similar to the negative rod-plane gaps, the prebreakdown currents showed variations with the applied voltage, gas pressure, mixture ratio and the field configuration. Figure 5.11 shows the steady component of the prebreakdown current as a function of the applied voltage and the mixture ratio. These measurements were carried out in a 20 mm gap using 1 mm diameter anode at a total pressure of 200 kPa. For a particular voltage and mixture ratio, the prebreakdown current decreased when the gas pressure was increased and was lower than that observed for the negative rod-plane gaps. The variations in the prebreakdown current with gas pressure, mixture ratio and the applied voltage were similar for various electrode systems studied.

The magnitude of the corona current prior to breakdown varied with the gas pressure, mixture ratio, gap length and the diameter of the rod anode. In general, these currents were up to 50% lower than those observed in the case of the negative polarity. The corona currents prior to breakdown exhibited a peak for a mixture ratio which was affected by the total gas pressure as shown in figure 5.12. Figure 5.13 shows the effect of gas pressure and gap length on magnitudes of corona currents prior to breakdown for 1% and 95% SF_6-N_2 mixtures.

The voltage-current characteristics for the positive rod-plane gaps in SF_6-N_2 mixtures can also be expressed as

$$I = CV[V - V_o] \qquad 5.1$$

where V_o is the minimum discharge onset voltage. The value of the constant C was affected by the gap length, gas pressure, mixture ratio and

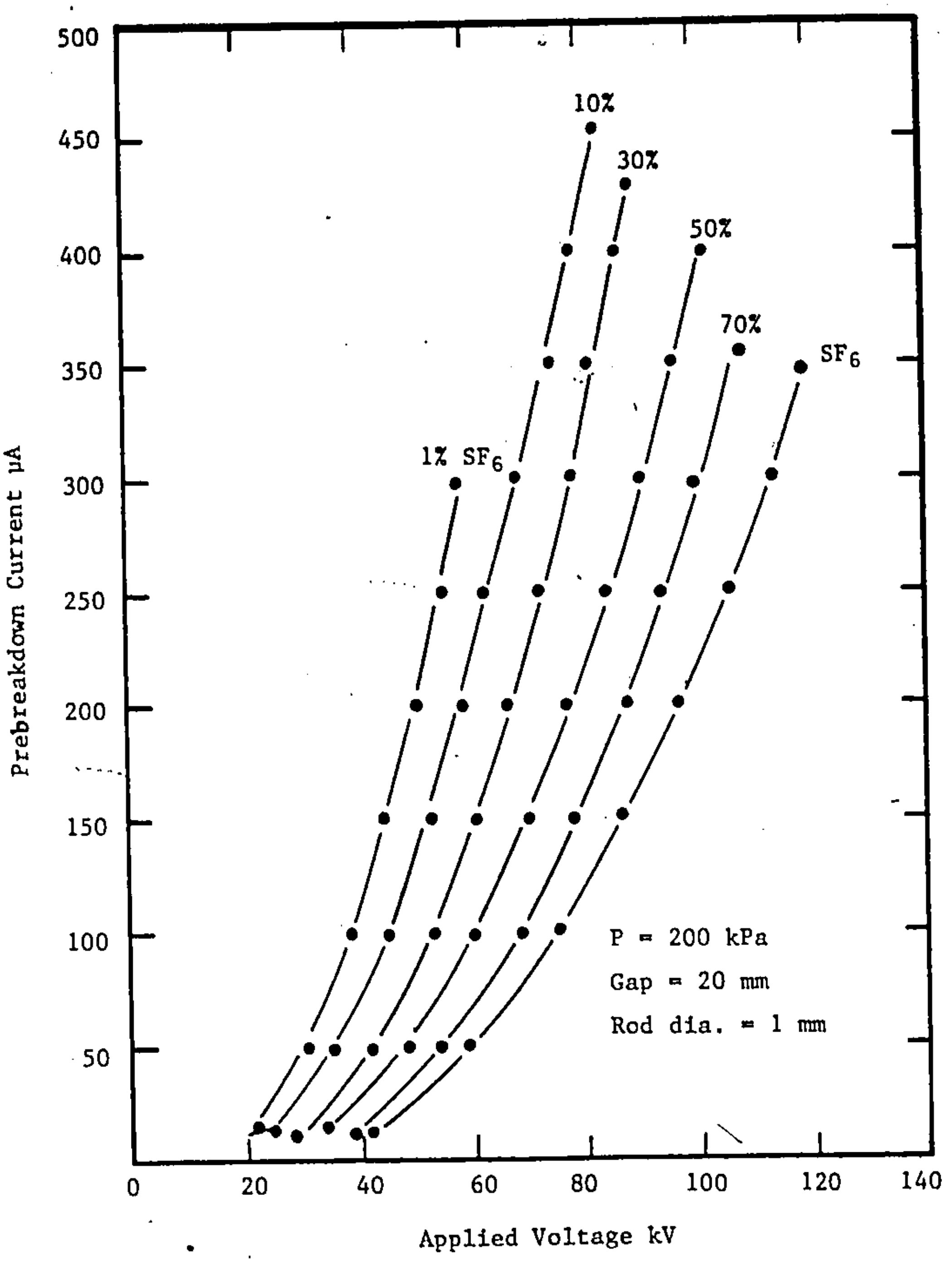

Figure 5.11 - Effect of applied voltage and gas mixture ratio on corona current in a positive rod-plane gap.

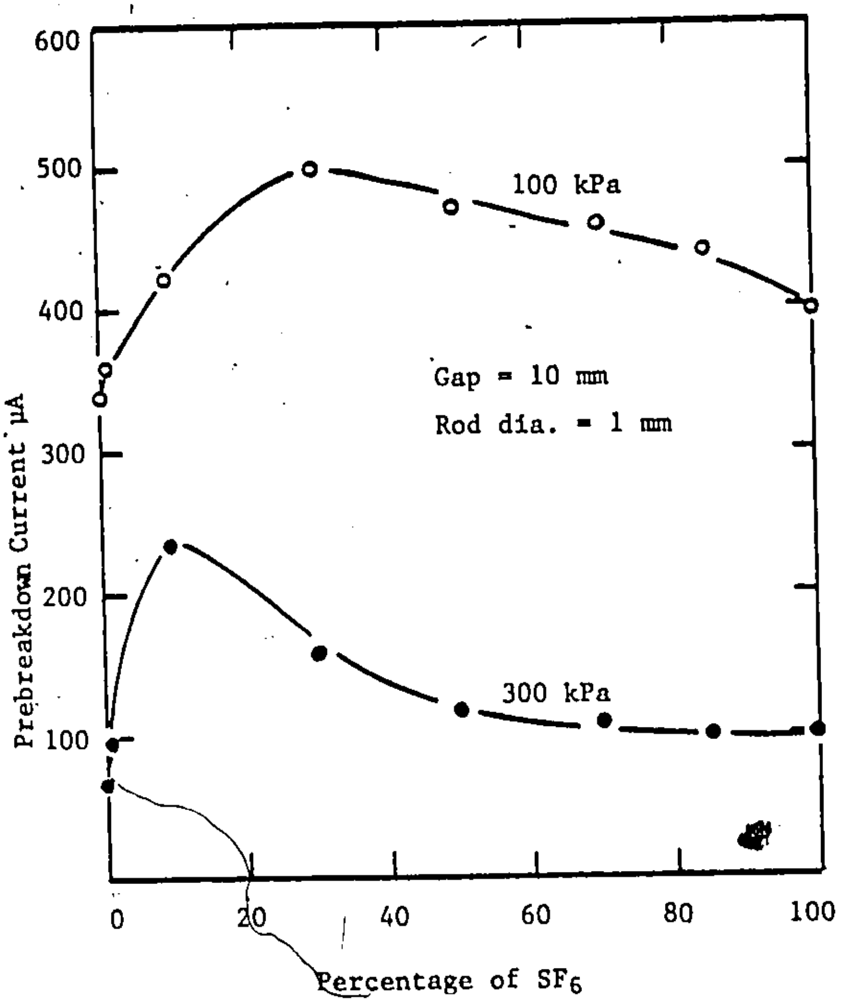

Figure 5.12 - Effect of gas pressure and mixture ratio on current prior to breakdown in SF_6-N_2 mixtures.

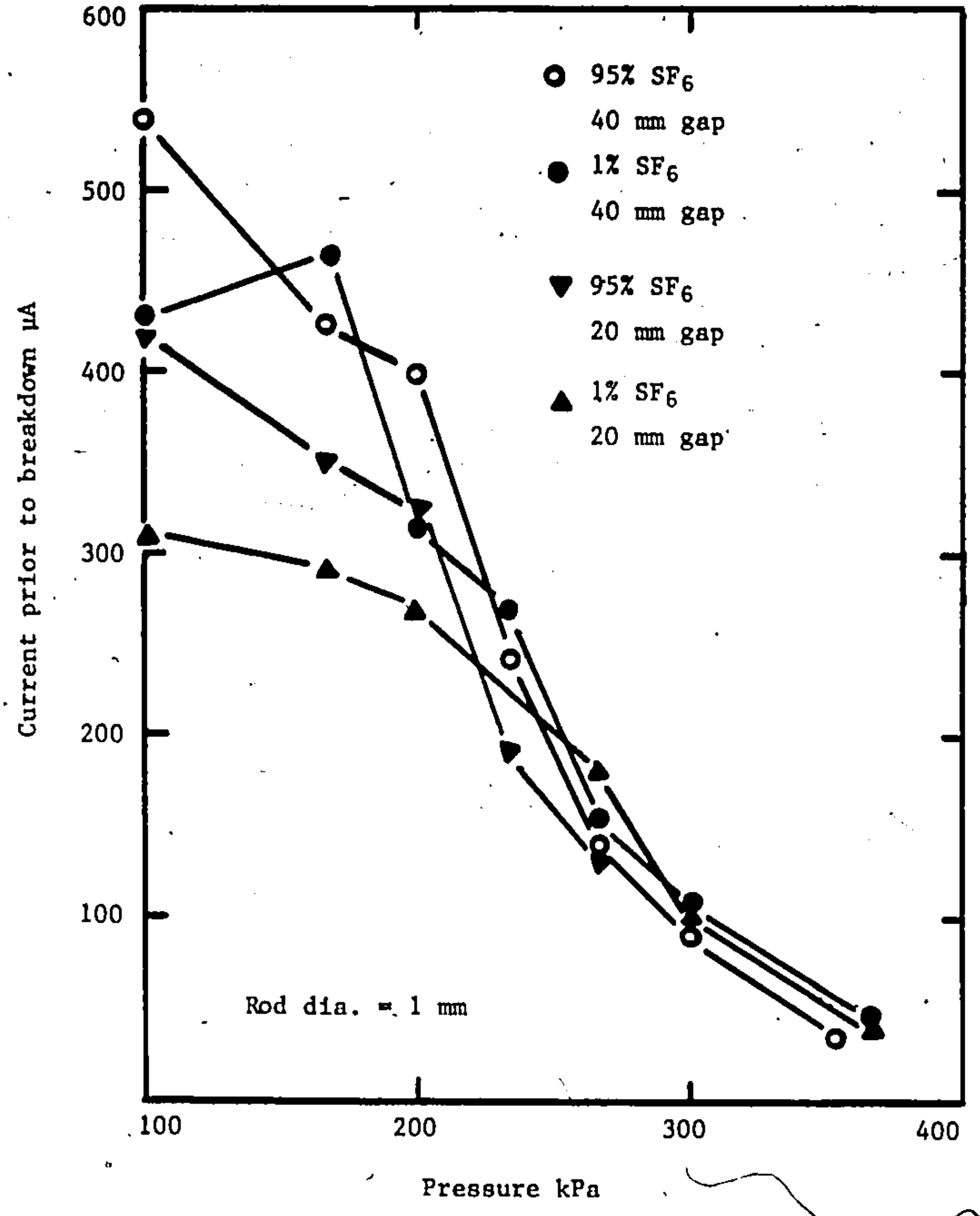

Figure 5.13 - Effect of gap length and gas pressure on the current prior to breakdown in SF_6-N_2 mixtures for positive rod-plane gaps.

the diameter of the anode. The value of the constant C for positive rod-plane gaps was very close to that obtained for the negative rod-plane gaps under identical test conditions. Figure 5.14 shows the variations in the value of the constant C with the mixture ratio for a 20 mm gap using 1 mm anode at a total gas pressure of 200 kPa. Similar to the negative polarity, the curve in figure 5.14 indicates that when the first few parts percent of SF_6 are added to nitrogen, most of the free electrons are attached to SF_6 molecules forming heavy negative ions and thereby reducing the value of the constant C. Any further addition of SF_6 has relatively little effect on the negative ion population and hence the value of the constant C.

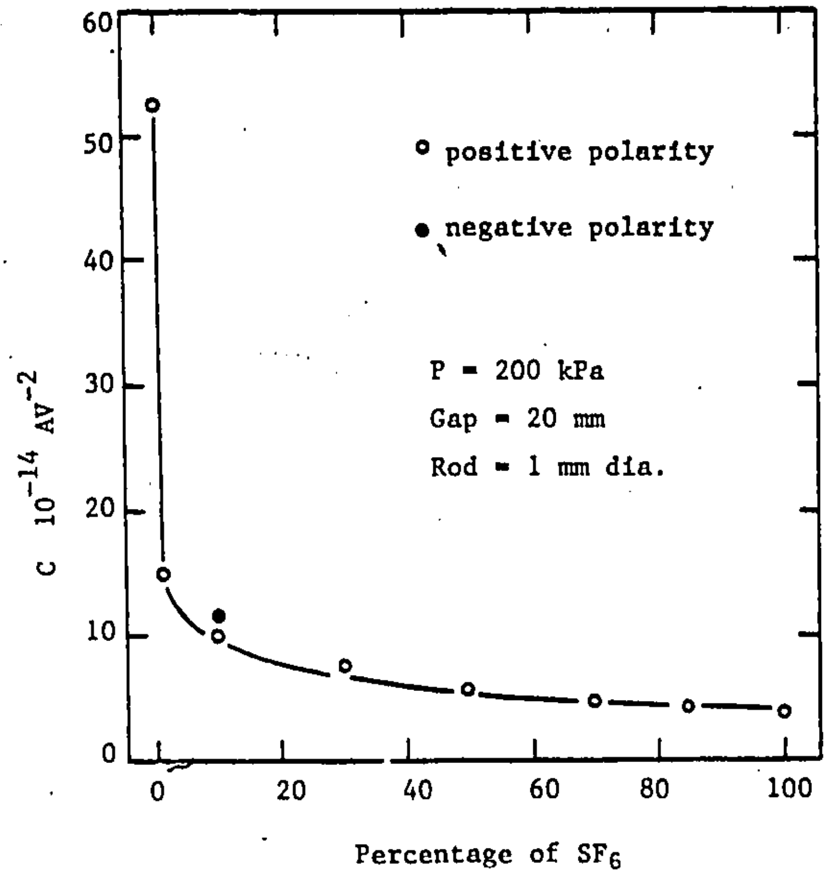

Figure 5.14 - Variation of the constant C with gas mixture ratio in a positive rod-plane gap.

CHAPTER VI

BREAKDOWN STUDIES OF THE POSITIVE ROD-PLANE GAPS

6.1. Introduction

The breakdown in SF_6 and SF_6-N_2 mixtures is found to be corona stabilized over a certain pressure region. Above this pressure, the discharge onset usually leads to breakdown without any corona discharges. According to Hazel [11], the rate of rise of the applied voltage does not significantly affect the breakdown voltage levels for SF_6 in the corona stabilized pressure region. However, the rate of rise has a significant influence on the test results in the pressure region where steady corona discharges do not precede the breakdown. In such cases, the breakdown levels are the lowest and have less scatter when the rate of rise of the applied voltage is of the order of 1 kV/min. In view of these findings, the applied voltage was raised upto about 70% of the expected breakdown value at a rate of 1 kV/sec and thereafter at a rate of 1 kV/min upto breakdown.

6.2. The Breakdown Behavior of SF_6

The breakdown voltages of compressed SF_6 for positive rod-plane gaps have been reported in the literature [11-15]. The general character of the breakdown under such conditions is the existance of a pressure range over which the breakdown voltage is substantially higher than the corona threshold and a breakdown in this region occurs in the presence of a steady corona. Above this pressure, the discharge onset directly leads to sparkover. In order to gain a better understanding of breakdown under such conditions, discharge voltages of rod-plane gaps in pure SF_6 were investigated.

Figure 6.1 shows the breakdown voltage as a function of the gas pressure for a 20 mm gap using 1 mm diameter rod anode. For comparison, the discharge onset voltages for single pulse and steady corona activity are also included. The general behavior of the breakdown voltage as a function of the gas pressure can best be explained by dividing the pressure into five regions as shown at the top of the figure. The characteristics of the regions A, B, D and E were investigated previously by Hazel [11] and agree well with the present investigations.

The breakdown voltage in region A is much higher than the onset level and increases almost linearly with pressure. In region B, the breakdown voltage is a non-linear function of the gas pressure and decreases with increasing pressure after attaining a maximum value at a certain pressure. The difference between the corona onset and breakdown voltage levels is quite appreciable in this region. In region C, the breakdown voltage-pressure curve has a discontinuity. The width of this region is about 15 kPa for the gap under discussion. In this region, as the applied voltage is increased gradually, a breakdown occurs at about 74 kV. When the applied voltage is increased beyond this level, a breakdown does not occur until the applied voltage is raised to about 120 kV. A breakdown would not occur at any other value of applied voltages in between these two levels. Whereas no steady prebreakdown current is detected before the spark occurs at the lower voltage level, a prebreakdown current of several microamperes is measured before the spark occurs at the upper voltage level. Usually there is a small scatter in the breakdown voltage values for each level. Furthermore, when the voltage is reduced gradually from the upper level, no breakdown is recorded at voltages corresponding to the lower voltage level. In such cases, the steady corona disappears at a level which is significantly lower than

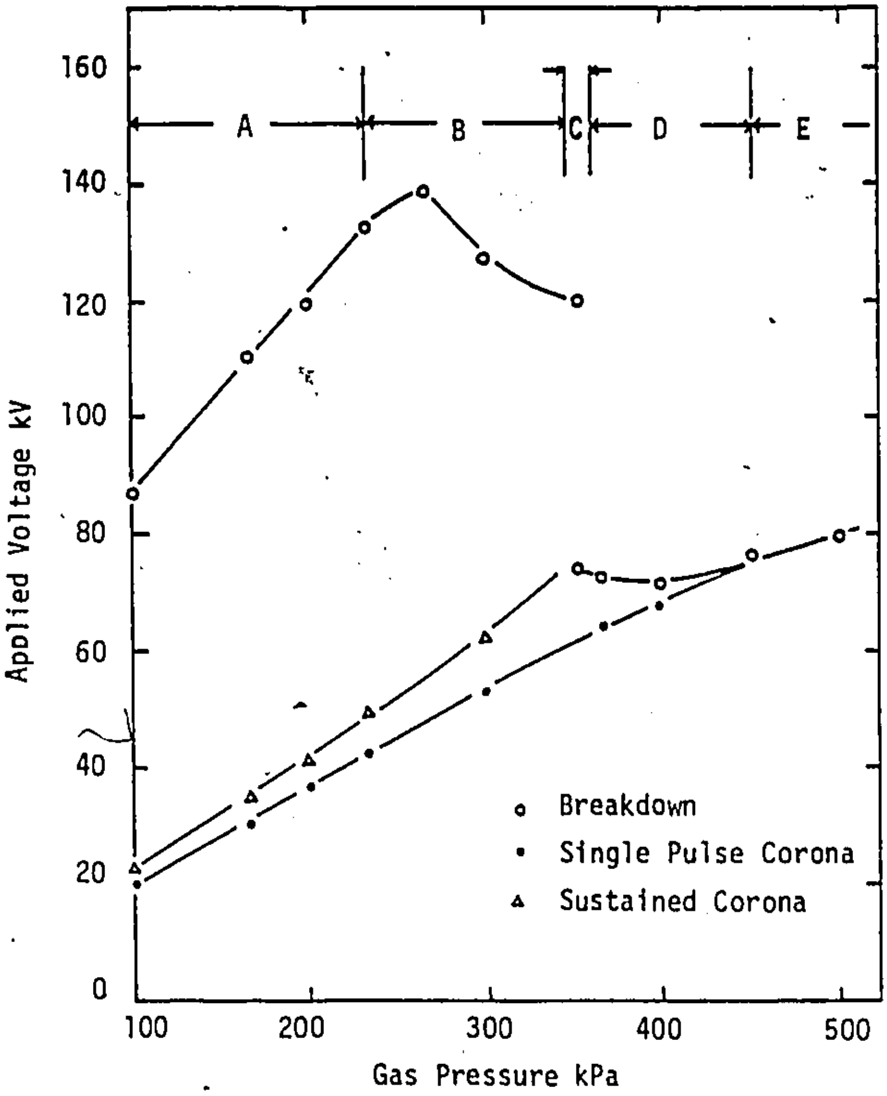

Figure 6.1 - Breakdown voltage-pressure characteristics of SF_6 for a 20 mm positive rod-plane gap. Diameter of rod electrode is 1 mm.

the lower breakdown voltage level. In region D, there is no steady corona discharge prior to the breakdown, although single pulse or momentary corona discharges might occur before the breakdown. The difference between the breakdown and the corona onset voltages is very small in this region and decreases with increasing gas pressure, until it reduces to zero at critical pressure, P_c. In region E, there is no prebreakdown activity of any type prior to the breakdown of the test gap.

The discontinuity observed in the breakdown voltage-pressure characteristics of Figure 6.1 was earlier hinted by Hazel and Kuffel [13] but was not explored in detail. Cookson and Wootton [16] also observed that a 25 mm rod-rod gap insulated with 200 kPa of SF_6 had two 60 Hz breakdown levels at 70 and 100 kV. However, like others [12, 15], they measured the breakdown voltages at discrete pressures with significant increments and did not observe the discontinuity for other gaps that they studied. Consequently they described this observation as an "unusual characteristic". Similarly Works and Dakin [14] apparently encountered the same phenomenon when they reported that in some cases their breakdown studies of the positive rod-plane gaps appeared to indicate two distinct breakdown voltage levels at a single gas pressure falling in the negative slope region of the breakdown voltage-pressure characteristics of SF_6.

In order to understand the effect of the field non-uniformity on the breakdown behavior of SF_6 in general and the discontinuity in particular, breakdown voltages of 20 and 40 mm rod-plane gaps using 1, 1.5, 2, 3.16, 6.3 and 12.6 mm diameter rod anodes were investigated. As an extremely small diameter anode, the needle anode shown in figure 2.2 was also used in some measurements. Figures 6.2 and 6.3 show the results of these measurements. Single pulse corona onset voltage levels for these gaps

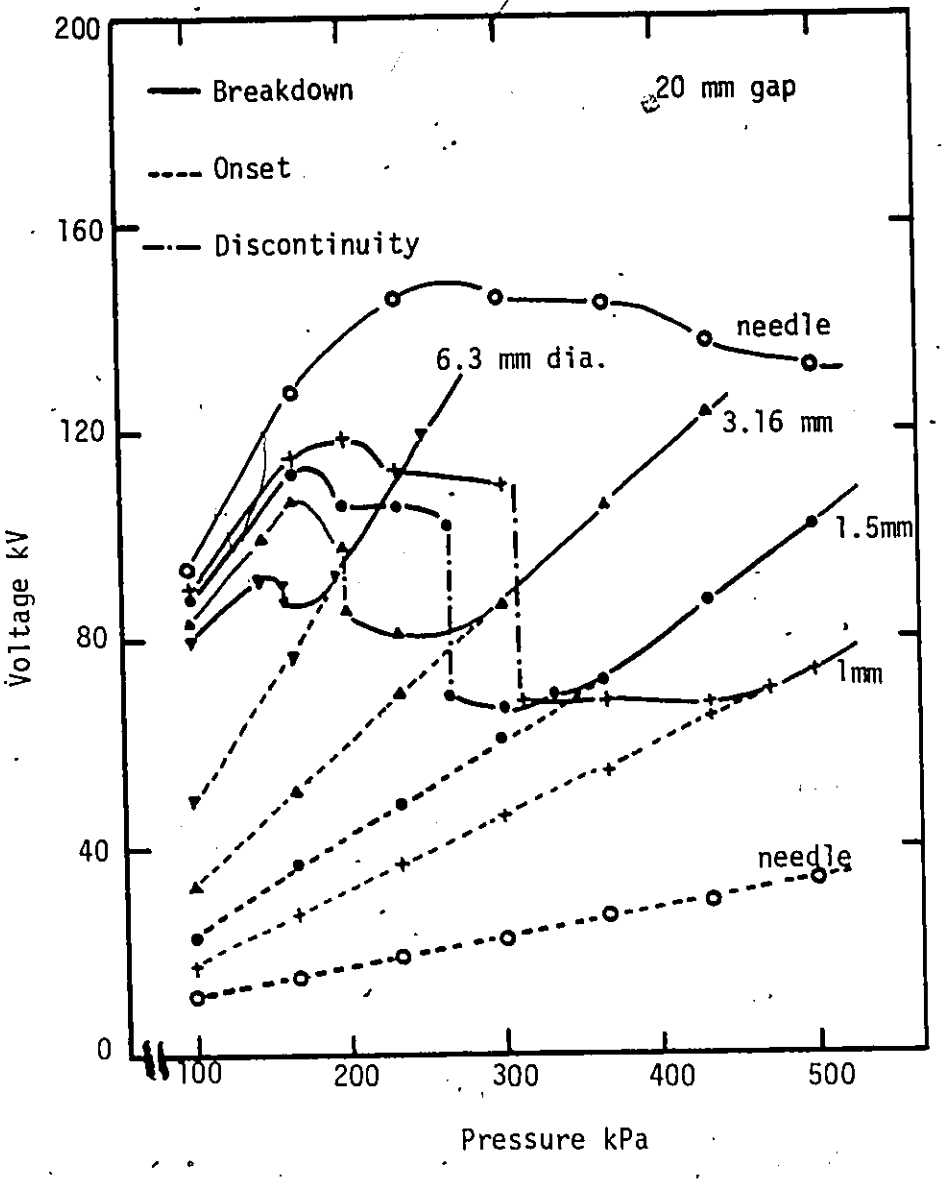

Figure 6.2 - Effect of the rod diameter on the breakdown voltage-pressure characteristics of SF_6 for a 20 mm positive rod-plane gap.

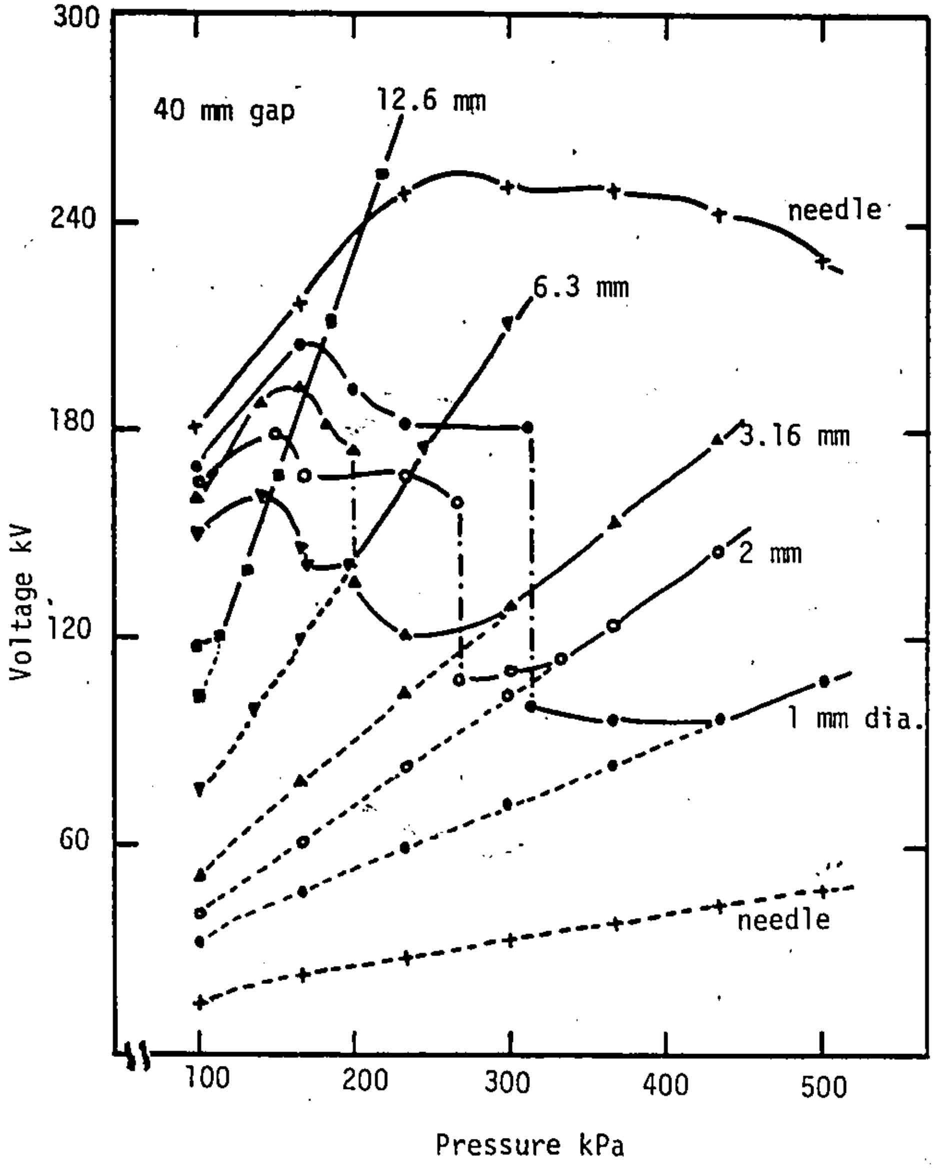

Figure 6.3 - Effect of the rod diameter on the breakdown voltage-pressure characteristics of SF_6 for a 40 mm positive rod-plane gap.

are also included in these figures. A comparison of figures 6.2 and 6.3 with 6.1 indicates that in general the breakdown behavior of all the gaps is similar to that of the 1 mm diameter anode. The pressure P_d at which the discontinuity occurs and the critical pressure P_c are higher for gaps having smaller diameter anodes. For the needle electrode, these pressures definitely seem to exceed 500 kPa, the highest pressure investigated in our studies. In the pressure range over which the breakdown is corona stabilized, the difference between the corona onset level and the breakdown voltage level is the highest for the needle electrode and the lowest for the 12.6mm diameter rod anode. Therefore, at low pressures, the breakdown voltage is the highest for the needle electrode and is the lowest for the 12.6 mm rod anode for the same gap length. The corona onset voltages on the other hand behave in the opposite fashion and are the lowest for the needle electrode and the highest for the 12.6 mm diameter rod anode. This behavior of the positive rod-plane gaps is very similar to that of negative rod-plane gaps shown in figure 4.5. Furthermore, the difference between the two breakdown voltage levels corresponding to the discontinuity pressure P_d is higher for the smaller diameter anodes and the discontinuity is more distinct for smaller anodes. Also the discontinuity pressure P_d as well as the critical pressure P_c are primarily affected by the diameter of the rod electrode and more or less are independent of electrode separation.

6.3. The Breakdown Behavior of SF_6-N_2 Mixtures

The breakdown and corona onset measurements show that SF_6-N_2 mixtures behave similar to pure SF_6. The breakdown of mixtures containing as low as 0.1% SF_6 exhibits behavior shown in figures 6.1 - 6.3. Figure 6.4 shows the breakdown voltage-pressure characteristics for a

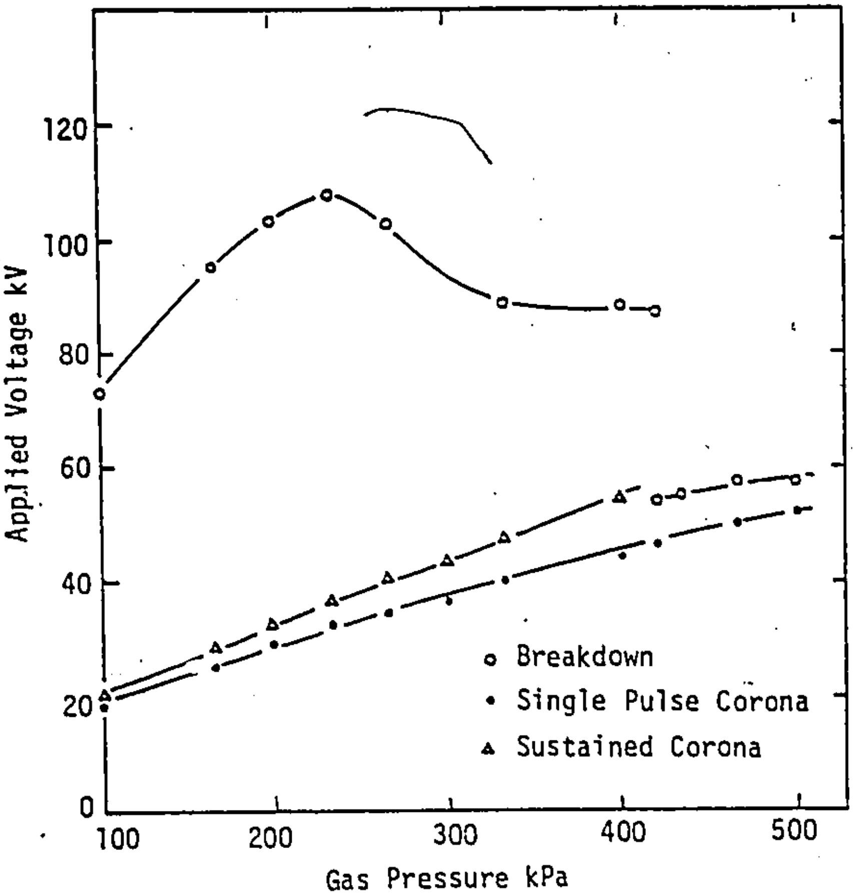

Figure 6.4 - Breakdown voltage-pressure characteristics of a 50% SF_6-N_2 mixture for a 20 mm rod-plane gap. Diameter of the rod electrode is 1 mm.

20 mm positive rod-plane gap insulated with a 50% mixture. Figure 6.5 shows similar characteristics for a 45 mm gap insulated with a 1% SF_6-N_2 mixture. The breakdown levels and the discontinuity pressure in SF_6-N_2 mixtures are different from those observed in pure SF_6 as shown in figures 6.1 - 6.5. Besides, the critical pressure P_c at which the breakdown and the corona onset voltages coincide is higher in mixtures than in pure SF_6. The critical and the discontinuity pressures depend on the mixture ratio and are higher in all the mixtures than those in pure SF_6. Figure 6.6 shows the changes in the discontinuity pressure with mixture ratio for a 20 mm gap and 1 mm anode. Furthermore, the pressure at which the maximum breakdown voltage was recorded was roughly the same in SF_6 and in mixtures having SF_6 content higher than about 10%. For mixtures with SF_6 content below 10%, this pressure was higher than that observed in pures SF_6 and increased with decreasing SF_6 content. In general, the breakdown in SF_6-N_2 mixtures is corona stabilized over a wider pressure range as compared to pure SF_6.

Figure 6.7 presents the breakdown voltages for a 20 mm gap using 1 mm rod anode as a function of mixture ratio for different pressures. For pressures of 100 and 200 kPa, the behavior of the breakdown voltage is similar to that observed for negative rod-plane gaps. In such cases, the addition of about 5% SF_6 almost doubles the breakdown voltage of nitrogen. Any further addition of SF_6 causes an increase in the breakdown voltage but at a relatively lower rate. Furthermore, the breakdown voltage of SF_6 is higher than that for all the mixtures and pure nitrogen. For pressures of 300 and 400 kPa, the breakdown behavior is not similar to the preceeding lower pressures of 100 and 200 kPa. In these cases, some of the mixtures have higher breakdown strength than that of pure SF_6. For example, in figure 6.7, the mixtures having 5 to 85% SF_6 have breakdown

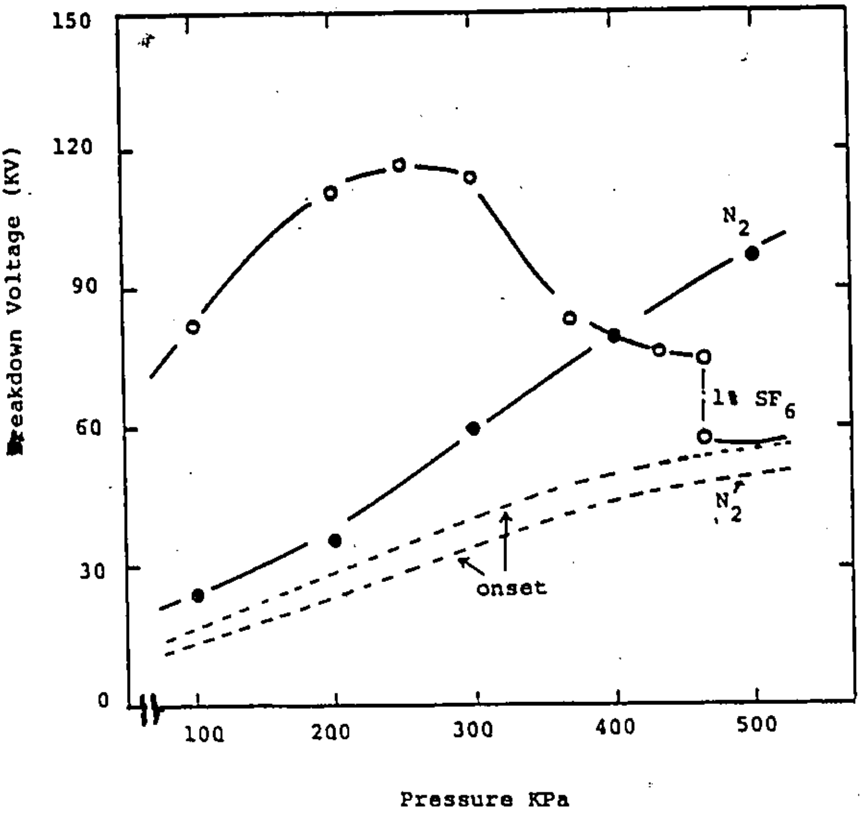

Figure 6.5 - Effect of gas pressure on breakdown and corona onset voltages of N_2 and 1.0% SF_6-N_2 mixture for a 45 mm rod-plane gap using 1 mm diameter rod anode.

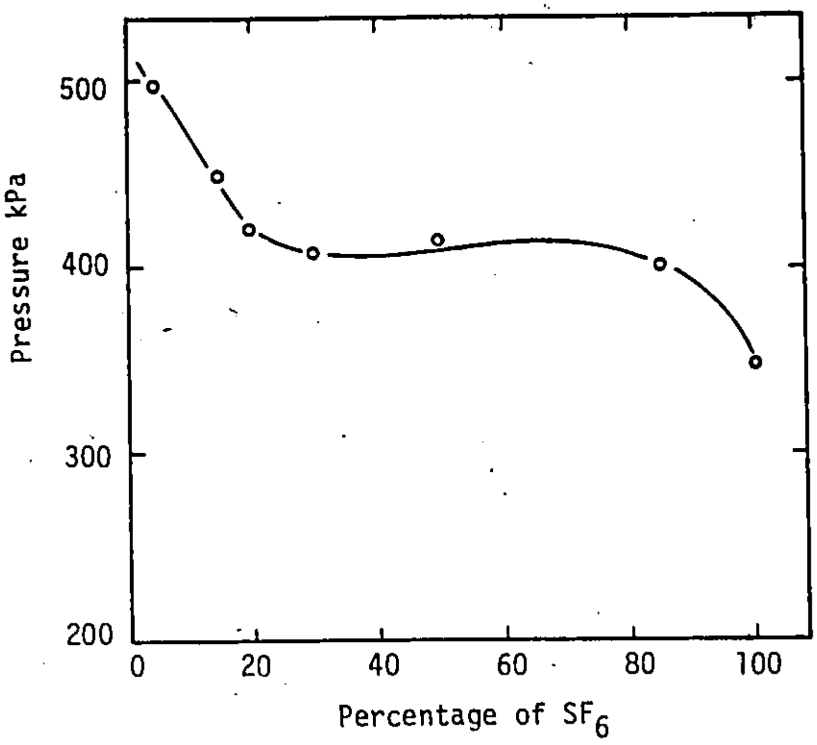

Figure 6.6 – Variation of the discontinuity pressure P_d with gas mixture ratio.

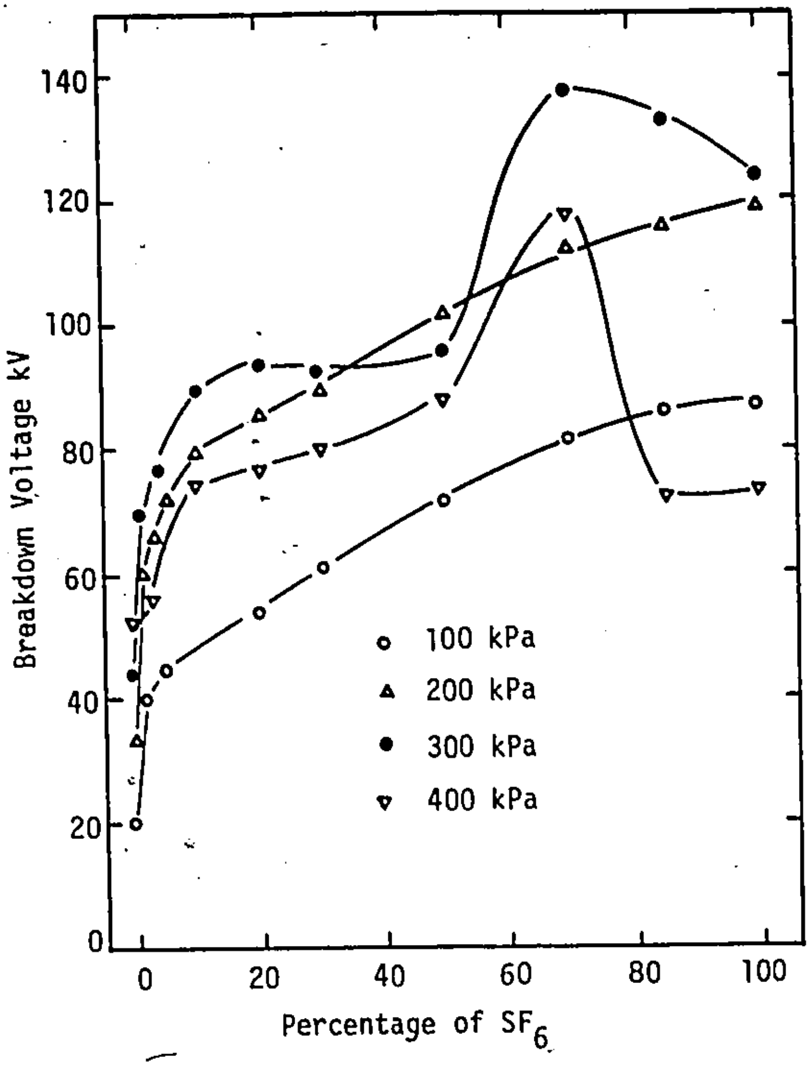

Figure 6.7 - Breakdown voltage-mixture ratio characteristics for a 20 mm rod-plane gap using 1 mm diameter rod anode.

strength higher than that of pure SF_6 at a total gas pressure of 400 kPa. At this pressure, the breakdown voltage of a 60% mixture is roughly 1.5 times that of pure SF_6 for otherwise similar experimental conditions. This is due to the fact that in mixtures, the breakdown is corona stabilized over a wider pressure range and the stabilization processes are more effective in some pressure regions.

The breakdown voltage of mixtures having SF_6 content less than 30% was even lower than that of pure SF_6 at 500 kPa as shown in figure 6.8. This drop in the breakdown voltage is, however, not reflected in the corona onset measurements. The onset voltages of all the mixtures are always higher than that of pure nitrogen as shown in figures 5.9 and 5.10. The breakdown in nitrogen in highly non-uniform field gaps occurs in the presence of corona discharges. Both the corona onset as well as the breakdown voltages of nitrogen increase almost linearly with pressure in the pressure range investigated as shown in figure 6.5. In mixtures, on the other hands, the breakdown is corona stabilized only at low pressures. The breakdown voltage of mixtures is therefore pressure dependent in a non-linear fashion. At low pressure, the space charges generated due to the corona discharges help to increase the breakdown voltage of mixtures substantially over that of pure nitrogen. However, as the gas pressure is increased, the ability to increase breakdown voltage is reduced. The difference between the breakdown voltage of the mixtures and of pure N_2 is therefore reduced. As the gas pressure is further increased, the discharge onset directly leads to a breakdown. In such cases, the onset and the breakdown voltage levels of the mixture coincide. This is not the case for pure nitrogen as shown in figure 6.5. The breakdown voltages of the mixtures containing small SF_6 contents are therefore

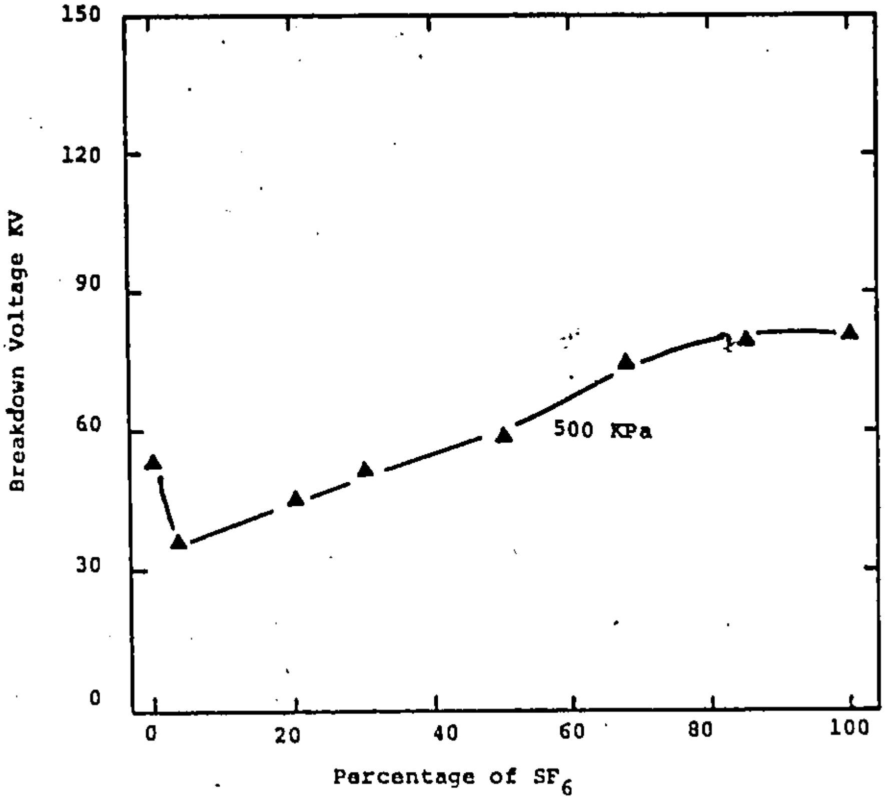

Figure 6.8 - Breakdown voltage-mixture ratio characteristics for a 20 mm rod-plane gap using 1 mm diameter rod anode.

lower than that of pure nitrogen at such high pressures. Similar behavior has also been observed[7, 17] under the applications of positive impulse voltages. Cookson and Wootton [18] have also reported that the 60 Hz breakdown voltage of SF_6-N_2 mixtures with SF_6 content below 20% is lower than that of pure nitrogen at a total pressure of 780 kPa for a 75 mm parallel plane gap in the presence of 6.4 mm long and 0.4 mm in diameter copper particles.

The breakdown characteristics of SF_6-N_2 mixtures weresimilar for the other gaps investigated. Figure 6.9 shows the breakdown voltage as a function of the mixture ratio for a 40 mm rod-plane gap using 1 mm rod anode. The characteristics are similar in every respect to those of a 20 mm gap as already discussed (figure 6.7 and 6.8).

6.4. The Spark Trajectory Studies

In addition to the breakdown voltage measurements, a study of the spark trajectories of SF_6, N_2 and SF_6-N_2 mixtures was carried out. Such a study has provided useful information in the past [11,13,19]. For various gaps investigated, the spark paths were mostly straight and were relatively unaffected by the gas pressure in the case of pure nitrogen. The trajectories in SF_6 and SF_6-N_2 mixtures were similar to each other and were affected by the total gas pressure. For SF_6 and all its mixtures, the spark paths are relatively straight in the pressure region A defined in figure 6.1. In this region, the breakdown voltage increases almost linearly with pressure. In region B, where the breakdown voltage is a non-linear function of the gas pressure, the spark trajectories exhibit a pronounced curvature. In region C, the breakdown sparks corresponding to the upper breakdown level have a pronounced curvature. The trajectories were relatively straight when the breakdown occurred

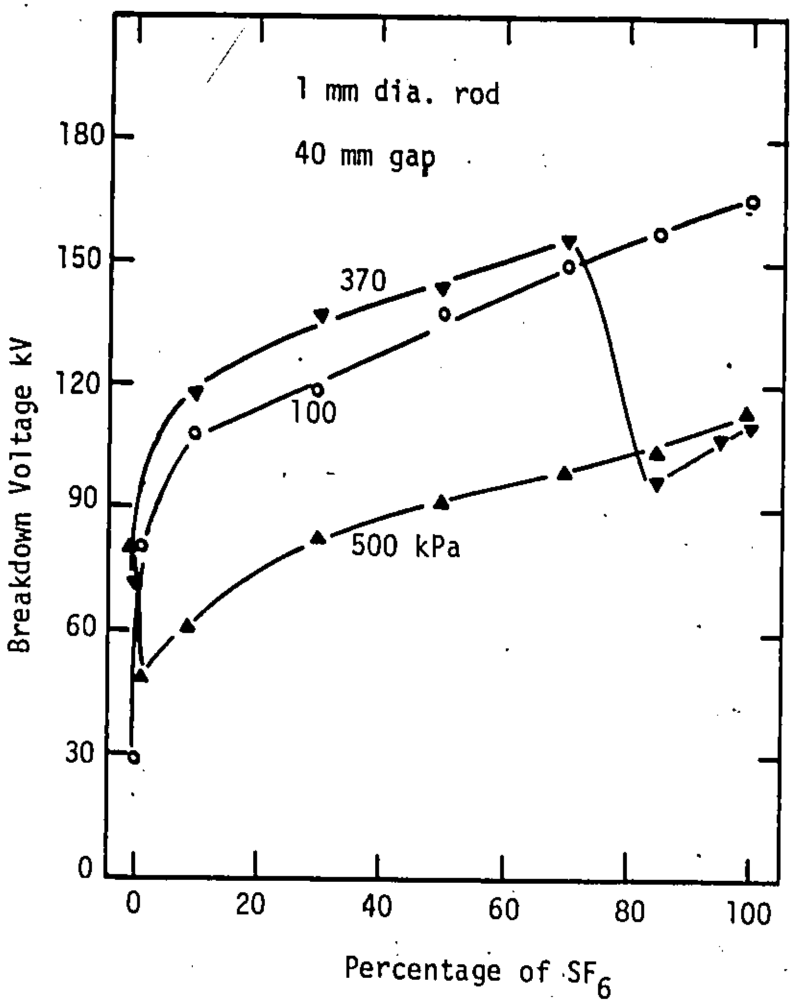

Figure 6.9 - Breakdown voltage-mixture ratio characteristics for a 40 mm rod-plane gap.

at the lower voltage level. In region D and E, the spark paths were generally straight. Figure 6.10 shows the spark channels for a 50%, SF_6-N_2 mixtures at different gas pressures for a 20 mm gap and 1 mm rod anode. The breakdown voltage-pressure characteristics for this gap have already been discussed in figure 6.4. It is interesting to note the spark paths corresponding to the discontinuity pressure of 420 kPa for the two different breakdown voltage levels. The picture for the upper breakdown voltage of 89.1 kV represents three consecutive sparks under similar test conditions.

6.5. Discussion

The prebreakdown studies of positive rod-plane gaps presented in the previous chapter confirm the earlier [11,13] findings that the corona discharge in SF_6 insulated gaps is a streamer phenomenon from the inception to the breakdown level. The present investigations show that SF_6-N_2 mixtures having SF_6 content higher than 1% exhibit a prebreakdown and breakdown behavior which is very similar to that of pure SF_6. In mixtures, the corona activity is a streamer phenomenon and the breakdown voltage-pressure characteristics show all the features observed in pure SF_6 as discussed in the previous sections.

In Figure 6.1, the breakdown voltage levels are much higher than the corona onset levels in regions A and B. As corona streamers advance in the gap in succession, they emit photons which can excite or ionize the gas molecules. The positive ions generated in the streamers drift towards the cathode. The electrons produced in the high field region are quickly drawn into the anode. However, the electrons generated in the low field region due to photoionization of the gas molecules will attach to the SF_6 molecules forming negation ions. These negative ions can suffer field induced detachments if the ratio $E/p \geq 0.9$ kV/kPa cm[20].

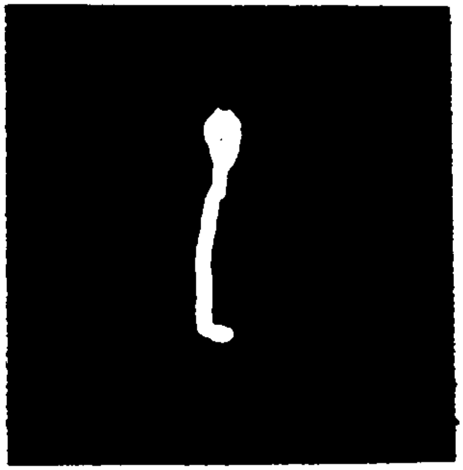

P = 100 kPa, V = 73 kV

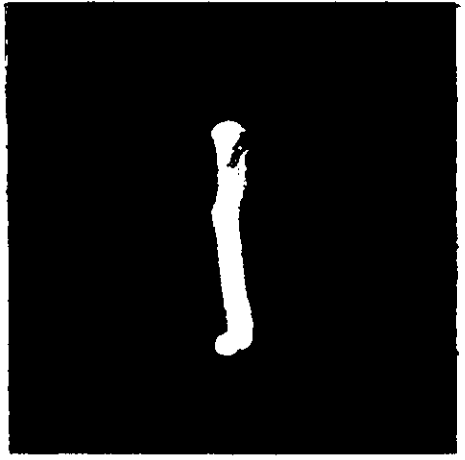

P = 200 kPa, V = 105 kV

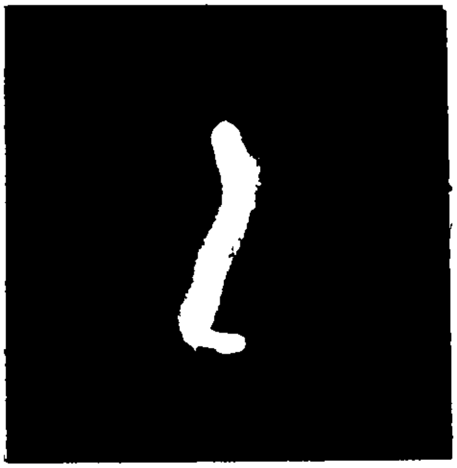

P = 235 kPa, y = 110.5 kV

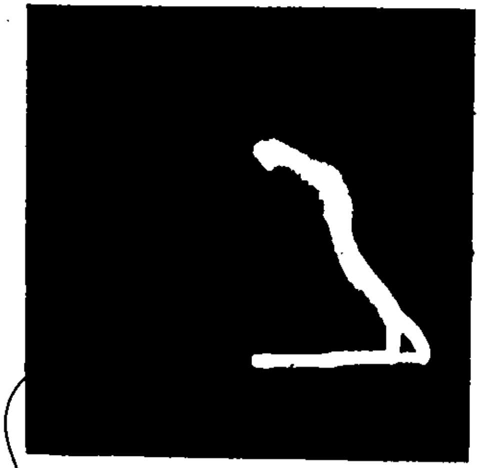

P = 270 kPa, y = 104.8 kV

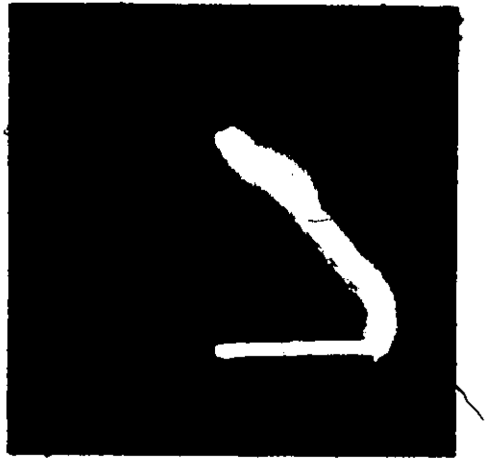

P = 300 kPa, V = 94.8 Kv

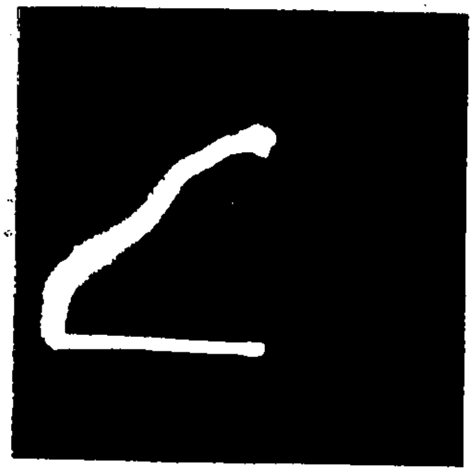

P = 335 kPa, y = 90.2 kV

Figure 6.10 -- continued.

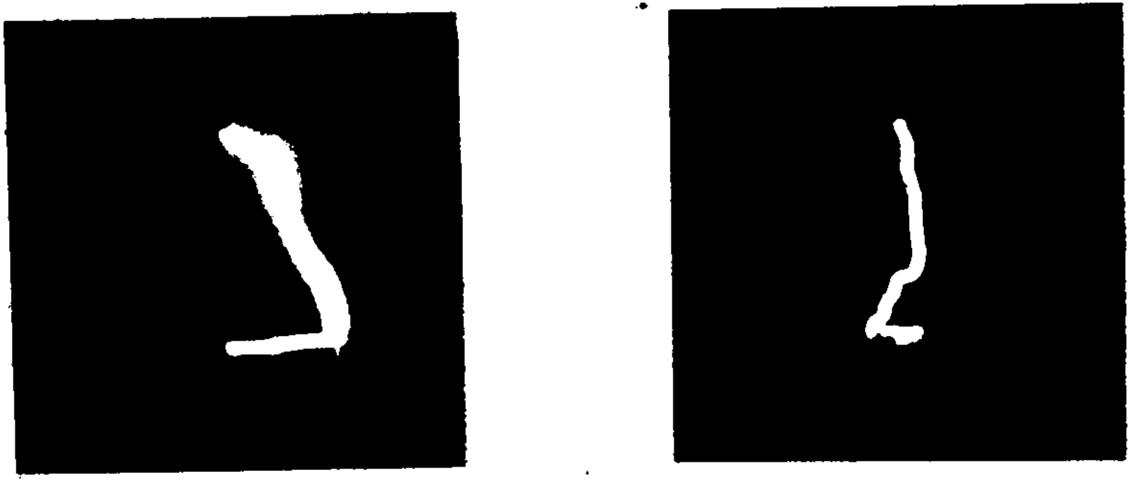

P = 400 kPa, V = 89.7 kV

P = 420 kPa, V = 55 kV

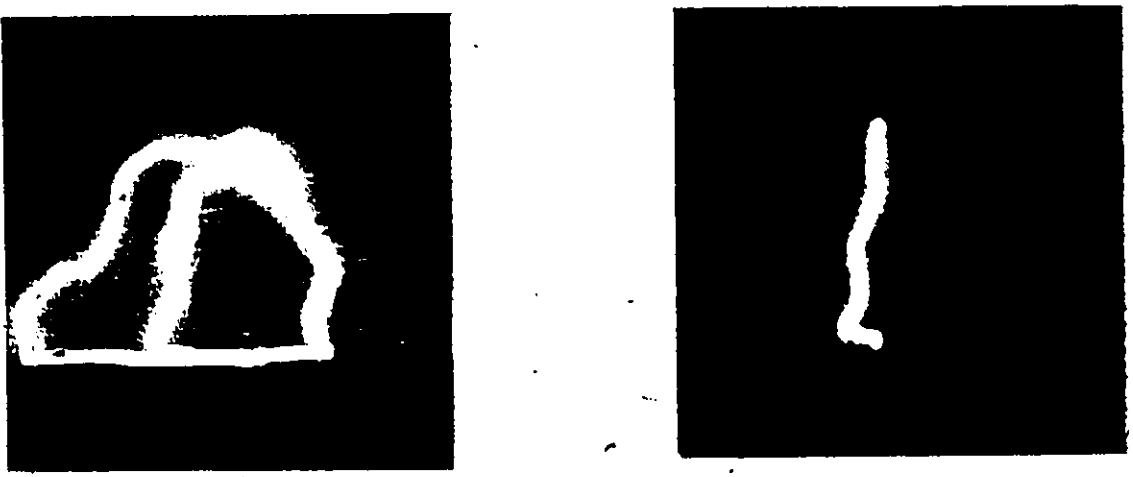

P = 420 kPa, V = 89.1 kV

P = 500 kPa, V = 58 kV

Figure 6.10 - Spark trajectories for a 20 mm positive rod-plane gap filled with a 50 % SF_6-N_2 mixture. Diameter of the rod electrode is 1 mm.

The maximum field strength for a 20 mm gap using 1 mm diameter rod is about 22.5 times the average field in the gap [21]. Using the corona onset levels given in figure 5.9, it is seen that the maximum field in the space charge free gap is always ≥ 1.50 kV/kPa cm. For example, for a 50% SF_6-N_2 mixture, the field at the anode tip is roughly 2.20 kV/kPa cm corresponding to the onset level given in figure 5.9. Thus these negative ions can suffer detachment once they approach the high field region near the anode. If the rate of formation of the negative ions equals that at which they are being removed on reaching the anode or by field induced detachment, then a stable negative ion space charge results which enhances the field near the anode. This negative ion space charge and the positive ion space charge drifting towards the cathode creates a low field barrier outside the enhancement zone. Thus while the space charge enhances the propagation of streamers in the close proximity to the anode, it inhibits their propagation farther in the gap.

The study of the spark trajectories indicates that the breakdown sparks in region A are straight. Thus in this region, whenever a streamer, confined by the space charge is able to penetrate the low field barrier, a breakdown occurs. With increasing gas pressure, the lateral diffusion of the space charge is reduced and in region B, the low field paths which pass around this space charge region offer less resistance to the propagation of the streamers than the space charge barrier. Thus in this region, the breakdown is initiated by the streamers circumventing the space charge region. This would account for the decrease in the breakdown voltage when the gas pressure is increased in this region. The curvature of the spark trajectories in this region and the observations [22] that, the curvature of the breakdown sparks is changed if the space charge is shifted from near the anode tip by a transverse flow of the gas further support this hypothesis.

As the gas pressure is increased, the lateral diffusion of the electrons in the streamer tip is reduced. The photon absorption coefficient of the gas increases with increasing pressure and thus a greater percentage of the photons produced by the streamers is absorbed sufficiently close to the streamer tip to initiate secondary avalanches. This causes an increase in the space charge accumulation at the streamer tip which enhances the local field and thus the ability of the streamers to propagate. The space charge is localized to a higher degree at higher pressures as a result of the reduced diffusion of the electrons. This increases the electron-ion collision rate and in consequence increases the rate of photon generation and hence the avalanche production at the streamer tip. Furthermore, since the mean free paths of the ionizing photons are reduced at higher gas pressure, the probability of formation of a steady negative ion space charge to enhance the field near the anode tip decreases at high gas pressures. Thus the low field barrier becomes less effective and the ability of the streamers to propagate in the gap is enhanced. Therefore, in regions D and E no steady corona materializes and the breakdown takes place instead. This is consistent with the observation that the difference between the onset and the breakdown voltages decreases with increasing pressure in region D and ultimately reduces to zero in region E.

Region C is a transitional region between the corona stabilized and non stabilized breakdown. It is interesting to note that while conditions are favorable for corona streamers to propagate and bridge the gap at lower voltage levels, a breakdown and only a small increase in the electric field is enough to attain conditions necessary for a steady corona to materialize. Once this is achieved, the corona stabilization mechanism becomes effective and the gap breaks only if the voltage is raised substantially. In such cases, if the applied voltage is reduced gradually, a breakdown does not occur at a voltage corresponding to the lower breakdown voltage level. This is because steady corona is present and the space charge due to this steady corona discharge inhibits the streamer propagation into the gap to produce a breakdown.

The width of the pressure region in which breakdown is corona stabilized in SF_6 is related to the range of photons which are capable of causing photoionization or photo-detachments, processes which are necessary to maintain the sustained corona discharges near the anode. The increase in the width of the stabilization region in SF_6-N_2 mixtures shown in figure 6.6 suggests that the mean free path of such photons is increased in the mixtures. This is consistent with the measurements of Blair et al [23]. Furthermore, since more light is emitted in SF_6-N_2 mixtures during the corona discharges, it appears that the range of the photons capable of causing photoionization or photo-detachments in the mixtures is larger than for the photons of high energy required in pure SF_6. Consequently the photoionization or photo-detachment in the low field regions is more effective in SF_6-N_2 mixtures than that in pure SF_6. Therefore, the effective radius of the ion cloud is larger in the mixtures than that in SF_6 resulting in a more effective corona stabilization process in SF_6-N_2 mixtures. Our measurements indicate that the breakdown voltage of 85% SF_6-N_2 mixture for a 20 mm gap is practically the same as that of pure SF_6 over most of the pressure range while it is greater than that of pure SF_6 in some pressure regions. For gaps larger than 20 mm, this gap has a higher breakdown voltage than that of pure SF_6 over most of the pressure range.

CHAPTER VII

THEORETICAL ANALYSIS OF THE DISCHARGE CHARACTERISTICS

7.1. Breakdown Mechanisms in SF_6

Under normal conditions a gas is almost a perfect insulator. However, some free electrons and ions are always present due to ionization processes. Under the influence of an applied electric field, the free electrons may gain sufficient energy to ionize a neutral gas molecule on collision. The number of electrons thus produced in the path of a single electron travelling a unit distance in the direction of the applied electric field is known as the Townsend first ionization coefficient α. Several types of ionization processes in SF_6 have been suggested [24]. The following reaction requires the lowest electron energy of 15.9 eV to ionize a gas molecule upon impact[25];

$$SF_6 + e \longrightarrow (SF_6^+)^* + 2e \longrightarrow SF_5^+ + F + 2e \tag{7.1}$$

In SF_6, negative ions are formed when either a low energy electron attaches itself to a neutral gas molecule resulting in a "direct attachment", or when it attaches to one of the constituents of the molecule after dissociation resulting in a "dissociative attachment". Previous studies have indicated that SF_6^- and SF_5^- are the predominant negative ions resulting from electron collisions, exceeding other possible negative ions such as F^-, F_2^-, SF_2^-, SF_3^-, and SF_4^- at least by a factor of one hundred [26-28]. The formation of the majority of SF_6^- ions is initiated by the reaction [26, 28];

$$SF_6 + e \longrightarrow (SF_6^-)^{*1} \tag{7.2}$$

where $(SF_6^-)^{*1}$ is a metastable ion with a lifetime of the order of 10μsec. This reaction is a resonance capture process with a maximum cross-section of 10^{-15} cm^2 at an electron energy of 0.05 eV. There are several possible reactions subsequent to (7.2). Some of them are

$$(SF_6^-)^{*1} \longrightarrow SF_6 + e \qquad (7.3)$$

$$(SF_6^-)^{*1} + (SF_6)_o \rightarrow (SF_6^-)_o + (SF_6)_v \qquad (7.4)$$

$$(SF_6^-)^{*1} + (SF_6)_o \rightarrow (SF_6)_o + (SF_6^-)_v \qquad (7.5)$$

Reaction (7.3) is called "autodetachment". Reactions (7.4) and (7.5) involve a collision with a neutral gas molecule and the resulting negative ion is termed as a "collision stabilized ion". Subscripts o and v refer to zero order and excited vibrational states respectively. Reaction (7.5) is the more probable of the last two reactions.

The formation of the majority of SF_5^- ions follows a somewhat similar process. Initially a metastable ion is formed by the reaction

$$SF_6 + e \longrightarrow (SF_6^-)^{*2} \qquad (7.6)$$

The lifetime of $(SF_6^-)^{*2}$ is exceedingly short and as such, the following subsequent reaction almost invariably occurs.

$$(SF_6^-)^{*2} \longrightarrow SF_5^- + F \qquad (7.7)$$

The attachment processes in SF_6 are described by the electron attachment coefficient η, which is the number of attachments produced in the path of an electron travelling a unit distance under the influence of the applied electric field. Both these coefficients, α and η, are strongly dependent on the applied electric field [1].

There are a number of possible inelastic collisions which do not increase the ion population but play a significant role in the overall determination of the discharge properties of the gas. Equally significant are the dissociation reactions which produce both a positive and a negative ion such as

$$SF_6 + e \longrightarrow SF_5^+ + F^- + e \qquad (7.8)$$

The increase dN in the number of electrons along the path dx in the direction of the applied electric field due to the combined ionization and attachment processes is given by:

$$dN = N(\alpha-\eta)dx \tag{7.9}$$

where N is the initial number of electrons. For $\alpha > \eta$, equation (7.9) leads to an exponential growth of the electron population, eventually resulting in the breakdown of the insulation.

Two types of breakdown mechanisms are generally used to describe the breakdown processes in gases. According to the "Townsend Mechanism", a succession of electron avalanches initiated at the cathode causes a breakdown of the gas. Under non-uniform field conditions, the number of electrons N at the anode compared to the initial electrons N_0 at the cathode can be written as [1]

$$\frac{N}{N_o} = \frac{1 + \int_o^d \exp[\int_o^x (\alpha-\eta)dx]\ \alpha dx}{1 - \gamma\int_o^d \exp[\int_o^x (\alpha-\eta)dx]\ \alpha dx} \tag{7.10}$$

where the secondary ionization coefficient γ is the number of secondary electrons for each primary electron produced as a result of ionizing processes such as electron emission from the cathode by positive ion bombardment or photoelectric emission from the cathode.

Thus the Townsend criterion for breakdown in non-uniform field gaps is derived from equation (7.10) as

$$\gamma \int_o^d \exp[\int_o^x (\alpha-\eta)dx]\ \alpha dx = 1 \tag{7.11}$$

Equation (7.11) can be modified for application to uniform field gaps as

$$\frac{\gamma\alpha}{\alpha-\eta}\,[\exp(\alpha-\eta)d - 1] = 1 \tag{7.12}$$

The Townsend breakdown criterion of equation (7.11) or (7.12) is of little use to the high voltage design engineer because the secondary ionization coefficient γ is a very sensitive function of the electrode surface condition and the degree of gas purity. Measurements of γ have so far been made only at pressures below 3.4 kPa [1] and these values are not valid for pressures of technical importance. It is therefore difficult to apply the Townsend criterion in a meaningful way to engineering problems. Furthermore, the Townsend mechanism is unable to explain the breakdown under steep voltage surges in some cases.

In the streamer mechanism it is assumed that the growth of a single electron avalanche becomes unstable before reaching the anode. This results in the formation of fast moving streamers from the avalanche head. These streamers form a highly conducting channel across the gap, which ultimately causes the collapse of the applied voltage. The basic mechanism behind the formation of these streamers is assumed to be the photoionisation in the gas. Though a satisfactory quantitative theory for the streamer formation has not been formulated, Meek [29] developed the following criterion for streamer formation in non-uniform field gaps;

$$(\alpha-\eta)_x \exp\left[\int_0^x (\alpha-\eta)dx\right] = K_1 \; E_x \left[\frac{x}{\rho}\right]^{0.5} \qquad (7.13)$$

In this equation, x denotes the avalanche length at the moment when streamers are formed. $(\alpha-\eta)_x$ is the apparent Townsend first ionization coefficient at the avalanche head, ρ is the gas density and K_1 is a constant. A similar equation was proposed independently by Raether [30] who suggested that a critical number, 10^8, of charge carriers is necessary to transform an avalanche into a streamer. Meek's equation was modified by Pedersen [31-32] to obtain the following well known streamer criterion;

$$\int_0^{x_c} (\alpha-\eta)dx = K \qquad (7.14)$$

where x_c is the critical avalanche length which is the distance between the highly stressed electrode and the point in the electrode gap where $\alpha = \eta$, and K is a constant. The limiting case of the streamer criterion is obtained by setting K = 0 in equation (7.14) which gives

$$\int_0^{x_c} (\alpha - \eta)dx = 0 \tag{7.15}$$

Thus the limiting value of the breakdown strength in SF_6 is obtained by setting

$$\alpha = \eta \tag{7.16}$$

which is satisfied at a threshold value of the field intensity. This value of the field intensity is referred to as the "critical" or the "limiting" field intensity in $(E/p)_{lim}$. Its value for SF_6 at normal atmospheric pressure is 89.5 kV/cm. Since, for $\alpha < \eta$ an electron avalanche should not grow in an electronegative gas, $\alpha = \eta$ sets the threshold condition for the growth of electron avalanches. In a practical case an electron avalanche will grow when α is slightly greater than η.

7.2. Streamer Breakdown Criterion for SF_6

The streamer breakdown criterion of equation (7.14) can be used to determine the lowest possible voltage which can cause a breakdown in SF_6. Both the ionization and the attachment coefficients α and η are affected by the applied electric field. According to the measurements reported in the literature [33-37] the values of $\frac{\alpha}{p}$ and $\frac{\eta}{p}$ can be approximated in the vicinity of the region where $\frac{\alpha}{p} = \frac{\eta}{p}$ by the following relationships:

$$\frac{\alpha}{p} = 23(E/p) - 12.34 \quad (\text{kPa cm})^{-1} \tag{7.17}$$

$$\frac{\eta}{p} = -4(E/p) + 11.35 \quad (\text{kPa cm})^{-1} \tag{7.18}$$

Thus the following expression can be used for the effective ionization coefficient $\bar{\alpha}$;

$$\frac{\bar{\alpha}}{p} = \frac{\alpha-\eta}{p} = \beta[(E/p) - (E/p)_{lim}] \quad (\mathrm{kPa\ cm})^{-1} \tag{7.19}$$

where $\beta = 27\ \mathrm{kV}^{-1}$ and $(E/p)_{lim}$ is 877.5 $\mathrm{V(kPa\ cm)}^{-1}$ for pure SF_6. Here E[kV/cm] denotes the applied electric field and p[kPa], the SF_6 pressure referred to at a temperature of 20°C.

Using equation (7.19), the streamer breakdown criterion of equation (7.14) can be expressed as

$$\beta[\int_o^{x_c} E(x)dx - p \bullet x_c \bullet (E/p)_{lim}] = K \tag{7.20}$$

Thus in order to evaluate the left hand side of equation (7.20), a detailed knowledge of the electric field distribution in the gap is required.

In a uniform field gap E(x) is constant throughout the gap and x_c is equal to the gap length d. The breakdown voltage V_d in a uniform field gap, as obtained from equation (7.20), is therefore given by

$$V_d = E \bullet d = \frac{K}{\beta} + \left(\frac{E}{p}\right)_{lim} \bullet p \bullet d \tag{7.21}$$

For uniform or nearly uniform field gaps, the streamer formation directly grows to a breakdown. However, in non-uniform field gaps, it is not always the case. In such gaps, the streamers develop into a steady corona discharge at low pressures. As discussed in the previous chapters, the breakdown voltage is substantially higher than the corona inception level due to the stabilization effects of the corona generated space charges. In such cases, therefore, the criterion for streamer formation corresponds to the corona inception.

In a non-uniform field gap, the critical avalanche length x_c is generally a very small fraction of the total gap length d. Therefore the electric field in the region of interest, i.e., in the vicinity of the highly stressed electrode along its axis of symmetry, can be approximated by [38].

$$E(x) = \frac{E_{max}}{\left(1 + \frac{x}{R}\right)^2} \tag{7.22}$$

where E_{max} is the maximum field in the gap, i.e., the field at the tip of the highly stressed electrode and

$$\frac{1}{R} = \frac{1}{2} \left[\frac{1}{R_1} + \frac{1}{R_2}\right] \tag{7.23}$$

where R_1 and R_2 are the radii of curvature of the highly stressed electrode in two directions mutually orthogonal to each other.

The critical avalanche length x_c can be determined from equation (7.22). Since $\left(\frac{E}{p}\right)_{lim} = \frac{E(x_c)}{p}$, the value of x_c is therefore given by;

$$x_c = R \left[\sqrt{\frac{E_{max}}{\left(\frac{E}{p}\right)_{lim} \bullet p}} - 1\right] \tag{7.24}$$

Substitution of equations (7.22) and (7.24) into equation (7.20) yields;

$$\beta R \left[\sqrt{E}_{max} - \sqrt{\left(\frac{E}{p}\right)_{lim} \bullet p}\right]^2 = K \tag{7.25}$$

Therefore, the maximum electric field strength at breakdown is given by;

$$\frac{E_{max}}{p} = \left(\frac{E}{p}\right)_{lim} \left(1 + \frac{C_1}{\sqrt{pR}}\right) \tag{7.26}$$

where the constant C_1 is calculated from

$$C_1 = \sqrt{\frac{4 \bullet K}{\beta \bullet (E/p)_{lim}}} \tag{7.27}$$

Using the field utilization factor $u = \frac{E_{av}}{E_{max}}$ i.e., the ratio of the average field E_{av} and the maximum field E_{max}, the discharge voltage for a non-uniform field gap insulated with SF_6 can be expressed as

$$V_d = E_{av} \bullet d = E_{max} \bullet u \bullet d \tag{7.28}$$

Using E_{max} as given in equation (7.26), equation (7.28) can be written as

$$V_d = \left(\frac{E}{p}\right)_{lim} \bullet u \bullet p \bullet d \bullet \left(1 + \frac{C_1}{\sqrt{pR}}\right) \tag{7.29}$$

Thus equations (7.21) and (7.29) give the minimum discharge inception voltages for uniform and non-uniform field gaps insulated with compressed SF_6 [38]. These expressions are for electrodes with smooth surfaces. The influence of electrode surface roughness can be introduced in the calculations as suggested by Pederson [39-40] and will be discussed later.

7.3. Streamer Breakdown Criterion for SF_6-N_2 Mixtures

Equation (7.14) can be used to formulate a breakdown criterion for SF_6-N_2 gas mixtures if the effective ionization coefficient is known for the mixtures. However, to our knowledge such measurements have not been reported in the literature. On the other hand, the values of the ionization coefficient for pure nitrogen have been reported in the literature and are approximated by the expression [40-41]

$$\frac{\alpha}{p} = A \exp\left(- \frac{B}{(E/p)}\right) \tag{7.30}$$

where $A = 66\ (\text{kPa cm})^{-1}$ and $B = 2.15\ \text{kV}\ (\text{kPa cm})^{-1}$.

The possibility of calculating the ionization and attachment coefficients of gas mixtures has been discussed in several reports [42-44] from the respective values of these coefficients for pure gases. Ermel [42] assumed that the ionization coefficient for a two component gas mixture, α_m, can be represented by

$$\frac{\alpha_m}{p} = \left[\left(\frac{\alpha}{p}\right)_1^1 + y\left(\frac{\alpha}{p}\right)_2^1\right] \Big/ (1 + y) \qquad (7.31)$$

where $y = \frac{p_2}{p_1}$ is the partial pressure ratio of the two constituents gases, while $\left(\frac{\alpha}{p}\right)_1^1 = f_1(E/p)$ and $\left(\frac{\alpha}{p}\right)_2^1 = f_2(E/p)$ are the ionization coefficients for the individual gases when mixed. If there are any gas interactions, $\left(\frac{\alpha}{p}\right)_1^1$ and $\left(\frac{\alpha}{p}\right)_2^1$ will differ from the pure gas values $\left(\frac{\alpha}{p}\right)_1$ and $\left(\frac{\alpha}{p}\right)_2$ and equation (7.31) will not be valid. In such cases the ionization coefficients can be obtained only by actual measurements. A similar argument applies for the attachment coefficient. If gas interactions are neglected, the effective ionization coefficient for a two component gas mixture is assumed to be approximated by

$$\frac{\bar{\alpha}_m}{p} = \frac{(\alpha_m - \eta_m)}{p} = \left[\left(\frac{\bar{\alpha}}{p}\right)_1 + y\left(\frac{\bar{\alpha}}{p}\right)_2\right] \Big/ (1 + y) \qquad (7.32)$$

Assuming that equation (7.32) is valid for SF_6-N_2 mixtures, their effective ionization coefficients can be calculated using equations (7.19), (7.30) and (7.32). The values of these coefficients are thus given by

$$\frac{\bar{\alpha}_m}{p} = Z\,\beta[(E/p) - (E/p)_{lim}] + (1 - Z)A\exp\left(-\frac{B}{(E/p)}\right) \qquad (7.33)$$

Here, p is the total gas pressure and $Z = \frac{p(SF_6)}{p}$ is the partial pressure ratio of SF_6. Figure 7.1 contains the values of $\frac{\bar{\alpha}_m}{p}$ as functions of (E/p) for several SF_6-N_2 mixtures. As can be seen, for mixtures having $Z \geq 5\%$, $\frac{\bar{\alpha}_m}{p}$ is almost a linear function of (E/p) in the region of interest, that is, where $\alpha_m = \eta_m$. Although $\frac{\bar{\alpha}_m}{p}$ is not a linear function of (E/p) in this region for mixtures having $1\% \leq Z \leq 5\%$, it can be assumed to be approximately linear in the narrow range of $0 \leq \frac{\alpha_m}{p} \leq 4$ (kPa cm)$^{-1}$, resulting in a negligible error in the calculations. Therefore for SF_6-N_2 mixtures with $1\% \leq Z \leq 100\%$, the effective ionization coefficient can be expressed as [6]

$$\frac{\bar{\alpha}_m}{p} = \beta_m \left[(E/p) - (E/p)^1_{lim}\right] ; \tag{7.34}$$

where $\beta_m = f_1(Z)$ and $(E/p)^1_{lim} = f_2(Z)$ are constants for a particular mixture ratio. The values of β_m and $(E/p)^1_{lim}$ are given in Table 7.1. From this table it is clear that even for mixtures with 5% $SF_6 (Z = 0.05)$, β_m is considerably higher than that in common gases such as air, nitrogen, ect. Therefore the assumptions made in deriving equations (7.21) and (7.29) are valid for SF_6-N_2 mixtures. Thus it is proposed that the discharge inception voltages for SF_6-N_2 mixtures can be expressed as

$$V_d = \frac{K_m}{\beta_m} + (E/p)^1_{lim} \bullet p \bullet d \tag{7.35}$$

in uniform field gaps and

$$V_d = (E/p)^1_{lim} \bullet u \bullet p \bullet d \bullet \left(1 + \frac{C_m}{\sqrt{pR}}\right) \tag{7.36}$$

in non-uniform field gaps. Here

$$C_m = f_3 \ (Z) = \sqrt{\frac{4 \bullet K_m}{\beta_m \bullet (E/p)^1_{lim}}} \tag{7.37}$$

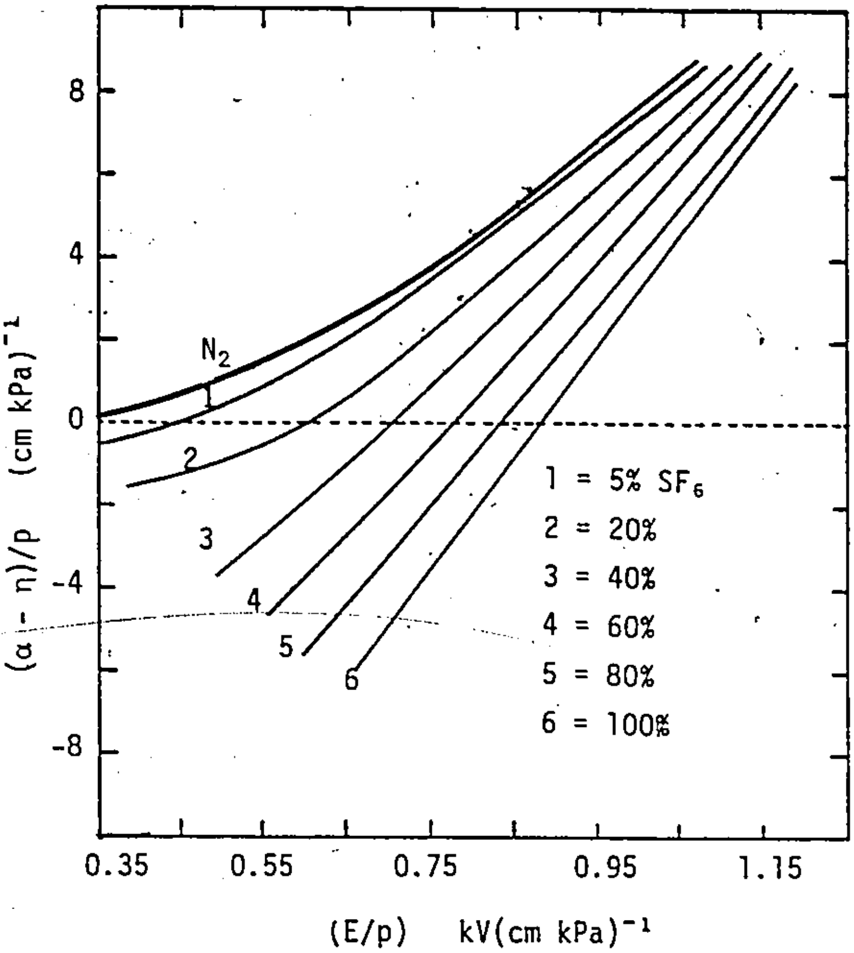

Figure 7.1 - Effective ionization coefficients for SF_6-N_2 mixtures.

TABLE 7.1

Variations of β_m, $(E/p)^1_{lim}$ and C_m with SF_6 Content for SF_6-N_2 Mixtures

$Z = \frac{p(SF_6)}{p}$ %	β_m kV^{-1}	$\left(\frac{E}{p}\right)^1_{lim}$ $V(kPa\ cm)^{-1}$	$C_m (kPa\ cm)^{\frac{1}{2}}$
100	27	877.5	1.33
95	26.44	866.6	1.35
90	25.87	855.4	1.37
85	25.29	843.6	1.40
80	24.69	831.4	1.43
75	24.08	818.8	1.46
70	23.47	804.9	1.49
65	22.79	790.9	1.52
60	22.10	775.4	1.55
55	21.40	759.5	1.59
50	20.60	742.4	1.64
45	19.80	724.0	1.68
40	19.08	704.2	1.73
35	17.95	682.8	1.80
30	16.86	658.9	1.87
25	15.63	632.3	1.96
20	14.20	602.1	2.10
15	12.5	566.4	2.29
10	10.5	521.0	2.56
5	8.0	439.2	3.10
1	5.0	350.0	3.70

The value of the constant K_m can be found from the expression [40]

$$\bar{\alpha}_m (E_s) \bullet d = K_m \tag{7.38}$$

where E_s is the measured value of the 'Paschen curve' breakdown field strength. From experimental data, it is found that $K(SF_6) = 10.5 \pm 3$ [45-46]. A similar analysis for pure nitrogen utilizing values of α obtained from equation (7.30) and the uniform field breakdown voltages reported by CIGRE [47] shows that the value of K for nitrogen lies between 5 and 8. Therefore, it is safe to assume that $K_m \leq K(SF_6)$. Using this assumption in equation (7.37), the resulting values of the constant C_m are given in Table 7.1. Thus equations (7.35) and (7.36), along with the values of constants β_m, C_m and $(E/p)^1_{lim}$ as given in Table 7.1, can be used to calculate the minimum discharge inception voltages for uniform and non-uniform field gaps insulated with SF_6-N_2 gas mixtures having SF_6 contents between 1% and 100% by pressure.

Figure 7.2 shows the variations in $(E/p)^1_{lim}$ when the gas mixture ratio is changed. The value of $(E/p)^1_{lim}$ for a 0.1% mixture is roughly 260 $V(kPa\ cm)^{-1}$. Figure 7.2 shows that the addition of the first 5% of SF_6 increases this value to 440 $V(kPa\ cm)^{-1}$. However, further increase of SF_6 from 5 to 50% increases the limiting value of the field strength to about 740 $V(kPa\ cm)^{-1}$. A still further increase of the SF_6 content from 50 to 100% increases this value to only 877.5 $V[cm\ kPa]^{-1}$. Thus the addition of the first few parts percent of SF_6 increases the value of $(E/p)^1_{lim}$ considerably and any further increase of SF_6 content in the mixture, though causes an increase in $(E/p)^1_{lim}$, but not with a similar effectiveness, producing in this manner a "saturation tendency" in the $(E/p)^1_{lim}$ - mixture ratio characteristics. When (E/p) is less than $(E/p)^1_{lim}$, α is less than η in electronegative gases and their mixtures,

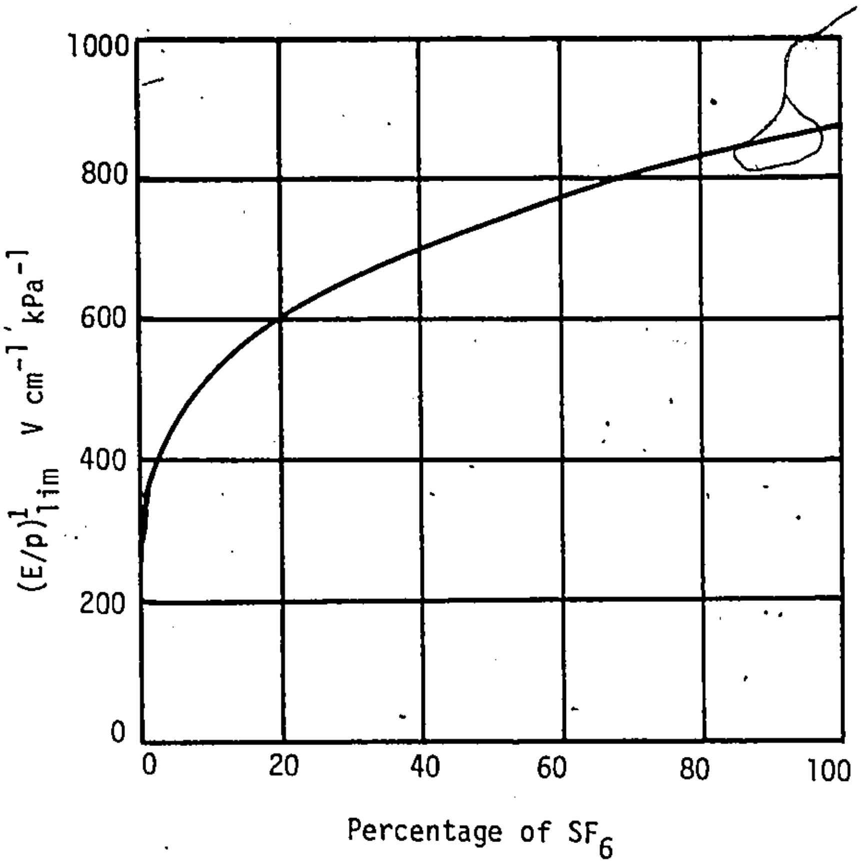

Figure 7.2 - Variation of $\left(\frac{E}{p}\right)^1_{lim}$ with gas mixture ratio.

and the electron avalanches cannot grow. Thus $\alpha = \eta$ sets the threshold condition for the growth of electron avalanches and $(E/p) = (E/p)^{1}_{lim}$ gives the limiting value of the field strength which can cause a breakdown in the uniform field gaps [1]. Therefore the breakdown and corona onset voltages of SF_6-N_2 mixtures in uniform and non-uniform field gaps respectively as functions of the mixture ratio should display a behavior similar to that of figure 7.2. It is interesting to note the similarities between figure 7.2 and figures 3.11, 5.9 and 5.10 which were experimentally obtained for SF_6-N_2 gas mixtures.

7.4. The Electrode Surface Roughness Effects in SF_6-N_2 Mixtures

The electrode surface roughness can cause a considerable reduction of the threshold for breakdown in SF_6 insulated devices. The surface roughness causes localized microscopic regions in the gas near the electrodes with field strength much higher than the macroscopic average field. Depending on the gas pressure, such regions of enhanced field strength can result in a large reduction of the breakdown strength [1].

For perfectly smooth electrodes, the macroscopic breakdown field strength $\left(\frac{E}{p}\right)_o$ in a uniform field gap will be approximately equal to $\left(\frac{E}{p}\right)_{lim}$. However, the macroscopic breakdown field strength in a uniform field gap with surface defects will be lower than the limiting field strength according to [39,40];

$$\left(\frac{E}{p}\right)_o = \xi \left(\frac{E}{p}\right)_{lim} \qquad 0 < \xi < 1. \tag{7.39}$$

where ξ is the roughness factor which depends in a very complicated way upon the microscopic structure of the surface and a direct calculation of ξ is almost impossible. However, the basic quantities controlling ξ can be derived from a simple model consisting of a smooth plane with a hemispherical protrusion of radius R. Using the streamer breakdown criterion and taking into account the perturbed field along the axis of symmetry of the protrusion, Pedersen [39] has shown that the protrusion will have no effect on the breakdown field strength of SF_6 if

$$pR \leqslant \frac{K}{\beta\left(\frac{E}{p}\right)_{lim}\phi(\xi)} \tag{7.40}$$

in which

$$\phi(\xi) = 1 - 3\sqrt[3]{\frac{1}{4}\,\xi(1-\xi)^2} \tag{7.41}$$

The maximum value of the product PR which can be tolerated in SF_6 without loosing the dielectric strength due to the electrode surface roughness $(pR)_{SF_6}$ can be obtained from equation (7.40) by setting $\xi = 1$. Therefore $(pR)_{SF_6}$ is given by

$$(pR)_{SF_6} = \frac{K}{\beta\left(\frac{E}{p}\right)_{lim}} \tag{7.42}$$

The value of $(pR)_{SF_6}$ is approximately 4 kPa mm. From above, we propose that the maximum value of the product pR which may be tolerated in SF_6-N_2 mixtures can be expressed as

$$(pR)_{mix} = \frac{K_m}{\beta_m\left(\frac{E}{p}\right)^{1}_{lim}} \tag{7.43}$$

From equation (7.42) and (7.43), one can obtain the ratio of the maximum permissible product of gas pressure and protrusion height in SF_6-N_2 mixtures and that of pure SF_6. This can be expressed as

$$\frac{(pR)_{mix}}{(pR)_{SF_6}} = \frac{\left(\frac{E}{p}\right)_{lim} \bullet \beta}{\left(\frac{E}{p}\right)^{1}_{lim} \bullet \beta_m} \tag{7.44}$$

Equation (7.44) is obtained assuming $K_m \approx K(SF_6)$. Using equation (7.44) and the values of β_m and $(E/p)^1_{lim}$ as given in Table 7.1, one can calculate $(pR)_{mix}$. The expression given in equation (7.44) is plotted in figure 7.3 as a function of the percentage of SF_6. It is seen that a higher value of the product pR compared to that of pure SF_6 can be tolerated in SF_6-N_2 mixtures without losing the breakdown strength.

For values of product greater than those obtained from equations (7.42) and (7.43), the breakdown field strength is determined as follows:

$$(pR)^1_{SF_6} = \frac{K}{\beta(E/p)_{lim}\,\phi(\xi)} = \frac{K}{\beta(E/p)_{lim}\,\phi[(E/p)_o]} \tag{7.45}$$

for pure SF_6 and

$$(pR)^1_{mix} = \frac{K_m}{\beta_m \left(\frac{E}{p}\right)^1_{lim} \phi(\xi)} = \frac{K_m}{\beta_m \left(\frac{E}{p}\right)^1_{lim} \phi\left[\left(\frac{E}{p}\right)_o\right]} \tag{7.46}$$

for SF_6-N_2 mixtures.

Figure 7.4 shows the variations in the values of surface roughness factor ξ as a function of the variable "RATIO" which is defined as;

$$\text{RATIO} = \frac{(pR)^1_{SF_6}}{(pR)_{SF_6}} = \frac{(pR)^1_{mix}}{(pR)_{mix}} \tag{7.47}$$

Figure 7.5 shows the maximum value of the breakdown strength as a function of the product pR for SF_6 and SF_6-N_2 mixtures containing 20 and 50% SF_6. It is interesting to note that the breakdown field strength of a 50% mixture is almost 85% that of pure SF_6 for perfectly smooth electrodes. However, for a hemispherical protrusion of height 100 μm at a pressure of 500 kPa, the breakdown field strength of a 50% mixtures is about 94% that of pure SF_6. In SF_6 insulated cables, this maximum surface roughness is usually about 150 μm [48]. Therefore in such systems at pressures of technical importance, the breakdown strength of 50% mixture is expected

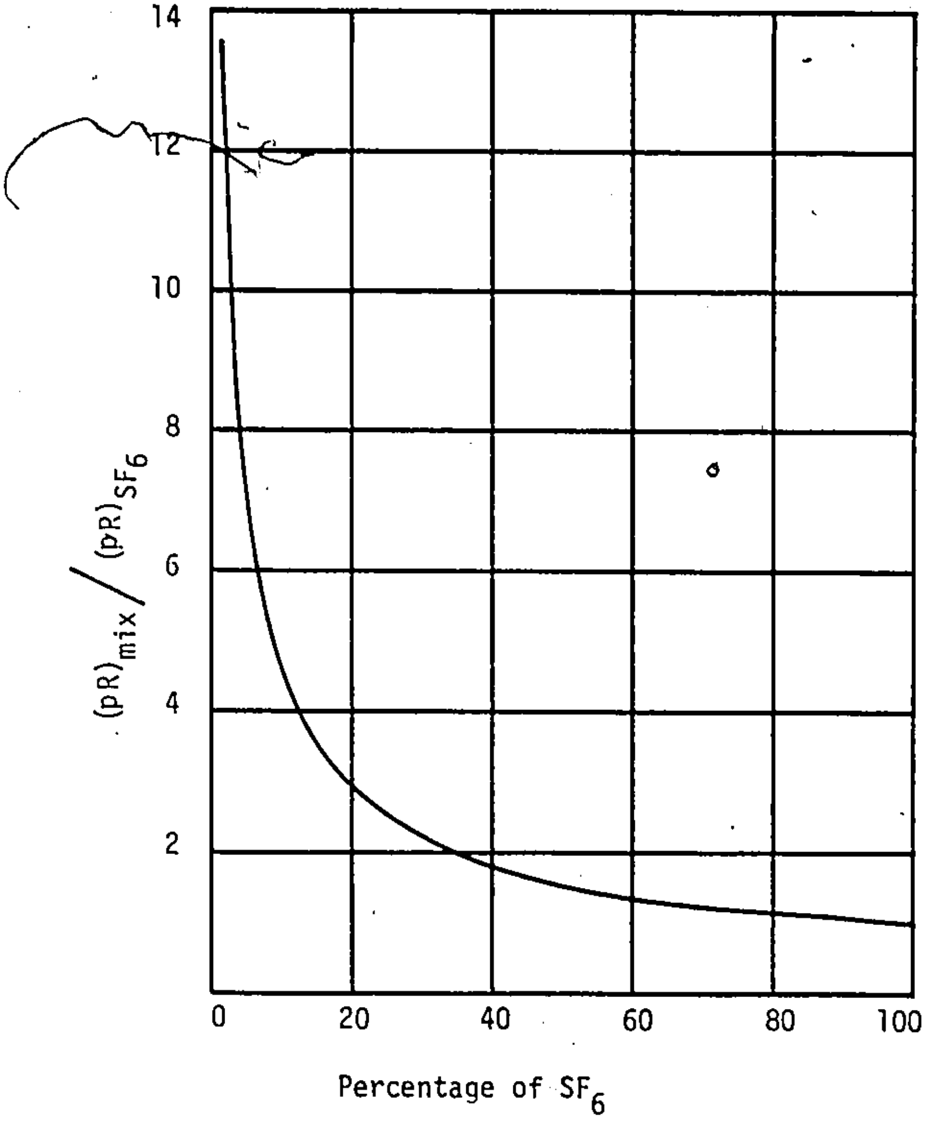

Figure 7.3 - Relative limits for the onset of surface roughness effects in SF_6-N_2 mixtures.

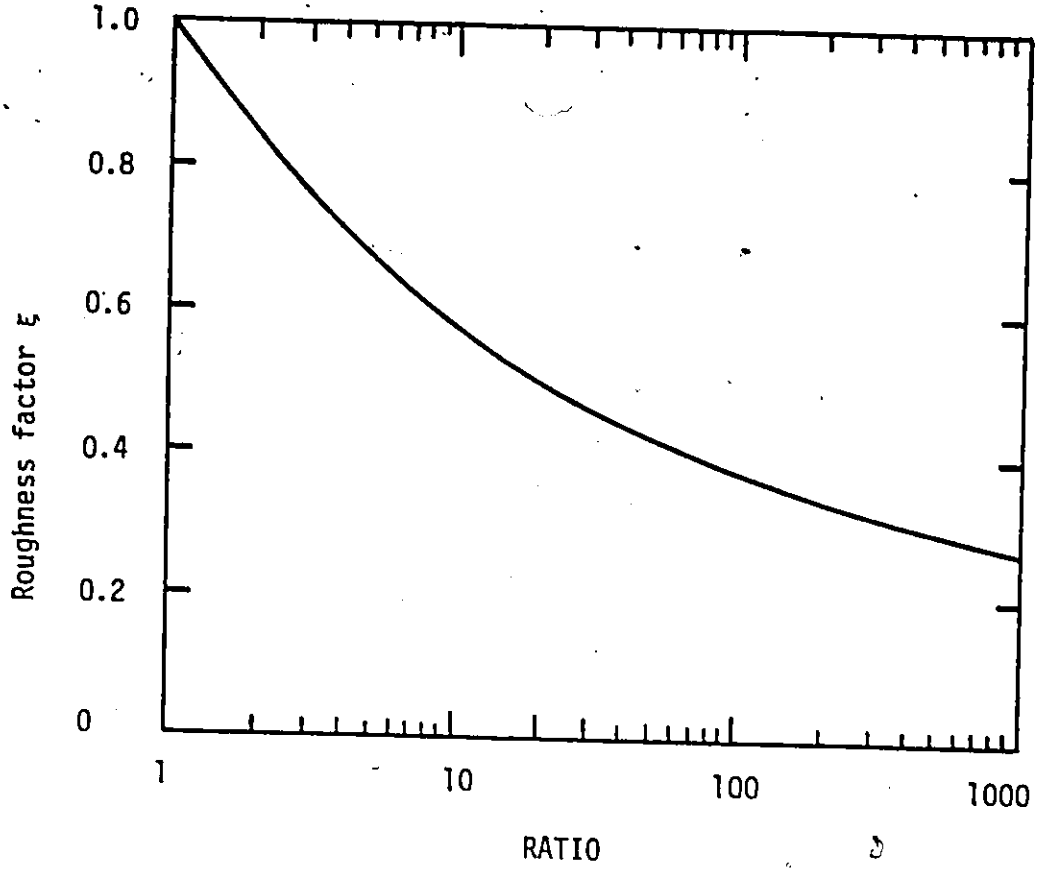

Figure 7.4 - Effect of the variable RATIO on surface roughness factor ξ for SF_6 and SF_6-N_2 mixtures.

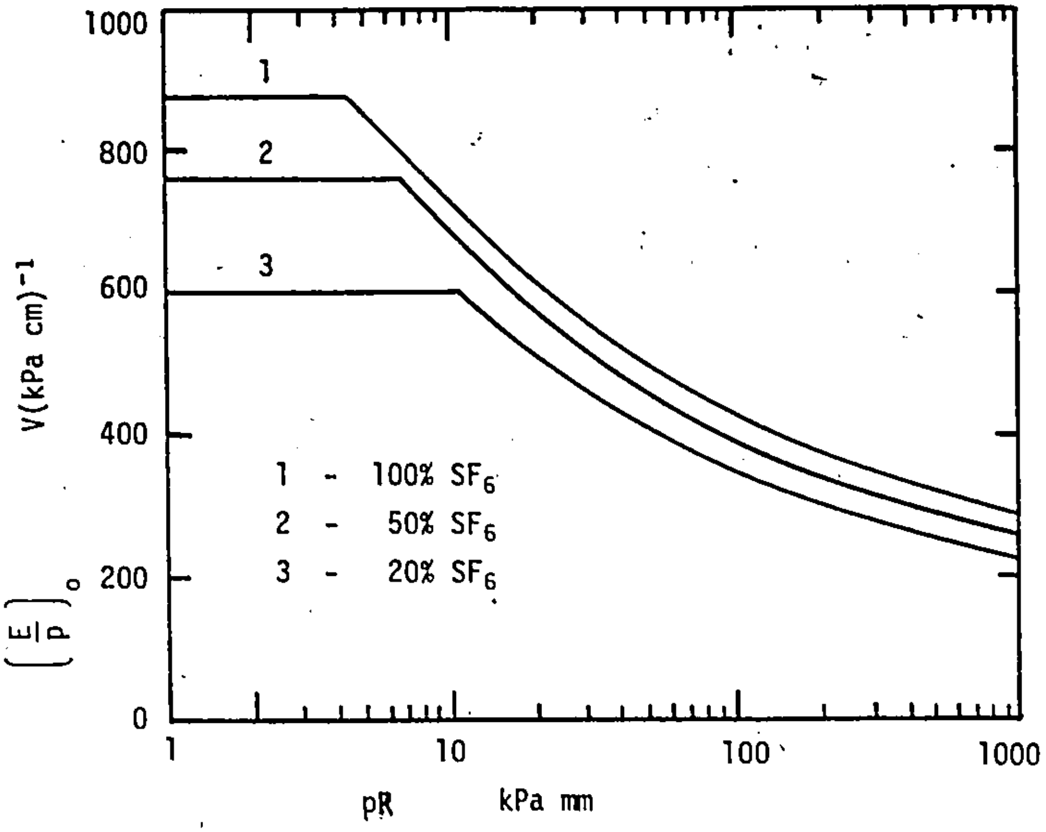

Figure 7.5 - Breakdown limitations in SF_6 and SF_6-N_2 mixtures from surface roughness. $(E/p)_o$ is the limiting value of the breakdown field strength for rough electrodes.

to be almost as high as that of pure SF_6. Thus the breakdown voltages of SF_6-N_2 mixtures are expected to be less sensitive to the electrode surface imperfections.

7.5. Comparison of Calculated and Measured Discharge Inception Voltages

(a) Plane-plane gaps

Uniform field breakdown voltage measurements for SF_6-N_2 mixtures have been reported in the literature by Pace et al [10], Ermel [42] and Wieland [43]. Using equation (7.35) we calculated the discharge inception voltages with parameters β_m and $\left(\frac{E}{p}\right)^{1}_{\lim}$ as given in Table 7.1. A good agreement was found between these and the measured values reported in the literature. The calculated values are shown in figure 7.6 as a function of the gas mixture ratio for different values of the product pd. The breakdown voltage levels measured by Wieland [43] are also included for comparison.

(b) Sphere gaps

Sphere-sphere and sphere-plane gaps are usually used to study the effect of small field non-uniformities on the breakdown voltage characteristics of compressed gases and and gas mixtures. Table 7.2 contains the field utilization factor u for sphere-sphere and sphere-plane gaps for different values of the parameter $\frac{d}{D}$, where D is the sphere diameter. These factors were calculated by Fiegel et al [49] and Russel [50] respectively. Using a 51-mm diameter sphere and a 130 mm diameter plane electrode, we measured the breakdown voltages of a 10 mm SF_6-N_2 insulated gap. Direct voltages of positive polarity were applied to the sphere electrode in these measurements. The measured and calculated values agree quite favorably as shown in Figure 7.7.

Howard [12] has measured the 50 Hz breakdown voltages for a sphere-sphere electrode system using 50 mm diameter sphere electrodes and gaps of upto 5 mm. Calculated values using equation (7.36) differ only slightly

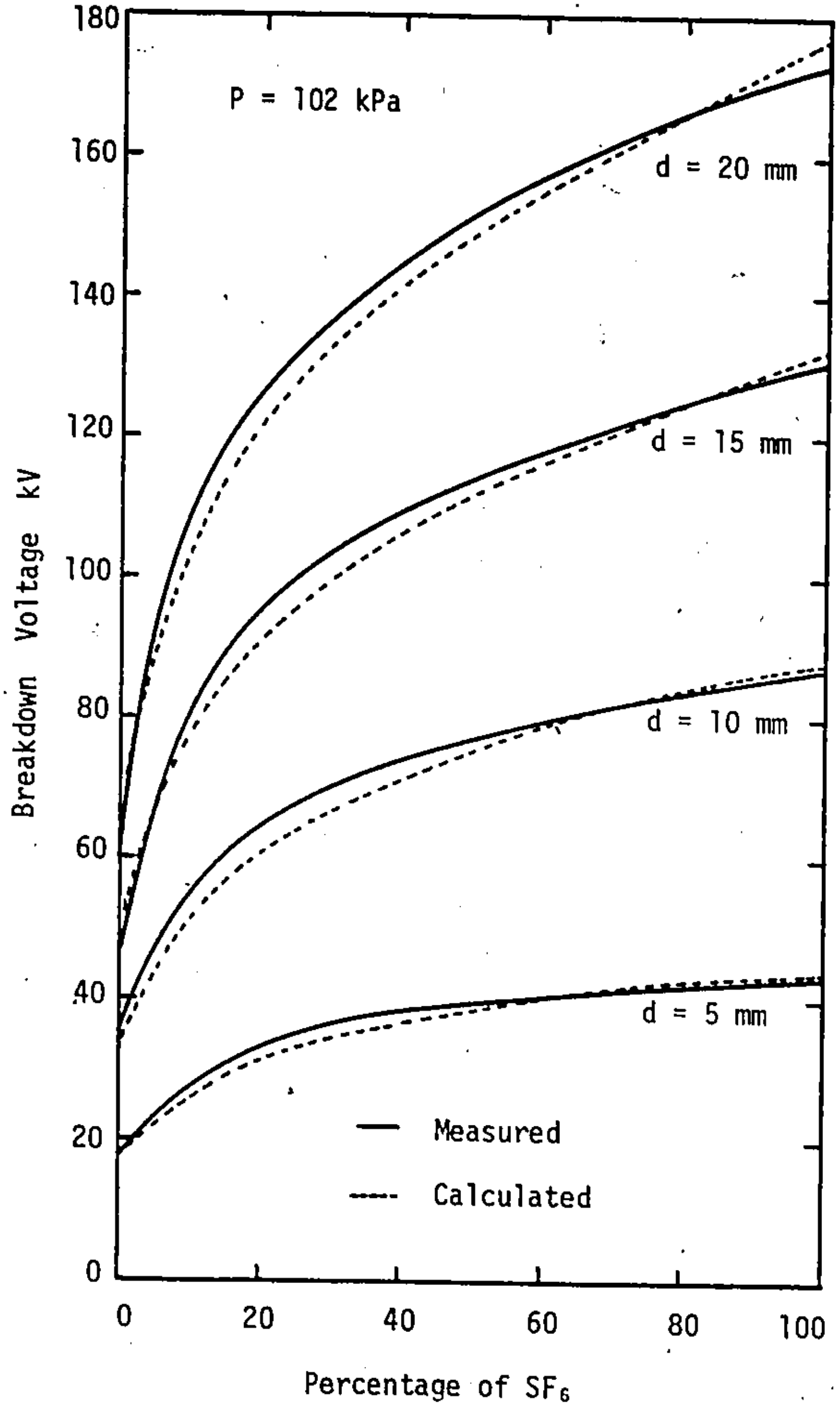

Figure 7.6 - Measured and calculated values of uniform field breakdown voltages in SF_6-N_2 mixtures.

TABLE 7.2

Field Utilization Factors For Sphere-Plane and Sphere-Sphere Gaps [49,50].

	Field Utilization Function u	
$\frac{d}{D}$	Sphere-Plane	Sphere-Sphere
0.1	0.876	0.932
0.2	0.777	0.877
0.3	0.691	0.818
0.4	0.620	0.761
0.5	0.556	0.705
0.6	0.512	0.660
0.8	0.431	0.582
1.0	0.373	0.517

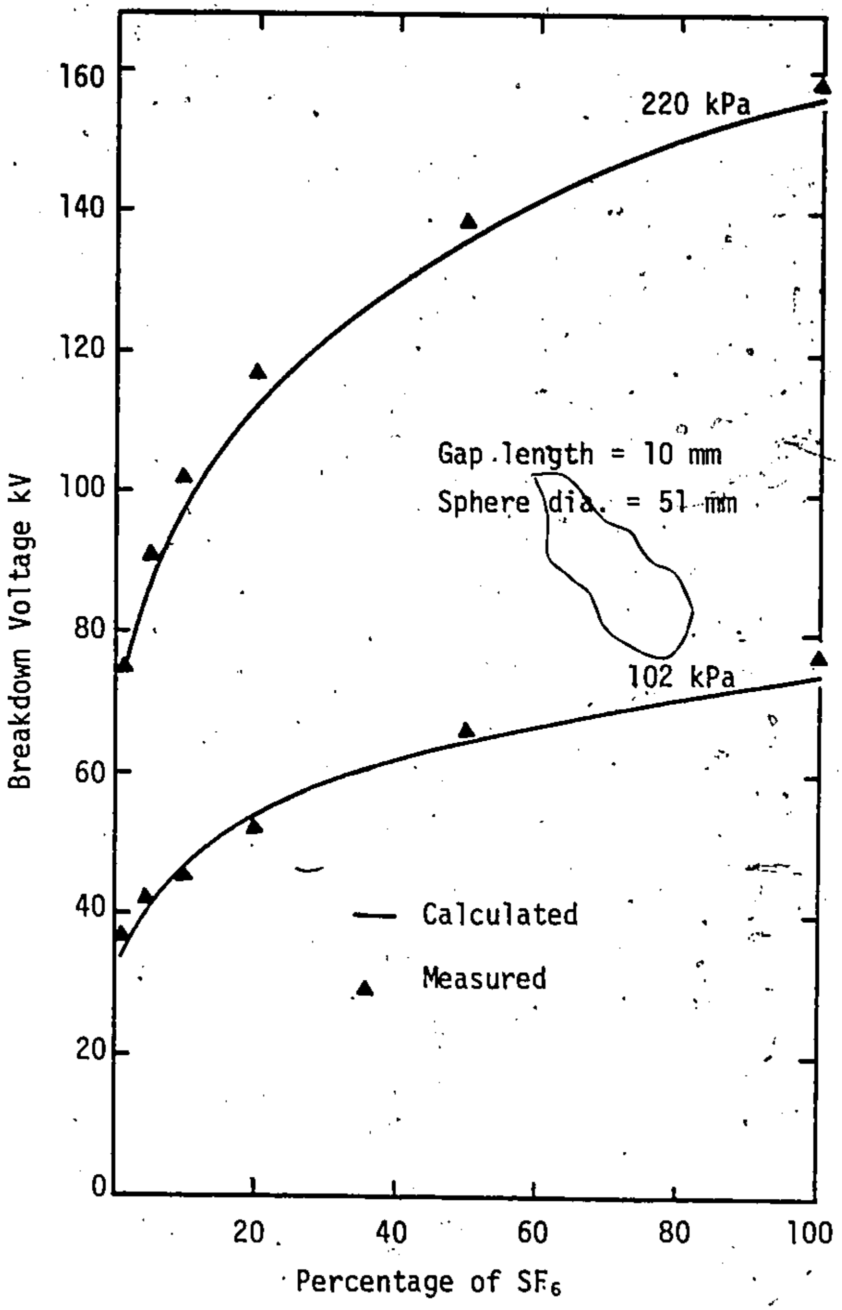

Figure 7.7 - Breakdown voltage as a function of gas mixture ratio and pressure for sphere-plane gap filled with SF_6-N_2 mixtures.

from his measurements as shown in figure 7.8.

(c) Cylindrical electrode systems

The field utilization factor u for a coaxial cylindrical electrode system having inner and outer electrodes of radii R_i and R_o respectively is given by

$$u = \frac{R_i}{R_o - R_i} \ln\left(\frac{R_o}{R_i}\right) \tag{7.48}$$

The discharge inception voltages were calculated for SF_6-N_2 mixtures at a total pressure of 102 kPa for three coaxial systems having R_i equal to 4, 7.5 and 14 mm. R_o = 20 mm was used in all these calculations. These values are given in Figure 7.9. For comparison, the static field breakdown voltages for both polarities as measured by Christophorou et al [51] have also been included.

(d) Rod-plane gaps

Rod-plane gaps are usually used to study the prebreakdown and breakdown characteristics in highly non-uniform field gaps. For SF_6 and SF_6-N_2 mixtures at low pressures, the corona inception occurs first and the breakdown voltage is usually higher than the corona inception level. At higher pressures, depending on the diameter of the rod electrode, the polarity of the applied voltage and the percentage of SF_6 in the mixture, the discharge onset can directly lead to a breakdown and therefore the breakdown and corona onset voltages coincide as discussed earlier. The streamer criterion of equation (7.36) should therefore predict the minimum of the corona inception or the breakdown voltages for a particular pressure.

The field factors $F = \frac{1}{u}$ have been calculated by Azer et al [21] for hemispherically capped rod-plane gaps using the finite element method. For gaps having $0.8 \le \frac{d}{R} \le 40$, where R is the radius of the electrode,

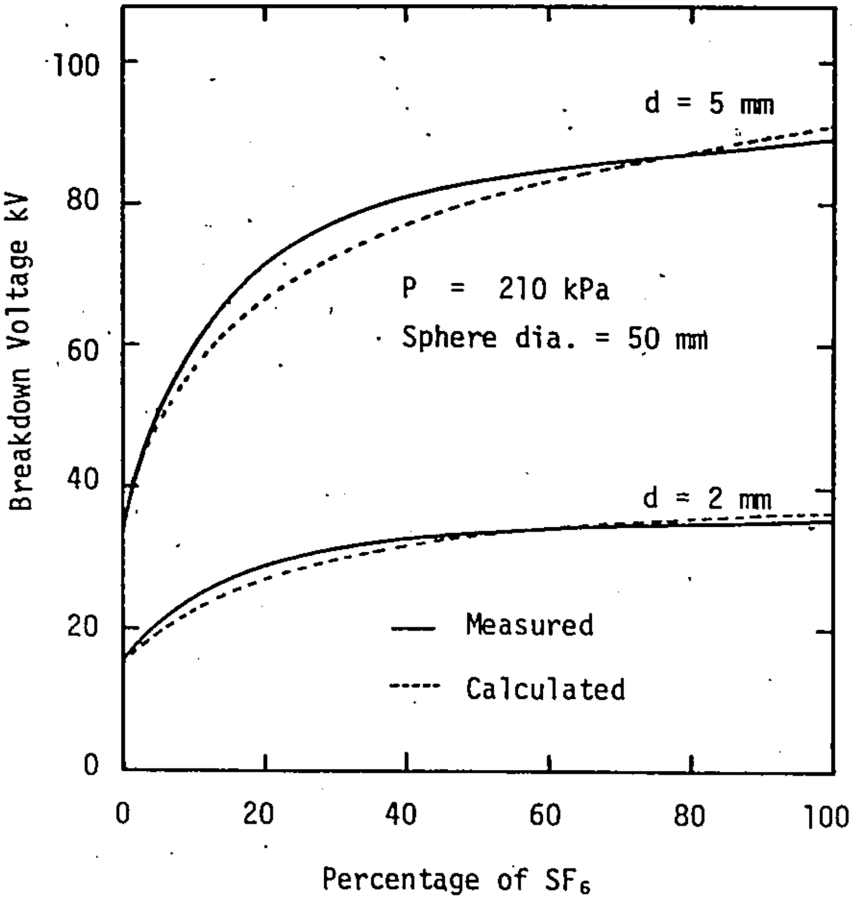

Figure 7.8 - Measured and calculated values of breakdown voltages for sphere-sphere gaps filled with SF_6-N_2 mixtures.

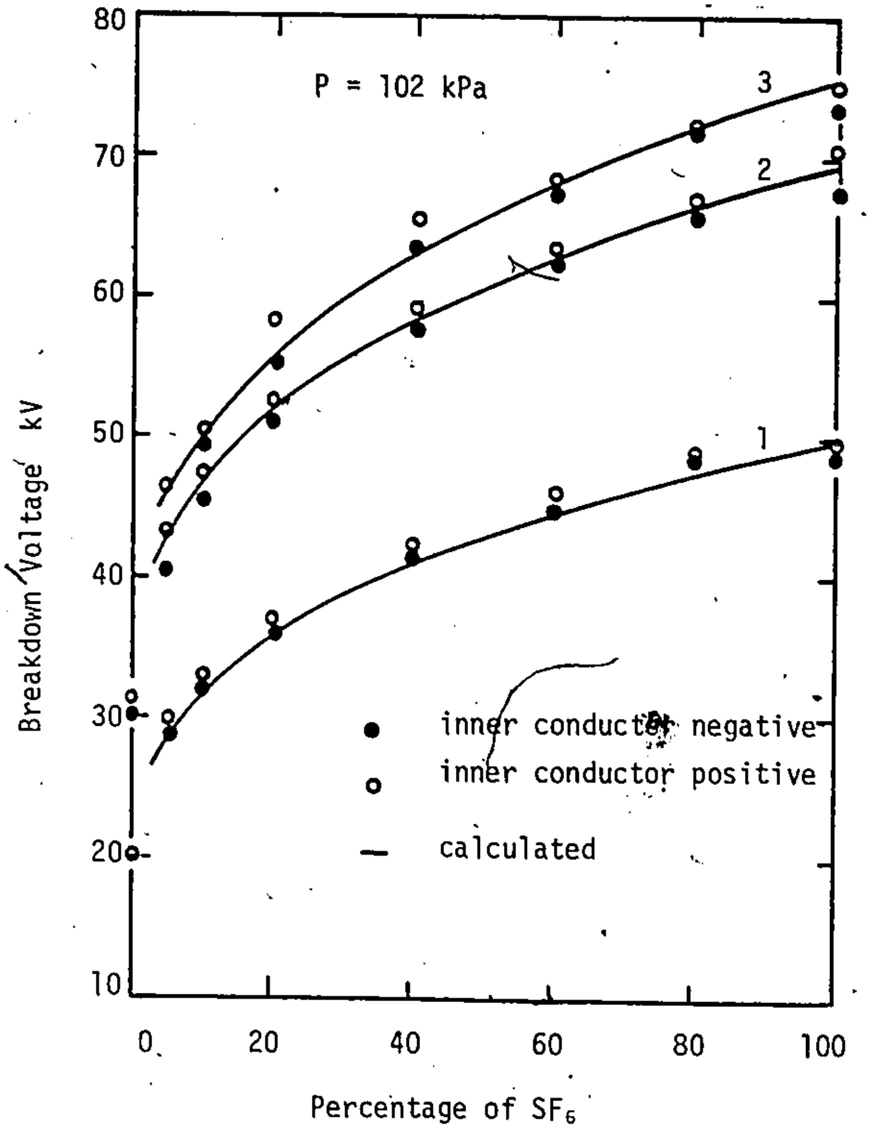

Figure 7.9 - Measured and calculated values of static field breakdown voltages for SF_6-N_2 mixtures in coaxial electrode systems. The radius of outer cylinder is 20 mm while that of inner cylinder is (1) = 14 mm, (2) = 4 mm, (3) = 7.5 mm.

they showed that

$$F = \frac{1}{u} = 0.6162 \left(\frac{d}{R}\right)^{0.9716} + 1.1377 \qquad (7.49)$$

Using the field factors given by equation (7.49) and the streamer criterion of equation (7.36), the discharge inception voltages were calculated for rod-plane gaps. In such gaps, the corona onset level is strongly affected by the polarity of the applied voltage and is usually the lowest when the rod electrode is the cathode as discussed in chapter III and V. Usually the corona inception is in the form of single isolated pulses. As the applied voltage is increased, steady corona becomes dominant. The onset levels for the steady corona are higher than those at which single pulse activity is observed. In figure 7.10, the measured values of the inception levels for single pulse corona activity are given when a negative direct voltage is applied to a 1 mm rod electrode. Figure 7.11 shows the results of similar measurements using 12.6 mm diameter rod cathode. In this case, there was no corona prior to the breakdown of the test gap and therefore the measured values are the breakdown voltage levels. Figure 7.12 through 7.17 contain the minimum voltage at which the discharge activity was observed for SF_6 and SF_6-N_2 mixtures containing 10 and 50% SF_6. These measurements were made using 10 and 40 mm long rod-plane gaps over the pressure range of 100 to 500 kPa. Hemispherically capped rod electrodes having diameters of 1, 2, 3.16 and 6.3 and 12.6 mm were used for these measurements. For the 12.6 and 6.3 mm diameter rods, no corona activity was observed prior to breakdown in these mixtures over a certain pressure range. The measured values given are the minimum levels at which either corona or breakdown was observed when the applied voltage was being raised or lowered gradually. ~~For~~ For comparison, calculated values are also included in these figures. As can be seen, the calculated

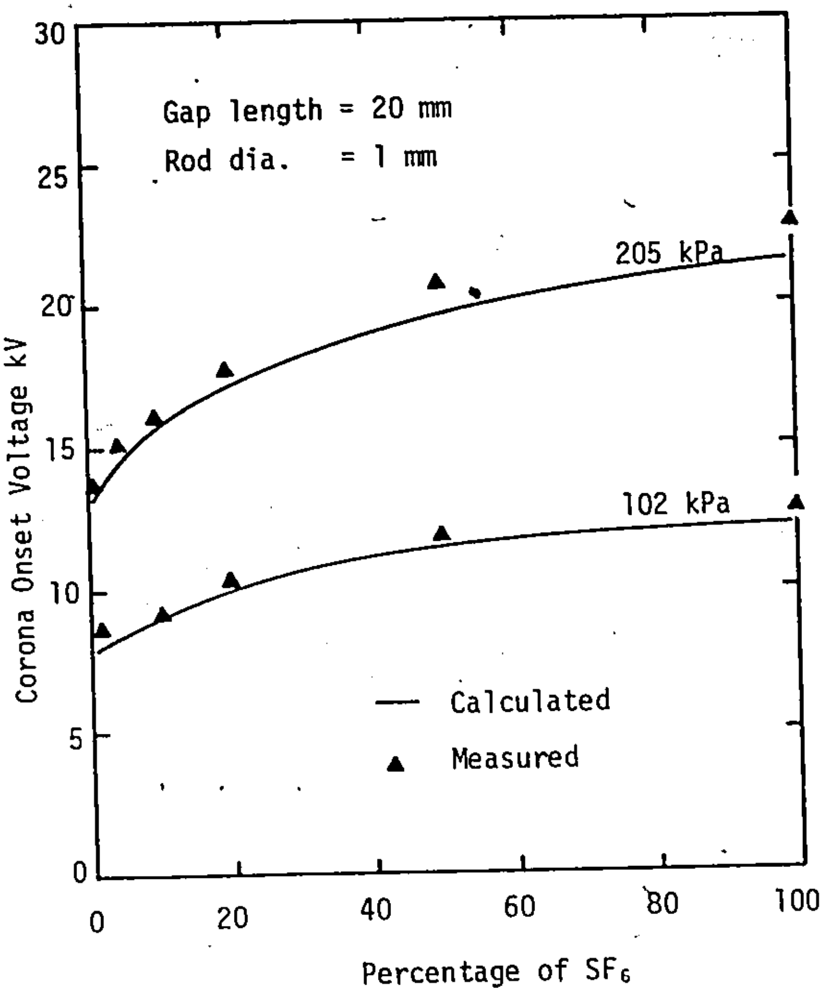

Figure 7.10 - Dependence of the corona onset voltage on mixture ratio for SF_6-N_2 mixtures.

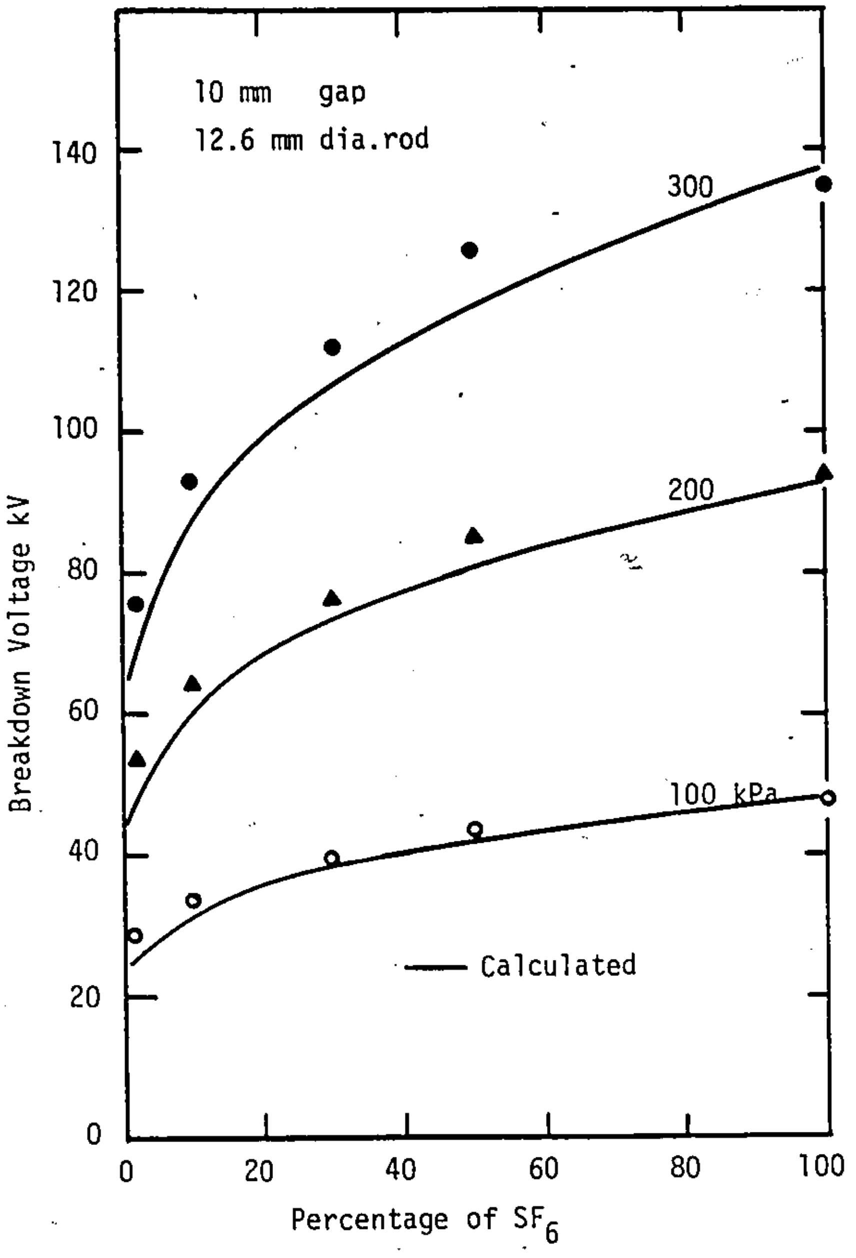

Figure 7.11 - Effect of pressure and mixture ratio on breakdown voltage of rod-plane gap filled with SF_6-N_2 mixtures.

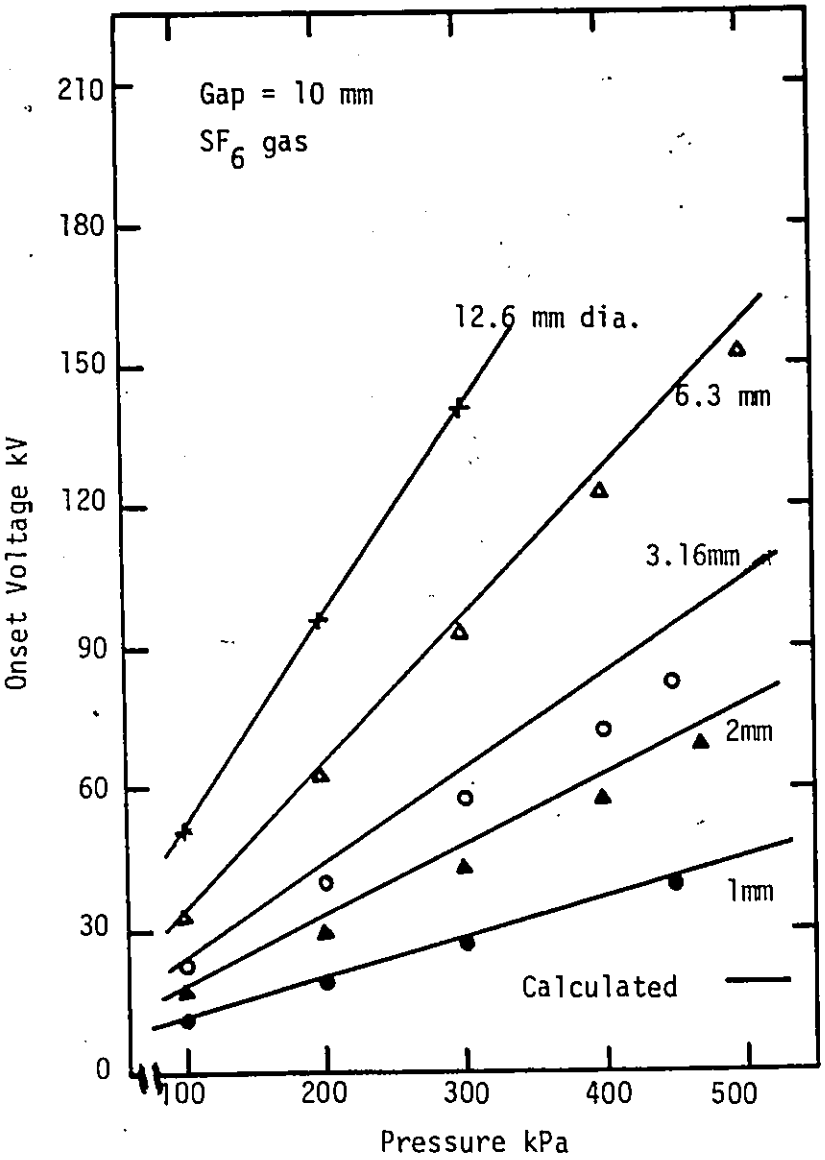

Figure 7.12 - Calculated and measured values of the minimum discharge voltage of SF_6 as a function of gas pressure and rod diameter.

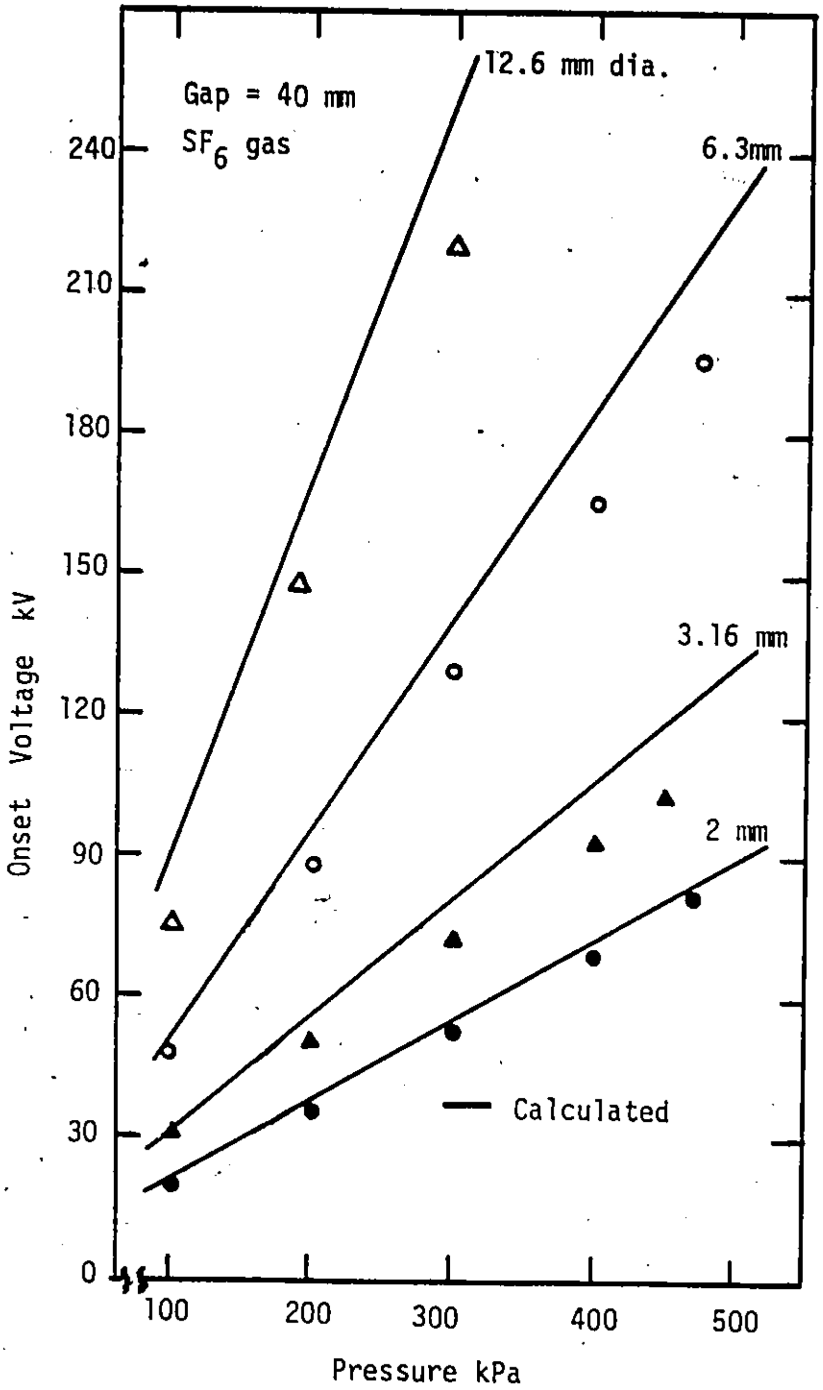

Figure 7.13 - Calculated and measured values of the corona onset voltages of SF_6 for negative rod-plane gaps.

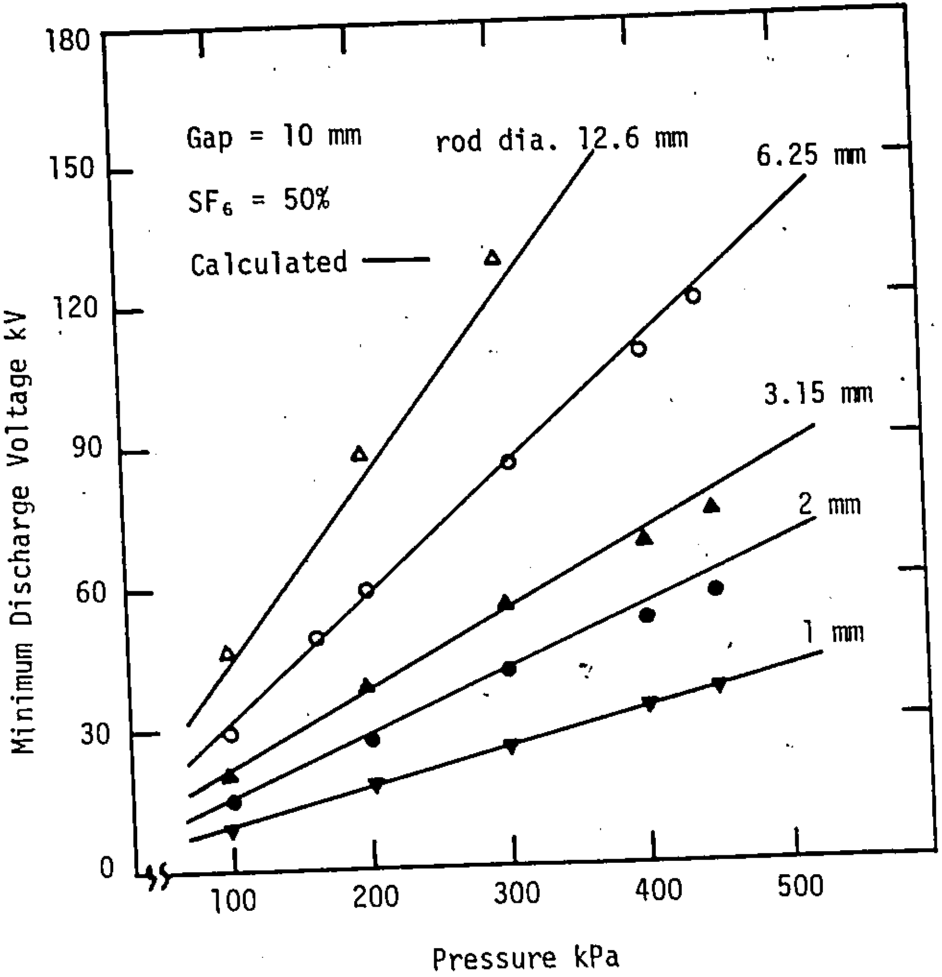

Figure 7.14 - Minimum discharge voltage as a function of gas pressure and rod diameter for a 50% mixture.

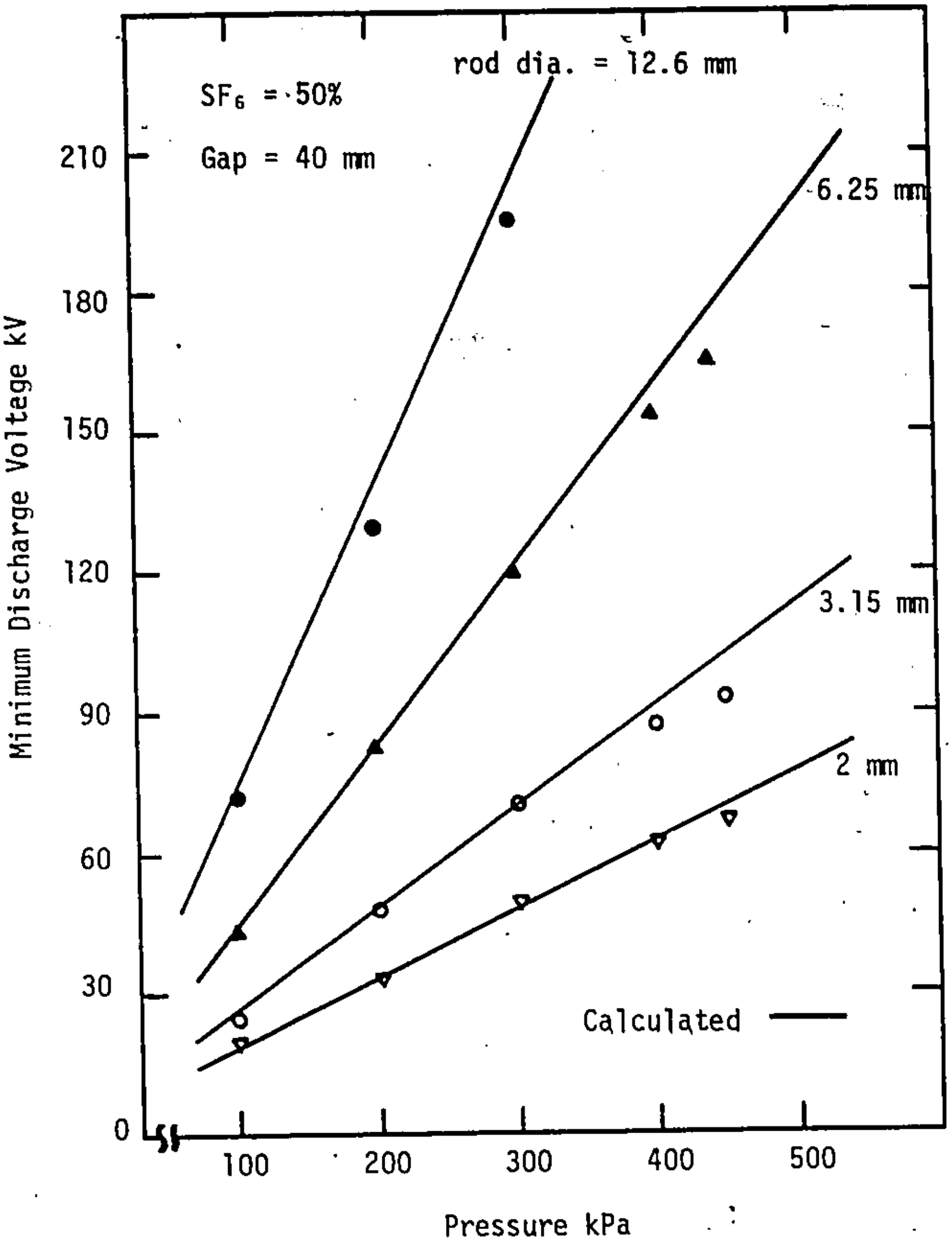

Figure 7.15 - Minimum discharge votlage as a function of gas pressure and rod diameter for a 50% mixture.

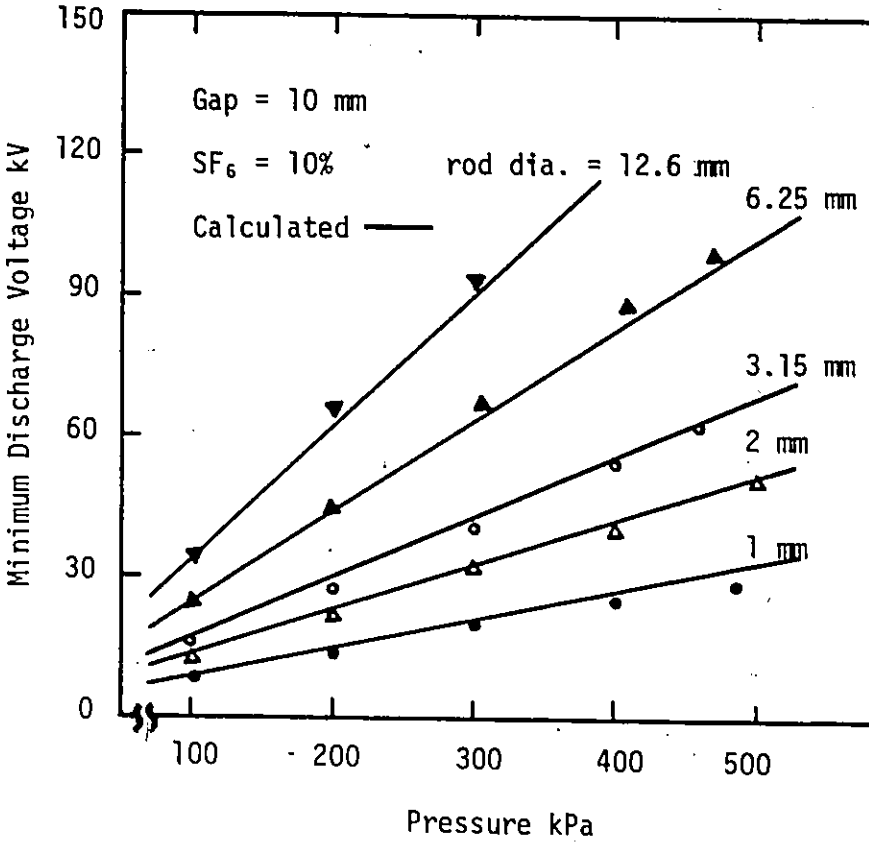

Figure 7.16 - Minimum discharge voltage as a function of gas pressure and rod diameter for a 10% mixture.

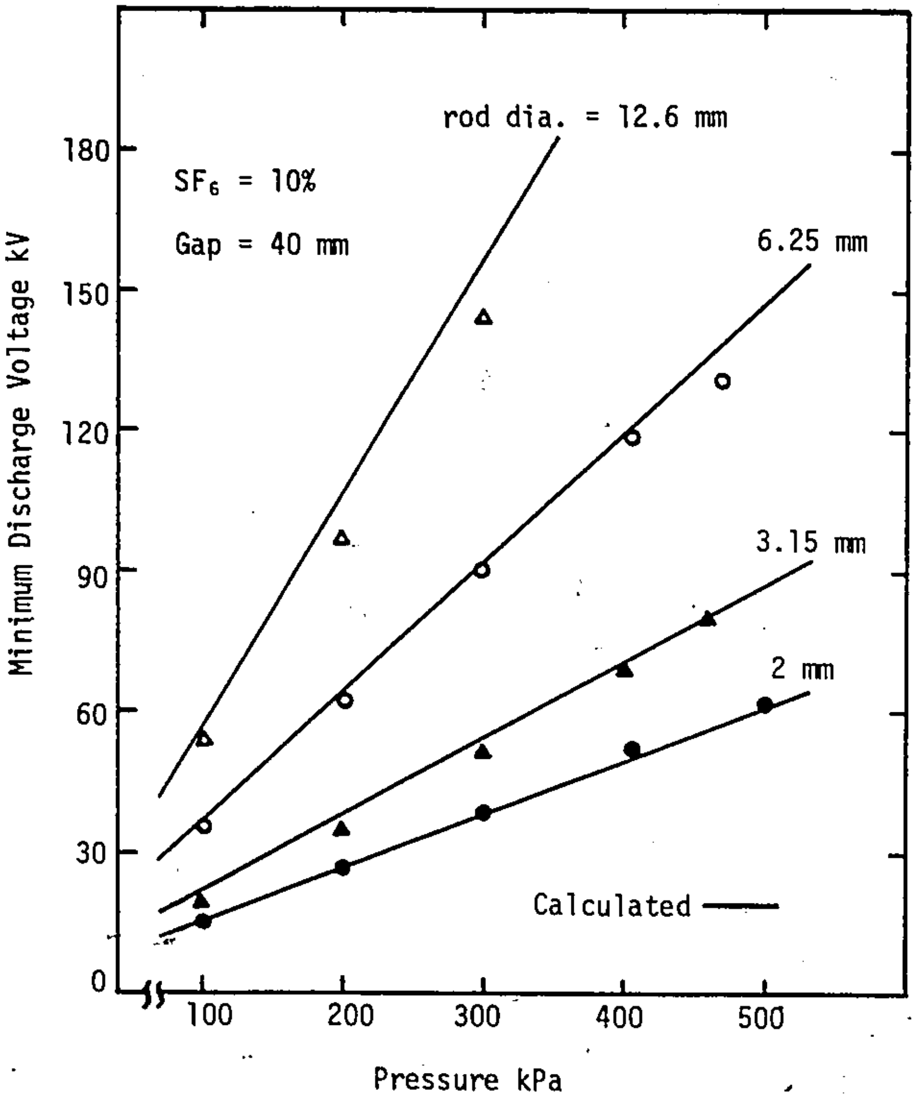

Figure 7.17 - Minimum discharge voltage as a function of gas pressure and rod diameter for a 10% mixture.

values are in good agreement with the experimental measurements for these mixtures over most of the pressure range. However, for pure SF_6 at higher pressures, the measured values are sometimes lower than calculated. Although the electrodes were polished and cleaned thoroughly prior to these measurements, the electrode surface changes during the measurements. It is expected that the surface roughness can become of the order of 10 microns due to sparking. Therefore, the roughness effects can reduce the breakdown strength at higher pressures as discussed in the previous section. Thus the difference between the measured and the calculated values at higher pressures in the case of pure SF_6, is due, at least in part, to the electrode surface conditions.

When alternating voltages are applied to the rod-plane gaps corona inception usually occurs during the negative half of the voltage cycle. Although no measurements have been reported for 60 Hz onset voltages of SF_6-N_2 mixtures, it is expected that the inception levels for alternating applied voltages will be close to those measured using negative direct applied voltages. Thus it can be said with reasonable certainty that the criterion proposed here can be used to calculate the discharge inception voltages for gaps having varying degrees of field uniformities with a great degree of accuracy.

CHAPTER VIII

DISCUSSION OF THE EXPERIMENTAL RESULTS

8.1. Introduction

One of the prime objectives of this work is to gain insight into the processes which characterize the behavior of SF_6-N_2 gas mixtures subjected to non-uniform electric fields. There are a variety of elastic and inelastic collision reactions which can in part determine the performance of SF_6 and N_2 under electrical stresses. The presence of a non-uniform electric field renders an analytical study difficult, as the energy distribution of electrons and ions changes from point to point in the gap. Furthermore, the presence of positive and negative space charges in the gap makes it difficult to determine the true electrical stress at any point in the gap. Although no chemical reaction is expected between SF_6 and N_2, the problem of dealing with mixtures is more complicated than individual gases. Therefore, it is extremely difficult to formulate a comprehensive explanation of the observed discharge phenomena in a non-uniform field gap in terms of the significant collision interactions which take place in highly stressed, high pressure, SF_6-N_2 gas mixtures. This is mainly due to the fact that very little or no information is available in the literature about most of these reactions. Investigations in the study of the fundamental physical interactions have been carried out only under uniform fields and at low pressures in pure gases.

Due to a large number of parameters governing the processes in mixtures, a comprehensive quantitative analysis of the observed discharge phenomena in SF_6-N_2 mixtures is extremely difficult. This applies especially to the experimental observations regarding the prebreakdown corona currents and the corona stabilized breakdown levels. Therefore, the following discussion is devoted to a qualitative explanation of the characteristics of the corona discharges in SF_6-N_2 mixtures. Much of this discussion is in reference to the corona studies in air and consequently a summary of the pertinent characteristics of these discharges is first presented. Furthermore, the breakdown characteristics of positive and negative rod-plane gaps are discussed in detail. Some new experimental data on non-uniform field breakdown in SF_6-He mixtures are included for comparison. Finally, a semi-empirical criterion regarding corona free breakdown in SF_6 is discussed and modified for applications to SF_6-N_2 mixtures.

8.2. Prebreakdown Studies

Since Townsend first initiated an intensive investigation of electrical discharges in gases, most of the studies carried out are devoted to the analysis of the various forms of corona in air because of its importance as high voltage insulation. The strongly electronegative gases and their mixtures which have found a widespread use only in recent years, have received little attention so far. It has been suggested that there is little difference between corona discharges in air and other electronegative gases such as SF_6 [52]. The results of the present investigations have proven the contrary.

8.2.1. Cathode corona in air

The various forms of the static field corona in rod-plane gaps of high field non-uniformity in air at atmospheric pressure will be summarized in this section. When the voltage across a rod-plane gap is gradually increased, a saturation current of the order of 10^{-14}A is measured. No ionization takes place in this region. With a further increase in the voltage, an abrupt current increase signals the development of ionization producing regular current pulses. These pulses, first reported in 1937 by O'Day [9] were studied in detail by Trichel [9] in 1938 and are hence known as Trichel pulses. Raising the applied voltage further does not result in a change of the corona mode for a considerable voltage range. Trichel pulses are extremely regular in their amplitude and repetition rate. The repetition rate of such pulses increases and their amplitude decreases gradually as the applied voltage is increased. However, the shape of the current pulse remains basically unaltered. The average prebreakdown current I varies with the applied voltage as [52];

$$I = C(V - V_o)^m \qquad (8.1)$$

where V_o is the onset level of the regular Trichel pulse corona dnd C and m are constants. The constants C and m as well as the voltage V_o are functions of the rod radius and the gap length, and C also depends on the pressure.

The visual character of a single Trichel pulse is difficult to record photographically because it is extremely faint. However, there are four distinct regions of the discharge in analogy to the glow discharge at low pressures. These regions are Crook's darkspace, the negative glow, the Faraday dark space and the positive column. The brightest part of this corona mode is the positive column which extends only a few millimeters into the gap . The Trichel pulse continuously shifts its position on the cathode surface. This makes the visual appearance more like a luminous cone. On large cathodes several such cones may develop simultaneously, forming regular patterns.

When the applied voltage is increased beyond the 'critical frequency' of about 10^6 sec^{-1}, a sudden transition from the Trichel pulse mode to a steady corona take place. No large change in the average prebreakdown current accompanies this transition. In appearance this corona mode is extremely stable, as the name implies. Like the Trichel pulse, the discharge region in this mode can be subdivided into a bright spherical negative glow and a less bright positive column separated by a thin dark regional (Farady dark space). The glow mode of the corona differs from the Trichel pulse mode only in that it is continuous rather than intermittent. The physical structure of the ionization process is, however, the same for both modes. The glow mode may exist simultaneously with the Trichel corona, but at different locations of a large cathode.

When the applied voltage is increased, the glow discharge continues to persist until a breakdown occurs. In long gaps another type of corona called "negative streamers" or "feathers" is observed prior to breakdown. It appears only at very non-uniform field configurations and thus be observed only at large electrode spacings at very high voltages. In short gaps this corona mode is unstable and at once leads to a breakdown. During this mode, feather-shaped discharges develop from the negative glow portion of the corona. The positive column shrinks to form the feather stem that extends towards the anode with very little or no branching. The current associated with this mode is made up of a steady component with superimposed regular pulses. The rise time of these pulses is of the order of 0.5 μsec which is extremely long when compared with the rise time of a few nanoseconds for all other pulsating corona modes. This long rise time is due to the relatively slow build up of the feather-like discharge advancing slowly through a gap filled with negative ion space charge. The discharge tip is subjected to diffusion and deflection by the negative ions. This results in the appearance of a multitude of these feather-like discharges, and therefore this type of corona is sometimes called the "brush discharge".

8.2.2. Cathode corona in SF_6 and SF_6-N_2 mixtures

The results of the present investigations of corona discharges in SF_6 and SF_6-N_2 mixtures described in chapter III indicate substantial differences between the corona in air and that in SF_6 or SF_6-N_2 mixtures. These differences exist both in the visual appearance and in the prebreakdown current associated with these discharges.

In air, the prebreakdown current at the onset of corona discharge is usually composed of individual pulses which are regular in amplitude, time separation and waveshape. In SF_6 and SF_6-N_2 gas mixtures, however, the prebreakdown current pulses at the discharge onset vary at random in amplitude as well as time separation. This is probably due to the non-availability of the initiatory electrons in the strongly electronegative SF_6 and its mixtures. In air, Trichel pulse corona exists over a considerable voltage range and leads to the glow corona when the frequency of the Trichel pulses approaches to 10^6 sec^{-1}. In SF_6 and SF_6-N_2 mixtures having SF_6 content above about 5%, the single pulse corona leads to a series of pulses in rapid succession (momentary discharge). This type of corona current is not observed in air. However, the most obvious difference appears at the onset of a steady prebreakdown current.

In air, the onset of such a steady current coincides with the inception of a glow discharge, whereas in SF_6 and SF_6-N_2 mixtures, it coincides with the appearance of a very narrow well defined filamentary discharge which is considerably different from the glow discharge in air. The discharge in air is usually concentrated at one point on the cathode which can wander around as a result of the cleaning action of the cathode surface due to positive ion bombardment. For large cathodes, the concentrated discharge can appear on more than one point simultaneously depending upon the applied voltage, the rod diameter and the gas pressure etc. However, the visual appearance of these discharges remains practically the same from the onset of the Trichel pulse corona to the ultimate breakdown of the test gap unless negative streamers can materialize. The visual appearance of corona in air is very similar to that of air-N_2 mixtures. Figure 8.1(a-e) shows the changes in the character of the cathode corona when the applied voltage across a 40 mm gap filled with N_2 containing less than 0.1% of air is gradually increased. Except at the onset region where irregular Trichel pusles were observed (Figure 8.1(a)), the corona character remains basically the same when the gap voltage is increased as shown in figure 8.1(b-e). The appearance of this corona is very different from the corona observed in a 1.5% SF_6-N_2 gas mixture for otherwise identical test conditions as shown in figure 8.1(f). As discussed in chapter III, the visual appearance of the cathode corona in SF_6 is similar to that in the SF_6-N_2 mixtures. The corona of figure 8.1(f) is composed of numerous well defined bright channels of varying length along different portions of the cathode surface. Each filament appears to be a small streamer. In gaps filled with SF_6-N_2 mixtures, these streamers exist from the very inception of the discharge upto the

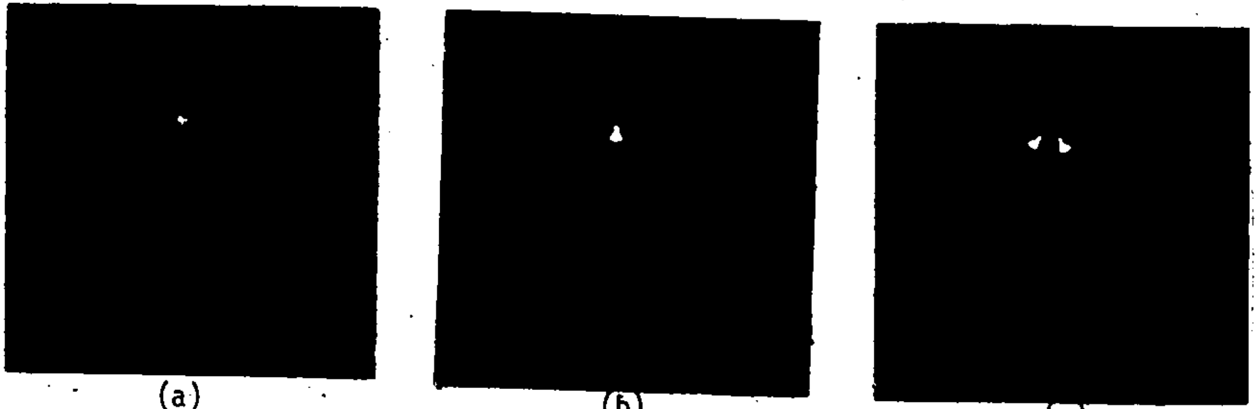

(a)
v = 40 kv
P = 100 kPa
exposure = 10 msec

(b)
v = 50 kv
P = 100 kPa
exposure = 10 msec

(c)
v = 63.8 kv
P = 100 kPa
exposure = 10 msec

(d)
v = 65.8 kv
P = 100 kPa
exposure = 10 msec

(e)
v = 71 kv
P = 100 kPa
exposure = 10 msec

(f)
v = 87.5 kv
P = 100 kPa
exposure = 10 msec

Figure 8.1 - Static field cathode corona in a 40 mm gap for 12.6 mm diameter rod electrode

(a) - (e) = corona in N_2 containing less than 0.1% of air

(f) Corona in an SF_6-N_2 mixture containing 1.5% of SF_6

breakdown. Since the corona onset levels measured experimentally agree reasonably well with the calculated values for the streamer formation, there is little doubt that the bright filamentary discharge channels observed in SF_6 and SF_6-N_2 mixtures are individual corona streamers. Though the visual appearance of the corona discharges in long rod-plane gaps using smaller rod radii had a diffused glow-like appearance especially at low gas pressures and for mixtures having low SF_6 content, both the appearance and the associated corona current in these cases is still different from that observed in air. The glow in air is concentrated at a point on the electrode and is conical in shape similar to those shown in figure 8.1(b→e). In SF_6-N_2 mixtures, it has a spherical shape as shown in figure 3.7(c-d). The corona current associated with a glow discharge in air is steady in magnitude while that observed in SF_6-N_2 mixtures having $SF_6 \geq 20\%$ always contained pulses of considerable magnitude superimposed on the steady levels. In such mixtures under no conditions absolute steady currents were recorded. However, for mixtures having SF_6 content between 1 and 20%, glow like steady currents could be observed for time periods ranging from microseconds to milliseconds which were always followed by pulses superimposed on the steady level. Only for mixtures having SF_6 content below 0.1%, it was possible to observe pure glow-like currents over certain voltage ranges. Thus in SF_6-N_2 mixtures having 1 to 100% SF_6 glow corona, like the one observed in air, does not materialize.

The Trichel corona pulses in air are regular in time separation which is related to the negative ion clearing time in the gap. In air, a Trichel pulse does not materialize until the negative ion space charge left by the previous pulse drifts away leaving the gap free of space charge. This is not the case in SF_6. As seen in figure 3.5(c), in a momentary discharge, a series of current pulses are observed in rapid succession before the current drops to zero. Mobility measurements of SF_6^- [26,27,53], the predominant negative ions in SF_6 discharges, yield a typical value of about 0.45 cm^2 $(volt.sec)^{-1}$ at a gas pressure of 100 kPa. In a field having $\frac{E}{p}$ values of the order of $\left(\frac{E}{P}\right)_{lim}$ i.e., 0.8775 kV $(cm\ kPa)^{-1}$, a negative ion would drift a mean distance of about 0.4 mm in one microsecond. Thus a total time of about 50 μsec is required to clear a 20 mm gap. This is roughly the decay time of the last current pulse shown in figure 3.5(c). However, between the first and the last current pulses of figure 3.5(c), the average duration of each small pulse is roughly 10 to 15 microseconds. This situation is similar to the current pulses shown in figure 3.5(e). Thus the oscillograms of figure 3.5 (c and e) suggest that it is not essential for an SF_6 filled gap to be totally free from the negative ion space charge created by the previous corona pulse before the subsequent corona discharge can materialize. Hence the discharge can occur even if part of the gap contains negative ion space charge. This hypothesis is further supported by the oscillograms shown in figure 3.5(f and g) where both the prebreakdown current and the photomultiplier output show a maximum repetition rate of the order of 1 pulse per microsecond at the onset of a steady discharge which certainly does not allow for a substantial clearing of the negative ions produced during the previous discharge. Figures 3.5(c) to (e) also indicate that the first pulse in a momentary discharge has relatively higher amplitude compared to the following pulses. Further 3.5(e) shows that when the time separation between two consecutive pulses is close to 50 μsec, a pulse magnitude of the order of the initial big pulse is observed. Thus the big pulses are observed when the gap is, in all probability, almost clear of the space charges, while the small pulses are observed , when the gap is partially filled negative ions.

In a momentary discharge there are usually a large number of small pulses before the discharge completely chokes off. It appears that the discharge is completely choked off when the low field region is entirely filled with negative ion space charge which reduces the field in the neighborhood of the cathode to a level below the threshold necessary for the streamer formation.

An increase in the applied voltage beyond the inception level of the momentary discharges should in theory decrease the probability of the discharge extinction. This appears to the case since an increase in applied voltage usually results in longer durations for the momentary discharges and in reduced time separation between two successive discharges. This behavior continues until at a certain voltage level, for reasons not fully understood, a continuous discharge appears. However, it is interesting to note that the average value of the prebreakdown current during a continuous discharge, if corrected for the higher applied voltages, is similar to that for the momentary discharge activity when averaged over the time periods for which such discharges exist. Furthermore, the current and the light output waveforms for the momentary and sustained discharges are very similar except that the lattter does not suffer a self extinction. However, the transition from a momemtary to sustained discharge is abrupt with respect to a change in the applied voltage. The transformation is marked with a very large increase in the average corona currents. A reversal to a momentary discharge results only when the gap voltage is reduced. Therefore, at the inception level, there is a discontinuous change in the probability of discharge extinction. Thus, in spite of the similarities, it appears that the two types of discharge phenomena are not entirely similar.

It is likely that a transformation from a momentary to a sustained discharge occurs when the former attains a sufficient repetition rate to generate enough amounts of foreign products (due to chemical reactions caused by high energy electrons and photons) to alter the gas properties. Changes in the chemical composition will alter the photon spectrum and their absorption properties and, to a lesser degree, cause changes in the ionization and attachment coefficients [9]. Experimentally it was observed that the transition from a momentary to a sustained discharge was marked by a sudden increase in the momentary discharge repetition rate and an accompanying rise in the direct current level. This suggests a run-away process in which each discharge contributes to accumulation of the foreign products in the gas. This promotes further discharges, and as the accumulation increases, so does the repetition rate until the discharge becomes sustained. This discharge, once established, generate sufficient chemical by-products to maintain itself at voltages below the onset level and thus the offset voltages are lower than the onset values.

An inspection of the surface conditions of the electrodes subjected to extensive breakdown and corona discharges showed that the discharges in SF_6 and SF_6-N_2 mixtures resulted in the discoloration of the anode surface. This discoloration appeared to be some form of insulating layer which was very evident on the plane anode. This layer probably resulted from the chemical reactions between the constituent radicals of SF_6 generated in the discharges, and the anode.

In general, the prebreakdown behavior of SF_6-N_2 mixtures is very similar to that of pure SF_6. This is due to the fact that even the mixtures containing as low as 5% of SF_6 in N_2 are strongly electronegative and have an effective ionization coefficient which behaves similar to pure SF_6 as discussed in the previous chapter. Thus corona discharges in all such mixtures resemble more or less the discharges in pure SF_6. The most obvious difference was that the discharges in SF_6-N_2 mixtures were bright and not as bluish as those observed in pure SF_6. It also appeared that as though the length and number of corona streamers was larger in SF_6-N_2 mixtures than in pure SF_6 for a given field configuration. This is due to the fact that, (a) the effective ionization coefficient for a given value of E/p is higher in the mixtures than in pure SF_6, (b) the critical avalanche length, X_c, necessary to transform an avalanche into a streamer is larger in SF_6-N_2 mixtures than in pure SF_6, and (c) the absorption coefficients of SF_6 are higher than those of the mixtures.

Using equation (7.24) and (7.26), it is possible to express X_c as:

$$X_c \simeq \left[\frac{R \cdot K_m}{p \cdot \beta_m \cdot (E/p)^{1}_{lim}} \right]^{0.5} \tag{8.2}$$

Table 8.1 contains the value of the critical avalanche length for a 40 mm rod-plane gap using 12.6 mm diameter rod electrode when filled with SF_6-N_2 mixtures at a total pressure of 100 kPa. An examination of Table 8.1 indicates that for conditions corresponding to the discharge threshold, the region of ionization activity, i.e., where $\alpha > \eta$, and consequently the length of the corona streamers is more in SF_6-N_2 mixtures than in pure SF_6. Furthermore, this length increases as the SF_6 content in the mixture is reduced. Also the range of corona streamers is related to the mean free paths of the ionizing photons. The streamers advance more into the gap if the mean free path of the ionizing photons is large [9]. The measurements reported by Blair et al [23] indicate that the mean free paths of photons in SF_6-N_2 mixtures increase when the SF_6 content in the

TABLE 8.1

Critical Avalanches Length X_c for SF_6-N_2 Mixtures

Gap Length = 40 mm, Rod Dia. = 12.6 mm

SF_6 (%)	X_c (mm)
100	0.53
75	0.58
50	0.66
30	0.75
20	0.84
10	1.02
5	1.25
1	1.75

mixtures is reduced. Thus the region of discharge activity will increase when SF_6 component in the mixtures is reduced.

With increase in the gas pressure for a given mixture, the length and number of corona streamers reduce. This reduction in the length is, at least in part, due to the relatively smaller values of the critical avalanche length X_c at high gas pressures which is inversely proportional to the square root of the pressure. Also when the gas pressure is increased, the density of positive and negative ion space charges increases because of the reduced ion drift and diffusion velocities. The mean free paths of the photons are also reduced. This results in an uneven distribution of the space charges in the gap with a strong space charge barrier along the axis of symmetry of the rod electrode. Consequently the streamers have a tendency to form away from the tip and propagate in the gap circumventing the space charge barrier as shown in figure 3.9. The inclination of the streamers increases in general with gas pressure. As discussed in chapter VI, the probability of the cathode directed streamers increases with pressure. The same is true for the anode directed streamers. Thus depending on the field configuration and the dielectric medium, there exists a pressure above which anode directed streamers can propagate all the way to the cathode and initiate a spark at the discharge onset. Therefore, in the negative rod-plane gaps, corona discharges do not materialize above such pressures and a breakdown takes place instead. Since the photoemission and absorption characteristics of SF_6-N_2 mixtures are expected to change with the gas mixture ratio, the critical pressure is also expected to vary with the mixture ratio.

Another interesting feature of the coronas in SF_6-N_2 mixtures is highlighted by studying the difference between the visual appearance of corona in pure N_2 and in SF_6-N_2 mixtures containing minute traces of SF_6

as impurity. In pure N_2, the photons have long mean free paths as shown in figure 3.10 where they are seen illuminating the plane electrode as well as the chamber walls. This is very different from that of a mixture containing 0.05% of SF_6 as shown in figure 3.10. It appears that the addition of a small amount of SF_6 as impurity to nitrogen substantially modifies its absorption characteristics. Similar behavior has also been observed in our study of the negative impulse coronas in nitrogen and SF_6-N_2mixtures containing less than 1% of SF_6 [7].

8.2.3. Anode corona in air

The summary of anode corona in air discusses the discharges in a rod-plane gap in air at atmospheric pressure [9,52,54]. Under these conditions, the discharge at the anode surface goes through three distinct modes of; onset pulses, glow discharge (Hermstein's glow), and prebreakdown streamers respectively with increasing gap voltages.

As the gap voltage is gradually increased, the sudden appearance of current pulses marks the formation of streamer or burst pulse discharge. The pulses occur at random and intermittently and their initial frequency depends on the intensity of some ionizing agent acting as a catalyst. The frequency of the streamer pulses, and hence the average prebreakdown current, shows a considerable increase with the applied voltage. The onset current pulses contain either streamer or burst pulses or mixtures of the two. A streamer discharge essentially leads to the formation of ionized gas channel normal to the electrode surface. The current resulting from such a discharge appears as a single pulse with a rise time of the order of 20 to 40 nanosecondsand a decay time to half its peak value of the order of 100 nanoseconds. A burst pulse results from a weak streamer and a burst pulse ionization has a tendency to spread radially over the anode surface. Due to these reasons burst pulses are also known as "corrupt streamers". The burst pulse current generally appears as a sequence of pulses with smaller amplitudes and slower rise times than those for streamer pulses. A sequence of such pulses can exist for durations of the order of 100 μsec. According to Loeb [9], it is the mean free path of ionizing photons relative to the ionizing length, which is the minimum distance from the anode surface to the point where $\alpha = \eta$, which determines whether a streamer or burst pulse will occur. If the mean free path is much larger than the ionizing length, a burst pulse will occur, otherwise streamer pulses will appear.

Both the streamer and burst pulses occur at random and are irregular in amplitude. The reasons for their random and irregular occurrence lies in the distortion of the electrostatic field caused by the positive and negative ions present in the gap after a streamer has developed. These space charges distort the original field so that a new streamer cannot develop before they have cleared the gap. Since their density and distribution depend on the intensity of the preceeding streamer, the time required to clear the gap will be highly fluctuating. Sometimes a streamer starts to propagate into an area that has not been completely cleared of the space charges and will thus get "choked" resulting in a current pulse with a slow rise time and small magnitude. This has been referred to as burst pulse. The repetition rate of streamer pulses in the onset region is a function of the applied voltage as well as geometry of the anode. Maximum repetition rates of the order of several kHz have been observed.

When a negative ion space charge of sufficient density accumulates around the anode, a transition from the intermittent streamers corona mode to a steady glow occurs. The conditions are not favorable for the establishment of a glow discharge in the absence of a negative ion space charge of sufficient density and negative ions will become neutralized at the anode. This clears the way for a new streamer to develop. In the case of sufficient negative ion space charge density, the locally enhanced field is high enough to lead to a Townsend type of self-sustaining discharge with photoionization of the gas molecules as the main source of secondary electrons. Consequently a thin sheet of ionized gas exists between the negative ion space charge and the anode. This type of discharge is stable because the ionizing radiation from the discharge creates electrons that form negative ions. These ions drift towards the anode and compensate for the loss in the density of negative ions due to diffusion and recombinations. In the case of large anodes, a glow corona may exist with streamers simultaneously developing at other locations. The discharge current from a glow corona has a direct current component with a small ripple of frequency of the order of 1 MHz. The glow discharge derives its name from its visual appearance which is a closely adhering soft glow over the anode surface.

The glow corona suppresses the devlopment of streamer type discharges. Streamers reappear only after the applied voltage is increased considerably beyond the onset level necessary for a glow discharge. The characteristics of these streamers are very similar to those of the onset streamers. However, because these streamers ultimately initiate a complete breakdown of the gap, they are termed as "prebreakdown streamers". The frequency of these streamers varies from ≈ 10^3 sec^{-1} near their onset to about $10^4 sec^{-1}$ before breakdown. These streamers are one of the most conspicuous modes of static field anode corona in air because they are relatively bright and long, and because they cause an appreciable amount of acoustic noise and radio interference.

8.2.4. The anode corona in SF_6 and SF_6-N_2 mixtures

The earlier studies [11,13] about the anode corona in SF_6 and the present investigations regarding static field corona discharges in SF_6 and SF_6-N_2 mixtures indicate that there are several differences between the anode corona in air and that in SF_6 and SF_6-N_2 mixtures. The most obvious difference exists at the onset region of a steady corona current. In air, the onset of a steady corona current coincides with the inception of Hermstein type glow discharge. However, in SF_6 and SF_6-N_2 mixtures, it coincides with the appearance of a narrow, well defined filament having a bright root. The visual manifestations of the discharge in SF_6 and SF_6-N_2 mixtures and the prebreakdown current resulting from such a discharge indicates that a sustained discharge in SF_6 and SF_6-N_2 mixtures is a sequence of streamer pulses. The filamentary discharge in SF_6 and SF_6-N_2 mixtures exhibits no diffused tip and the discharge column is very narrow. The appearance of this filament is quite different from the brush-like discharge observed in air in the onset pulse region. The brush discharge exhibits a diffuse tip in the low field region which is the result of a branching of the streamers that constitute the discharge. The appearance of the filamentary discharges in SF_6 is primarily due to small mean free paths of the photoionizing radiation which primarily affects the discharge in two ways: the spread of ionization over the anode surface in the form of burst pulses is reduced, and the branching of the streamer type ionization growth is curtailed. The discharge is constricted in a narrow channel. As suggested by Weissler and Mohr [55], the channel of positive ions created by a streamer is rapidly neutralized by electron-positive ion recombinations and electron attachments producing negative ions. Because of the latter, a neutral but still highly ionized gas channel remains. Therefore the subsequent streamers prefer to follow the existing channel and this gives the discharge a highly confined appearance. Due to the highly localized nature of this discharge, a local temperature rise and some chemical changes in the gas may stabilize the discharge [56].

Since the repetition rate of momentary discharges is virtually the same as the repetition rate of pulses constituting a sustained discharge, it is therefore likely that a momentary discharge is a sequence of streamer pulses which suffer self-extinction. The repetition rate of pulses in a momentary discharge is of the order of one pulse per microsecond. If one assumes a mobility of the positive ions similar to that of the negative ions in an SF_6 discharge, the positive ions will drift over a mean distance of about 0.04 cm/μsec in a field having an $E/p = 0.8775$ kV(cm kPa)$^{-1}$ as discussed previously. Thus the pulse repetition rate of the momentary discharges does not allow for a substantial clearing of the positive ions produced by the previous streamer. This space charge reduces the voltage gradients at the anode surface and consequently inhibits subsequent streamer discharges. However, many of these ions are eliminated by recombining with the electrons produced in the streamers. Also since SF_6 is highly electronegative, a large number of the negative ions is formed in SF_6 and SF_6-N_2 mixtures. These negative ions neutralize the positive ion space charge to a large degree especially in the low field regions. Thus through several mechanisms, the inhibiting effect of the space charge created by streamer ionization is reduced rapidly allowing such a high repetition rate. Pulses following the initial pulse of a momentary discharge are somewhat smaller than the initial pulse as shown in figure 5.6(b,d,e,f and g) indicating an incomplete neutralization of the streamer space charge.

The sequence of pulses following the initial pulse of a momentary discharge displays an almost successive increase in magnitude as shown in figure 5.6(b,c and f). Thus it appears that the field at the anode surface is enhanced with the passage of each pulse. Only the formation of a negative ion space charge sheath can account for such an enhancement. This sheath is created by the attachment processes between SF_6 molecules and the electrons produced in the low field regions by streamer ionization. Photoionization in this low field region can also be an important factor. The negative ions thus produced in the low field regions drift towards the anode. Their mutual repulsion as well as atraction towards the positive ions drifting in the direction of the cathode tend to spread the advance of the negative ions laterally over the anode surface. Most of these electrons either recombine with the positive ions or suffer field induced detachment before reaching the anode as discussed earlier in chapter VI. Thus, a dynamic separation exists between the negative ion space charge and the anode surface. In this region, the electrostatic field for a given applied voltage is greater than that obtained when there is no negative ion space charge sheath. Furthermore, the negative ion space charge reduces the field between this space charge and the cathode. The growth phase of the momentary discharges indicates that the field enhancement is maintained over a distance sufficient for streamer development. The reduced voltage gradient between the negative ion space charge and the cathode inhibits the propagation of such streamers into the gap and therefore imposes a limit on the maximum current pulse which a streamer can induce. Hence the pulse amplitudes do not increase indefinitely and level off at some maximum value as is evident in figure 5.6(c).

The current oscillograms of figure 5.6 do not suggest an obvious reason for the self-extinction of the momentary discharges. It is possible that a movement of the negative ion sheath towards the anode causes a reduction in the field enhancement zone near the anode surface which prevents further streamers. Since the probability of field induced detachment of SF_6 negative ions changes rather slowly with a wide variation in the value of E/p, it is quite likely that statistical variations in the field enhancement distance occur due to fluctuations in the field induced detachment processes.

Similar to the negative polarity, the transition form a momentary discharge to a sustained discharge in positive rod-plane gaps is very abrupt with respect to a change in the gap voltage. This is marked by a large increase in the average prebreakdown current. The return to a momentary discharge occurs when the gap voltage is reduced below the onset level of a sustained discharge. It seems that the reasons for the transformation form a momentary discharge to a sustained discharge are similar to those discussed earlier for the cathode corona in SF_6 and SF_6-N_2 mixtures.

When the applied voltage is increased beyond the inception level of a steady discharge, the discharge extends very little into the gap. In such cases, the spread of the visible discharge with increasing gap voltages is observed for the most part to be tangential rather than normal to the electrode surface. This indicates that the low field barrier to the discharge growth is present at all voltages upto the breakdown. This low field barrier becomes stronger especially along the axis of the rod anode as the gas pressure is increased. This is primarily due to a reduced lateral diffusion at high gas pressures. Thus at such pressures, the corona streamers as well as the breakdown streamers are tangential to the rod anode as discussed earlier in chapters V and VI.

The discharge in SF_6-N_2 mixtures having SF_6 contents above a few parts percent is similar to that of pure SF_6. The discharge channels are bright and narrow and the corona activity is more or less confined to the vicinity of the anode. This is primarily due to the following two reasons: (i) The ionization and attachment coefficients of mixtures are very similar to those of SF_6 and are much different from the more common gases as discussed in the previous chapter. (ii) The mean free paths of the ionizing photons in SF_6-N_2 mixtures, though larger than those in pure SF_6, are considerably smaller than those in N_2 [23]. The reduced length of these paths result in smaller streamer lengths and reduced branchings.

Due to the relatively long mean free paths of the ionizing photons, the streamers in pure nitrogen are very large in length and show excessive branching as seen in figure 5.3. The addition of minute traces of SF_6 reduces the branching and the streamer length considerably as shown in figure 5.5. Thus it appears that the mean free paths of the ionizing photons in an SF_6-N_2 mixture containing less than 1% of SF_6 are considerably lower than those observed in pure nitrogen. This is consistent with our earlier observations about the corona discharges in such mixtures under the applications of impulse and negative direct voltages.

8.3. Breakdown Studies

It can be stated without any doubt that the presence of sustained corona discharges in both the positive as well as the negative rod-plane gaps considerably enhances the breakdown strength of systems insulated with SF_6 and SF_6-N_2 mixtures. The pressure over which this enhancement occurs is often referred to as the "corona stabilized breakdown region". The high pressure limit of this region at which the breakdown and the corona onset voltages coincide is known as the critical pressure P_c.

The results of the present investigations clearly indicate that the breakdown of both the negative and positive rod-plane gaps is corona stabilized in the low pressure region. At high pressures, however, the breakdown occurs in the absence of any corona discharges. The width of the corona stabilized breakdown region is much smaller for the positive rod-plane gaps as compared to the negative ones. Consequently, the critical pressure for the negative rod-plane gaps is higher than that observed for the positive ones as shown in figures 8.2 and 8.3. From these figures, it is clear that the critical pressure for the negative rod-plane gaps is almost twice that of the positive rod-plane gaps. Furthermore, the breakdown voltage for negative gaps is higher than that for the positive gaps in the low pressure end of the corona stabilized region. However, the reverse is the case at the higher pressures where the breakdown is not corona stabilized.

In the corona stabilized breakdown region at low pressures, the breakdown voltages increase linearly with pressure for both polarities of the applied voltage. The absolute width of the pressure region, where the breakdown voltage-pressure curve is linear, is much wider for the negative gaps as shown in figures 8.2 and 8.3. In these regions, the sparks follow straight paths for both the polarities of the applied voltages. As the gas pressures are increased, the breakdown voltages attain maximum values followed by reductions in magnitudes with increasing gas pressures, as shown in the figures 8.2 and 8.3. For both the positive and negative rod-plane gaps, the breakdown sparks show pro-

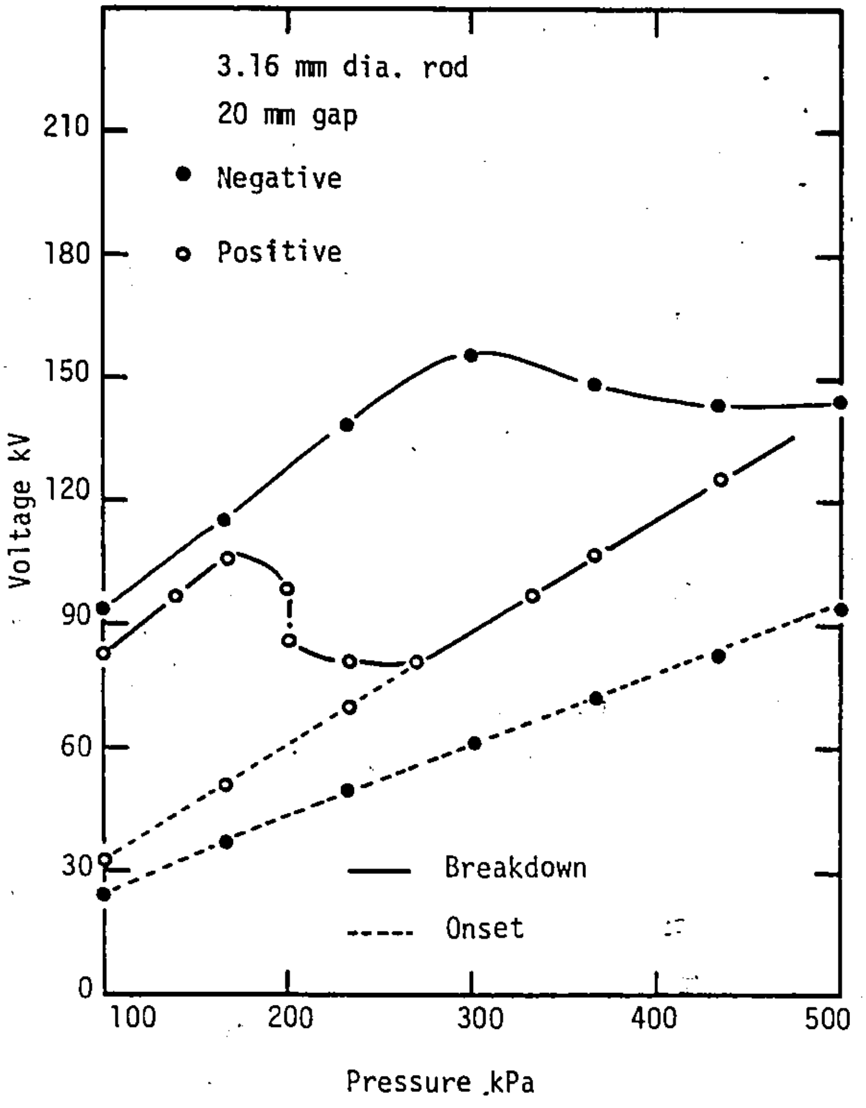

Figure 8.2 - Effect of gas pressure on the breakdown voltage behavior of positive and negative rod-plane gap filled with SF_6.

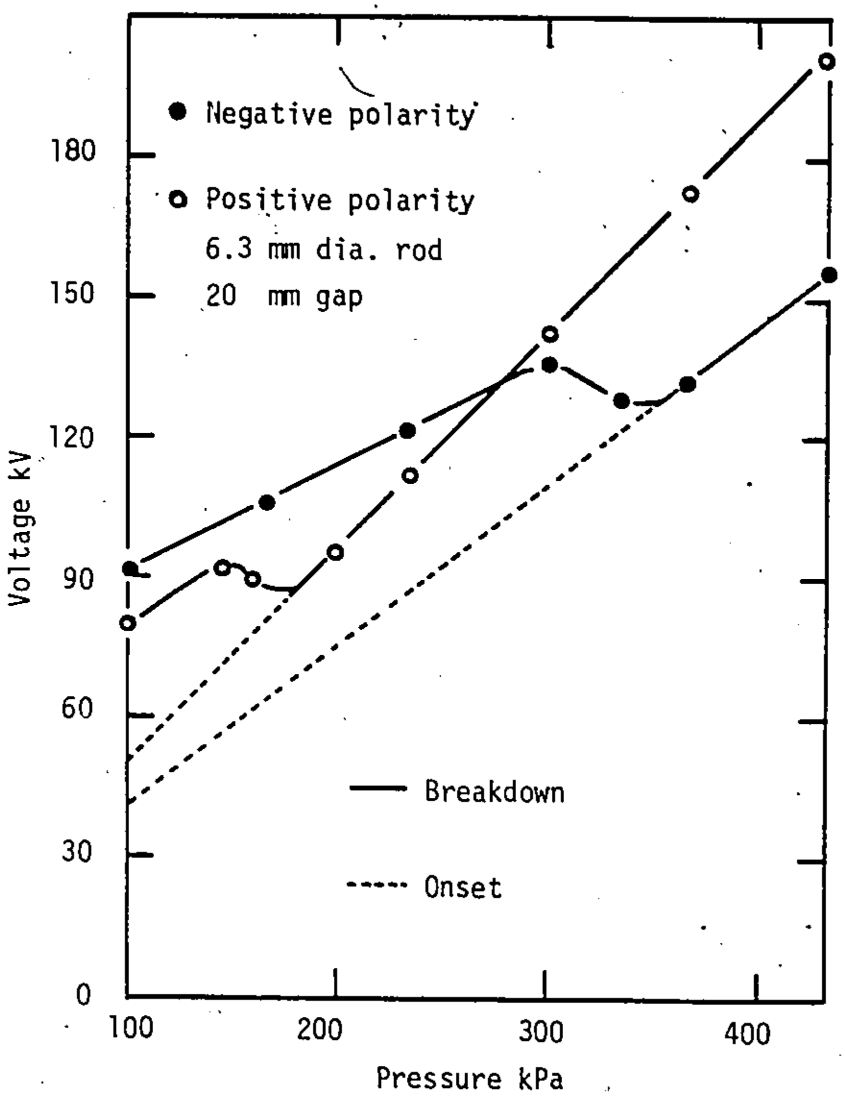

Figure 8.3 – Effect of gas pressure on the breakdown voltage behavior of positive and negative rod-plane gap filled with SF_6.

nounced curvature to the axis of the rod electrodes. When the gas pressure are further increased, breakdowns no longer take place in the presence of continuous corona discharges, although single or momentary corona discharges might occur before breakdown. In these pressure regions, the breakdown voltages remain almost unchanged with increasing pressures and the spark trajectories are straight. Above the critical pressures, the first avalanche grows to a breakdown in both cases and the spark paths are straight. Though a discontinuity similar to that observed in the breakdown voltage-pressure characteristics for a positive rod-plane gap was not observed for the negative gaps, the possibility of such a discontinuity cannot be ruled out. It is quite likely that extremely non-uniform field gaps with smaller diameter cathodes have discontinuities in the breakdown voltage-pressure curves especially at high values of the gas pressures not investigated in our studies.

The threshold voltage for the single pulse corona is higher for the positive rod-plane gaps as shown in figures 8.2 and 8.3. Furthermore, the magnitudes of the average prebreakdown currents for a given applied voltage and gas pressure are larger in the negative rod-plane gaps when compared with those observed for the positive gaps. This is probably due to the fact that the secondary ionization processes such as photoionization of the gas, photoemission from the cathode, and electron emission from the cathode due to positive ion bombardment are more effective when the rod cathode is in the high field region such as in the negative rod-plane gaps. Furthermore, when the highly stressed electrode is the cathode, the chances of field emitted electrons, initiating corona discharges are present especially at high values of the gas pressures. These reasons and the fact that it is easier for the positive than the negative streamers to propagate and bridge the gap make the corona stabilization processes more effective, especially at low pressures, for the negative rod-plane gaps. Consequently the corona stabilized breakdown region is wider in the case of the negative rod-plane gaps compared to that of the positive gaps.

At low pressures, the breakdown voltages of SF_6 and SF_6-N_2 mixtures is higher for the negative rod-plane gaps. This is due to the fact that it is more difficult for the negative streamers to advance in a divergent field as compared to the positive streamers. In the case of negative rod-plane gaps, an avalanche starts from the highly stressed cathode and the electrons diverge outward from a high field to a lower field region. Thus any electrons created by photoionization will move ahead of the streamer head to create new avalanches and thus move into a rapidly declining field region. Furthermore, when the streamer propagates in the presence of corona discharges, the low field region is filled with slowly drifting negative ions. This makes the streamer propagation farther into the gap extremely difficult unless the external fields are high enough to ensure the effective fields at the streamer tip ≥ 0.8775 $kV(cm\ kPa)^{-1}$ in the case of pure SF_6. On the other hand, for a positive rod-plane gap the electrons created ahead of the avalanche by photoionization travel towards the high field regions thereby creating more positive ion space charge at the avalanche head. In this fashion, the positive ion space charge is advanced towards the cathode maintaining the field at its tip and creating more electrons ahead of itself to continue the advance. This not only results in a lower value of the breakdown voltage for a positive rod-plane gap but also results in a much lower value for the critical pressure in such gaps.

The reduced gap voltages required for the propagation of the negative streamers causing a breakdown at extremely high pressures, figure 8.2 and 8.3, requires further investigations. However, it appears that at such high pressures the diffusion of electrons and ions is reduced considerably. Furthermore, the mean free paths for electrons and the ionizing photons are reduced considerably. Thus the new avalanches produced by photoionization effectively originate at the streamer tip. This helps in increasing the positive ion space charge density and hence maintains the field at the streamer tip as it advances into the gap regions where the applied field is otherwise declining rapidly. Thus at these high pressures, the ability of the positive and the negative streamers to propagate farther into the gap and resulting in a breakdown is more or less the same. However, as discussed earlier, the ionization activity starts at a relatively lower voltage level when the highly stressed electrode is the cathode, the breakdown voltage at such pressures is therefore lower for the negative rod-plane gaps.

The width of the corona stabilization regions in non-uniform field gaps is probably related to the mean free paths of the photons which can cause photo-ionizations or photo-detachments [16]. These processes are very important to maintain the steady corona discharges which in turn enhance the breakdown strengths of such gaps. In the previous chapters we have seen that, in general, the width of corona stabilization regions are more for SF_6-N_2 mixtures than that for pure SF_6. From the information reported in the literature [23], it appears that the mean free paths of the ionizing radiations vary with the mixture ratios and are higher in SF_6-N_2 mixtures than in pure SF_6. The present investigations of SF_6-N_2 mixtures show that the critical pressure P_c, the discontinuity pressure P_d and the pressure P_m where corona stabilization effects are maximum for a given field configuration are all affected to a certain extent when the mixture ratio is changed. The variations in P_c and P_d with mixture ratios are shown in figures 4.8 and 6.6 respectively for negative and positive rod-plane gaps. The pressure P_m remains almost unchanged for SF_6-N_2 mixtures having SF_6 content above a few parts percent. In order to fully comprehend and appreciate the effect of photoionization on the discharge behavior of mixtures, mixtures of SF_6 and helium were investigated. The breakdown behavior of such mixtures was found to differ from that of SF_6-N_2 mixtures. Although, the breakdown voltage-pressure characteristics for both mixtures were similar, the pressures P_m, P_c and P_d behaved differently with change in mixture ratios for SF_6-He mixtures. As shown in figure 8.4 and 8.5, though the pressure P_m has different values for different mixtures, the partial pressure of SF_6 corresponding to the pressure P_m is almost the same for a given electrode gap. The pressures P_c and P_d behave similar to P_m as shown in these figures. In figure 8.6, curve 1 shows the variations in the pressure P_c with the mixture ratio for a 40 mm negative rod-plane gap using 6.3 mm rod electrode and filled with SF_6-He mixtures. However, the partial pressure of SF_6 corresponding to the critical pressure P_c for each mixture ratio is almost the same as shown in curve 2 of figure 8.6. Thus the corona free breakdown for a given SF_6-He mixture for the investigated electrode geometry occurs at a pressure P_c such that the partial pressure of SF_6 of the mixture is roughly 300 kPa. Figure 8.7, curve 1, show the discontinuity pressure P_d as a function of the mixture ratio for a 20 mm gap using 1 and 3.16 mm diameter rod anodes. Here again, the partial pressure of SF_6 for each gap corresponding to the discontinuity pressure is more or less independent of the gas mixture ratio as shown in the figure. Thus it is obvious that when He is added to SF_6, the pressures P_m, P_d and P_c are all increased such that at their new values, the partial pressures of SF_6 are relatively unchanged from their respective

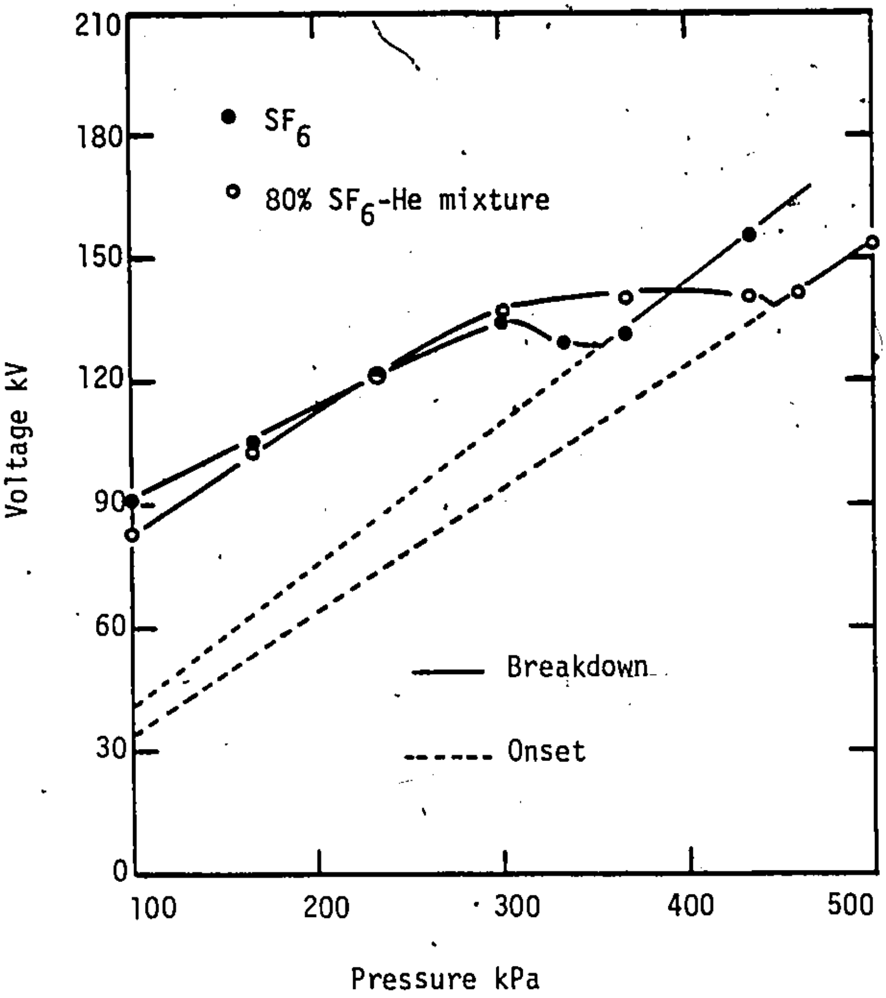

Figure 8.4 - Breakdown voltage-pressure characteristics of SF_6 and 80% SF_6-He mixture for a 20 mm negative rod-plane gap using a 6.3 mm rod cathode.

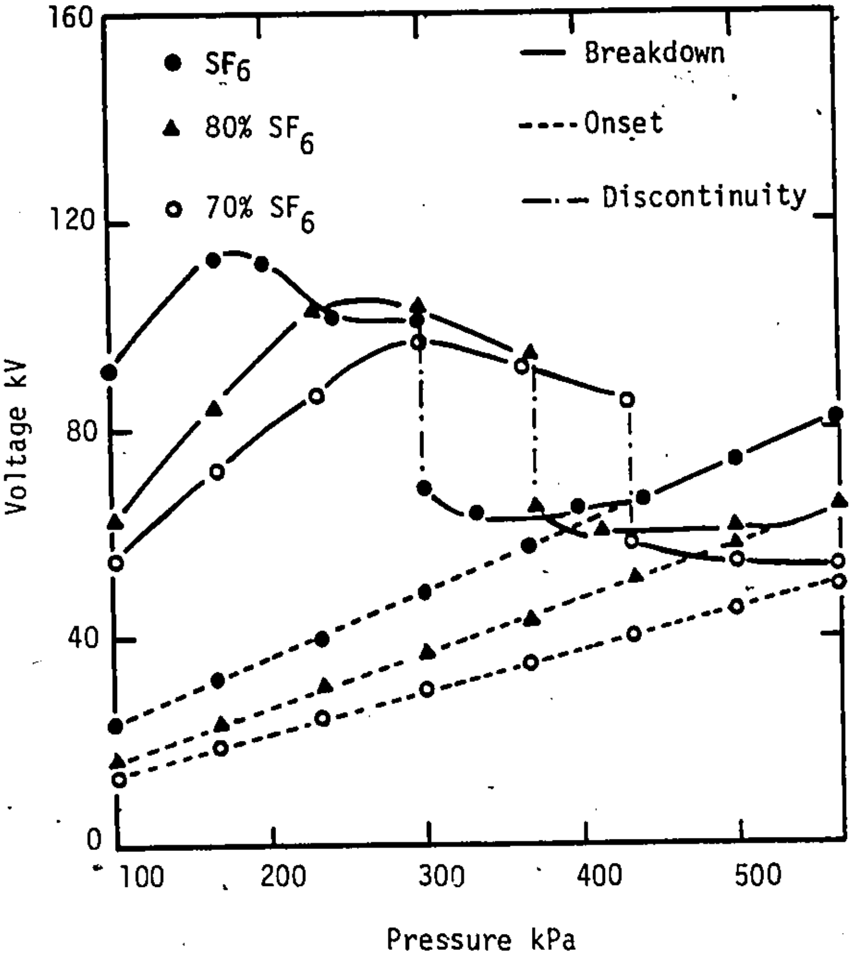

Figure 8.5 – Breakdown voltage-pressure characteristics of SF_6 and SF_6-He mixtures for a 20 mm positive rod-plane gap using 1 mm diameter rod electrode.

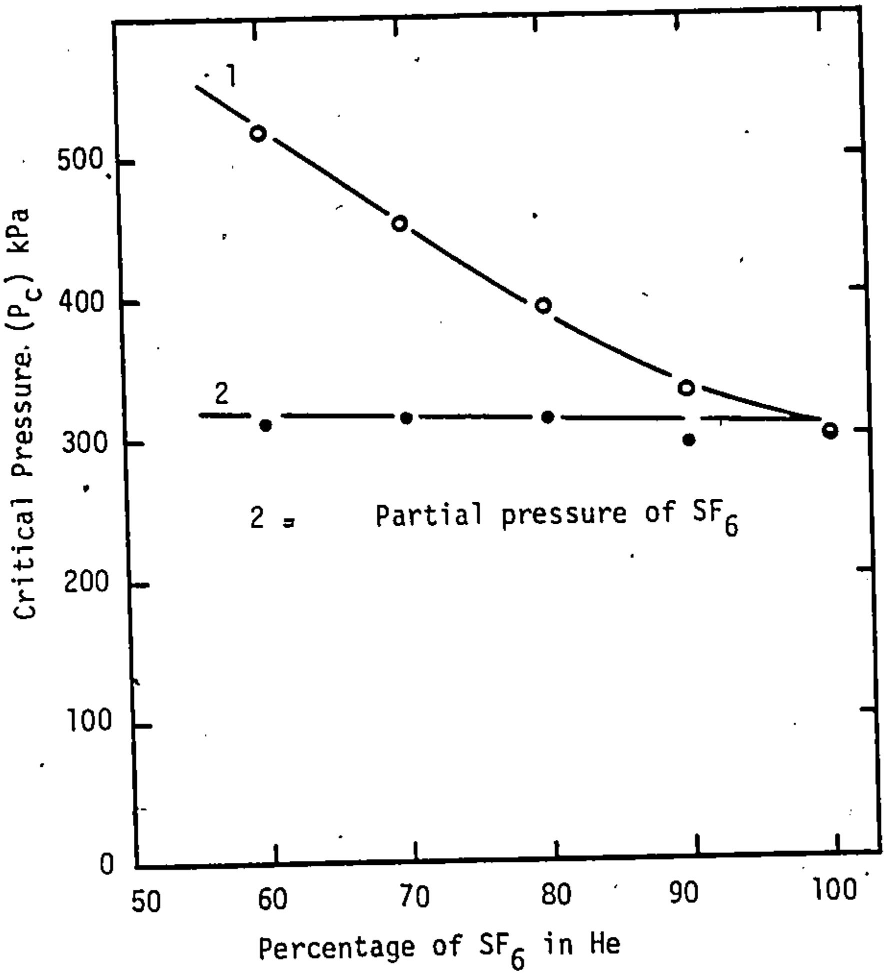

Figure 8.6 – Effect of gas mixture ratio on the critical pressure of a 40 mm negative rod-plane gap using 6.3 mm diameter rod cathode and filled with SF_6–He mixtures.

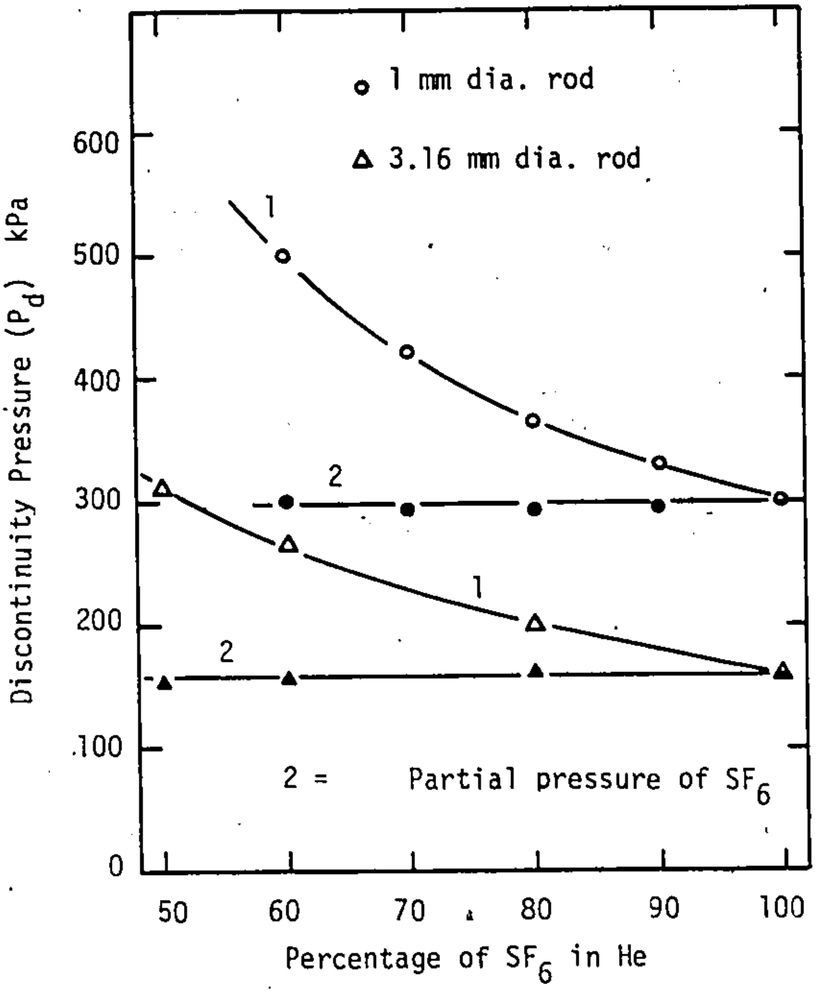

Figure 8.7 – Effect of gas mixture ratio on the discontinuity pressure of 20 mm positive rod-plane gaps filled with SF_6-He mixtures.

values in pure SF_6. This is probably due to the transparent nature of He to the photons which play an important role in the stabilization process. Thus when the mixture ratios are changed, the ranges and mean free paths of these photons are affected only by the SF_6 molecules present in the mixture. Consequently the partial pressure of SF_6 for the maximum stabilization is almost independent of the mixture ratio. The same argument supports the behavior of SF_6-He mixtures with respect to the pressures P_c and P_d. Wootton and Cookson [57] have reported that the partial pressure of SF_6 corresponding to the pressure P_m is unaffected by the mixture ratio when voltages of power frequency are applied across parallel plane gaps in the presence of 6.4 mm long and 0.45 mm diameter particles. The present investigations and those reported in the literature [57] indicate that SF_6 mixtures with other gases such as N_2, CO_2 and air do not show a behavior similar to that observed in SF_6-He mixtures because these gases do not have the required transparency to photons.

The breakdown voltages of the negative and the positive rod-plane gaps filled with SF_6 at low pressure of about 100 kPa increase with decreasing rod radii as shown in figures 4.5, 6.2 and 6.3. Azer and Comsa [21] have similarly reported that the 60 Hz breakdown voltages for rod-plane gaps insulated with SF_6 decreases with increasing rod diameter for small rod sizes. Similarly Cookson and Farish [58] observed that the 60 Hz breakdown voltage levels of SF_6 insulated coaxial electrode systems containing spherical particles decrease with increasing particle size. Thus, it is obvious that non-uniform field gaps using small electrodes have a higher breakdown strength, especially at low pressures in pure SF_6. As seen from equation 8.3, the critical avalanche length at the onset of a streamer type discharge is proportional to the square root of the rod radius. Thus at the discharge onset the length of the low field region, where α is less than η, will be more in an electrode system using a smaller diameter anode or cathode. Similarly, at any other value of the applied voltage, the field region with $\alpha < \eta$ will be larger in length for electrodes of smaller diameters. Also since at low pressures the corona discharges are present prior to the breakdown, this low field region is filled with slowly drifting negative or positive ions space charges for negative and positive gaps respectively. Consequently, the region with α less than η, acts as a barrier to the streamer propagation. Since the length of this barrier is affected by the rod diameter and is higher for smaller diameter rods, the corona stabilized breakdown voltages for such gaps are higher than those using rods with bigger sizes. This is, however, true only for extremely non-uniform field gaps. If the rod diameter is increased to such a value that the breakdown is corona free, the breakdown voltage increases with rod diameter thereby attaining a maximum value for the plane-plane gap.

8.4. Corona Free Breakdown in SF_6

The results of the present investigations and those reported in the literature [11-15] indicate that a breakdown in highly non-uniform field gaps insulated with SF_6 can occur in the absence of corona discharges at high gas pressure because the probability of streamer propagation is increased at such pressures. If the pressure is sufficiently high, the first streamer formed in the gas can bridge the gap and initiate a spark. In SF_6 and SF_6-N_2 mixtures, the corona free breakdown occurs at much lower pressure when the highly stressed electrode is the anode. Also since the critical pressure P_c under the applications of alternating applied voltages is more or less equal to its value obtained for positive rod-plane gaps, the criterion for corona free breakdown in SF_6 discussed in this section applies to alternating applied voltages as well.

The ability of a cathode directed streamer to propagate in the gas depends on the rate of growth of the position ion space charge at the streamer tip. This space charge is created by the secondary avalanches approaching the streamer tip. These avalanches are initiated by the electrons produced in the ionizing volume, that is, the volume surrounding the streamer tip where the total electric field strength E_t due to the applied voltage and streamer space charge is streamer directed, and $\frac{E_t}{p} \geq 0.8775$ kV/cm kPa. The number of secondary avalanches reaching the streamer tip is therefore proportional to the number of electrons produced in the ionizing volume. Electrons produced outside the ionizing volume suffer attachments producing negative ions and thus do not contribute to the streamer propagation.

For a given set of field conditions, the number of electrons produced in the ionizing volume is proportional to the photon absorption coefficient μ of the gas and the rate of photon production within the streamer tip. The photon absorption coefficient μ is proportional to the gas pressure p. Assuming that the photons are created at a point source and the ionizing volume is a sphere of radius r with its center at the point source, the probability P_i of a photon being absorbed in the ionizing volume is given by

$$P_i = \left(1-e^{-\mu r}\right) = \left\{1-y_1\ e^{-pr}\right\} \qquad (8.3)$$

where y_1 is a constant. Therefore, a linear increase in the pressure is accompanied by an exponential increase in the probability that a photon will create a free electron within the ionizing volume.

Thus the growth of the positive ion space charge at the streamer tip is a function of the total field strength E_t in the vicinity of the tip. For a cathode directed streamer to propagage in a direction in which the field intensity is decreasing, the space charge field must increase at a rate which can compensate for the rate of decrease of the applied field. The rate of increase of the space charge field is proportional to the rate of charge accumulation at the streamer tip, which in turn is proportional to the rate of photoionization and photo detachments in the ionizing volume.

From the above, it is evident that the probability of a corona free breakdown in SF_6 is a function of the rate of change of voltage gradients at the anode and the gas pressure. On the basis of this statement, Hazel [11] proposes the following hypothesis: A streamer initiated breakdown in SF_6 will occur in the absence of any corona, when the gas pressure is such that

$$\left.\frac{dE}{dx}\right|_{x=0} e^{-0.01p} \leq W \qquad (8.4)$$

where $\left.\frac{dE}{dx}\right|_{x=0}$ is the maximum rate of change of anode surface gradient in kV/cm^2 at the streamer onset voltage. p is the gas pressure in kPa and W is a constant. On the basis of his measurements of the critical pressure, Hazel [11] proposed a value of W = 200.

Using equation (7.22) and the streamer breakdown criterion of equation (7.26), one can express $\left.\frac{dE}{dx}\right|_{x=0}$ as;

$$\left.\frac{dE}{dx}\right|_{x=0} = -(2)\cdot\left(\frac{E}{p}\right)_{\lim}\cdot\frac{1}{R}\cdot p\cdot\left(1+\frac{C_1}{\sqrt{pR}}\right) \tag{8.5}$$

With equations (8.4) and (8.5), one can write the semi-empirical criterion for the corona free breakdown in compressed SF_6 [11] as

$$\left(\frac{E}{p}\right)_{\lim}\cdot\frac{1}{R}\cdot p\cdot\left(1+\frac{C_1}{\sqrt{pR}}\right)\cdot e^{-0.01p} = 100 \tag{8.6}$$

An inspection of equation (8.6) indicates that the occurrence of a corona free breakdown depends only on the parameters p and R. The locus of p, R - combination which satisfy equation (8.6) is plotted in figure 8.8. The corona free breakdown criterion of equation (8.6) can be interpreted with reference to figure 8.8 as follows: Prebreakdown currents can be observed in SF_6 insulated systems possessing a p, R - combination lying to the left while corona free breakdown occurs with a p, R - combination lying to the right of the curve.

Figure 8.8 shows the maximum pressures at which single pulse corona and sustained corona discharges were observed experimentally using different rod geometries. Thus the calculations based on equation (8.6) yield a reasonably accurate prediction of the critical pressure P_c.

8.5. Corona Free Breakdown in SF_6-N_2 Mixtures

From the results presented so far, it is obvious that the critical pressures P_c for SF_6-N_2 mixtures are different from those observed in pure SF_6. The values of P_c generally increase when the SF_6 component in the mixture is reduced. As seen in figure 6.5, it appears that the critical pressure P_c in pure N_2 is extremely high compared to that observed in pure SF_6. Since the discharge behavior of SF_6-N_2 mixtures is very similar to that of pure SF_6 as discussed in the previous chapters, it is proposed that the corona free breakdown criterion of equation (8.6)

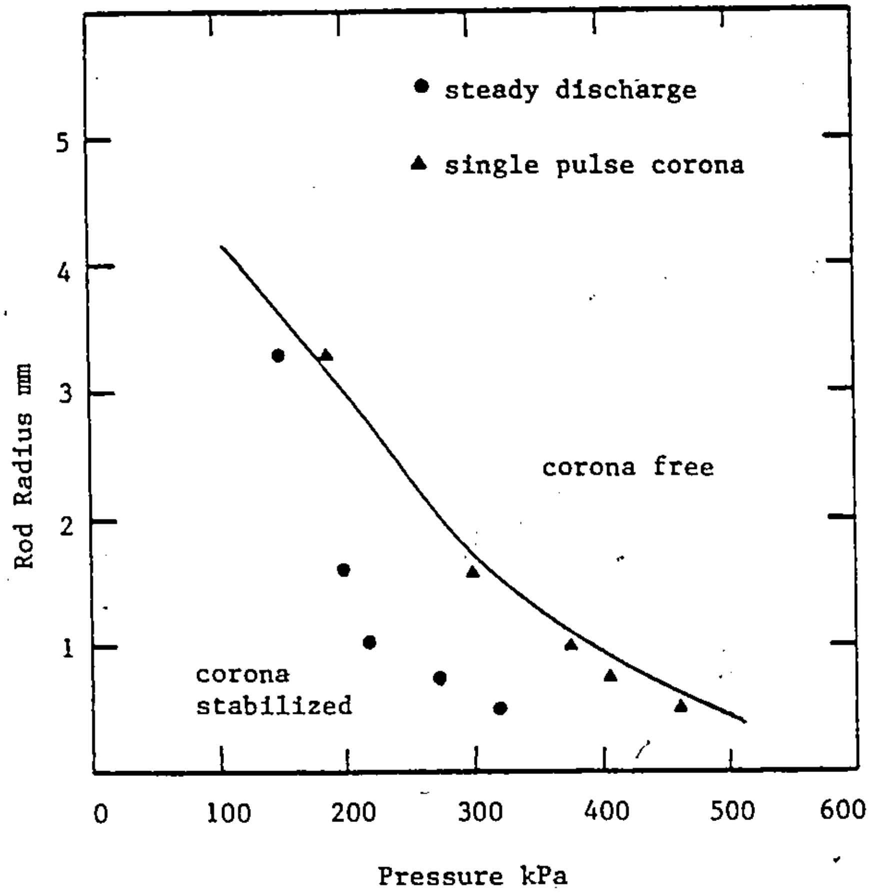

Figure 8.8 - Effect of rod radius on the onset pressure for corona free breakdown in positive rod-plane gaps filled with SF_6

can be modified to obtain a similar criterion for SF_6-N_2 mixtures. Accordingly it is proposed that the corona free breakdown in SF_6-N_2 mixtures occur when

$$\left(\frac{E}{p}\right)^{1}_{\text{lim}} \cdot \frac{1}{R} \cdot p \cdot \left[1 + \frac{C_m}{pR}\right] \cdot e^{-0.01p} = 100Z \qquad (8.7)$$

where $Z = \dfrac{p(SF_6)}{p}$ is the partial pressure ratio of SF_6 and $\left(\frac{E}{p}\right)^{1}_{\text{lim}}$ and C_m are functions of Z as shown in Table 7.1. Figure 8.9 shows the calculated and measured values of the critical pressure P_c for SF_6-N_2 mixtures in a 20 mm gap using 1 mm diameter rod anode. Thus from figure 8.9, it appears that equation (8.7) gives a reasonable prediction of the corona free breakdown pressures for SF_6-N_2 mixtures. In figure 8.10, the locus of p, R combination satisfying equation (8.7) is plotted for pure SF_6 and SF_6-N_2 mixtures containing 50 and 20% SF_6. It is obvious that, in general, the critical pressure P_c is higher for mixtures having smaller SF_6 contents.

8.6. Concluding Remarks

Based on the experimental and analytical studies described in this work, the following conclusions can be drawn.

The static field anode and cathode corona discharges in SF_6-N_2 mixtures are very similar to those observed in pure SF_6. Such discharges pass through three distinct modes of single pulse discharge, momentary discharge and sustained discharge activity with increasing applied voltages. The corona discharges in pure N_2 are substantially different from those observed in SF_6-N_2 mixtures containing small traces of SF_6. Moreover the corona discharges in SF_6-N_2 mixture are significantly different from those in air. At higher values of gas pressures or in more uniform field gaps, a complete breakdown may preclude the development of any type

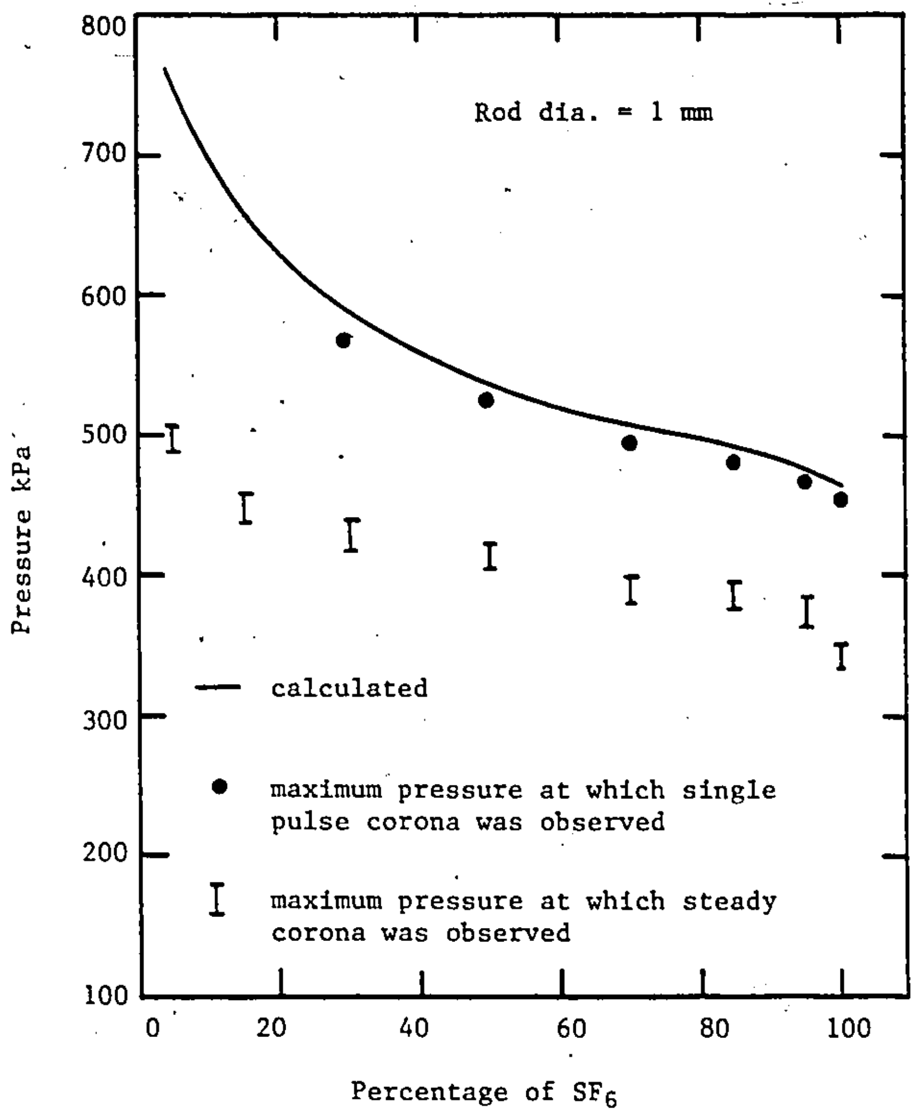

Figure 8.9 - Effect of gas mixture ratio on the critical pressure of a 20 mm positive rod-plane gap filled with SF_6-N_2 mixtures.

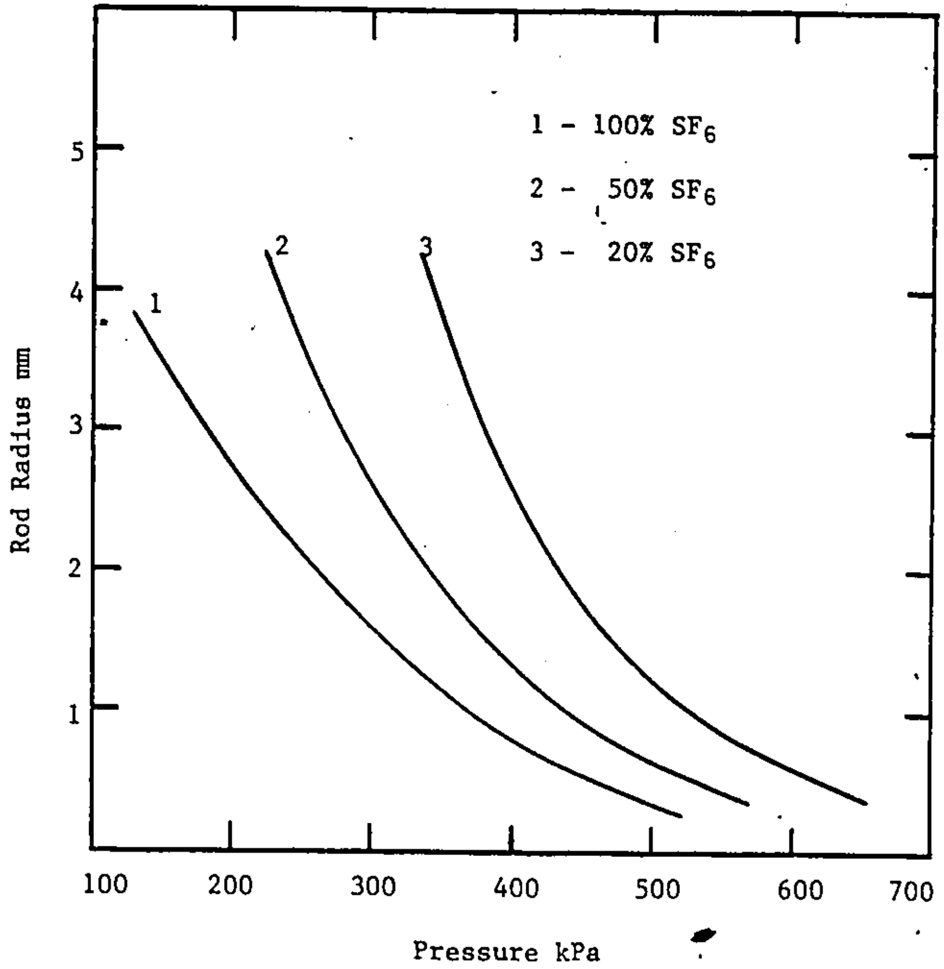

Figure 8.10 - Effect of rod radius on the onset pressure for corona free breakdown in SF_6 and SF_6-N_2 mixtures.

of corona discharges. The critical pressure which is the pressure above which corona discharges do not precede the breakdown depends on the polarity of the applied voltage, diameter of the rod electrode and gas mixture ratio. For a given electrode-gap arrangement and the mixture ratio, P_c is higher for the negative than that for positive rod-plane gaps. Also P_c has higher values for gaps filled with SF_6-N_2 mixtures than those filled with pure SF_6 for both polarities of the applied voltages.

The continuous corona discharges in SF_6 and SF_6-N_2 mixtures establish low field barriers to the propagation of breakdown streamers in positive and negative rod-plane gaps. Consequently, the breakdown voltages of non-uniform field gaps are much higher than the onset levels. The ability of these low field barriers to increase the breakdown voltage above the corona threshold level is affected by the polarity of the applied voltage, electrode-gap configuration, gas pressure and mixture ratio. In positive rod-plane gaps, the transition form the corona stabilized breakdown to one which occurs without any steady prebreakdown discharges is very abrupt. This results in a discontinuity in the breakdown voltage-pessure curve of such gaps. The pressure at which this discontinuity occurs is higher in SF_6-N_2 mixtures than in pure SF_6. In negative rod-plane gaps, this transition does not appear to be as abrupt as in the positive gaps and occurs at higher values of gas pressures.

In general, the corona stabilization processes operate over a wider pressure range for the negative than the positive gaps. Also both the theoretical as well as experimental studies incidate that for positive rod-plane gaps, the corona stabilization processes are operative over a wider pressure range in SF_6-N_2 mixtures as compared to pure SF_6.

The breakdown voltages of negative rod-plane gaps filled with N_2 are very sensitive to the presence of SF_6 as impurity. The breakdown voltage of pure N_2 for a 20 mm rod-plane gap using 1 mm rod cathode is almost doubled when 0.02% of SF_6 is added. In general, the breakdown voltage of negative gaps is the highest for pure SF_6.

For positive gaps, the breakdown voltage of SF_6 and SF_6-N_2 mixtures is strongly affected by the total gas pressure. At low pressures such as 100 kPa, the breakdown voltage-mixture ratio curves are similar for both the positive and the negative rod-plane gaps and the breakdown voltages of SF_6 are higher than those of SF_6-N_2 mixtures. At higher values of gas pressures such as 500 kPa, the breakdown voltages of mixtures containing less than 30% SF_6 are even lower than those of pure N_2. At moderate gas pressures such as 300 kPa to 400 kPa, the breakdown voltages of certain mixtures can be upto about 70% higher than those of pure SF_6. However, the corona onset voltages of SF_6-N_2 mixtures for both positive and negative rod-plane gaps behave similarly with respect to changes in the gas pressure. The onset voltages are lower for the negative gaps and for such gaps onset voltage-mixture ratio characteristics are similar to the uniform field breakdown voltage-mixture ratio curves.

The analytical studies show that the streamer breakdown criterion presented in this work can be used to estimate the discharge inception voltages of SF_6-N_2 mixtures with reasonable degree of accuracy for gaps having varying degrees of field non-uniformities. Furthermore, these studies indicate that compared to pure SF_6, SF_6-N_2 mixtures are less sensitive to the electrode surface defects.

From the point of view of application of SF_6-N_2 mixtures in gas insulated devices, the present studies indicate that the discharge behavior of 50% SF_6-N_2 mixtures is very similar to that of pure SF_6. The uniform field breakdown strength of such a mixture is expected to be about 85-95% that of pure SF_6 depending on the electrode surface conditions. In non-uniform field gaps, such a mixture will have a higher breakdown strength than pure SF_6 for pressures of technical interest. Also it can be operated at pressures considerably higher than 600 kPa which is the upper limit for SF_6 insulated devices. Moreover, similar to pure SF_6, such mixtures are non-flammable, non-toxic and carbon free but are relatively less expensive. Furthermore, compared to pure SF_6, the thermal characteristics of 50-50, SF_6-N_2 mixtures are not significantly degraded [59]. Thus it appears that SF_6-N_2 mixtures can be used instead of pure SF_6 in compressed gas transmission lines resulting in considerable savings in the overall cost of such systems.

REFERENCES

[1] N.H. Malik and A.H. Qureshi, "Breakdown Mechanisms in Sulphur-Hexafluoride". IEEE Trans. on Elect. Insul., Vol.EI-13, No.3, 1978, pp.135-145.

[2] N.H. Malik and A.H. Qureshi, "A Review of Electrical Breakdown in Mixtures of Sulphur-Hexafluoride and Other Gases". IEEE Trans. on Elect. Insul., Vol.EI-14, No.1, 1979, pp.1-13.

[3] N.H. Malik, A.H. Qureshi, G.D. Theophilus and M.R. Raghuveer, "Prebreakdown Phenomenon in SF_6-N_2 Mixtures at Various Pressures". Proc.1978 IEEE International Symposium on Electrical Insulation, Philadelphia, Pennsylvania, USA, 1978, pp.140-145.

[4] N.H. Malik, A.H. Qureshi and G.D. Theophilus, "Breakdown and Prebreakdown Phenomena in SF_6-N_2 Gas Mixtures." Proc. VIII International Symposium on Discharges and Electrical Insulation in Vacuum, Albuquerque, New Mexico, USA, 1978, pp.F7.1 -F7.14.

[5] N.H. Malik, A.H. Qureshi and G.D. Theophilus, "Static Field Breakdown of SF_6-N_2 Mixtures in Rod-Plane Gaps." IEEE Trans. on Elect. Insul., Vol.EI-14, No.2, 1979, pp.61-69.

[6] N.H. Malik and A.H. Qureshi, "Calculation of Discharge Inception Voltages in SF_6-N_2 Mixtures." IEEE Trans. on Elect. Insul., Vol.EI-14, No.2, 1979, pp.70-76.

[7] A. Yializis, N.H. Malik, A.H. Qureshi and E. Kuffel, "Impulse Breakdown and Corona Characteristics for Rod-Plane Gaps in Mixtures of SF_6 and Nitrogen With Less than 1% SF_6 Content." IEEE paper F79 157-9, PES Winter Meeting, New York, N.Y., Feb. 4-9, 1979.

[8] G.L. Weissler, "Positive and Negative Point-to-Plane Corona in Pure and Impure Hydrogen, Nitrogen, and Argon." Physical Reviews,

Vol.63, No.3, 1943, pp.96-107.

[9] L.B. Loeb, "Electrical Corona; Their Basic Physical Mechanisms." U.C.L.A. Press, Berkeley, California, USA, 1965.

[10] M.O. Pace, L.G. Christophorou, D.R. James, R.Y. Pai, R.A. Mathis and D.W. Bouldin, "Improved Unitary and Multi-Component Gaseous Insulators." IEEE Trans. on Elect. Insul., Vol.EI-13, No.1, 1978, pp.31-36.

[11] R.L. Hazel, "D.C. Breakdown and Corona Characteristics of Sphere and Rod-Plane Gaps Insulated With Compressed Sulphur-Hexafluoride." Ph.D. Dissertation, University of Windsor, Windsor, Canada,1974.

[12] P.R. Howard, "Insulation Properties of Compressed Electronegative Gases." Proc. IEE, Vol.104, Part A, No.13, 1957, pp.123-138.

[13] R. L. Hazel and E. Kuffel, "Static Field Anode Corona Characteristics in Sulphur-Hexafluoride." IEEE Trans. on P.A.S., Vol.PAS-95, No.1, 1976, pp.178-186.

[14] C.N. Works and T.W. Dakin, "Dielectric Breakdown of Sulphur-Hexafluoride in Non-Uniform Field Gaps." Trans. of AIEE, Vol.72, Part I, 1953, pp.682-687.

[15] T.R. Foord, "Some Experiments on Positive Point-to-Plane Corona and Spark Breakdown of Compressed Gases." Proc. IEE, Vol.100, Part II, No.78, 1953, pp.585-590.

[16] A.H. Cookson and R.E. Wootton, "AC Corona and Breakdown Characteristics for Rod Gaps in Compressed Hydrogen, SF_6 and Hydrogen-SF_6 Mixtures." IEEE Trans. on P.A.S., Vol.PAS-97, No.2, 1978, pp.415-423.

[17] E. Kuffel and A. Yializis, "Impulse Breakdown of Positive and Negative Rod-Plane Gaps in SF_6-N_2 Mixtures." IEEE Trans. on P.A.S., Vol. PAS-97, No.6, 1978, pp.2359-2366.

[18] A.H. Cookson and R.E. Wootton, "Particle Movement and Gas Breakdown in High Pressure Nitrogen and Sulphur-Hexafluoride." Proc. 3rd International Conference on Gas Discharges, IEE Conf. Publication No.118, 1974, pp.385-388.

[19] A. Yializis, "Impulse Breakdown Characteristics for Rod-Plane Gaps in Mixtures of Sulphur-Hexafluoride and Nitrogen." Ph.D. Dissertation, University of Windsor, Windsor, Canada, 1978.

[20] M. Eccles, A.N. Prasad and J.D. Craggs, "Electron Detachment in Sulphur-Hexafluoride." Electronics Letters, Vol.3, No.9, 1967, pp.410-411.

[21] A.A. Azer and R.P. Comsa, "Influence of Field Non-uniformity on the Breakdown Characteristics of Sulphur-Hexafluoride." IEEE Trans. on Elect. Insul., Vol.EI-8, No.4, 1973, pp.136-142.

[22] O. Farish, R.C. Davidson and D.J. Tedford, "Corona Stabilization and the Critical Pressure in SF_6 and in SF_6-N_2 Mixtures." Conf. on Electrical Insulation and Dielectric Phenomena, Colonie, New York, Oct. 17-20, 1977.

[23] D.T.A. Blair and N.M. MacLeod, "Radiation in the Vacuum Ultra-Violet from Discharges in Gas Mixtures." Proc. 4th International Conference on Gas Discharges, IEE Conf. Publ. No.143, 1976, pp.401-403.

[24] D. Kind, "Gas Insulated Energy Transmission Systems." Trans. of South African Institute of Elect. Engineers, Vol.65, Part 12, 1974.

[25] V.H. DiBeler and F.L. Mohler, "Dissociation of SF_6, CH_4 and SiF_4 by Electron Impact." J.Res. U.S. National Bureau of Standards, Washington, D.C., Vol.40, January 1948.

[26] E.W. McDaniel and M.R.C. McDowell, "Low Field Mobilities of the Negative Ions in Oxygen, Sulphur-Hexafluoride, Sulphur Dioxide and Hydrogen Chloride." Phys.Rev., Vol.114, No.4,1959, pp.1028-1037.

[27] K.B. McAfee, Jr., "Pulse Technique for Measurement of the Probabilty of Formation and Mobility of Negative Ions." J. of Chemical Physics, Vol.23, No.8,1955, pp.1435-1440.

[28] F.C. Fehsenfield, "Electron Attachment to SF_6." J. of Chemical Physics, Vol.53, No.5, 1970, pp.2000-2004.

[29] L.B. Loeb and J.M. Meek, "The Mechanism of Electrical Spark." Stanford University Press, Stanford, California, 1941.

[30] H. Raether, "Electron Avalanches and Breakdown in Gases." Butterworth Press, London, England,1964.

[31] A. Pedersen, "Calculation of Spark Breakdown or Corona Starting Voltages in Non-Uniform Fields." IEEE Trans. on P.A.S., Vol.PAS-86, No.2, 1967, pp.200-206.

[32] A. Pedersen,"Criteria for Spark Breakdown in Sulphur-Hexafluoride." IEEE Trans. on P.A.S.,Vol.PAS-89, No.3, 1970, pp.2043-2048.

[33] M.S. Bhalla and J.D. Craggs, "Measurements of Ionization and Attachment Coefficients in Sulphur-Hexafluoride in Uniform Fields." Proc. Phys. Soc., Vol.80, 1962, pp.151-160.

[34] L.B. Loeb, "Basic Processes of Gaseous Electronics." California University Press, 1955, pp.415.

[35] J. Dutton, F.M. Harris and G.J. Jones," Ionization, Attachment and Breakdown in SF_6." Nature, Vol.227, August 1970, pp.702-703.

[36] H.A. Boyd and G.C. Crichton, "Measurement of Ionization and Attachment Coefficients in SF_6." Proc. IEE, Vol.118, No.12, 1971, pp.1872-1877.

[37] U.N. Maller and M.S. Naidu, "Sparking Potentials and Ionization Coefficients in SF_6." Proc. IEE, Vol.123, NO.12, 1976, pp.107-108.

[38] T. Nitta and Y. Shibuya, "Electrical Breakdown of Long Gaps in Sulphur-Hexafluoride." IEEE Trans. on P.A.S., Vol.PAS-90, No.3,

1971, pp.135-145.

[39] A. Pedersen, "The Effect of Surface Roughness on Breakdown in SF_6." IEEE Trans. on P.A.S., Vol.PAS-94, No.5, 1975, pp.1749-1754.

[40] A. Pedersen, "Estimation of Breakdown Voltages in Compressed, Strongly Electronegative Gases and Gas Mixtures." 1977 Conf. on Electrical Insulation and Dielectric Phenomena, Colonie, New York, Oct.17-20, 1977.

[41] O. Farish, O.E. Ibrahim and B.H. Crichton, "Effect of Electrode Surface Roughness on Breakdown in Nitrogen-SF_6 Mixtures." Proc. IEE, Vol.123, No.10, 1976, pp.1047-1050.

[42] M. Ermel, "Das N_2-SF_6-Gasgemisch als Isoliermittel der Hochspannungstechnik." ETZ-A, Bd-96, H-5, 1975, pp.231-235.

[43] R.G. Baumgartner, "Dielectric Characteristics of Mixtures of Sulphur-Hexafluoride (SF_6) and Nitrogen (N_2)." Proc. 3rd International Conf. on Gas Discharges, IEE Conf. Publ. No. 118, I974, pp.366-369.

[44] V.A. Wiedland, "Gasdurchschlagsmechanismen in electronegativen gasen (SF_6) und in gasgemischen." ETZ-A, Bd.94, H-7, 1973, pp.370-373.

[45] P.W. Karlsson and A. Pedersen, "Inherent Limitations in Uniform Field Discharge Data for SF_6." IEEE Trans. on P.A.S., Vol.PAS-91, No.4, 1972, pp.1597-1601.

[46] A. Pedersen, P.W. Karlsson, E.Bregnsbo and T.M. Nielsen, "Anomalous Breakdown in Uniform Field Gaps in SF_6." IEEE Trans. on P.A.S., Vol.PAS-93, No.6, 1974, pp.1820-1826.

[47] T.W. Dakin, G. Luxa, G. Oppermann, J. Vigreux, G. Wind and H. Winkelnkemper, "Breakdown of Gases in Uniform Fields: Paschen Curves for Nitrogen, Air and Sulphur-Hexafluoride." Electra, No.32, 1974, pp.64-70.

[48] A. Diessner and R. Durschner, "Bemussung einpoliger, SF_6-Isolierter 420-kV-Rohrleiter." Elektrizitatswirtschaft, Vol.73, No.5, 1974, pp.124-128.

[49] H.E. Fiegel and W.A. Keen, Jr., "Factors Influencing the Sparkover Voltage of Asymmetrically Connected Sphere Gaps." Trans. of AIEE, Vol.76, Part I, July 1957, pp.307-316.

[50] A. Russel, "The Dielectric Strength of Air." The Philosophical Magazine, London, England, Vol.XI, 1906, pp.237-276.

[51] L.G. Christophoru, D.R. James, R.Y. Pai, R.A. Mathis, M.O. Pace, D.W. Bouldin, A.A. Christodoulides and C.C. Chan. "High Voltage Research (Breakdown Strength of Gaseous and Liquid Insulators)." Oak Ridge National Laboratory Report, ORNL/TM-6113, 1977, pp.25-28.

[52] E. Nasser, "Fundamentals of Gaseous Ionization and Plasma Electronics", Wiley, New York, 1971.

[53] M.S. Naidu and A.N. Prasad, "Mobility and Diffusion of Negative Ions in Sulphur Hexafluoride", J. Phys. D. Appl. Phys., Vol.3, 1970, pp.951-956.

[54] G.W. Trichel, "The Mechanism of the Positive Point to Plane Corona in Air at Atmospheric Pressure", Physical Review, Vol.55, 1939, pp.382-390.

[55] E.I. Mohr and G.L. Weissler, "Positive Corona in Freon-Air Mixtures", Physical Review, Vol.72, 1947, pp.294-297.

[56] S.K. Berger, "Der Einfluss Von Elektrodenoberflachenstorungen Auf Die Dielektrische Festigkeit Von Luft", Ph.D. Dissertation ETH Zuerich, 1978.

[57] R.E. Wootton and A.H. Cookson, "AC Particle-Initiated Breakdown in Compressed Gas Mixtures of SF_6 with He, N_2 and CO_2", Proc. 5th

International Conf. on Gas Discharges, IEE Conf. Publ.No.165, pp.177-180.

[58] A.H. Cookson and O. Farish, "Particle Initiated Breakdown Between Coaxial Electrodes in Compressed SF_6", IEEE Trans. on P.A.S., Vol. PAS-92, 1973, pp.871-876.

[59] A.H. Cookson, T.F. Garrity and R.W. Samm, "Research and Development in the United States on Three-Conductor and UHV Compressed Gas Insulated Transmission Lines for Heavy Load Transmission", CIGRE paper 21-09, August 30 - September 7, 1978.

VITA AUCTORIS

1949	Born in Punjab, Pakistan on January 17th.
1973	Graduated from the West Pakistan University of Engineering and Technology, Lahore with BSc degree in Electrical Engineering
1973-75	Lecturer in the Electrical Engineering Department, University of Engineering and Technology, Lahore, Pakistan
1976	Graduated from the University of Windsor, Windsor, Ontario, Canada with a MASc degree in Electrical Engineering
1979	Candidate for PhD degree in Electrical Engineering at the University of Windsor, Windsor, Ontario, Canada.